Tooling Performance in Micro Milling: Modelling, Simulation and Experimental Study

A thesis submitted for the degree of Doctor of Philosophy

by

Tao Wu

School of Engineering and Design, Brunel University

December 2012

Abstract

With the continuing trend towards miniaturization, micro milling plays an increasingly important role in fabrication of freeform and high-accuracy micro parts or components directly and cost-effectively. The technology is in kinematics scaled down from the conventional milling, however, existing knowledge and experiences are limited and comprehensive studies on the micro tooling performance are essential and much needed particularly for the process planning and optimization.

The cutting performance of micro tools is largely dependent on the dynamic performance of machine tools, tooling characteristics, work material properties and process conditions, and the latter three aspects will be focused in the study. The state of the art of micro milling technology with respect to the tooling performance has been critically reviewed, together with modelling work for performance prediction as well as metrology and instrumentation for the performance characterization.

A novel 3D finite element method taking into account the geometry of a micro tool, including the tool diameter, rake angle, relief angle, cutting edge radius and helix angle, has been proposed for modelling and simulation of the micro milling process. Validation through well-designed micro milling trials demonstrates that the approach is capable of characterizing the milling process effectively. With the support of FEM simulation developed, the tooling geometrical effects, including those from helix angle, rake angle and cutting edge radius with influences on cutting forces, tool stresses, tool temperatures, milling chip formation and temperatures have been comprehensively studied and compared for potential micro tool design and optimization purposes.

In an effort to prolong the tool life and enhance the tooling efficiency, DLC and NCD coatings have been deposited on micro end mills by PE-CVD and HF-CVD processes respectively. Corresponding cutting performance of these coated tools have been assessed and compared with those of WC micro tools in both dry and wet cutting conditions so as for better understanding of the coating influence on micro tools.

Furthermore, the cutting characteristics of the DLC coated and uncoated tools have been analysed through verified plane-strain simulations. The effects of coating friction coefficient, coating thickness and UCT have been determined and evaluated by design of simulation method.

Mechanical, chemical and physical properties of a work material have a direct influence on its micro-machinability. Five most common engineering materials including Al 6061-T6, C101, AISI 1045, 304 and P20, have been experimentally investigated and their micro milling behaviours in terms of the cutting forces, tool wear, surface roughness, and micro-burr formation have been compared and characterized.

Feed rate, cutting speed and axial depth of cut constitute the complete set of process variables and they have significant effects on the tooling performance. Fundamental understanding of their influences is essential for production engineers to determine optimum cutting parameters so as to achieve the maximum extension of the tool life. 3D FE-based simulations have been carried out to predict the process variable effects on the cutting forces, tool stresses, tool temperatures as well as micro milling chip formation and temperatures. Furthermore, experimental approach has been adopted for the surface roughness characterization. Suggestions on selecting practical cutting variables have been provided in light of the results obtained.

Conclusions with respect to the holistic investigation on the tooling performance in micro milling have been drawn based on the research objectives achieved. Recommendations for future work have been pointed out particularly for further future research in the research area.

Acknowledgements

First and foremost I would like to take this opportunity to express my gratitude to my supervisor, Professor Kai Cheng, for his enthusiastic scientific support, insightful guidance, and patient throughout the course of this research. Without his precious advice and encouragement, the completion of the PhD project would not have been possible.

I would like to thank Brunel University and the UK Technology Strategy Board (TSB) for their financial support which made this research possible. I am also grateful to my colleagues, Mr. Paul Yates, Mr. Feifei Jiao, Dr. Xizhi Sun, Dr. Dehong Huo and Dr. Robin Wang for their assistance in the micro milling trials and valuable discussions.

Project partners including Bristol University and Diameter Ltd, as well as Kistler (UK) Ltd, have also to be acknowledged for their support, assistance and constructive suggestions in this research project.

I am deeply indebted to my parents, Jiaqing Wu and Guilan Li, for their continuous encouragement and support. Finally, special thanks to my wife Dr. Juan Luo for all her love, encouragement and affection throughout this crucial time of my life.

Table of Contents

Abbreviations

BUE   Built up edge

CAD   Computer aided design

CAM   Computer aided manufacturing

CBN   Cubic boron nitride

CCD   Charge-coupled device

CP   Conventional processing

CVD   Chemical vapour deposition

DLC   Diamond-like carbon

DOC   Depth of cut

DOE   Design of experiment

ECAP   Equal channel angular pressing

EDM   Electrical discharge machining

FEM   Finite element method

FE-SEM   Field emission scanning electron microscope

FGD   Fine-grained diamond

FIB   Focused ion beam

HF-CVD   Hot filament chemical vapour deposition

LIGA   Lithography, electro plating, and moulding

MCT   Minimum chip thickness

MD   Molecular dynamic

MEMS   Micro electro mechanical system

NCD   Nano-crystalline diamond

OFHC   Oxygen-free high conductivity

PE-CVD   Plasma enhanced chemical vapour deposition

PMMA   Polymethylmethacrylate

PVD   Physical vapour deposition

SEM   Scanning electron microscope

TMS   Tetramethylsilane

UCT   Uncut chip thickness

WC   Tungsten carbide

2D   Two-dimensional

3D   Three-dimensional

Nomenclature

A	Plastic equivalent strain in Johnson-Cook constitutive model (MPa)
B	Strain related constant in Johnson-Cook constitutive model (MPa)
C	Strain-rate sensitivity constant in Johnson-Cook constitutive model
E	Specific cutting energy (N/mm^2)
F_f	Cutting force component in feed direction (N)
F_n	Cutting force component in normal direction (N)
F_r	Resultant cutting force (N)
F_{ra}	Cutting force component in radial direction (N)
F_{ta}	Cutting force component tangential to cutting direction (N)
f_z	Feed per tooth (µm)
h	Radial depth of cut (mm)
h_c	Value of UCT (µm)
h_{cl}	Low UCT (µm)
h_{ch}	High UCT (µm)
h_f	Tool flank wear (µm)
h_0	Distance between tip point and reference line of a tool before cutting (µm)
h_t	Distance between wear point and reference line of a tool after cutting (µm)
$L_{\widehat{AB}}$	Tool-work cutting edge contact length (mm)
m	Thermal softening exponent in Johnson-Cook constitutive model
n	Strain hardening exponent in Johnson-Cook constitutive model
P	Pitch height (mm)

R Radius of cutting tool (mm)

r Tool cutting edge radius (mm)

T_{melt} Melting temperature of work material (K)

T_{room} Room temperature (K)

t_m Value of MCT (mm)

t_c Coating thickness (μm)

w Width of cutting section (mm)

α Rotation angle for bottom engaging point of a cutter (deg)

α_e Axial depth for cutting edge points (mm)

α_p Axial depth of cut (mm)

β Helix angle (deg)

γ Cutting rotation angle (deg)

$\bar{\varepsilon}$ Equivalent plastic strain (mm/mm)

$\dot{\bar{\varepsilon}}$ Plastic strain rate (s^{-1})

$\dot{\bar{\varepsilon}}_0$ Reference strain rate (s^{-1})

θ Difference of rotation angle between bottom and top engaging point (deg)

μ Coefficient of friction

$\bar{\sigma}$ Von Mises flow stress (MPa)

σ_n Normal stress (MPa)

τ_f Frictional stress on tool rake surface (MPa)

φ Friction angle between tool and chip (deg)

List of Figures

List of Tables

Chapter 1 Introduction

1.1 <u>Background of the research</u>

During the last 1-2 decades, the demand for high-accuracy miniature and micro features or components has experienced a phenomenal growth in various sectors including aerospace, medical, automotive, electronics, telecommunication, optics, etc. Some specific applications include micro channels for lab-on-chips, micro fuel cells, fluidic micro-chemical reactors, micro-nozzles for high-temperature jets, micro-holes for fibre optics, micro-moulds and deep X-ray lithographic masks (Chae et al., 2006; Liu et al., 2004a; Vogler et al., 2003). For micro electro mechanical systems (MEMS) only, Yole Development's analysis shows that the overall MEMS market is expected to grow from $8 billion in 2010 to $18 billion in 2015, while the emerging MEMS markets have the potential to add a further $2.2 billion to the overall MEMS market by 2015 (Yole Developpement, 2010). This emerging trend and the reported developments indicate micro parts and systems are becoming more and more important, both for enhancing product performance and diversity as well as for enhancing industrial economic growth.

To support this growth and cope with the diverse requirements of a wide range of applications, there is a growing need for a fast, direct, reliable and repeatable approach to fabricate freeform and high accuracy features or components out of a diverse range of engineering materials. Some traditional manufacturing procedures, such as plasma etching and LIGA, are primarily applicable to silicon or silicon-like materials on planar geometries and lack the ability to produce high aspect ratio three-dimensional components (Jackson et al., 2006; Liu et al., 2004a). Due to these limitations, researchers have turned to the miniaturization of mechanical manufacturing processes to address the aforementioned requirements (Bruno et al., 1995).

One alternative micro-mechanical fabrication method of growing importance is micro milling. It is a newly emerging, but fast-growing technology, and it has the capability of

creating freeform microstructures with complex shapes ranging from tens of micrometers to a few millimetres in size out of various materials, such as metals and metal alloys (Brecher et al., 2008; Takeuchi et al., 2006; Bang et al., 2005; Weck et al., 2001; Weule et al., 2001), polymers (Friedrich et al., 1996), and silicon (Rusnaldy et al., 2008; Rusnaldy et al., 2007). Fig. 1.1 shows some examples of high-quality or high aspect ratio features produced by micro milling various materials.

<div align="center">(a)   (b)   (c)</div>

<div align="center">(d)   (e)   (f)</div>
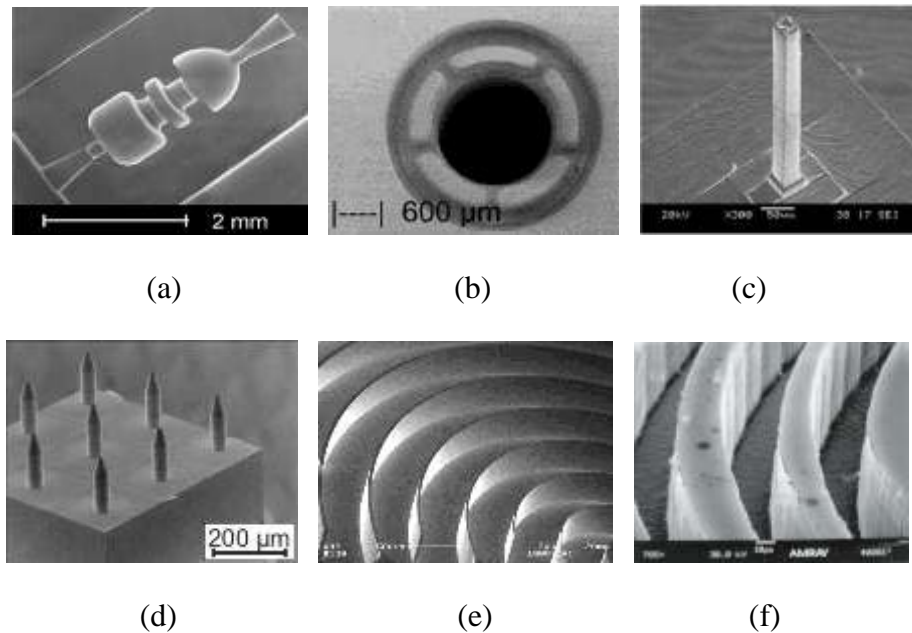
Fig. 1.1 Examples of high-quality or high aspect ratio micro features

(a) and (b) Micro moulds (steel) (Brecher et al., 2008; Weule et al., 2001), (c) and (d) Micro columns (brass) (Takeuchi et al., 2006; Bang et al., 2005), (e) Micro walls (nickel silver) (Weck et al., 2001), (f) Micro trenches (PMMA) (Friedrich et al., 1996)

Micro milling possesses numerous advantageous characteristics, such as flexibility, cost-efficiency, repeatability and high form accuracy, and it also features as a major means for shaping real three-dimensional parts in the small and medium lot sizes. So far, it has found a broad spectrum of important applications, including:

- Medical: Dental implants, bridges, hip prosthesis, bone plates and screws, spinal hook, surgical forceps and scissors, micro pumping mechanisms, etc.

- Watch-making: Precision watch cases, wristwatch parts, movements, electrodes, dial, etc.

- Electronics: Micro moulds for inserted connectors, miniature electronic devices, micro sensors, lab-on-a-chip, radio-frequency identification chips, etc.

- Optics: Micro lens arrays, optical devices, etc.

- Aerospace: Mould for planetary gear wheels, miniature devices for rockets, micro gyroscope components, micro valves and servo devices, etc.

- Others: Moulds for rings and pendants, components for measuring devices, injection nozzles, electrodes for cutting inserts, etc.

Some specific micro-milled components mentioned above are illustrated in Fig. 1.2.

(a)	(b)	(c)
(d)	(e)	(f)
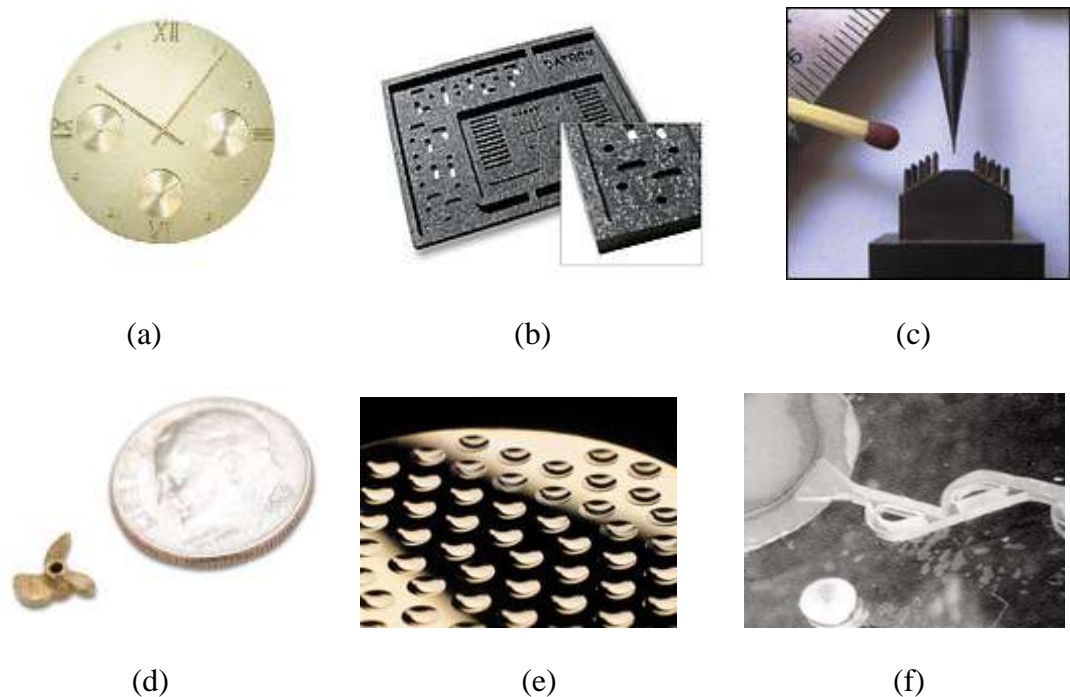
Fig. 1.2 Examples of micro-milled components

(a) Precision watch dial (Willemin Macodel, 2010), (b) Soldering frame (Datron Dynamics, 2010), (c) Micro electrode (Cimatron Group, 2010), (d) Micro propeller (Inventables, 2010), (e) Wafer-level optics (Kaleido Technology, 2010), (f) Micro valve (Design News, 2010)

Potential industrial applications as well as advantageous process capabilities enable the micro-mechanical cutting technique more and more promising, and thus there have received widespread interest in enhancing scientific understandings of the technology.

Although micro milling emerges as a newly developing method, it is in nature originally and directly scaled down from the conventional milling. The two cutting processes have the similar kinematics, and the cutting process can be characterized by mechanical interaction of a sharp tool with the work material, causing breakage inside the material along defined paths, and eventually leading to removal of the useless part of the workpiece in the form of chips (Alting et al., 2003).

Micro milling plays an increasingly important role in bridging the gap between the traditional precision macro and the emerging micro machining for making functional components. Nevertheless, a number of critical issues, arise on transition of mature macro-domain knowledge into the micro level, which influence the underlying mechanisms of the process, resulting in changes in the chip-formation process, cutting forces, vibrations and process stability, and the generation and subsequent character of the resulting machined surface (Liu et al., 2004a). These constraints, for example, unpredictable tool life and premature tool failures, significant downsized tool-work interactions, are mainly resulting from the miniaturization of machined components, cutting tools and processes, making the manufacturing technique considerably challenging in achieving favourable cutting performance.

In the study, tooling performance is referred as the cutting performance of micro tools, and it is universally weighted by a combination of characterization methods, such as the cutting forces, chip formation, tool wear and life, dimensional accuracy and surface finish. Research on this aspect has the potential to improve the tool design and optimize the cutting process. At present, scientific knowledge on the factors governing the tooling performance has not been systematically examined yet and the present capability of the manufacturing technique needs to be continually developed to meet current and future production demands. It would therefore be of great significance to address a comprehensive insight so as for further extending its industrial applications.

This research is partially in conjunction with the UK Technology Strategy Board (TSB) project Smart and Effective Engineering Manufacturing (SEEM) with grant contract number BD266E. The main objective of this project is to develop, apply and optimize diamond-like carbon and nano-crystalline diamond coatings on cutting tools so as to prolong the tool life and improve the cutting performance of tools. It also concerns with

developing an embedded sensing system for detecting and monitoring the real-time conditions of cutting tools.

1.2 <u>Tooling performance relevant challenges</u>

Currently, micro milling has being implemented and progressed at a breakneck speed, but the shaping of micro-scale devices has raised numerous scientific and technological challenges that are highly relevant to the tooling performance. The following issues constitute main limitations for the cutting technique reaching its full industrial potential.

1.2.1 Tool run-out

Tool run-out is characterized as misalignment or eccentricity between the axis of rotation of the spindle and the axis of symmetry of the tool (Chae et al., 2006). A small run-out may cause negligible effect in macro-scale milling, while in micro-scale milling, it can result in unstable periodic variations in chip load and forces. As a result of the tool run-out, it is common that one cutting edge performs machining while the other does not, leading to uneven wear on the tool cutting edges (Li, 2009), as an example is shown in Fig. 1.3.

(a) Wear on the 1st cutting edge   (b) Wear on the 2nd cutting edge
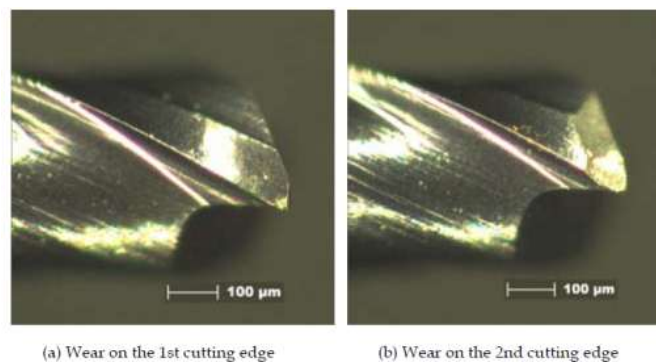
Fig. 1.3 Uneven cutting edge wear resulting from the tool run-out (Li, 2009)

It is clearly seen that one cutting edge wears more intensive than another one for the two-flute cutter. In such case, the cutter become blunt quickly, leading to significant force variations, chatter, and rougher surface profile as well as increasing the possibility of tool failures. Additionally, tool run-out influences micro-burr formation drastically (Lee et al., 2002).

The causes of tool run-out include asymmetric tool geometry, imperfect tool alignment in tool holder, mismatch between the tool holder and machining spindle, mass imbalance, eccentricity of spindle bearings, and vibration of tools during machining, etc (Lee et al., 2005). Run-out of a micro tool tip is a combination of error sources. Controlling and reducing the tool run-out is critical for improving the tool life and machining accuracy. In order to minimize the micro tool run-out, not only well-designed and manufactured tool but also precision tool holder and spindle are required. For an ultra-precision spindle, run-out inaccuracy should be controlled within 1µm so as to ensure high geometric accuracy of machined components (Kern, 2010). With existing equipment and techniques, the tool dynamic run-out is extremely difficult to determine due mostly to the very small dimensions of micro tools. Consequently, characterizing, controlling and reducing micro tool run-out presents a major consideration for the development of micro milling machines so as to achieve favourable cutting performance.

1.2.2 Tool wear and life

In conventional cutting, the tool wears gradually and the tool life criterion is commonly determined based on dimensional accuracy and quality of machined parts. Due to reduced structural stiffness and strength of micro tools, these end tool life criteria cannot be employed as premature tool failures occur frequently.

In normal conditions, the sharp cutting edges of miniature tools wear out rather rapidly, leading to large force variations and significant tooling performance deterioration (Bao et al., 2000c). Fig. 1.4 shows examples of cutting forces and burr formation variations using new and worn tools. When this phenomenon continues for an extended period of time, the increasing forces and stresses resulting from the wear may lead to fatigue-related breakages of micro tools (Tansel et al., 1998a).

While in extreme conditions, premature tool failures take place. For a well-designed and manufactured micro tool, there might be two reasons associated with the tool breakages: One is because the process conditions are not properly selected, leading to the cutting forces beyond critical strength limit of the tool. Another is due to chip clogging inside the tool flutes in only a few rotations, resulting in high cutting forces, stresses and temperatures.
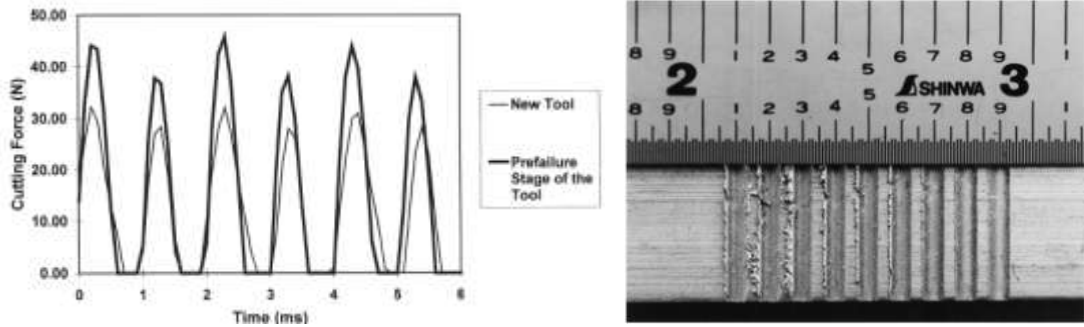
Fig. 1.4 Cutting force and burr formation variations under new and worn tools (Bao et al., 2000c)

Tool rotation deviations, partial fracture of cutting edges, and machining vibrations due to impurities of work materials also give rise to the probability of tool breakages. Unpredictable tool life and premature tool failures obstruct further cutting operations and prolongation of the micro tool life presents a key topic for researchers. In principle, excellent dynamic performance of micro milling machines, optimal design and fabrication of micro tools, free cutting homogeneous work materials as well as appropriate operating conditions can be beneficial for reducing the tool excessive wear as well as improving its lifespan.

1.2.3 Micro-burr formation

In micro-mechanical machining, burr formation is inevitable. The presence of high surface-to-volume burrs not only reduces part accuracy and quality but also affects its assembly and functionality. In conventional machining, deburring is routinely performed to meet specified tolerance and accuracy requirements. However, it cannot always be applied on micro-sized parts because of tiny part features as well as high surface quality requirements. Furthermore, burr removal process is often a major obstacle in terms of time，efforts and automation. Moreover, the functionality of micro products cannot be well maintained as it required due to alteration of inherent material characteristics across the deburring zones. Consequently, micro-burr formation should be controlled and minimized as far as possible.

A variety of influential factors, including tooling properties, work materials and process conditions, could more or less affect the micro-burr formation. Aurich et al. (Aurich et

al., 2009) summarized potential burr control strategies including:

- Tool and tooling: tool geometry alteration, proper tool material selection corresponding to the work material, coating technology, tool size.

- Coolant: application method, coolant media, application location.

- Process parameters: proper combination of cutting speed, feed, etc.

- Work material: replacing work material for less burr or preferable burr type.

- Work geometry: design change.

- Process sequencing: order of processes.

- Tool path and machining strategies: better tool path planning and effective machining strategies.

As micro-burr formation is a simultaneously integrated result of many factors, it may not be sufficient to achieve smaller burrs by changing one or two sources. Burrs minimization should be considered at all stages, from part design to the entire manufacturing process. So far, optimal combinations of these influential factors so as to control and minimize micro burrs are largely dependent on the part features being machined.

1.2.4 Optimum performance

In most cases, the performance of micro tools needs to be balanced. The holistic considerations for this aspect consist of the tool wear and life, geometric accuracy and quality of machined parts, material removal rate, etc. In case the tooling behaviours are opposite from each other, such as longer tool life but lower productivity, optimization of the micro cutting process becomes necessary and it is mainly determined based on specific application requirements.

In practice, appropriate process conditions have the most effective effects on the improvement of tooling performance. In conventional milling, they are always adopted by recommendations of tool suppliers or experiences of machine operators. However, for micro-scale milling, the operating conditions used are quite conservative due to the

high cost and fragility of micro tools. Proper selection of process conditions so as to achieve a satisfactory compromise among tooling performance needs to be addressed before this technology can reach its full potential in cost-effective, high throughput micro manufacturing.

1.3 Aim and objectives

The aim of this research is to comprehensively investigate the cutting performance of tools in micro milling dedicated for potential improvement of the micro cutting process. The motivation for the study mainly stems from the analysis of the tooling performance relevant process constraints, which indicate that dynamic performance of micro milling machines, cutting tool characteristics, work material properties as well as process conditions are the key factors in determining effective tooling performance. The investigation focuses primarily on the latter three aspects, in particular cutting tools, employing both simulation and experiments based approaches. The distinctive objectives for the study include:

(1) To critically review the state of the art of micro milling technology relevant to the tooling performance.

(2) To propose a novel approach for modelling and simulation of the micro milling process.

(3) To investigate tooling geometrical effects of micro tools and the associated micro milling performance.

(4) To evaluate the performance of DLC and NCD coatings deposited on micro tools.

(5) To obtain scientific understandings of work materials and process variables effects on the tooling performance.

1.4 Chapter plan of the thesis

This thesis is divided into nine chapters, as illustrated in Fig. 1.5.
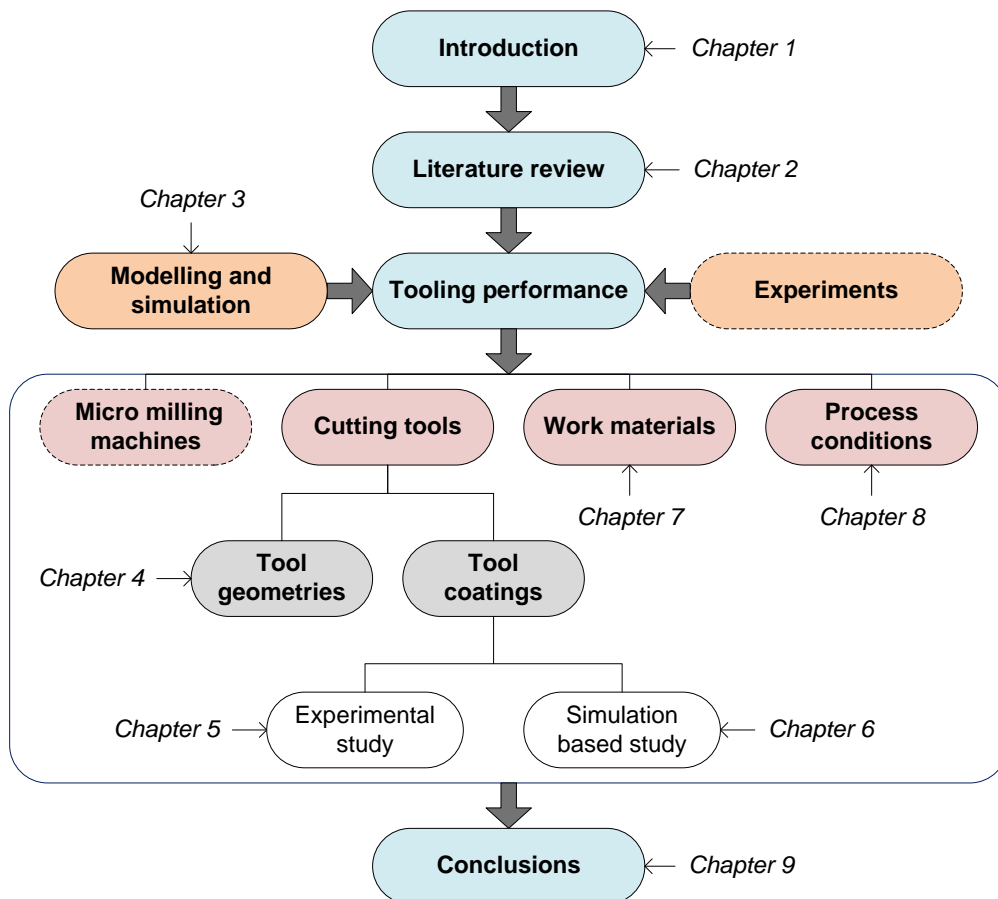
Fig. 1.5 Chapter plan of the thesis

The brief synopsis of each chapter is laid out in the following:

Chapter 1 introduces the research background, scientific and technological challenges, the aim and objectives, and the structure of the thesis.

Chapter 2 reviews the state of the art of micro milling technology from the tooling performance viewpoint, covering machines, micro tooling and processes. Micro milling mechanics is surveyed in depth, followed by the introduction of modelling efforts. Essential metrology and instrumentation for performance characterization are also highlighted.

Chapter 3 proposes a novel three-dimensional (3D) finite element method for effective modelling and simulation of the micro milling process. The proposed approach is validated through well-designed cutting trials.

Chapter 4 comprehensively investigates tooling geometrical effects on micro milling performance using the finite element method proposed in ***Chapter 3***. FE-based simulations are carried out under different helix angles, rake angles and cutting edge radius so as to determine respective influence on the tooling performance.

Chapter 5 introduces the characteristics of diamond-like-carbon (DLC) and nano-crystalline diamond (NCD) films deposited on micro end mills. The cutting performance of these coated tools is compared with that of uncoated tungsten carbide tools in both dry and wet slot milling for the evaluation purpose.

Chapter 6 assesses the cutting performance of DLC coated micro tools under various coating conditions using FE-based plain-strain simulations. The influence of coating friction coefficient, coating thickness and uncut chip thickness on the tooling performance are statistically analysed through design of simulation method.

Chapter 7 emphasizes on experimental investigation of the work materials' micro-machinability. Micro milling trials on work samples with different engineering materials are undertaken and the relevant tooling performance are presented, evaluated and discussed.

Chapter 8 explains systematic study of the process variables effects on the micro milling performance employing both simulation and experiments based approaches. Suggestions on selecting appropriate process variables are also given based on the research results.

Chapter 9 draws conclusions resulting from this investigation and makes recommendations on improving this area of research in the future.

Chapter 2 Literature Review

2.1 Introduction

In this chapter, the state of the art of micro milling technology that are highly relevant to the tooling performance, covering ultra-precision micro milling machines, cutting tools, work materials and process conditions, are firstly surveyed in a comprehensive manner. Fundamental cutting mechanics, including micro-cutting mechanism, size effects, chip formation and minimum chip thickness as well as work material microstructure effect are then emphasized. Modelling of the micro milling process for performance prediction is also reviewed in depth, and essential metrology and instrumentation for performance characterization are lastly introduced in brief.

2.2 State of the art of micro milling on the tooling performance

The principles of micro milling are similar to those of conventional milling operations, as components and products need to be fabricated within predefined quality, cost and time constraints. Four fundamental issues affecting the tooling performance, including ultra-precision micro milling machines, cutting tools, work materials together with process conditions, as shown in Fig. 2.1, play an important role for implementing the technology to high value manufacturing in various sectors.
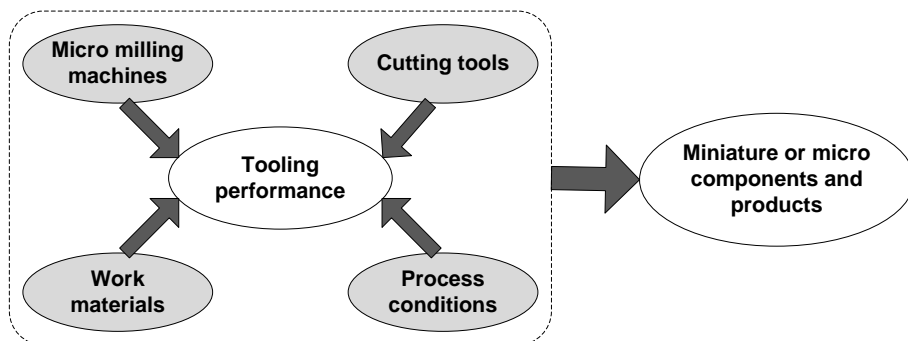
Fig. 2.1 Fundamental aspects affecting the tooling performance in micro milling

2.2.1 Micro milling machines

Excellent capabilities and quality of machine tools are vital for producing high quality micro-sized products. To meet the requirements for high dimensional accuracy, good form and surface finish, micro milling machines are required to have high static stiffness, good thermal stability, low motion errors and high damping or dynamic stiffness (Huo et al., 2009a).

In addition, a high cutting speed is necessary to achieve good tooling performance and high material removal rate so as to maintain acceptable productivity (Chae et al., 2006). Because of tiny diameters for the micro tools, micro milling machines are commonly equipped with high revolution, low thermal expansion and low run-out spindles.

Furthermore, multi-axis configurations of machines are also critical for ensuring greater process flexibility and higher form accuracy in machining freeform features. The advantage is manufacturing without the need for resetting thus greatly increasing productivity and eliminating re-clamping errors.

At the early stage of micromachining development, the cutting trials are mainly carried out on precision conventional machines, which is not cost effective, less flexible and tedious in use. Along with increased understandings of the cutting process and special requirements for the machines, numerous precision and ultra-precision machine tools, as shown in Fig. 2.2 (a-f), have been designed and configured with good micro milling capabilities (Fanuc, 2010; Kern, 2010; Kugler, 2010; Makino, 2010; Moore, 2010; Sodick, 2010).

Apart from the commercial machines, a five-axis ultra-precision micro milling machine, as illustrated in Fig. 2.3, has been built jointly by UPM Ltd and Brunel University, featuring a small footprint with good energy efficiency, low production cost and high machining accuracy (Huo et al., 2009a; Huo et al., 2009b). The overall footprint is only about $1m^2$ and its aerostatic bearing spindle is capable of producing speed up to 200,000 rpm (Huo et al., 2010). The further detailed specifications of the machine tool see Appendix III.

(a)   (b)   (c)

(d)   (e)   (f)

Fig. 2.2 Commercial micro milling machines

(a) KERN Micro (Kern, 2010)   (b) FANUC ROBONANO α-0iB (Fanuc, 2010)   (c) Sodick AZ250L (Sodick, 2010), (d) Kuglar Micromaster (Kugler, 2010) (e) Moore Nanotech 350UPM (Moore, 2010) (f) Makino Hyper2J (Makino, 2010)

Fig. 2.3 Ultra-precision micro milling machine UltraMill (Huo et al., 2010)

Main specifications of the above ultra-precision machine tools are summarized in Table 2.1, which provides a comprehensive comparison of characteristics and the state of the art of micro milling machines.

Table 2.1 Main specifications of the ultra-precision micro milling machines

	KERN Micro	FANUC ROBO NANO α-0iB	Sodick AZ250L	Kuglar Micromaster	Moore Nanotech 350UPM	Makino Hyper 2J	Brunel UltraMill
Configurations	Three linear axes and two rotary axes	Three linear axes and two rotary axes	Three linear axes	Three axes (standard) or five axes (optional)	Three axes (standard) or four axes (optional)	Three linear axes	Three linear axes and two rotary axes
Base structure	Polymer concrete	Cast iron base with concrete	Box-shape structure without overhang	Solid granite	Cast epoxy-granite base with carbon fibre reinforcements	Granite base	Natural granite
Vibration isolation	N/A	Air and oil damper	Counter-balance tables	Passive air dampers	Self levelling air isolation system	N/A	Squeeze film damper
Controller	Heidenhain	Fanuc	Sodick	Multiprocessor path control	Delta Tau	Fanuc	Delta tau
Spindles	Vector-controlled spindle	Static air bearing, air turbine	pneumatic static bearing, air turbine	hydrostatic bearing	Liquid cooled air bearing	N/A	Aerostatic bearing
Speed range (rpm)	Up to 160,000	Up to 50,000	Up to 120,000	Up to 200,000	200~60,000	3,000~40,000	Up to 200,000
Motion accuracy (µm)	<0.1	<0.2	N/A	±0.5	<0.05	±0.3	<1
Drive system	AC Servo	Linear motors and built-in servo motors	AC coreless linear motor	Linear motor	Brushless DC linear motor	N/A	Brushless drive motors
Drive system resolution (nm)	N/A	1	3	N/A	0.034	2	5
Work volume (mm)	250×220×200	280×150×40	250×150×100	300×300×200	350×350×150	200×150×150	150×150×80

In addition, numerous efforts have been taken to develop miniature machines and micro factories for fabricating precision micro components (Li et al., 2008; Lee et al., 2006; Bang et al., 2005; Okazaki et al., 2001; Tanaka, 2001). These very small footprint machines and factories are capable of reducing production cost, saving energy and increasing flexibility. At present, however, they are mainly used for research purpose as

application perspectives are still unclear due to their lack of rigidity as well as base vibration problems (Okazaki et al., 2004).

2.2.2 Cutting tools

2.2.2.1 Tool materials

Tool materials, coatings together with tool geometries are the most important factors determining effective tooling performance. The best tool materials have high hardness combined with adequate toughness and chemical stability at high temperature (Childs et al., 2000). Any given material does not generally have outstanding properties in all respects. Many types of materials, ranging from high speed steel, carbide, ceramics, to cubic boron nitride (CBN) and diamond can be used to fabricate micro tools. A comparison of their performance and applicable work materials are shown in Table 2.2 and Table 2.3 respectively.

Table 2.2 Comparison of typical tool material performance (Childs et al., 2000)

	Hot hardness	Toughness	Wear resistance	Thermal shock resistance	Cutting speed	Surface finish	Material costs
High speed steel	Low	High	Low	High	Low	Low	Low
Carbide	↓	↑	↓	↑	↓	↓	↓
Ceramics	↓	↑	↓	↑	↓	↓	↓
CBN	↓	↑	↓	↑	↓	↓	↓
Diamond	High	Low	High	Low	High	High	High

Table 2.3 Typical tool materials and their applicable work materials (Childs et al., 2000)

	Soft non-ferrous	Cast iron	Carbon and low alloy steels	Hardened steels	Nickel-based alloys	Titanium alloys
High speed steel	√	×	O	×	×	×
Carbide	√	√	√	O	√	O
Ceramics	×	√	√	O	√	×
CBN	×	O	×	√	O	O
Diamond	√	×	×	×	×	√

(√: Good, O: Suitable, ×: to be avoided)

Among these tool materials, diamond has some outstanding mechanical, chemical and physical properties, the high hardness enables sharper cutting edges, a much lower rate of wear and longer tool life as compared to other materials. However, high cost, brittleness and chemical affinity to iron have restricted its applications. For commercial micro tools, the most common and popular material is ultra-fine grain (normally grain size less than 0.5μm) cobalt-bonded tungsten carbide due to comparably low cost, high hardness, strength and adequate wear resistance characteristics. Of the most importance is that it is suitable for machining a wide variety of engineering materials including hardened steels. The performance of tungsten carbide tools is largely dependent upon the composition and grain size. The content of cobalt can affect the tool physical properties. A smaller amount of cobalt will result in higher hardness but brittleness of tools, generally, the finer grain size, the higher micro hardness, and vice versa.

2.2.2.2   Tool coatings

The microstructure that gives a tool its required hardness or toughness may not give the best wear resistance. Theoretically, tungsten carbide tools can be employed in machining almost all engineering materials, but they suffer from severe wear in case of cutting hard materials. In order to prolong the tool life and improve tooling performance, hardness, toughness and wear resistance of a tool material must be consistently maintained during machining operations.

Coating techniques potentially offer a promising solution to meet this need. They also enable the possibility of dry machining due to a lower friction coefficient between tools and work materials (Heaney et al., 2008). Coatings should be harder than the substrates in order to resist wear, be more inert to resist chemical wear and must adhere well to the substrates (Childs et al., 2000).

Aramacharoen et al. (Aramcharoen et al., 2007) reported that AlCrTiN coated micro mills provide better performance in machining hardened die steels in terms of reduced tool wear and improved surface quality as compared to the uncoated ones. In the later research (Aramcharoen et al., 2008), the authors compared the performance of TiN, TiCN, TiAlN, CrN and CrTiAlN films and demonstrated that these physical vapour depositions (PVD) coatings help reducing cutting edge chipping and the edge radius

wear as well as burr size. Among these coatings, TiN coatings deliver the best results.

The most common coatings for commercial micro tools are titanium-based and TiAlN in particular. Although carbide tools with diamond coating layers have recently come on to the market (Union Tool, 2010), they are not widely employed and are still under research. Diamond coatings for micro mills are advantageous and promising because they are capable of reducing flute clogging by eliminating adhesion of the work material to the tool surface, reducing tool wear due to high hardness and reducing cutting forces due to low friction coefficients against many materials (Heaney et al., 2008). Therefore, there has been strong interest in applying diamond films upon micro tools for improving the cutting performance.

Torres et al. (Torres et al., 2009) successfully coated fine-grained diamond (FGD) and nano-crystalline diamond (NCD) films onto tungsten carbide micro end mills using a hot-filament chemical vapour deposition (HF-CVD) process. The grain size of FGD is between 0.5~1μm, whereas for NCD is less than 0.1μm. They studied the performance of both coated tools by dry slot milling of aluminium and there was a dramatic improvement in tool integrity, lower wear rate, no observable adhesion and a significant reduction in the cutting forces compared to the performance of uncoated ones. However, in the study, the diamond coatings experienced severe delaminating due to insufficient bonding strength to the substrate, resulting in catastrophic tool fracture of the cutting edges. The authors suggested further development is indispensable for improving coating adherence upon tungsten carbide so as to increase longevity of diamond coatings. In order to achieve good adhesion, substrate surface pre-treatment, such as acid etching, is considered as an effective process (Jackson et al., 2003).

2.2.2.3   Tool geometries

The typical geometries and shapes of micro tools are directly scaled down from those of conventional tools due to their analogous cutting process (Fleischer et al., 2008). Micro tools are geometrically referred as tools with cutting diameter smaller than Ø1mm, and they are commonly seen in square and ball-nosed tips in the market, as illustrated in Fig. 2.4.

(a) Square tip   (b) Ball-nosed tip

Fig. 2.4 Micro tools in different tips (Union Tool, 2010)

Optimum geometrical configuration of micro tools is desirable for achieving better structural stiffness and strength, eliminating chip clogging and therefore improving the cutting performance. Li (Li, 2009) analysed the effects of structural features on the strength of cutting edges employing finite element method (FEM) and reported that negative rake angle, lower helix angle and relief angle can significantly reduce the maximum stress level on the cutting edge corners while there is only a slight stress effect caused by alteration of cutting edge radius. Fang et al. (Fang et al., 2003) performed an investigation on three types of micro tools in terms of rigidity, breakages and cutting performance in order to improve the tool life and quality of machined parts. Based on the FEM analysis and experimental study, they concluded that semi circle-based end mills have both highest rigidity and best tooling performance when compared to those of typical two-fluted and triangle-based end mills. Fleischer et al. (Fleischer et al., 2008) optimized a single-edged micro tool by means of structural stability analysis.

2.2.2.4   Tool fabrication

Fabrication of micro tools is essential for the application of micro cutting technology. Imprecise geometry and the irregularity of tools often negate the advantages of ultra-precision process control, state of the art machine tools and ultra fine tuning of process parameters (Dornfeld et al., 2006). In general, grinding is a traditional technique for manufacturing both conventional and micro tools. The quality of the tools is largely dependent upon the properties of the grinding wheel, such as abrasive grit size and grinding edge radius. Grinding for micro tool fabrication is rarely reported except for diamond grinding attempted by Schaller et al. (Schaller et al., 1999). With the decrease in tool diameter below Ø100μm, such technology becomes extremely challenging due to a reduction in tool rigidity and the requirements for tighter tolerances and sharper cutting edges.

Focused ion beam (FIB), which is cutting force free, is capable of producing micro tools with high quality, but not on a commercial scale. Adams et al. (Adams et al., 2001) fabricated a number of high speed steel and tungsten carbide micro end mills around Ø25μm diameter and 2, 4, 5 cutting edges by FIB sputtering processes. The cutting edge radius of these tools was less than 0.1μm and Fig. 2.5 shows these good quality tools in different shapes. Ali (Ali et al., 2006) also fabricated micro end mills of Ø20μm diameter with different aspect ratios by the same process and experiments on PMMA indicated surface finish of 80nm Ra could be achievable. In addition, Friedrich and his colleagues (Friedrich et al., 1996; Vasile et al., 1996) developed some two-flute and four-flute micro end mills in Ø22~100μm diameter with a submicron edge radius using an FIB micro machining process. These tools exhibited good form quality in micro milling high aspect ratio features as shown in Fig. 1.1 (f).
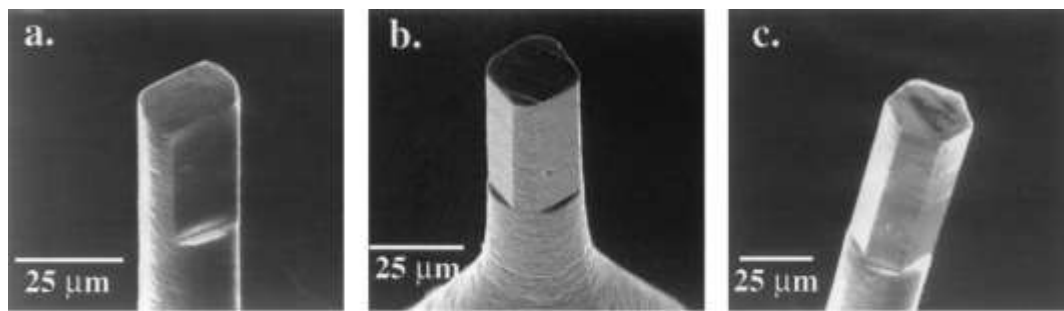
(a) Two cutting edges   (b) Four cutting edges   (c) Six cutting edges

Fig. 2.5 Micro tools fabricated by FIB (Adams et al., 2001)

In addition to FIB, electrical discharge machining (EDM) is another potential process for fabricating micro tools. Egashira et al. (Egashira et al., 2003) developed micro ball end mills with a radius of 10μm using EDM. Fleischer et al. (Fleischer et al., 2008) showed the feasibility of manufacturing tungsten carbide end mills with helical shapes in Ø50μm and Ø100μm diameters and with semi-circular shapes employing wire EDM technique. Cheng et al. (Cheng et al., 2009) also fabricated polycrystalline diamond ball end mills of Ø300μm diameter based on the wire EDM process. End mills of Ø50μm diameter with noncircular cross-sectional profiles were produced utilizing a similar process by Yan et al. (Yan et al., 2009), and micro grooving tests on electroless nickel plating demonstrated good performance of these tools in terms of wear and form quality. Some of the aforementioned EDM-fabricated micro tools are shown in Fig. 2.6.

(a)   (b)
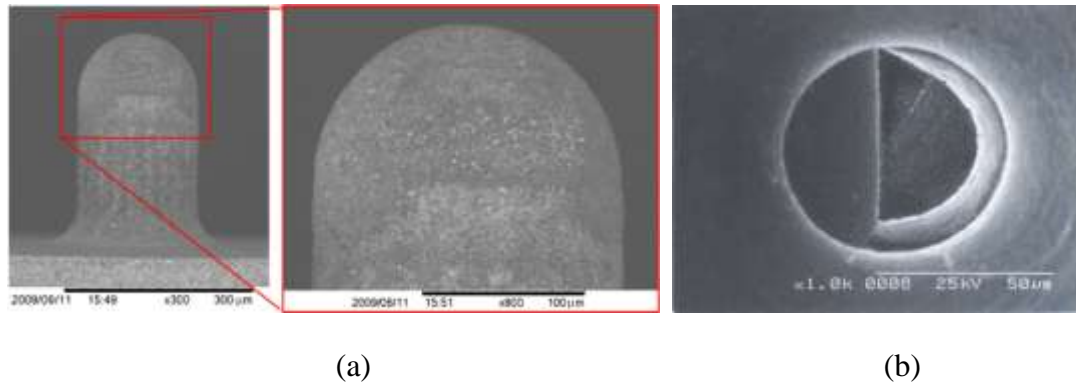
Fig. 2.6 Micro tools fabricated by EDM: (a) Polycrystalline diamond ball end mill
(Cheng et al., 2009), (b) Tungsten carbide micro end mill (Yan et al., 2009)

2.2.3 Work materials

Work materials affect the tooling performance in a direct way and selection of proper
work materials is largely dependent on applications, i.e. components and products.
Different industrial sectors require specific materials, such as stainless steel and
titanium alloys for medical devices, aluminium alloys for aerospace, hardened steel for
moulds and silicon for electronics. However, the cutting performance or machinablity
characteristics of these materials vary widely due to respective mechanical, physical and
chemical attributes.

Fig. 2.7 illustrates the machinability of common metals as compared to that of stainless
steel 416 in conventional machining (PMPA: Precision Machined Products Association,
2010). In principle, aluminium alloys are the easiest metals to be machined, followed by
copper alloys, cast iron and steels.

The equivalent comparison with respect to micro-machinability has not been established
yet. Due to the well-known size effects resulting in possible changing in the process
physics, existing knowledge and experiences in macro domain cannot be applied
directly. The assumption of homogeneity and isotropy in work material properties is no
longer valid because micro-grain-structure size is often of the same order of magnitude
as the tool cutting edge curvature (Grum et al., 2003). Material properties, such as grain
size and orientation (Pham et al., 2009; Popov et al., 2006a), heat treatment (Schmidt et
al., 2002) and multiple phases (Vogler et al., 2003), which may have little or no

influence at large scales, might become dominant factors with strong influences on the cutting performance of tools in micromachining. This will be discussed extensively in work microstructure section of this chapter.
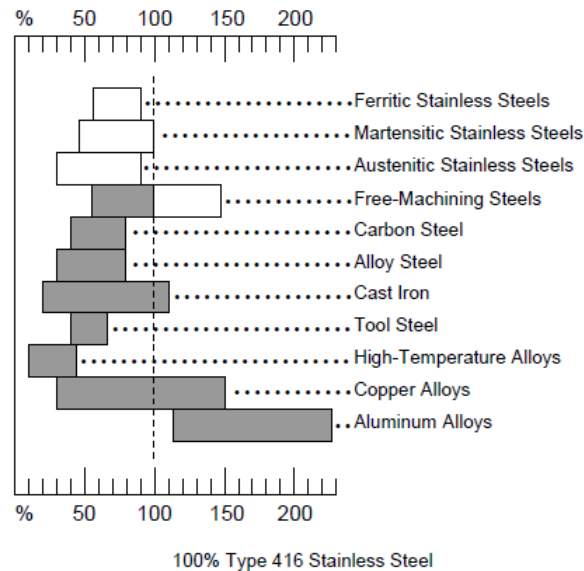
Fig. 2.7 Comparative machinability of common metals in conventional machining
(PMPA: Precision Machined Products Association, 2010)

The spectrum compatible materials can be tackled by micro milling are broad, including both metal and non-metal materials (Schueler et al., 2010; Shelton et al., 2010a; Shelton et al., 2010b; Gietzelt et al., 2008; Weinert et al., 2008; Rusnaldy et al., 2007; Bissacco et al., 2005; Uhlmann et al., 2005; Adams et al., 2001; Friedrich et al., 1996). When machining soft metal materials (e.g. aluminium alloys and copper), the failure of micro tools is mainly due to the edge wear. But in case of machining hard materials (e.g. tool steels), micro tools show rapid abrasive wear, edge chipping or premature breakages. In general, without considering any tool wear or dynamic influence, the harder work materials, the better surface finish as soft materials are more ductile and the elastic recovery gives rise to the surface roughness (Li, 2009). Softer materials can result in smaller burr size due to the lower tool wear rate (Schmidt et al., 2004). In micromachining high brittle non-metals, such as silicon and ceramics, excessive surface and subsurface cracking usually takes place due to very low fracture strain characteristics, and ductile mode machining is regarded as an effective approach for improving the surface finish (Dornfeld et al., 2006).

2.2.4 Process conditions

From process conditions point of view, the cutting performance of micro tools is determined by five main factors, as shown in Fig. 2.8. They are cutting speed, feed rate, depth of cut, cutting path and cutting fluid. Scientific understanding of their influence on the tooling performance will have the potential to optimize the cutting process.
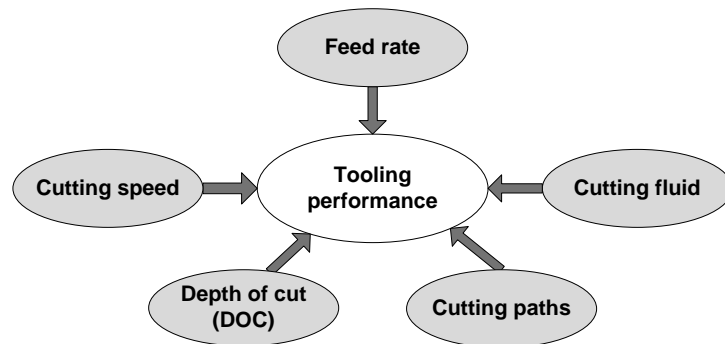
Fig. 2.8 Process conditions affecting the tooling performance

2.2.4.1 Process variables

In conventional milling, it is well established that increasing cutting speed, feed rate and DOC enhances the productivity and, reducing cutting speed as well as increasing feed rate and DOC will adversely affect the cutting performance of tools. Thus, to achieve both better performance and productivity, rising cutting speed is usually considered to be more effective. However, in micro milling, it is impossible to apply a cutting speed as high as that in macro-scale cutting due to the tiny tool diameters and spindle speed limitations on available machine tools.

Some researchers have observed and reported the influence of process parameters on the cutting performance of micro tools. In micro milling OFHC copper, Huo et al. (Huo et al., 2010) indicated that feed rate has a significant influence on surface roughness and burr height, whereas cutting speed has only a slight effect. Moreover, DOC has no significant effect on surface roughness. Rising cutting speed results in better surface finish (Uhlmann et al., 2005; Weule et al., 2001), shorter tool life (Zaman et al., 2006; Rahman et al., 2001) and smaller burrs (Aramcharoen et al., 2009). Due to size effects, decreasing feed rate tends to increase the surface quality (Klocke et al., 2009), and the

highest tool wear rate occurs at the lowest feed rate (Filiz et al., 2007). The larger the DOC, the higher the cutting forces but strangely lower wear rate (Rahman et al., 2001) and DOC has no obvious influence on the quality of machined surface (Vogler et al., 2004a).

Selection of appropriate process variables are of great importance for achieving optimum cutting performance, reducing lead time and enhancing productivity. In order to indentify optimal conditions for maximum tool life and minimum production cost, an optimized genetic algorithm was developed and demonstrated by Sreeram et al. (Sreeram et al., 2006).

2.2.4.2 Cutting path

To produce micro products with good accuracy and quality, micro milling is desired with efficient and reliable tool paths. Therefore, micro milling machines, cutting tools and the algorithm used to calculate the path in CAD/CAM systems need to be well coordinated to produce optimized tool trajectories and more stringent motion tolerances. This requires better distributed points on the tool path algorithm with greater accuracy than those in conventional machining.

Different machining strategies have a significant impact on the cutting performance. Dimov et al. (Dimov et al., 2004) reported that eight types of cutting paths in micro honeycomb structure milling can result in considerably different surface quality, and the best surface finish was achieved by the follow-hardwall and constant-load machining strategy. The authors claimed that the main consideration for selecting an appropriate machining strategy should be the maintenance of a constant chip load and the avoidance of tool breakages. Litwinski et al. (Litwinski et al., 2006) indicted that micro up milling generally leads to a better surface finish as compared to that in down milling, and there is almost no significant difference between zig cutting and contour parallel cutting in terms of machining quality.

2.2.4.3 Cutting fluid

The use of cutting fluid is generally advantageous with regard to the tooling performance and its two main functions are cooling and lubrication. Cutting fluid takes

away heat from both the cutting tool and workpiece, facilitates flushing of the chips from the cutting zone and minimizes cutting energy consumption by reducing friction at the tool-work interface. However, the flow pressure of flood fluid may be detrimental to the micro cutting behaviours (Dornfeld et al., 2006). If properly selected and applied, cutting fluid can make a substantial improvement on both tool life and machining quality (Weinert et al., 2005), as an example is shown in Fig. 2.9.
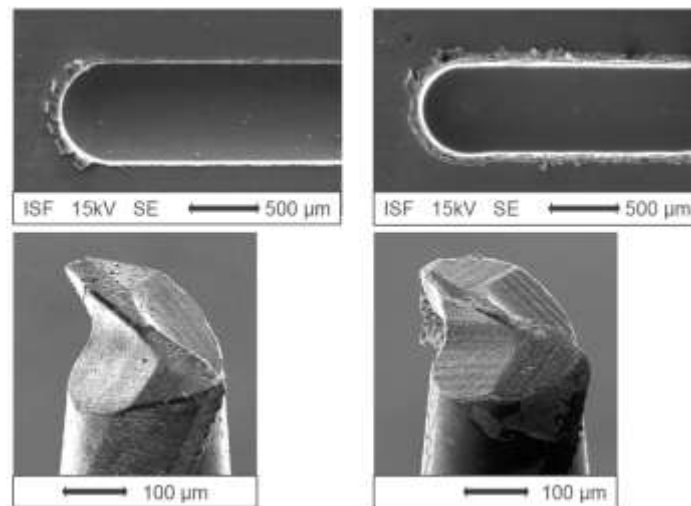
(a) Minimum quality lubrication   (b) Dry

Fig. 2.9 Performance improvement by minimum quality lubrication

(Weinert et al., 2005)

Jun et al. (Jun et al., 2008) observed a cooler cutting zone, lower cutting forces, significantly longer tool life and smaller burr formation when cutting fluid was present in comparison with corresponding performance under dry machining conditions. Aramcharoen (Aramcharoen et al., 2009) concluded that the choice of machining environment is the most significant factor for improving surface finish and reducing the tool wear in micro milling hardened tool steel, and the performance under minimum quantity lubrication is better than for dry milling or the use of flood coolant.

2.3   Micro milling mechanics

2.3.1 Micro-cutting mechanism

The main difference between micro-scale and macro-scale machining resides in the

cutting mechanism. In macro-scale cutting, the uncut chip thickness is far greater than the tool cutting edge radius, therefore, the edge corners can be neglected and the tools are assumed to be sharp. The effective rake angle is almost equal to the nominal tool rake angle. In this case, material removal is mainly achieved by shearing based on conventional cutting mechanism. When the uncut chip thickness decreases to the same order as the cutting edge radius of tools, the edges cannot be considered sharp anymore and the effective rake angle becomes negative. Material removal is then dominated by compressing or ploughing rather than shearing (Liu et al., 2004a). The schematic of cutting mechanisms in macro-scale and micro-scale cutting is shown in Fig. 2.10.

(a) Macro-scale cutting   (b) Micro-scale cutting
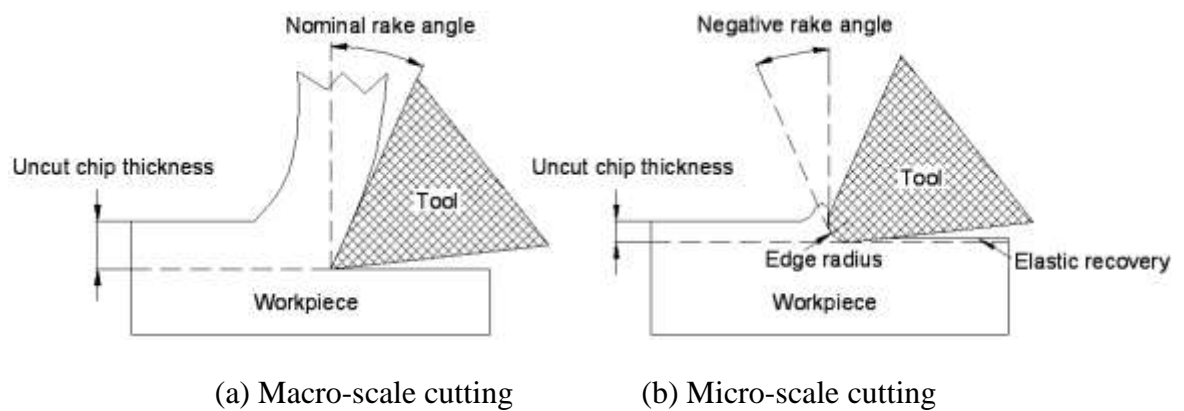
Fig. 2.10 Schematic of mechanisms at macro-scale and micro-scale cutting

When the uncut chip thickness is reduced to a critical value under specific cutting conditions, chips will not be formed and this value is termed as minimum chip thickness (MCT). Once the uncut chip thickness is smaller than the minimum chip thickness, not only a highly negative rake angle appears, but there is no work material removed and elastic recovery resulting from ploughing has a major influence on the surface generation (Vogler et al., 2004a). This ploughing phenomenon also significantly contributes to cutting force vibrations (Vogler et al., 2004b), increased burr formation (Lee et al., 2002) and larger specific cutting energy (Liu et al., 2007; Ng et al., 2006; Lucca et al., 1991).

2.3.2 Size effects in micro-scale cutting

In principle, two different aspects of size effects are of concern in micro-scale cutting. Firstly, when the uncut chip thickness becomes comparable to the tool cutting edge

radius and secondly, where the microstructure size of work materials has significant influence on the cutting mechanism (Dornfeld et al., 2006). Resulting from size effects, the influence of the tool cutting edge radius, negative rake angle, elastic recovery, minimum chip thickness and work microstructure become prominent with respect to the cutting forces, chip formation process, burr formation, vibration and process stability, energy consumption as well as the generation of machined surface (Liu et al., 2004a). Size effects in micro-scale cutting are summarized in Fig. 2.11.
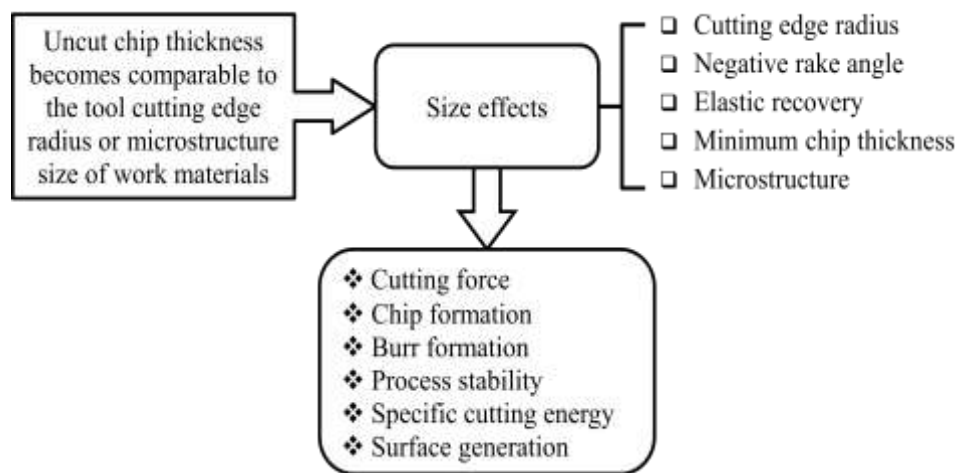
Fig. 2.11 Size effects in micro-scale cutting

2.3.3 Size effects related to micro milling

In micro milling, commercially available tools normally have the cutting edge radius ranging from 0.8μm to 5μm due to grain size and fabrication limitations. Along with scaling down of the tool geometry, applicable process parameters are limited in preventing possible tool deflection, excessive tool wear and premature breakages. Among these variables, feed rate is often selected to be much low so as to reduce the cutting loads. When the magnitude of feed per tooth tends to be the same order of the tool cutting edge radius or microstructure size of work materials, size effects play a significant role.

2.3.3.1 Chip formation and minimum chip thickness

Due to an intermittent cutting mechanism for micro milling, uncut chip thickness in the radial direction for each cutting passage varies from zero to the feed per tooth then to

zero. It is thus inevitable to encounter ploughing or rubbing because of the MCT effect. In cases where the feed per tooth is larger than MCT, ploughing and shearing mechanisms are present in one cutting pass, as schematically shown in Fig. 2.12. MCT at the exit direction is different from that of entrance side, which is likely to affect the micro-burr formation.
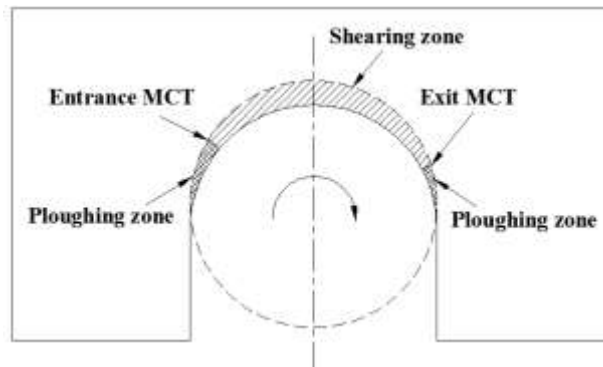
Fig. 2.12 Illustration of ploughing and shearing mechanisms in one cutting pass

When the radial depth of cut is smaller than MCT, the ploughing mechanism becomes dominant, but once radial depth of cut is larger than MCT, shearing of work materials takes place and chips can be formed. Ploughing dominant areas are located at the entrance and exit of the passage while the rest of the zone is dominated by shearing. In cases where feed per tooth is smaller than MCT, there are probably no chips formed during several consecutive revolutions of cutting because of the ploughing dominant mechanism and elastic recovery of work materials.

Weule et al. (Weule et al., 2001) observed the existence of minimum chip thickness in the micro milling process and noticed its significant impact on the achievable surface formation. A saw-tooth-like profile was detected in machining of SAE 1045 steel using around 5μm edge radii tools, which was explained as the MCT effect depicted in Fig. 2.13. Additionally, Liu et al. (Liu et al., 2006; Liu et al., 2004b) found cutting force and surface finish variations due to the influence of MCT, as shown in Fig. 2.14.

In micro-scale cutting, it is important to determine MCT so as to select appropriate process parameters for a given machining requirement. Some efforts have been taken to estimate MCT by simulation (Vogler et al., 2004a; Shimada et al., 1993), analytical formulation (Liu et al., 2006; Son et al., 2005), and experimentation (Kim et al., 2004;

Yuan et al., 1996). Studies show the value of MCT depends on the tool cutting edge radius, the properties of work materials, tool-work interface friction and process conditions used. And it usually lies between 5% and 42% of the tool cutting edge radius.

(a) Measured surface topography   (b) Theoretical surface profile
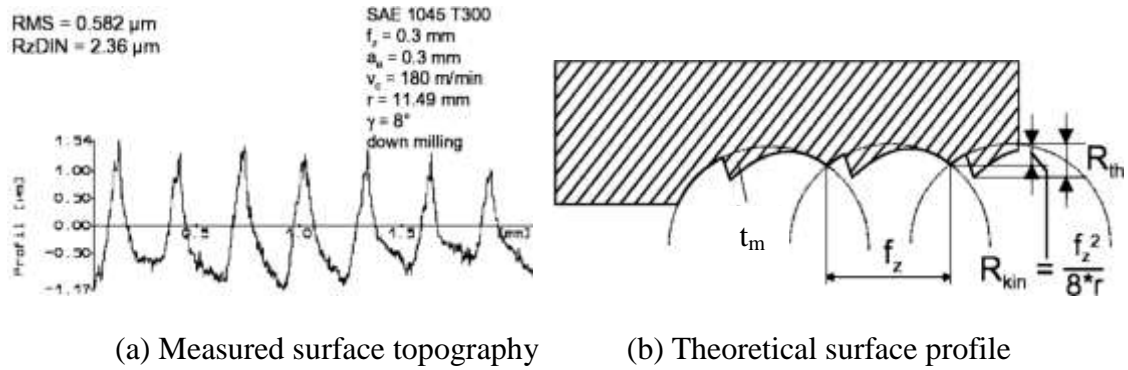
Fig. 2.13 The effect of MCT on surface profile (Weule et al., 2001)

(a) Cutting force (Liu et al., 2004b)   (b) Surface generation (Liu et al., 2006)
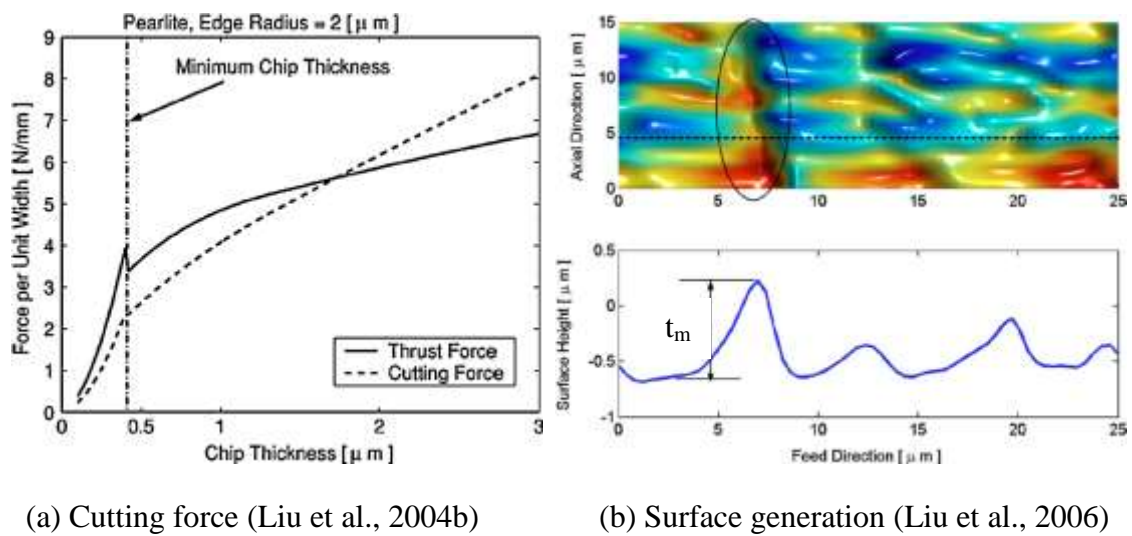
Fig. 2.14 The influence of MCT on cutting force and surface generation

Vogler et al. (Vogler et al., 2004a) studied MCT in micromachining of pearlite and ferrite materials based on a microstructure-level FEA model developed by Chuzoy et al. (Chuzhoy et al., 2002). They pointed out that the ratios of MCT to cutting edge radius were theoretically 0.2 for pearlite and 0.35 for ferrite. Molecular dynamics simulation was adopted by Shimada et al. (Shimada et al., 1993) to determine MCT in diamond cutting of aluminium and copper. They estimated that MCT could be as small as 5% of tool cutting edge radius for ductile metals.

Liu et al. (Liu et al., 2006) termed normalized minimum chip thickness as MCT to tool edge radius ratio and calculated the value for aluminium and carbon steel over a wide range of cutting speed and edge radius based on an analytical model. The normalized minimum chip thickness was found to be about 35-40% for Al 6082-T6 aluminium, 20-30% for AISI 1018 steel and 20-42% for AISI 1040 steel, as shown in Fig. 2.15. This also demonstrates a cutting speed effect on MCT.

(a) Al 6082-T6   (b) AISI 1018 and AISI 1040 steel
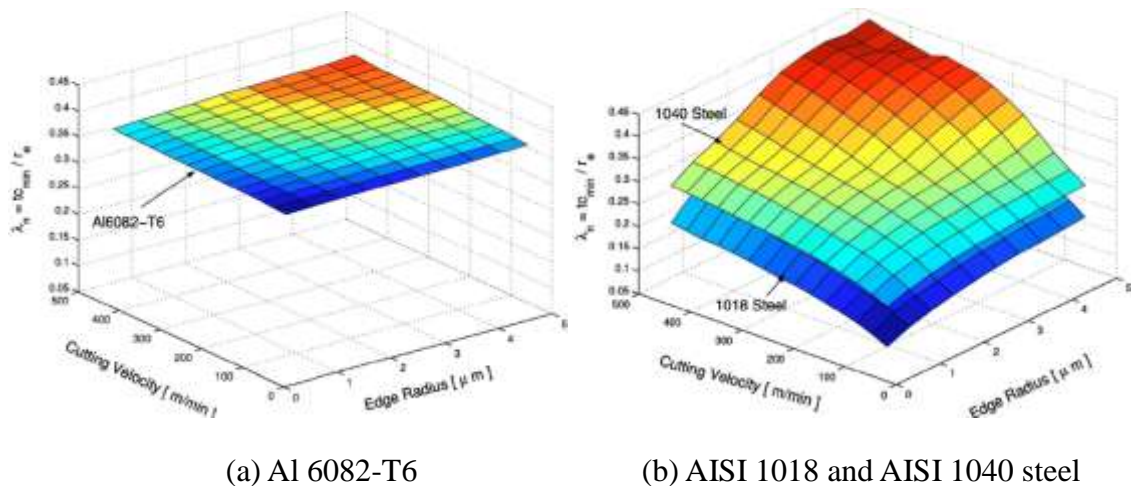
Fig. 2.15 Nominal MCT for different materials (Liu et al., 2006)

Son et al. (Son et al., 2005) concluded that MCT is determined not only by cutting edge radius but also by friction coefficient at the tool-work interface. The authors found that MCT ranged from 0.09µm to 0.12µm when using 0.5µm edge radii diamond tools in grooving aluminium, brass and OFHC copper.

Kim et al. (Kim et al., 2004) experimentally studied minimum chip thickness by cutting force fluctuation analysis, and the ratio of uncut chip thickness to the cutting edge radius was estimated to be between 22-25% for brass. Yuan et al. (Yuan et al., 1996) studied MCT by micro cutting of aluminium alloys with different edge radius tools, and concluded that tool sharpness has a considerable impact on MCT and surface integrity. The obtainable MCT was reported to be 0.05~0.2µm when using tools with an edge radius between 0.2~0.6µm.

2.3.3.2 <u>Work microstructure effect</u>

In conventional cutting, work materials are considered to be homogeneous and isotropic,

and chips are formed by shearing a bulk piece of material. In micro-scale cutting, however, the uncut chip thickness becomes the same order as the average grain size of work materials, where cutting is performed by fracturing an individual grain. In this case, the microstructure of work material should be treated as non-homogenous and anisotropic, which imposes a significant impact on the cutting mechanism.

Different material microstructures lead to different micromachining responses. Researchers have found that altering the microstructure of the work material, such as its grain size and crystallographic orientation, can affect the cutting forces (Yuan et al., 1994), chip formation (Simoneau et al., 2007; Simoneau et al., 2006a; Simoneau et al., 2006b), surface roughness (Cheung et al., 2002; Yuan et al., 1994) and burr formation (Min et al., 2006).

Vogler et al. (Vogler et al., 2003) studied the multiphase microstructure effects on the cutting force variation in micro end milling of both single-phase and multi-phase work materials. They observed the presence of higher frequency components of cutting force in the ductile iron experiments but not in the ferrite and pearlite machining. This was attributed to grain size and spacing of secondary phase in the material microstructure. In comparison with single-phase and multiphase surface generation in (Vogler et al., 2004a), they observed micro-milled surfaces on multiphase ductile iron are much rougher than those on single phase ferrite and pearlitic workpieces, as shown in Fig. 2.16. The cause of increased surface finish was explained as the result of phase boundary effects leading to a discontinuous chip formation process when micro milling multiphase materials. Fig. 2.17 illustrates corresponding chips in micro milling single phase ferrite and pearlite, multiphase ferritic and pearlitic DI materials.

To overcome non-homogeneity and anisotropy in work material properties, Schmidt et al. (Schmidt et al., 2002) suggested that work materials should be heat treated in finest and equidistant microstructure prior to the cutting process so as to achieve constant cutting loads, resulting in reasonable surface quality.

Popov et al. (Popov et al., 2006b) modified the microstructure of Al 5083 by equal channel angular pressing (ECAP) in order to achieve more homogeneous properties. The size of ECAP processed grains is observed to be five times smaller than those of the

CP material. The influence of microstructure on part quality and surface integrity was assessed by micro milling rib features and surface roughness was greatly improved by the reduction in grain size and material anisotropy. The similar material processing was performed by Pham et al. (Pham et al., 2009) on copper samples. It was found that surface roughness and surface defects were reduced significantly as a result of smaller grain size and refinement in mechanical and metallurgical properties at boundaries between the individual grains.
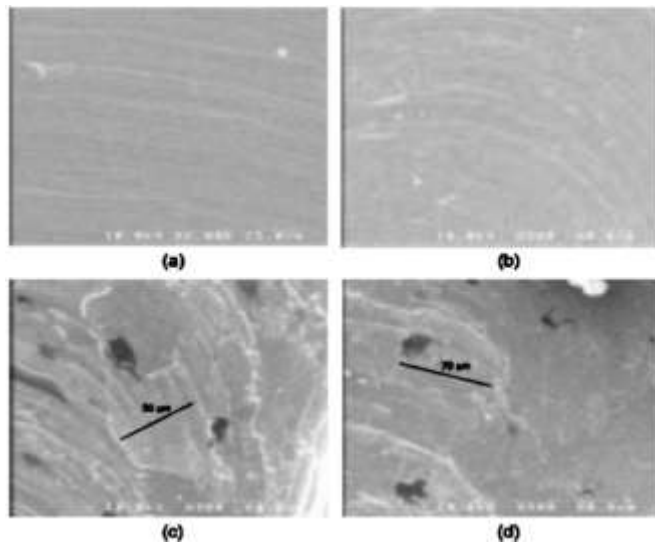
Fig. 2.16 Micro-milled slot floor surfaces for (a) Pearlite (b) Ferrite (c) Ferritic DI (d) Pearlitic DI (Vogler et al., 2004a)
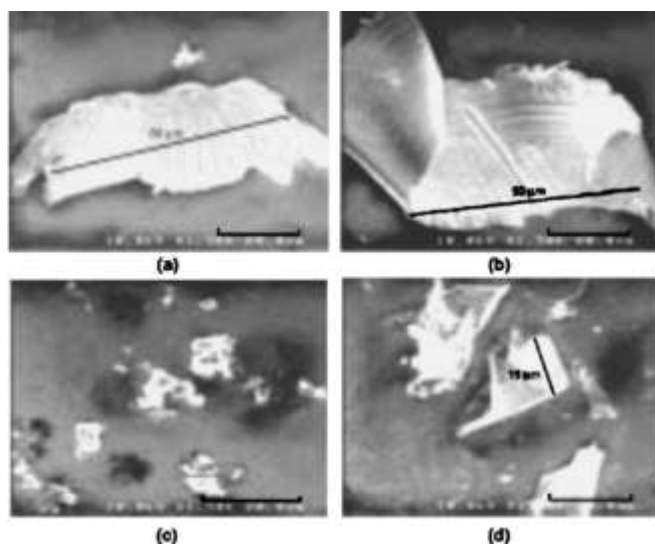
Fig. 2.17 Micro-milled chips for (a) Pearlite (b) Ferrite (c) Ferritic DI (d) Pearlitic DI (Vogler et al., 2004a)

2.4 <u>Modelling for performance prediction</u>

In micro cutting process, it is quite difficult to perform in-process observations and sometimes post-process measurements on tooling performance. Numerical modelling has become a good compliment to experimental approaches and it can offer a reasonable insight into certain verifiable trends or guidance on empirical research to assist further understanding of the process (Dornfeld et al., 2006).

Four key modelling methods, including molecular dynamic (MD) simulation, finite element method (FEM), multi-scale modelling and mechanistic modelling, are popularly used for characterization of nano/micro machining phenomena. The MD simulation is based on interatomic force analysis and it is more suitable for nanometric cutting. FEM is based on continuum mechanics principles, in which the materials are assumed to have continuous and homogeneous microstructures. This powerful technique has been mostly used for orthogonal cutting simulations (Davim et al., 2010; Deng et al., 2009; Khalili et al., 2009; Baker, 2006; Yen, 2004). The newly emerging multi-scale modelling techniques combine the strengths of both MD and FEM for wider length scale simulations, and mechanistic modelling is referred as developing an analytical model relating the process outputs to various input conditions, such as tooling geometries, work material properties and process conditions.

Among above approaches, FEM can be an attractive means for understanding isotropic machining mechanics at the micro-scale, and mechanistic modelling are commonly applied for the characterization of cutting forces (Bao et al., 2000a; Kang et al., 2008; Vogler et al., 2003), surface generation (Vogler et al., 2004a; Liu et al., 2007a) and chip formation (Liu et al., 2006; Kim et al., 2004).

2.4.1 Finite element modelling

2.4.1.1 <u>FEM software</u>

Several commercial tools are tailored for simulating the metal cutting process, among which DEFORM^{TM} (DEFORM, 2011) and AdvantEdge^{TM} (AdvantEdge, 2011) are widely used. DEFORM^{TM} is originally developed for analyzing metal forming processes, then extended to heat treatment, machining and mechanical joining

processes. DEFORM™-2D is widely adopted for orthogonal cutting simulations and DEFORM™-3D is for more complex processes requiring three-dimensional modelling, such as drilling. AdvantEdge™ is a CAE software solution specialized for cutting simulations, enabling users to analyze machining processes in 2D and 3D environments. Both systems feature automatic remeshing capabilities during large distortions as well as user friendly graphical interface.

Some other software, such as ABAQUS (Abaqus, 2011) and ANSYS LS-DYNA (ANSYS LS-DYNA, 2011), can also be used for the cutting process modelling. However, they are not universally adopted due to a large amount of knowledge and time required for setting up models at the pre-processor stage.

2.4.1.2 FEM procedures

The major input parameters for FEM simulations are illustrated in Fig. 2.18.
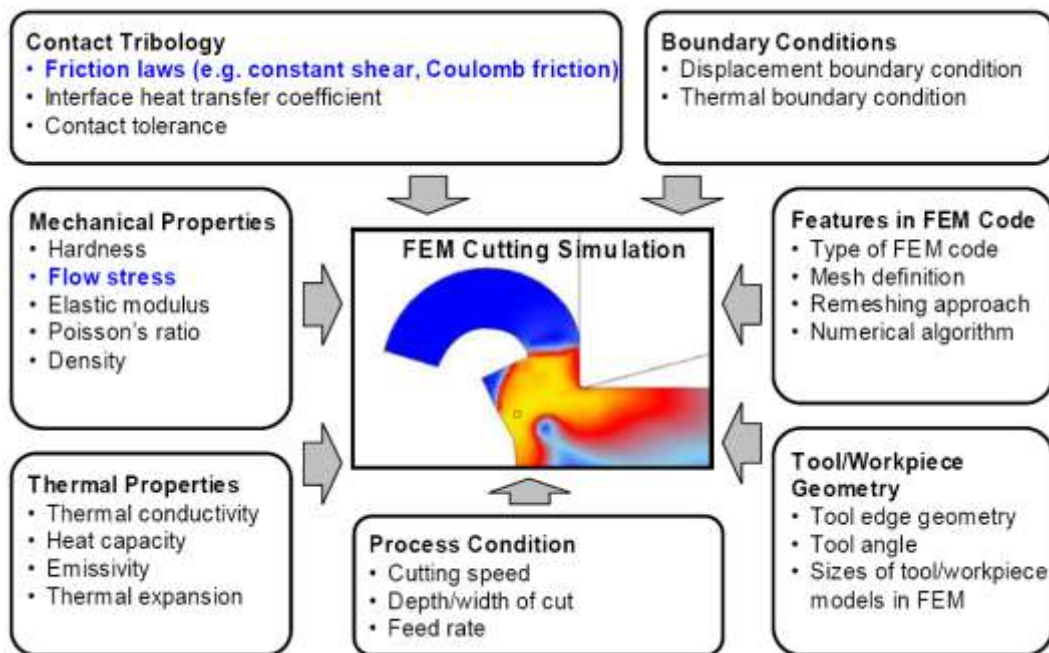
Fig. 2.18 Major input parameters for FEM simulations (Sartkulvanich, 2007)

The general steps for designing and analyzing a cutting process are:

- Selecting a FEM code

- Creating or importing tool and work models

- Meshing models

- Applying material properties

- Inputting cutting conditions

- Defining boundary conditions and inter-object relationships

- Running simulations

- Acquiring simulation results in the postprocessor

In order to speed up calculations without compromising the accuracy of simulation results, it is necessary to take appropriate simplifications or assumptions on tool and workpiece models as well as object types. In general, three-dimensional analysis is more accurate but time-consuming than the two-dimensional one, and elastic-plastic to plastic objects as well.

Work material flow stress model and tool-chip interface friction characteristics play an extremely crucial role in reliable and effective modelling of the cutting process. The flow stress, as a function of temperature, strain and strain rate, should be determined experimentally under wide temperature range and large deformation conditions. The main flow stress constitutive models used are summarized in table 2.4, among which Johnson-Cook model is frequently implemented and tabular data from Split-Hopkinson bar tests is also a promising one due to its ability to follow the true behaviour of a material.

The friction schemes at the tool-chip interface are very complicated and difficult to characterize. The contact regions and the friction coefficients between the tool and the chip are affected by various factors, such as material properties, cutting conditions, tooling geometries, etc. Whether sliding, shearing or combination of two behaviours dominates machining needs further investigation for specific applications. Özel (Özel, 2006) analysed the effects of friction models on the cutting forces, tooling stresses and tool-chip temperatures by orthogonal simulations and found that experimental measurement based variable friction model was more suitable for accurate prediction. The friction models for FE programs include constant sliding, constant shearing,

variable shearing, variable sliding, combination of constant shearing and sliding, and combination of variable shearing and sliding, among which pure sliding is considered as appropriate contact scheme at low cutting speed (Sheikh et al., 2007; Özel, 2006).

Table 2.4 Summary of main flow stress constitutive models

No.	Material model	Mathematical representations	Material constants
1	Tabular format	$\bar{\sigma} = \bar{\sigma}(\bar{\varepsilon}, \dot{\bar{\varepsilon}}, T)$	*N/A*
2	Oxley (Oxley, 1989)	$\bar{\sigma} = \sigma_1(\bar{\varepsilon})^n$	σ_1, n
3	Johnson and Cook (Johnson et al., 1983)	$\bar{\sigma} = [A + B(\bar{\varepsilon})^n]\left[1 + C\ ln\left(\frac{\dot{\bar{\varepsilon}}}{\dot{\bar{\varepsilon}}_0}\right)\right][1 - \left(\frac{T - T_{room}}{T_{melt} - T_{room}}\right)^m]$	*A, B, C, m, n*
4	Shirakashi and Usui (Shirakashi et al., 1970)	$\bar{\sigma} = A \cdot (\bar{\varepsilon})^n \cdot (\dot{\bar{\varepsilon}})^m \cdot [-\lambda(T - T_0)]$	*A, m, n, λ*
5	Zerilli and Armstrong (Zerilli et al., 1995)	$\bar{\sigma} = C_0 + C_1 \cdot exp[-C_2 T + C_3 T ln(\dot{\bar{\varepsilon}}) + C_4(\bar{\varepsilon})^{1/2} \cdot exp[-C_5 T + C_6 T ln(\dot{\bar{\varepsilon}})]$	$C_0, C_1, C_2, C_3, C_4, C_5$

2.4.1.3   FEM applications

Limited studies have been conducted using FEM for modelling of the micro milling process. Dhanorker and Özel (Özel et al., 2007; Dhanorker et al., 2006) developed a rigid-plastic plane-strain model to predict the cutting forces, temperature distributions and chip formation in the meso/micro scale milling processes. Predicted temperatures in the cutting zone were reported to be much lower whereas the specific cutting forces are larger as compared to those in conventional milling.

Wang et al. (Wang et al., 2009) studied the chip formation mechanism in micro milling of Al6061-T6 by adopting a similar approach. Chip formation calculations and analysis were undertaken based on proposed two-dimensional FE model, which was validated by comparisons of predicted cutting forces and chip formation with measured ones.

Afazov et al. (Afazov et al., 2010) performed a number of orthogonal cutting simulations to predict micro milling forces in an indirect manner. In the research, the

cutting forces in three directions were calculated based on a combination of the simulated force results and an uncut chip thickness analytical model.

2.4.2 Mechanistic modelling

2.4.2.1 Cutting forces

Bao and Tansel (Bao et al., 2000a) developed an analytical model for micro milling forces prediction based on Tlusty and Macneil's conventional model (Tlusty et al., 1975). Process conditions, tool geometry and work material were incorporated into the model, in which the chip thickness was calculated by considering the trajectory of cutting tool tip. The authors compared the differences of the proposed model with the conventional model, and concluded that the former estimates the cutting forces more accurately with an aggressive ratio of feed per tooth to tool radius, and the latter is only a special case of the former when the ratio becomes zero. Later, the authors modified their modelling work by taking the effects of tool run-out (Bao et al., 2000b) and tool wear (Bao et al., 2000c) into account. Based on the same conventional force model, Kang et al. (Kang et al., 2007) presented a cutting forces model of micro end milling considering the tool edge radius effects.

Zaman et al. (Zaman et al., 2006) introduced a first three-dimensional cutting force model for micro end milling operations. The theoretical chip area with the variation at tool rotation angle rather than uncut chip thickness was integrated and the predicted maximum cutting forces values are found well matched to the experimental results. Li et al. (Li et al., 2007) developed a three-dimensional force model considering the combination of tool tip trochoidal trajectory, tool run-out and minimum chip thickness effects, and instantaneous uncut chip thickness algorithms were used for cutting forces calculations.

Jun et al. (Jun et al., 2006b; Jun et al., 2006) developed a dynamic cutting force and vibration model considering both chip removal and ploughing cutting mechanisms in the micro milling process. The effects of minimum chip thickness, elastic recovery, and the elastic-plastic nature were taken into account in the chip thickness model. In the study, the authors noticed uneven variations for thrust force and attributed to the minimum chip thickness effect. In addition, the rate of increase for the cutting forces

was found to be much higher when the chip thickness is smaller than the minimum chip thickness compared to that when the chip thickness is larger than the minimum chip thickness.

Homogeneous microstructures of work material were assumed in above models. In an effort to better understanding cutting forces in micro milling heterogeneous materials, Vogler et al. (Vogler et al., 2003) developed a mechanistic model by using micro-structural mapping technique. A mapping of multiple phases was created to represent the actual work microstructure. Comparisons of actual and simulated microstructure of pearlitic and ferritic ductile iron are illustrated in Fig. 2.19. This model was capable of predicting higher frequency variation of cutting forces when micro-milling ductile iron. Through simulations, the authors attributed the frequency of the force variation to the spacing of the secondary phase, and the magnitude of this variation to the size of the secondary phase grains.
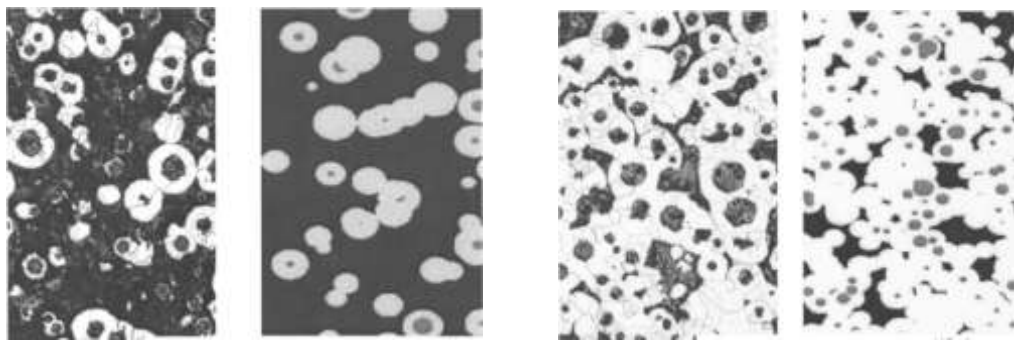
(a) Actual and simulated pearlitic DI   (b) Actual and simulated ferritic DI

Fig. 2.19 Comparisons of actual and simulated microstructure of ductile iron

In their later work, Vogler et al. (Vogler et al., 2004b) enhanced above force model by incorporating cutting edge radius effects. The minimum chip thickness resulting in two separate force generation mechanisms including slip-line plasticity model for shearing and interference volume for ploughing was modelled. Finite element simulations were performed for assisting the determination of the chip removal force model and the elastic deformation force model.

2.4.2.2   Surface generation

Vogler et al. (Vogler et al., 2004a) introduced a process model for the prediction of the slot floor surface generation in micro milling single-phase materials based on the tool geometry and the minimum chip thickness concept. The minimum chip thickness ratios were determined by orthogonal FE simulations. The model was shown to accurately predict both the feed rate trends and the magnitude of the surface roughness for ferrite and pearlite materials, and indicated that there exists an optimum feed rate for the smallest surface roughness due to trade-off between conventional feed effect and minimum chip thickness effect.

X. Liu et al.(Liu et al., 2007a; Liu et al., 2007b) developed surface generation models being capable of accounting for deterministic and stochastic surface roughness components for both sidewall and floor surfaces in micro end milling. The effects of the process kinematics, dynamics, minimum chip thickness and elastic recovery, and cutting edge serration as well as ploughing due to the significant tool edge radius effect were considered for the side wall surface model. For the floor surface model, the effects of the minimum chip thickness, elastic recovery, and the transverse vibrations were taken into account and the extent of ploughing at end cutting edge as well. Examples of the predicted deterministic surface topographies for side walls in up milling under different process conditions are shown in Fig. 2.20.
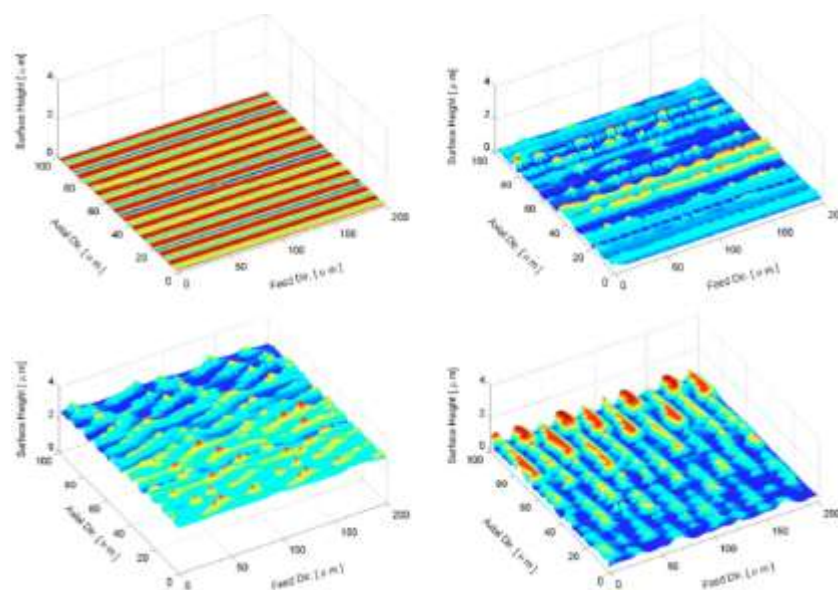
Fig. 2.20 Predicted 3D surface topographies under different process conditions

2.4.2.3 Chip formation

X. Liu et al. (Liu et al., 2006) developed an analytical model to predict the minimum chip thickness values based on molecular-mechanical theory of friction. The workpiece and the tool thermo-mechanical properties were incorporated into the model, which can account for the influence of cutting velocity and tool cutting edge radius on the minimum chip thickness. The authors found that the higher the carbon content, the larger the normalized minimum chip thickness for carbon steels, whereas for Al6082-T6, the normalized minimum chip thickness almost remain constant due to both the thermal softening effect and strain hardening effect.

Kim et al. (Kim et al., 2004) developed a static model of chip formation in micro milling, which is capable of accounting for the coupled minimum chip thickness and edge radius effects. The model was validated by verifying the level of periodicity present in the cutting forces at various feed per tooth. It was realized that the tool may rotate without removing any materials when the feed per tooth is smaller than the minimum chip thickness and that the periodicity of cutting forces is a function of the minimum chip thickness, feed per tooth, and position angle. The authors suggested the appropriate feed per tooth for a given tool diameter can be determined by an upper and lower limit, as shown in Fig. 2.21.
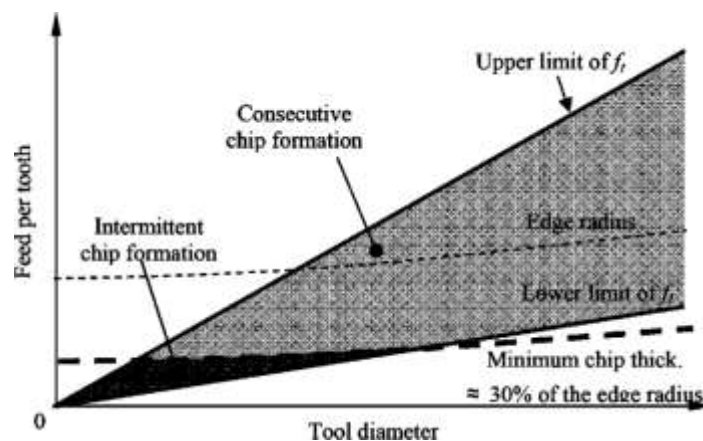
Fig. 2.21 Feed per tooth and the minimum chip thickness (Kim et al., 2004)

2.5 **Metrology and instrumentation for performance characterization**

Characterization of micro tools and machined micro or miniature features constitutes an

important part in micro milling. For performing precise inspection and measurements at the micro scale, 3D surface profilers, microscopes, process monitoring sensors and systems are widely adopted, the relevant features of which are given below.

2.5.1.1 3D surface profilers

A 3D surface profiler is an instrument for making quantitative measurements of surface texture. The characterization of a surface typically includes surface roughness and surface shape measurements. In most cases, surface profilers are used for 3D surface roughness measurement and analysis. Surface roughness reflects characteristic marks left by the machining process, which is a direct indicator for the quality of a machined surface, and it can affect a mechanical component's suitability for its function. Therefore, measuring surface topography and texture accurately in 3D is a crucial concern for industrial applications, particularly at micro and nano scale. Fig. 2.22 shows some typical non-contact and contact 3D surface metrology instruments.

(a)   Zygo NewView™ 7100 (Zygo, 2010)   (b) Wyko NT9080 (Veeco, 2010)   (c) Taylor Hobson Form Talysurf PGI 1240 (Taylor Hobson, 2010)

Fig. 2.22 Commercial 3D surface profilers

2.5.1.2 Microscopes

Microscopes are widely used for off-line inspection and measurements of tiny features. Basically, electronic microscopes, particularly scanning electron microscope (SEM), are commonly applied to observe chip formation, the state of micro tools and quality of micro features, as illustrated in Fig. 1.1, Figs. 2.4-2.5 and Figs. 2.15-17. SEM is an instrument that delivers high resolution images by using a focused beam of high-energy

electrons to generate a variety of signals at the surface of samples. These electron-sample interactive signals contain information including surface topography, chemical composition, crystalline structure and orientation of materials. Fig. 2.23(a) shows a typical scanning electron microscope ZEISS SUPRA 55VP (Zeiss, 2010), which has a resolution of 0.8 nm and magnification of up to 1,000,000 times.

In some cases, high magnification microscopes are not always necessary and a low magnification optical microscope is sufficient for laboratories and shop floor needs. In principle, an optical microscope can be equipped with several objectives to provide different magnifications, which can reach as high as 1,000 times. Fig. 2.23(b) illustrates a specialised optical microscope KERN µ-view with 450 times magnification for micro tooling checks (Kern, 2010). In addition to off-line inspection and measurement microscopes, some modern microscopes are equipped with CCD cameras, by which the machining process can be observed in real time.

(a) ZEISS SUPRA 55VP (Zeiss, 2010)   (b) KERN µ-view (Kern, 2010)

Fig. 2.23 Examples of scanning electron microscope and optical microscope

2.5.1.3   Process monitoring sensors and systems

Due to fragility of micro tools, excessive cutting forces and vibrations can significantly affect the overall quality of machined parts and longevity of tools. Therefore, on-line monitoring of operations becomes indispensable for evaluating, controlling and improving production processes so as to meet increasing precision and quality demands. Traditionally, two main monitoring approaches can be employed. One is direct monitoring, such as the aforementioned optical microscope with CCD cameras, by

which valuable cutting information can be observed or recorded directly. The other is an indirect method in which sensors like force sensors, acoustic emission (AE) sensors and accelerometers gather specific data correlated to cutting operations.

Among various indirect sensors, force dynamometer is the most common and effective tool. The forces generated in machining operations, reflecting interaction between cutting tools and work materials, have a direct impact on cutting performance such as tool wear or failure, quality of machined surface and accuracy of components. Therefore, it is necessary to characterize these forces quantitatively and precisely so as to examine, evaluate and optimize cutting processes. A force dynamometer is capable of performing the function accurately both in magnitude and direction by creating electrical signals proportional to the forces in three orthogonal directions. Ideally, a dynamometer should be developed and configured with high sensitivity, high rigidity, high natural frequency response, high linearity, low drift and low measuring threshold in order to achieve better static and dynamic characteristics.

The latest and most popular commercial miniature force dynamometers are Kistler MiniDyn series (Kistler, 2010). Fig. 2.24 shows one of the multi-component dynamometers. There are four 3-component piezoelectric force sensors mounted under high preload between the cover plate and the two lateral base plates inside the dynamometer. Its high sensitivity and rigidity as well as a 2mN threshold make it applicable to measuring extremely small forces for ultra-precision applications. The instrument has been extensively used by researchers for micro forces characterization and process optimization (Biermann et al., 2010; Park et al., 2009; Filiz et al., 2008; Lai et al., 2008; Rusnaldy et al., 2008).

Fig. 2.24 Dynamometer Kistler MiniDyn 9256C1 (Kistler, 2010)

Each sensor has its limitations. For example, it is difficult to capture and characterize the real-time state of tools by direct monitoring due to visually undetectable tool-work interface in micro-scale cutting. Some indirect sensors may not have the necessary signal-to-noise ratio and sensitivity required to adequately and reliably characterize surface finish, subsurface damage, and cutting forces at the ultra-precision scale due to extremely low cutting forces and low power consumption present (Dornfeld et al., 2006).

Fig.2.25 shows main application fields, level of precision and control parameters for some typical indirect sensors. To overcome their respective constraints, sensor fusion is regarded as an effective, flexible and reliable approach as the fusion and filtering of various process monitoring signals provide solutions for micro-control to enhance robustness and reconcile the limited frequency bandwidth of currently available sensors (Chae et al., 2006).
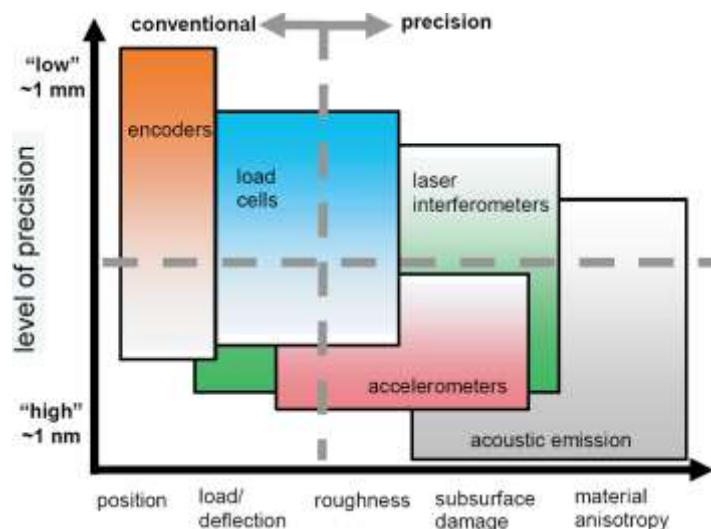
Fig. 2.25 Sensor application vs. level of precision and control parameters

(Lee et al., 2006)

Malekian et al. (Malekian et al., 2009) presented an integrated monitoring method consisting of AE sensor, force sensor, and accelerometer to examine tool condition during micro milling operations, as shown in Fig. 2.26. In the study, a vision system with CCD camera was utilised to observe actual tool state and measure edge corners of micro tools. Different bandwidth signals derived from various sensors were fused together through an adaptive neuro-fuzzy algorithm for the tool wear determination.
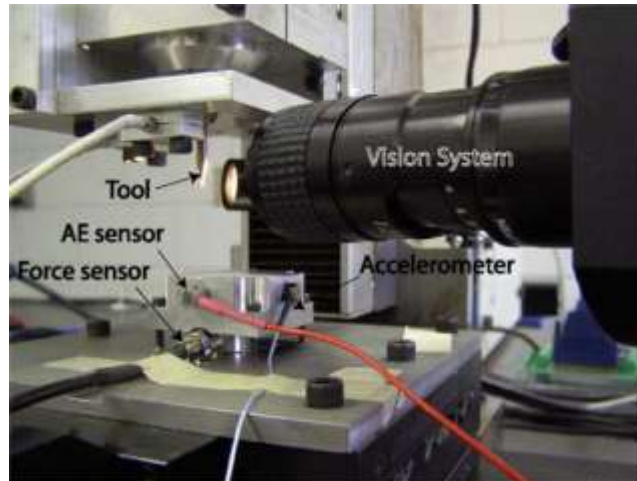
Fig. 2.26 An example of tool monitoring system (Malekian et al., 2009)

Gandarias et al. (Gandarias et al., 2006) proposed three indirect methods including reflective single-beam laser system, tool-work voltage monitoring system and off-line laser system for micro tool failure detection. Due to the fact that each system has its limitations, such as precise laser focusing or work material property requirements, the authors suggested an integrated system combining the advantages of reflective single-beam laser system and tool-work voltage monitoring system should be promising for further development of a tool monitoring system.

2.6   Conclusions

The chapter has presented a systematic review of the state of the art micro milling that is highly associated with the tooling performance. Modelling work for performance prediction as well as metrology and instrumentation for performance characterization has also been surveyed.

The review has revealed that the tooling performance can be dramatically affected by the performance of micro milling machines, cutting tool characteristics, work material properties and process conditions. Some concluding remarks can be drawn, but not limited to:

- The development of machines with ultra-precision micro milling capabilities has being extensively and successfully progressed.

- Knowledge related to optimal configuration of micro tools is relatively limited, including geometry optimization, appropriate diamond coating technology, etc.

- Little is known about comparative machinability of frequently used engineering materials at the micro-scale.

- There is no effective approach of selecting appropriate process conditions for optimum tooling performance.

- Mechanistic modelling for the micro milling process has been actively researched. However, 3D FE-based modelling and simulation approach is rarely available.

In order to make full use of the manufacturing technology for industrial applications, more work needs to be done to understand the micro cutting process. With the above in mind, there is a need to comprehensively realize the effects of cutting tool characteristics, work material properties as well as process conditions on the tooling performance for the potential process improvement. In addition, an effective FEM modelling approach is much essential for the performance prediction. These above issues will be addressed in the following chapters.

Chapter 3 Modelling and Simulation of the Micro Milling Process

3.1 Introduction

Modelling and simulation of the cutting process potentially allows designers and engineers to reduce the need for costly shop-floor trials, improves cutting tool design, optimizes process conditions and shortens the lead time in bringing a new product into the market. The finite element method (FEM), featuring reasonably accurate predictions on a user friendly graphical interface, has been widely employed for cutting processes modelling, simulation and optimization (Davim et al., 2010; Deng et al., 2009; Khalili et al., 2009; Baker, 2006; Yen, 2004; Klocke et al., 2001; Mamalis, 2001). However, at present, applying FEM for three-dimensional (3D) micro milling analysis is seldom reported, although 3D comprehensive analysis is essential and has many advantages in addressing the complexity in micro milling quantitatively.

In this chapter, a novel and effective finite element approach is proposed for modelling and simulation of the micro milling process under large deformations. A 3D tooling model considering a helix angle is developed for the cutting forces, tooling temperature distributions and chip formation prediction. Comparisons of predicted chip formation and cutting forces with the experimental results in dry slot milling are conducted for evaluation and validation of the proposed model.

3.2 Comparison of the two-dimensional and three-dimensional models

Two-dimensional (2D) plane-strain models are widely applied for orthogonal cutting process simulations (Davim et al., 2010; Deng et al., 2009; Khalili et al., 2009; Baker, 2006; Yen, 2004), and they also have been utilized for micro milling forces prediction

and chip formation analysis (Afazov et al., 2010; Wang et al., 2009; Dhanorker et al., 2008). For a 2D simulation, helix angle of the tool is neglected, which means chips only form and deform in planar direction and an example of predicted chip formation is shown in Fig. 3.1.
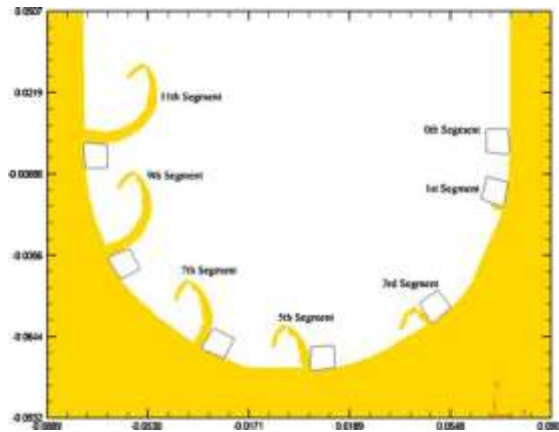
Fig. 3.1 An example of predicted chip formation in a 2D simulation (Wang et al., 2009)

In micro milling, radial depth of cut for one cutting pass, which corresponds to effective uncut chip thickness, is an important process parameter for determining cutting mechanics or behaviours. In order to identify the difference between 2D and 3D models, the relationship between the uncut chip thickness and other process variables needs to be formulated. The schematic diagram of a workpiece in full immersion slots milling is shown in Fig. 3.2.

      (a) 3D view   (b) top view
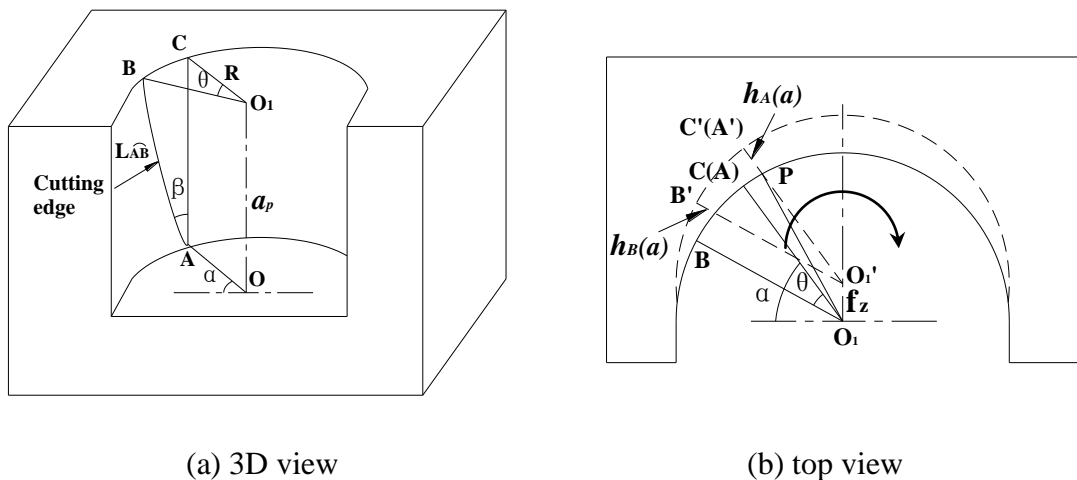
Fig. 3.2 Schematic diagram of a workpiece in full immersion slot milling

According to Fig. 3.2 (a), the tool-work contact length and the difference of rotation angle between bottom and top edge engaging point can be obtained by:

$$L_{\widehat{AB}} = \alpha_p / cos(\beta)$$

(3.1)

$$\theta \cong \alpha_p \cdot tan(\beta)/R$$

(3.2)

where α_p – Axial depth of cut;

β – Helix angle;

R – Radius of cutting tool.

From equation (3.1), it is obviously seen that the contact length is generally longer than axial depth of cut except for straight cutting edge (i.e. null helix angle) tools.

When the tooth of cutter advances to the next passage, as shown in Fig. 3.2 (b), A moves to A′ and B moves to B′, the effective uncut chip thickness for bottom edge engaging point A and for top edge engaging point B can be given as:

$$h_A(\alpha) = R + f_z \, sin(\alpha) - \sqrt{R^2 - [f_z cos(\alpha)]^2}$$

(3.3)

$$h_B(\alpha) = R + f_z \, sin(\alpha - \theta) - \sqrt{R^2 - [f_z cos(\alpha - \theta)]^2}$$

(3.4)

Where f_z – Feed per tooth;

α – Rotation angle for bottom edge engaging point.

Substituting equation (3.2) into (3.4), then the effective uncut chip thickness for B becomes:

$$h_B(\alpha) = R + f_z \, sin[\alpha - \alpha_p \cdot tan(\beta)/R] - \sqrt{R^2 - \{f_z \, cos[\alpha - \alpha_p \cdot tan(\beta)/R]\}^2}$$

(3.5)

And the effective uncut chip thickness for every point along cutting edge between A and B can be expressed:

$$h_B(\alpha, \alpha_e) = R + f_z\, sin[\alpha - \alpha_e \cdot tan(\beta)/R] - \sqrt{R^2 - \{f_z\, cos[\alpha - \alpha_e \cdot tan(\beta)/R]\}^2}$$

(3-6)

Where α ranges from 0 to π;

α_e – Axial depth for cutting edge points in the range of 0 to α_p.

For a 2D plane-strain model, it is assumed every point on the cutting edge has the same effective uncut chip thickness. While from equation (3.6), in which a helix angle is taken into account, the uncut chip thickness slightly varies along the tool cutting edge. Additionally, according to equation (3.1), there is a considerable difference for cutting edge contact length with and without a helix angle. Moreover, axial depth of cut is assumed to be equal to the height of the workpiece for the 2D model, which is less common for practical operations. Furthermore, in this case, it is impossible to apply bottom boundary conditions as well as predict the axial cutting force component.

Micro milling is an intermittent cutting process, and if the flutes of tools are straight, the whole tooth would impact the material at once, causing vibration and reducing accuracy and surface quality. Setting the flutes at an angle allows the tooth to engage work material gradually and smoothly so as to reduce vibration. Also, it is well known that a helical tooth profile plays a significant role in evacuating chips.

Based on above comparison and analysis, it is understood that the plane-strain model is relatively inaccurate for representing the practical cutting process, and micro milling simulations should ideally take all structural features including helix angle into consideration for the modelling development.

3.3 <u>Simulation software and its capabilities</u>

DEFORM[TM]-3D from Scientific Forming Technologies Corporation (SFTC), a robust and commercially available simulation system capable of analyzing three-dimensional flow of complex metal forming processes, is used in the study. The simulation code is based on an updated Lagrangian formulation that employs the implicit integration method designed for large deformations. The main features and capabilities of the software are:

- Simulation interface is user friendly graphical.

- Deformation and heat transfer are calculated in an integrated environment.

- Fully automatic, optimized remeshing is performed during simulation.

- Material models include elastic, rigid-plastic, thermal elastoplastic, thermal rigid-viscoplastic, porous and rigid.

- Point tracking deformation, contour plots, load-stroke prediction are available in the postprocessor.

- Multiple deforming body simulation allows for coupled die stress analysis.

- A self contact boundary condition allows a simulation to continue even after a lap or fold has formed.

- Multiple operations run sequentially without user intervention.

- Typical applications include forging, machining, rolling, extrusion, heading, drawing, cogging, upsetting and compaction.

3.4   Simulation developments

3.4.1 Tool modelling, meshing and boundary conditions

A Ø0.3mm diameter two-flute end mill (Magaforce 8500-Ø0.3mm) with a 30° helix angle is used in the modelling. Tool geometries including a 7° rake angle, 15° relief angle and 2.5µm cutting edge radius are measured by field emission scanning electron microscope (FE-SEM) Zeiss Supra 35VP and images of the tungsten carbide tool are shown in Fig. 3.3.

In micro end milling, the primary cutting edge is the side edge whereas the minor cutting edge is the bottom edge, and chip removal is mainly performed by the side cutting edge. Since feed per tooth is relatively low compared to axial depth of cut, the bottom cutting edge was ignored for modelling. Slots forming dimension errors due to cutting edge radius variations are also not taken into consideration. The primary cutting edge model, incorporating tool diameter, rake angle, relief angle, cutting edge radius

and helix angle, is developed through helical sweep protrusion by the commercial software Pro/Engineer. As for a tool with helix angle, pitch height can be calculated by:

$$P = 2\pi R / tan(\beta) \tag{4.7}$$

Where β − Helix angle;

   R − Radius of cutting tool.

The pitch height for a Ø0.3 mm diameter end mill with a 30° helix angle is 1.6324 mm.
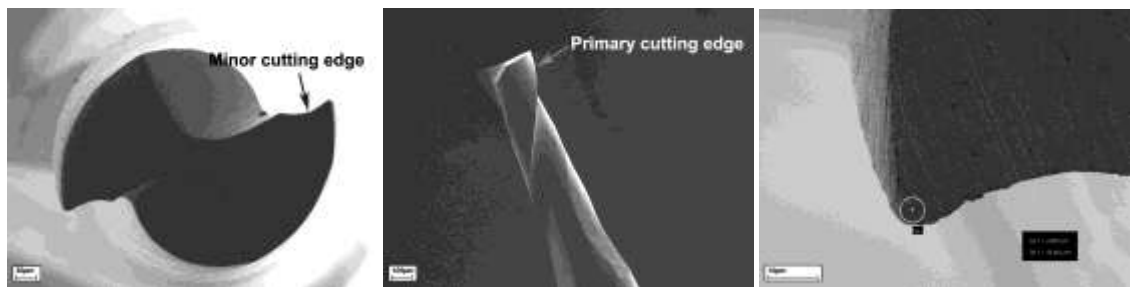
   (a) Bottom view   (b) Side view   (c) Measurement of cutting edge radius

Fig. 3.3 SEM images of the micro end mill

For tool meshing, tetrahedral elements and a mesh density window are used. The size of elements in the window to that of the rest of tool is set at 0.1, and total numbers of nodes and elements in the meshing are 3,165 and 13,181 respectively. For boundary conditions, heat exchanges between tool surfaces and environment are considered. Modelling and meshing of the primary cutting edge model is shown in Fig. 3.4.
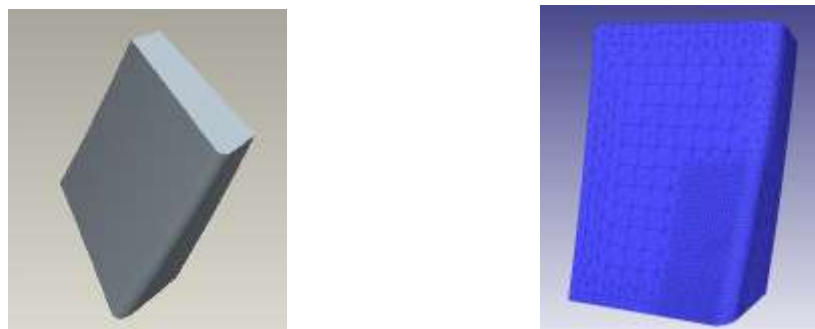
   (a) Modelling of the primary cutting edge   (b) Meshing of the primary cutting edge

Fig. 3.4 Modelling and meshing of the primary cutting edge

3.4.2 Workpiece modelling, meshing and boundary conditions

Simulation of full immersion milling is carried out. The modelling, meshing of work piece, cross-sectional dimensions and boundary conditions are shown in Fig. 3.5 (a-c).

(a)   (b)

(c)
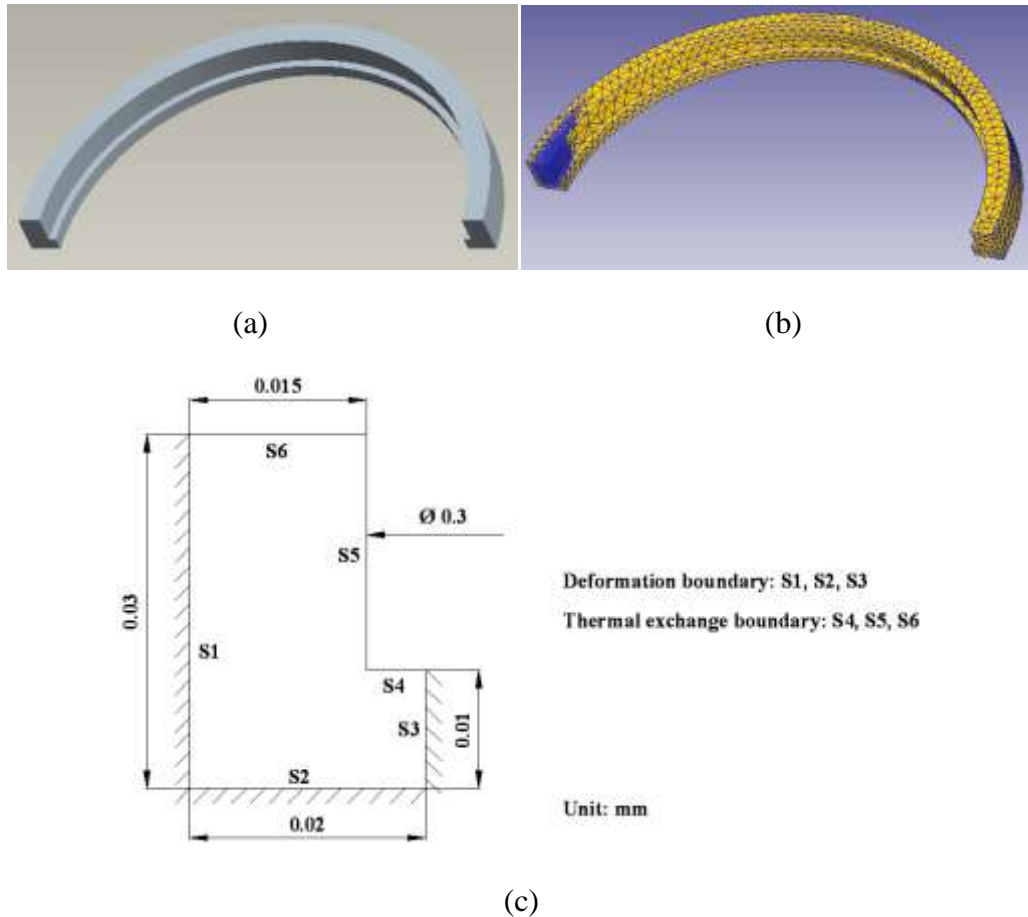
Fig. 3.5 Workpiece modelling, meshing, cross-sectional dimensions and boundary

conditions

A 180° rotation angle workpiece is modelled by Pro/Engineer. For meshing, tetrahedral elements and a mesh density window are adopted. The size ratio near the cutting edge in the density window to outside is set to be 0.02. The meshing window follows the movement of the tool during simulation to allow an excessively distorted mesh in the primary and secondary shear zones to be automatically remeshed without interruption. The total numbers of nodes and elements are 4,646 and 19,299 respectively. As shown in Fig. 3.5 (c), velocities of deformation boundary surfaces are fixed in three orthogonal directions and there exists thermal exchange between other free surfaces and the environment.

3.4.3 Work material flow stress

In metal cutting simulation, it is extremely vital to adopt accurate work material flow stress model to achieve desirably accurate predictions. The flow stress, which is dominated by temperature, strain and strain rate, should be determined experimentally under high temperature and large deformation conditions. AISI 1045 steel, low-cost medium carbon steel with adequate strength and toughness suitable for most engineering applications, is employed in my research.

Sheikh et al. (Sheikh et al., 2007) compared different flow stress models with experimental results for AISI 1045 steel and pointed out that the Johnson-Cook constitutive model produces the lowest percentage force errors at low, medium and high temperatures, and is recommended for cutting simulations over a wide range of cutting speeds. Therefore, a Johnson-Cook work material model is selected for coupled thermal deformation analysis. The Von Mises flow stress can be represented as follows:

$$\bar{\sigma} = [A + B(\bar{\varepsilon})^n] \left[1 + C \ln \left(\frac{\dot{\bar{\varepsilon}}}{\dot{\bar{\varepsilon}}_0} \right) \right] \left[1 - \left(\frac{T - T_{room}}{T_{melt} - T_{room}} \right)^m \right] \qquad (4\text{-}8)$$

where $\bar{\varepsilon}$ − The equivalent plastic strain;

$\dot{\bar{\varepsilon}}$ − The plastic strain rate;

$\dot{\bar{\varepsilon}}_0$ − The reference strain rate (normally $\dot{\bar{\varepsilon}}_0 = 1.0 \text{s}^{-1}$);

T_{melt} − Melting temperature of the work material;

T_{room} − Room temperature;

A − Plastic equivalent strain in Johnson-Cook constitutive model;

B − Strain related constant in Johnson-Cook constitutive model;

C − Strain-rate sensitivity constant in Johnson-Cook constitutive model;

m − Thermal softening exponent in Johnson-Cook constitutive model;

n − Strain hardening exponent in Johnson-Cook constitutive model.

Three sequential terms in the equation respectively account for strain hardening, strain rate and thermal softening effects on equivalent stress. The Johnson-Cook constants for

AISI 1045 steel, listed in Table 3.1, are determined by compression tests (Jaspers, 2002).

Table 3.1 AISI 1045 steel constants for Johnson-Cook flow stress model

A (MPa)	*B* (MPa)	*C*	*m*	*n*	T_{melt} (K)	T_{room} (K)
553.1	600.8	0.0134	1.0	0.234	1733	293

3.4.4 Chip-tool interface friction

Friction characteristics in the chip-tool interface together with the material flow stress data are the two most important inputs required for modelling and simulation of metal cutting process (Childs et al., 2000). However, how chips interact with the edges of tool and move across the rake surface and whether sliding, sticking or combination of two behaviours dominates in micro machining are still under investigation.

The contact schemes and the friction coefficients between the tool and the chip are affected by various factors, such as material properties, cutting conditions, tooling geometries, etc. Pure sliding is an appropriate friction scheme for conventional machining while in high speed cutting, sliding integration of a sticking model should be considered in terms of minor error of cutting forces (Sheikh et al., 2007). For micro milling, a higher spindle speed is chosen to achieve higher cutting speed; however, compared to conventional machining, cutting speed is relatively low due to the smaller tool diameter. Therefore, a pure sliding pattern is assumed reasonable and applicable. Based on Coulomb's law, the mathematical expression for frictional stress τ_f on tool rake surface is given by:

$$\tau_f = \mu\sigma_n \tag{4.9}$$

where $\sigma_n -$ The normal stress;

$\qquad \mu -$ Coefficient of friction.

The interface friction coefficient between tungsten carbide and AISI 1045 is chosen to be 0.4, which is based on a pin-on-disk test (Grzesik et al., 2002).

3.4.5 Process conditions and materials properties

Table 3.2 illustrates the process conditions, and tool and work material properties used for simulation. The properties of tool and workpiece are derived from the simulation software database and online source Matweb (Matweb, 2009).

Table 3.2 Summary of process conditions, tool and work material properties for the simulation inputs

Process conditions:

Cutting speed (m/min): 28.27

Feed per tooth (μm): 1

Axial depth of cut (μm): 20

Initial temperature for tool and workpiece (°C): 20

Convection coefficient (N/sec/mm/ °C): 0.02

Heat transfer coefficient (N/sec/mm/ °C): 45

Fraction of deformation energy transformed into heat: 0.9

Tungsten carbide properties:

Poisson's ratio: 0.24

Young's modulus (GPa): 690

Thermal conductivity (W/m/K): 84.02

Specific heat (J/kg/K): 203

Thermal expansion coefficient (μm/m °C): 5.2

AISI 1045 steel properties:

Poisson's ratio: 0.29

Young's modulus (GPa): 205

Thermal conductivity (W/m/K): 49.8

Specific heat (J/kg/K): 486

Thermal expansion coefficient (μm/m °C):

0 °C	20 °C	100 °C	200 °C	300 °C	400 °C	500 °C	600 °C
11.7	11.9	12.5	13	13.6	14.1	14.5	14.9

3.4.6 Simulation setup

In the study, the micro cutter is assumed to be rigid, and the work piece possesses a homogeneous and isotropic microstructure, and performs elastic-plastic deformations during simulations. The tool and workpiece are set to be master object and slave object

respectively, which means workpeice can deform according to the tool movement. Additionally, master-slave relationship between workpiece and itself is set up to ensure chips cannot penetrate back into the workpeice.

A maximum plastic strain failure criterion is adopted for chip separation and element separation occurs when a material critical plastic strain is reached. The initial positions of tool and workpiece models before simulation are illustrated in Fig. 3.6.
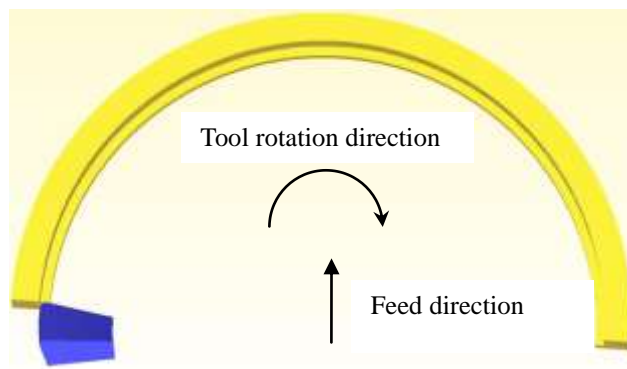
Fig. 3.6 Initial positions of the tool and workpiece models

3.5   <u>Simulation results</u>

The simulation is carried out under large deformations without considering process dynamic influences. Predicted cutting forces in the three orthogonal directions in one cutting pass are illustrated Fig. 3.7 and the maximum feed force, normal force and axial force are estimated to be 187mN, 212mN and 49.2mN. The tooling temperature distributions at different rotation angles are shown in Fig. 3.8, and the maximum tooling temperature at 45º, 90º and 135º are predicted to be 49°C, 78°C and 110°C, respectively.

Chip formation prediction at 45º, 90º and 135º rotation angle cutting are shown in Fig.3.9. It is obviously seen that chips flow along the tool helical direction, which reasonably matches the practical micro milling operations.

At a 45º rotation angle, radial depth of cut is considerably smaller as compared to the cutting edge radius, and the chip appears straight, largely due to the negative rake angle effect in the micro-scale cutting. Along with increasing radial depth of cut to feed per tooth as shown in Fig.3.9 (b), a complete spiral chip is produced as a result of helix

angle influence. When the cutting edge reaches the position of 135º rotation angle, fractured chip is observed owing to the maximum plastic strain failure criterion applied in the simulation.

(a) Feed forces   (b) Normal forces

(c) Axial forces
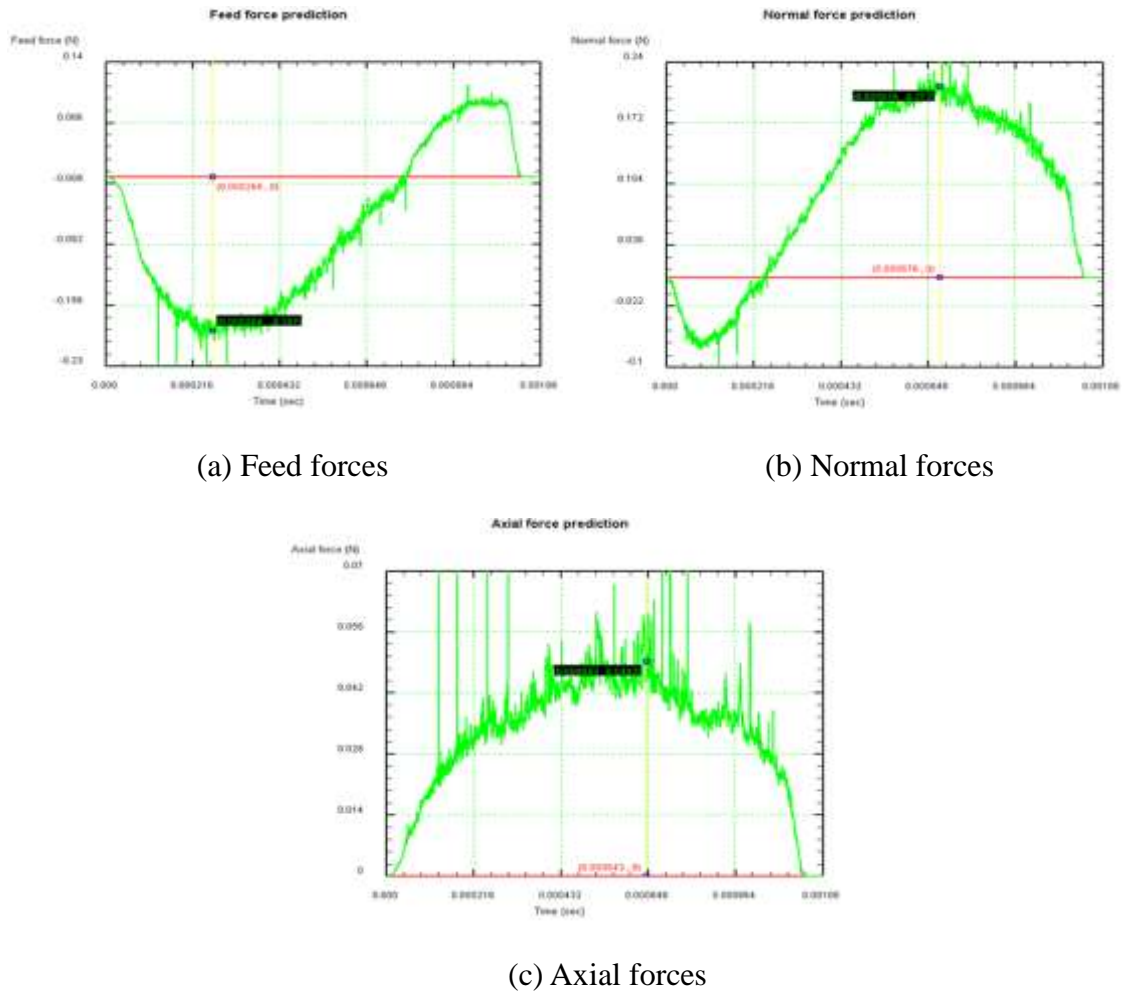
Fig. 3.7 Predicted cutting force components in one cutting pass

(a) 45º   (b) 90º   (c) 135º
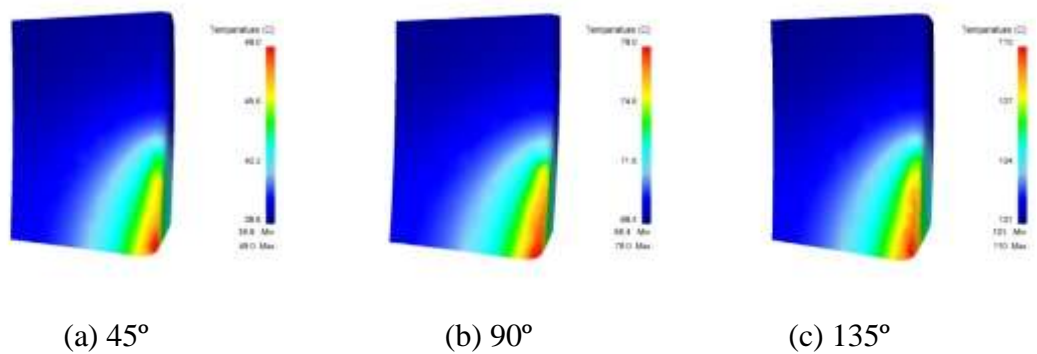
Fig. 3.8 Predicted tooling temperature distributions at different rotation angles

| (a) 45º | (b) 90º | (c) 135º |
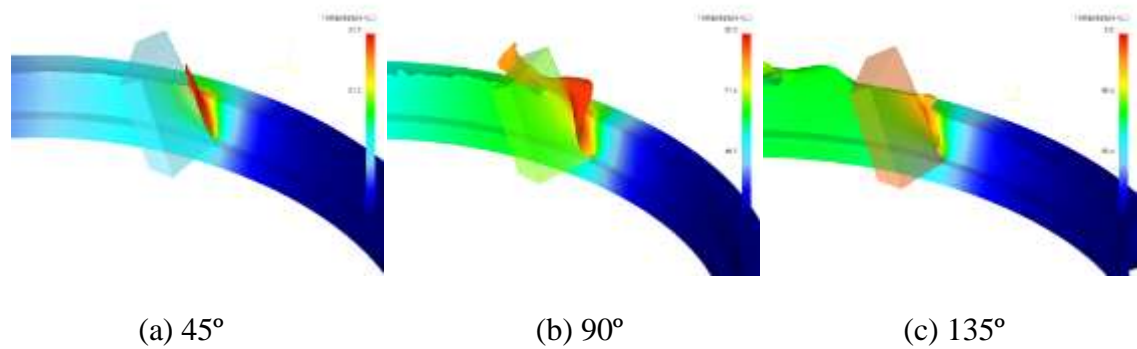
Fig. 3.9 Predicted chip formation at different rotation angles

3.6 <u>Verification through the cutting trials</u>

In order to verify the proposed FEM model, it is essential to make comparisons of simulated and experimental results on a quantitative basis. Measurements of cutting force components, one of the most important and accessible approaches can be achieved during machining operation, can satisfy the requirement. In addition, comparisons of predicted micro chip formation with experimental results are also adopted to verify the simulation results.

3.6.1 Experimental setup

The micro tool, as illustrated in Fig. 3.3, is used and the Ø3mm diameter tool shank is fixed in a precision spindle collet during experiments. Dry slot milling on an AISI 1045 sample is carried out on the ultra-precision micro milling machine UltraMill. Cutting forces are recorded by a Kistler dynamometer MiniDyn 9256C2 assisted with a four channel charge amplifier of 5070A. A/D data acquisition card 2855A4 is used for transferring signals to PC and software DynoWare is adopted for analyzing and evaluating the cutting forces. The sensitivity of the force sensor is set at −25.86 pC/N in the X axis direction, −13.07 pC/N in the Y axis direction, and −26.35 pC/N in the Z axis direction, which is based on calibration from Kistler. The sampling rate in the study is set at 32,000Hz, which enables sufficient sampling points in one recorded cutting pass. A digital camera Dino-Lite AD413TL is employed for the micro tool alignment. The setup of the cutting trials and micro tool alignment in Z (vertical) axis direction are shown in Fig. 3.10 and Fig. 3.11.

m
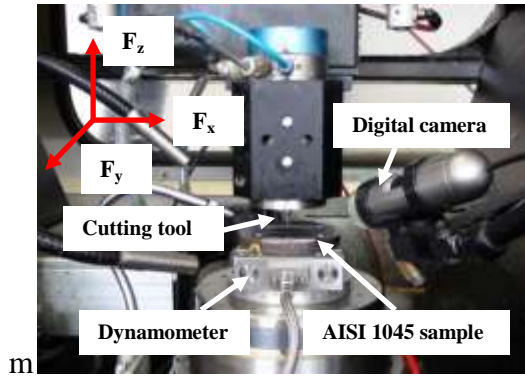
Fig. 3.10 Setup of the cutting trials   Fig. 3.11 Micro tool alignment
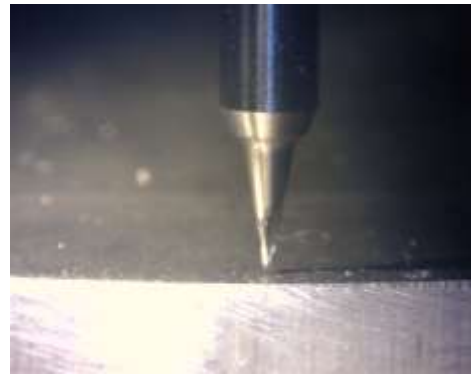
3.6.2 Comparison of the predicted and experimental results

The cutting force components in three directions after filtering are extracted and examples are shown in Fig. 3.12.
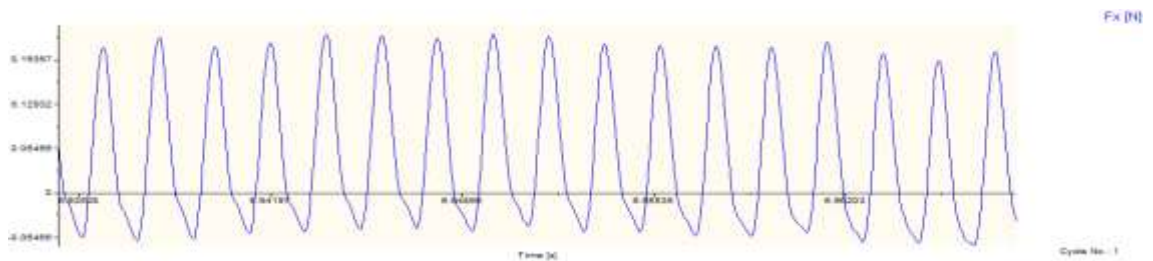
(a) Feed force component
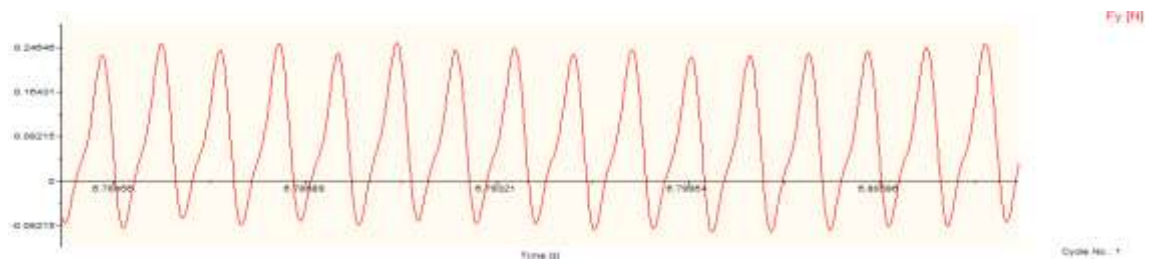
(b) Normal force component
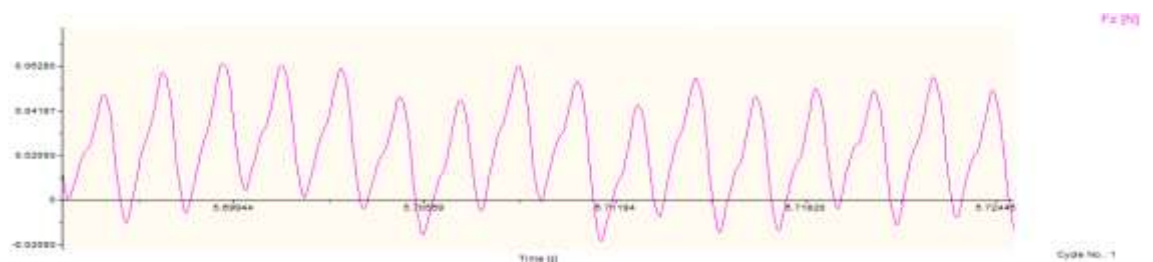
(c) Axial force component

Fig. 3.12 Examples of measured cutting force components

Averaged cutting forces in five consecutive cutting paths together with the predicted counterparts are plotted in Fig. 3.13, as a function of cutting rotation angle. The two curves are in good agreement except for slight variations. The errors may be due to simplified assumptions of the modelling inputs, such as the work material flow stress model and the tool-chip contact scheme. Size effects during micro milling operations may also lead to the force variations. Furthermore, measured maximum cutting forces in feed, normal and axial directions together with predicted ones are compared in Table 3.3. There are less than 8% deviations for normal and feed forces, and around 12% for axial forces, which demonstrates the reasonable accuracy of the simulation results.

(a) Feed forces

(b) Normal forces
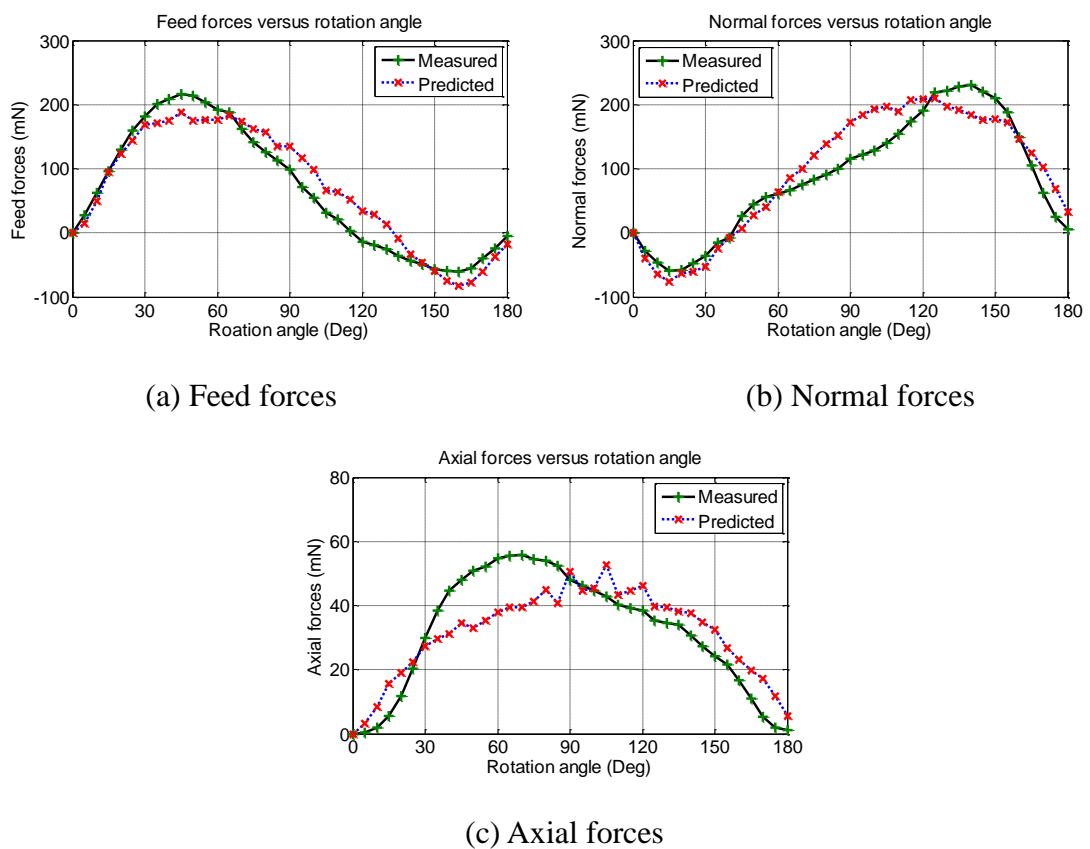
(c) Axial forces

Fig. 3.13 Comparison of the cutting force components

Table 3.3 Comparison of the measured and predicted maximum cutting forces

	Measured forces	Predicted forces	Deviations
Normal forces (mN)	221	212	4.1%
Feed forces (mN)	202	187	7.4%
Axial forces (mN)	56	49.2	12.1%

In addition, machined micro chips are collected and observed under a digital microscope Keyence VHX-1000. The predicted spiral shaped chip is well in agreement with collected micro chip examples (see Fig. 3.14). Based on the above comparison and analysis, it is concluded that the simulation is correct and convincing, and the 3D FE-based approach could provide reasonable accuracy for scientific understanding and characterization of the micro milling process, and the proposed model could be regarded as a benchmark model for studying the associated process performance including the cutting forces, tool stresses, tool temperatures and chip formation.

(a) Predicted chip formation   (b) Collected chip samples

Fig. 3.14 Comparison of predicted chip formation with collected chip samples

3.7   Conclusions

A novel 3D finite element method has been proposed for modelling and simulation of the micro milling process. Simulations considering tooling helix angle under large deformations have been carried out using a commercially available tool DEFORM™-3D. Cutting forces, tooling temperatures and chip formation in the simulation have been presented. Predicted cutting forces and micro chip formation show reasonable agreement with the measured results in well-designed cutting trials, and it demonstrates that the proposed modelling and simulation approach is capable of effectively characterizing the micro milling process with acceptable accuracy.

Chapter 4 Tooling Geometrical Effects of Micro tools and the Associated Micro Milling Performance

4.1 Introduction

Unpredictable tool life and premature tool failures remain major obstacles for application of the micro milling technology, and extension of the tool life presents a key issue for tool manufacturers and researchers.

For micro tool design, optimum tooling geometry is essential for achieving robust stiffness and mechanical strength, avoiding chip clogging and therefore improving tool life and tooling performance. Although dynamic cutting load is considerably low, micro tools easily suffer from deflection, chatter and premature breakages, resulted from dramatically reduced tool rigidity and bending strength. Stress concentration on sharp cutting edges may cause potential brittle fracture, damage part quality and lead to shorter tool life. High temperature accelerates tool wear development, which increases cutting forces and burr formation as well as degrades forming accuracy. Also, chip evacuation capability presents a key factor for determining tool life as inappropriate chip flow renders rise to possible blockage inside tool flutes, resulting in accumulated heat and high risk of sudden tool failures. Therefore, it is essential and much needed to adopt optimum geometrical features so as to achieve low cutting forces, tool stresses and temperatures, and avoid chip clogging. Furthermore, scientific understanding of tooling geometrical effects of a micro tool on its process performance becomes extremely vital for enhancing the tool life and cutting performance.

This chapter aims to investigate tooling geometrical effects on the micro milling performance in a comprehensive manner for the practical tool design and optimization purpose. In the study, the FE-based approach proposed in Chapter 3 is adopted and simulations using tools under different helix angles, rake angles and cutting edge radius are carried out. Comparisons of predicted cutting forces, tool stresses, tool temperatures

as well as chip formation are presented and discussed for determining individual influence so as to provide scientific knowledge and understanding for optimizing tool design and improving consequent cutting performance.

4.2 <u>Tooling geometry and characterization</u>

Micro end mills are considered in the study. The main geometrical features are diameter, flutes, radial rake angle, radial relief angle, helix angle and cutting edge radius, as schematically illustrated in Fig. 4.1. Because the primary cutting edge of a micro end mill is side edge, radial rake angle and relief angle are universally regarded as rake angle and relief angle for the tooling geometry measurement.

(a) Cross section of end mill   (b) Zoom in on a cutting edge   (c) Side view of end mill
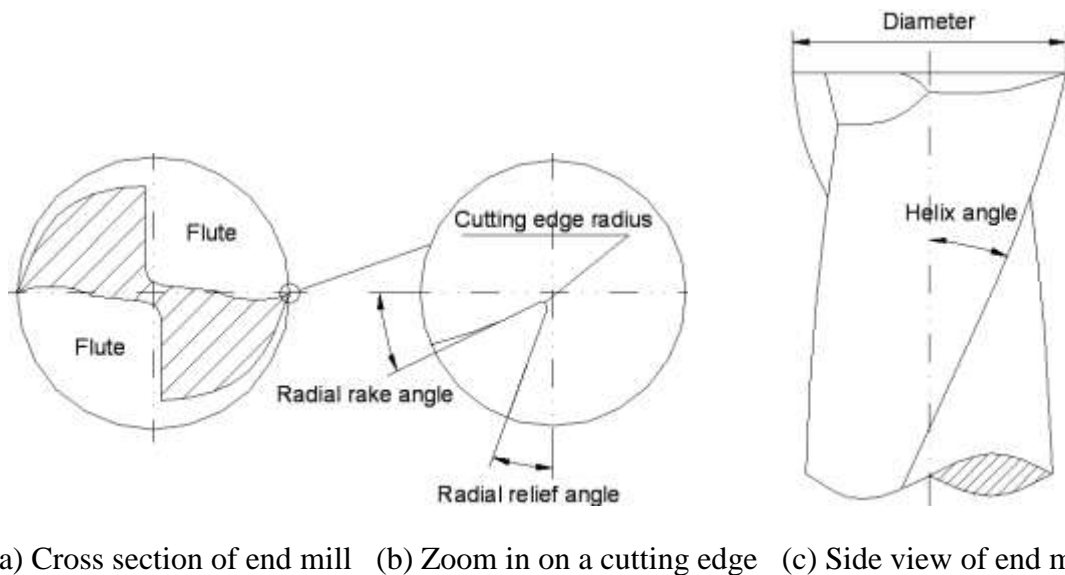
Fig. 4.1 Schematic illustration of a two-flute micro end mill

At present, commercially available micro end mills with Ø25μm diameter are emerging and smaller sizes down to Ø5μm are also available by a special order (Performance Micro Tool, 2010). With decreasing diameter, stiffness of tools tends to be weakening dramatically, which can easily cause tool deflection, unpredictable tool life and premature tool failures. Increasing radial rake angle and relief angle together with reducing cutting edge radius could lead to sharper but weaker tool tips, which imposes a major limitation on cutting edge strength. Generally, cutting edge radius for tungsten carbide micro tools are between 0.8~5μm due to restraints of the tool fabricating process. Selection of appropriate helix angle is crucial for both tool stiffness and chip

evacuation, and 30° helix angle is commonly employed for micro tools design and configurations.

4.3 <u>Investigation approach</u>

Experimentation is a traditional approach for micro cutting research. However, it appears to be costly and to some extent inaccessible for studying tooling geometrical effects on the associated process performance. With tiny dimension and complex configurations of micro tools, there is no experimental method by which stress distribution and tool temperatures on tips can be measured, in this case numerical method tends to the best solution for accurate estimation of the localized stresses and temperatures acting on the tool near the cutting edges.

Finite element method (FEM) possesses many potential advantages, such as user friendly graphical interface, reducing unnecessary cutting trials, shortening lead time, improving cutting tool designs as well as optimizing process conditions. Furthermore, it is capable of predicting cutting forces, chip flow and a distribution of tool temperatures and stresses under various cutting conditions. Therefore, FEM is chosen for the investigation approach.

4.4 <u>Simulation inputs</u>

The tool and workpiece models established in chapter 3 are used as benchmark models, and the detailed simulation inputs see Table 3.2. Simulations using different tooling geometries are carried out for understanding respective effects on process performance. Table 4.1 shows three geometrical input groups, including group 1 for four helix angle levels, group 2 for three rake angle levels and group 3 for three cutting edge radius levels.

For the tool modelling, pitch height for Ø0.3mm diameter tools with 15º, 30º and 45º helix angles are 3.5174mm, 1.6324mm and 0.9425mm, respectively. In the same group, when the specified feature changes, the values of the other features remain constant. Variations of tool diameter and relief angle are not considered and the total number of 3D simulations is 8. Predicted cutting forces, tool stresses, tool temperatures, chip

formation and temperatures with respect to different tool geometries are presented and discussed in the following sub-sections.

Table 4.1 Tooling geometries for the simulation inputs

	Helix angles	Rake angles	Cutting edge radius (µm)	Diameter (mm)	Relief angles
Group 1	0°, 15°, 30°, 45°	7°	2.5	0.3	15°
Group 2	30°	-7°, 0°, 7°	2.5	0.3	15°
Group 3	30°	7°	1, 2.5, 4	0.3	15°

4.5   Tooling geometrical effects on the micro milling performance

4.5.1 Influence of tooling geometry on cutting forces

Knowledge of the cutting forces in micro milling can be beneficial for improved machining accuracy, a higher production rate and preventing potential tool breakages (Huang et al., 2010). Predicted maximum feed forces, normal forces and axial forces using different tooling geometries are shown in Fig. 4.2.

Firstly, the effects of helix angles are tested. Four levels of helix angles are chosen, namely 0°, 15°, 30° and 45°, among which 30° helix angle is commonly used on commercial micro tools. From Fig. 4.2 (a), it is obviously seen that maximum feed forces and normal forces vary slightly under different helix angles whereas maximum axial force increase gradually along with increasing helix angles. Therefore, there is less impact for cutting forces in planar directions by altering helix angles. From tool development point of view, no obvious influences in terms of tool deflection are caused by changing helix angles as long as tool stiffness remains constant. At the tool rotation angle where the tool suffers the maximum cutting force, due to the fact that axial depth of cut is considerably low in micro milling, cutting edge contact length might be higher for high helix angle tools. Thus, cutting force per length unit becomes comparatively lower, which may reduce the possibility of edge fracture.

(a) Helix angles   (b) Rake angles

(c) Cutting edge radius
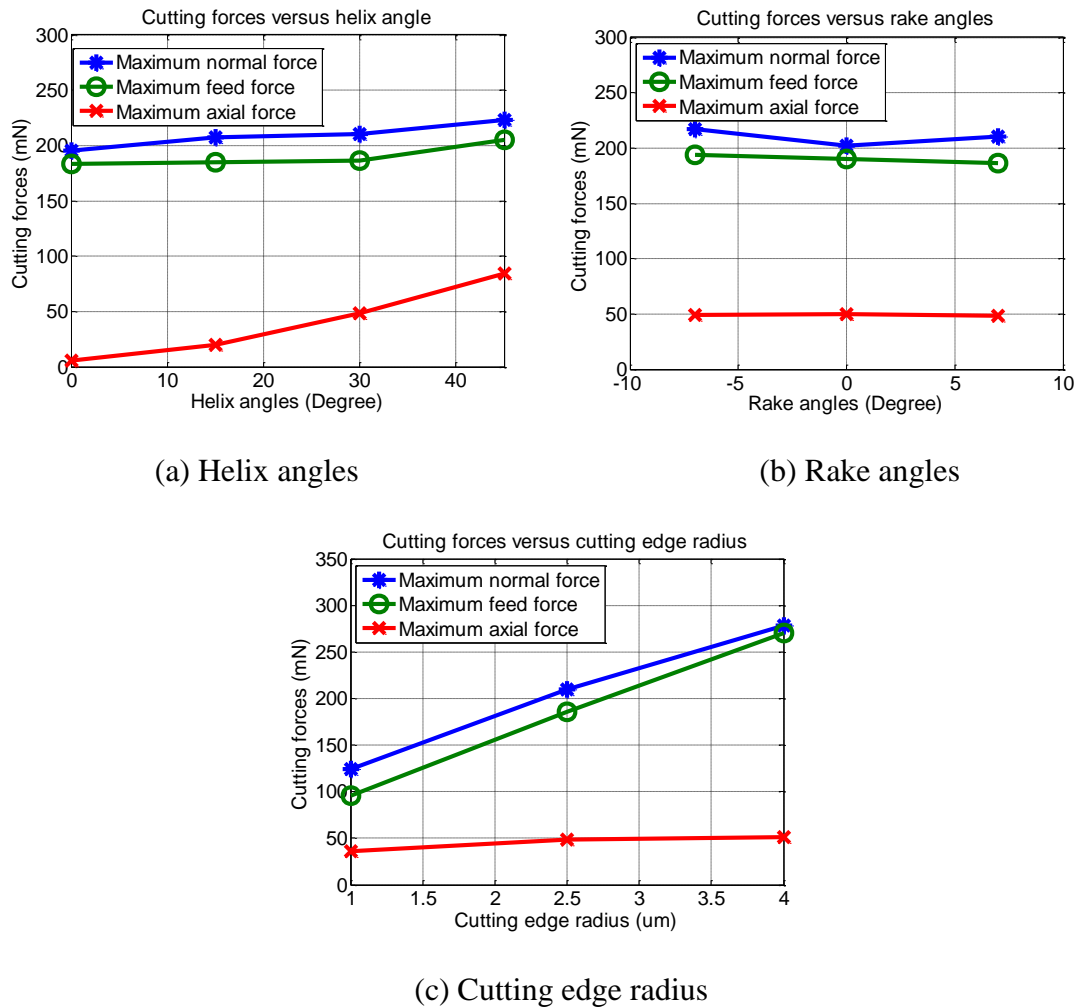
Fig. 4.2 Predicted cutting forces under different tooling geometries

Similar analyses are performed to understand rake angle and cutting edge radius effects on the cutting force components. From Fig. 4.2 (b), all the three force components vary rather slightly when rake angle changes from negative to positive, which means less significance for rake angle impact. And if cutting edge corner becomes dull, maximum feed force and normal force rise significantly whereas maximum axial force almost keeps constant, as depicted in Fig. 4.2 (c). According to above results and analysis, cutting edge radius has the most significant effect on the maximum feed and normal forces, whereas helix angle and rake angle have less impact. For the maximum axial force, helix angle plays the most important role than the other two structural features.

4.5.2 Influence of tooling geometry on tool stresses

Fig. 4.3 illustrates predicted tool stress values under the highest resultant forces during

one cutting passage. As seen from Fig. 4.3 (a), rising helix angles from 0° to 45° result in steadily increasing tool stresses. Probably it is mainly due to weakened cutting edges for high helix angle tools. According to Fig. 4.3 (b), rake angle also has considerable effect on maximum stresses at the cutting edge corner. Among all the three levels, the positive rake angle has the maximum stress and the negative rake angle has the minimum stress. Because the estimated cutting forces for tools with different rake angles vary little (see Fig. 4.2 (b)), this phenomenon can be explained by edge strengthening effects. Therefore, in hard milling or roughing applications, a negative rake angle is more preferable for maintaining good edge strength so as to reduce edge stresses. Sharp cutting edge corner also significantly reduces the level of maximum stresses, as shown in Fig. 4.3 (c). Although the tool cutting edge becomes weaker with smaller edge radius, cutting forces decrease greatly as well (see Fig. 4.2 (c)) and offset the cutting edge weakening effects. Therefore, the 1μm edge radius has the least tool stresses, followed by 2.5μm and 4μm.
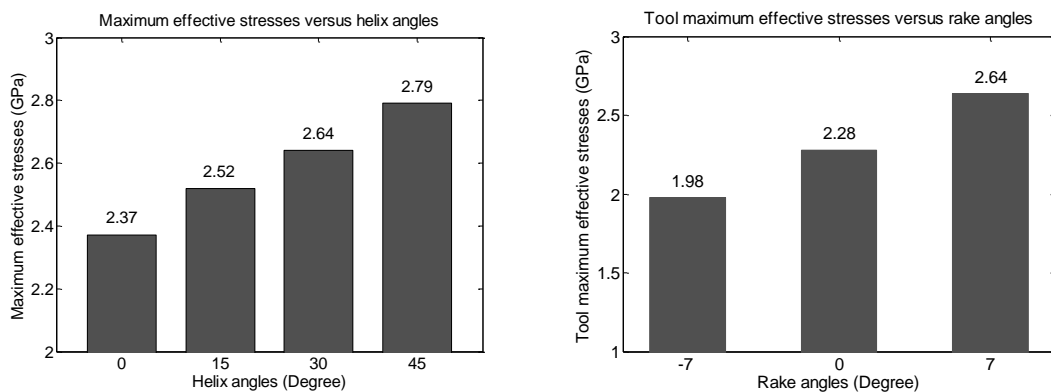
(a) Helix angles

(b) Rake angles
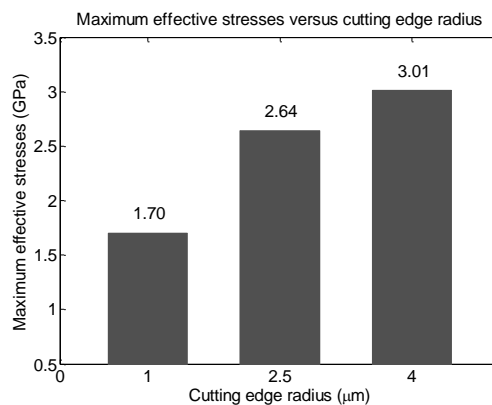
(c) Cutting edge radius

Fig. 4.3 Predicted tool stresses under different tooling geometries

4.5.3 Influence of tooling geometry on tool temperatures

An understanding of tool temperature distribution gives possible guidance for more rational tool designs and leads to an improved tool life. Heat generation in metal cutting is mainly caused by the large plastic deformation of the workpiece in the primary and secondary deformation zones as well as friction at the tool-chip and tool-workpiece interface. Fig. 4.4 shows predicted maximum temperatures on the primary cutting edges of tools employing different helix angles during one cutting pass. It is clearly seen that tools with higher helix angles are more likely to accumulate more heat on the tips, which may be explained by concentrated and reduced tool-chip contact area. From Fig. 4.5, high temperature zones tend to decline from tool-work interface line to cutting tip areas along with increasing helix angles.
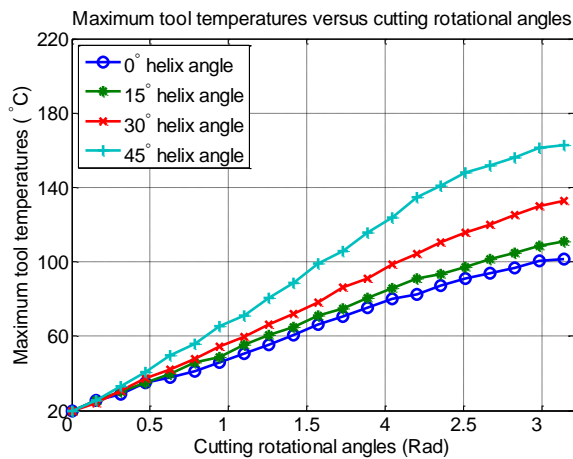
Fig. 4.4 Predicted tool temperatures under different helix angles

(a) 0°   (b) 15°   (c) 30°   (d) 45°
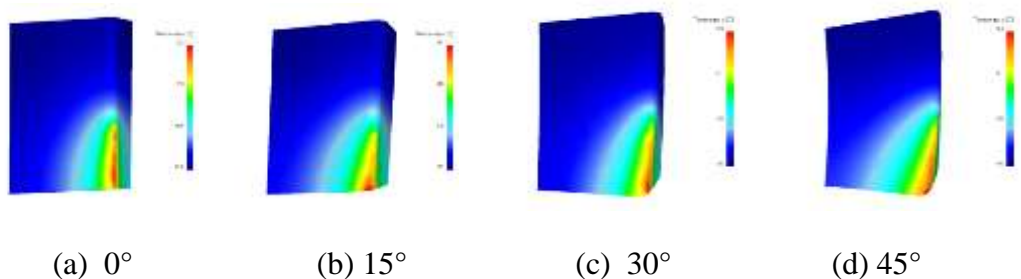
Fig. 4.5 Predicted tool temperature distributions under different helix angles after one cutting pass

From Fig. 4.6 and Fig. 4.7, it is clear that tool temperatures are also influenced by rake

angles, and negative rake angle has less impact on maximum tool temperature and positive rake angle has the most effect. Smaller cutting edge radius greatly reduces the level of heat generation as evident in Fig. 4.8 and Fig. 4.9, and compared to helix angle and rake angle, cutting edge radius has the most significant effect on the tool temperatures.

Since temperature distribution imposes a major impact on the tool wear development, resulting in significant wear rate on high temperature zones, cutting edge particularly for tip points may easily become worn and blunter. Therefore, major wear for a two-fluted end mill is mainly concentrated on two cutting tip points. To this point, for the sake of reducing tool temperature so as to reduce tool wear and extend tool life, high helix angle, positive rake angle and dull cutting edge may not suitable for high-duty operations.
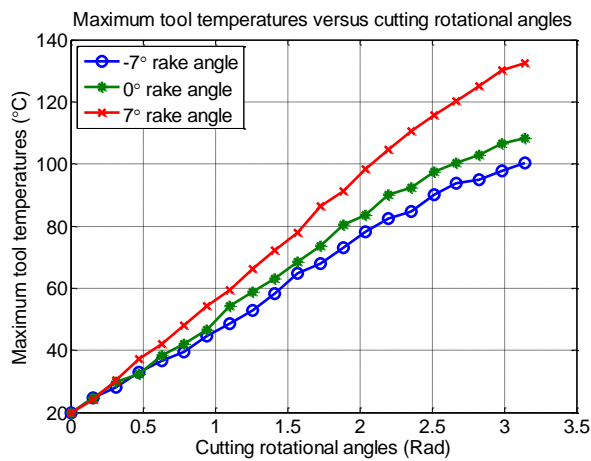
Fig. 4.6 Predicted tool temperatures under different rake angles

(a) -7°   (b) 0°   (c) 7°
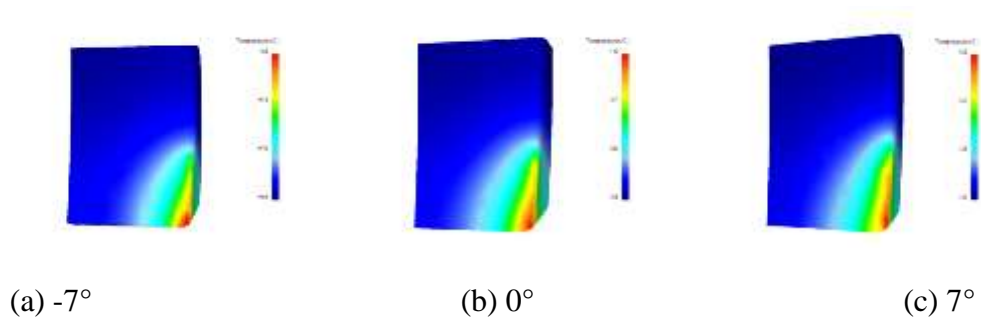
Fig. 4.7 Predicted tool temperature distributions under different rake angles after one cutting pass
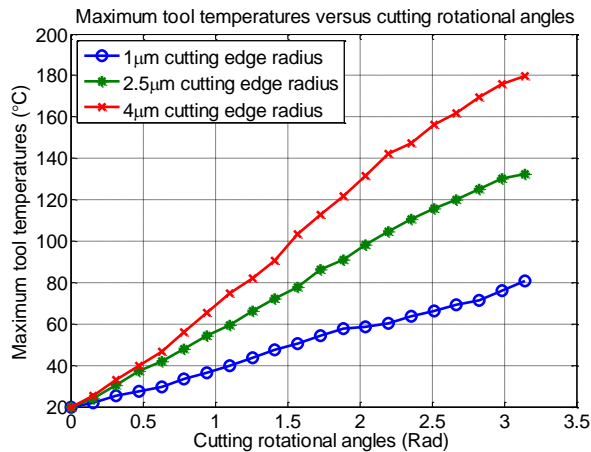
Fig. 4.8 Predicted tool temperatures under different cutting edge radius

(a) 1μm   (b) 2.5μm   (c) 4μm
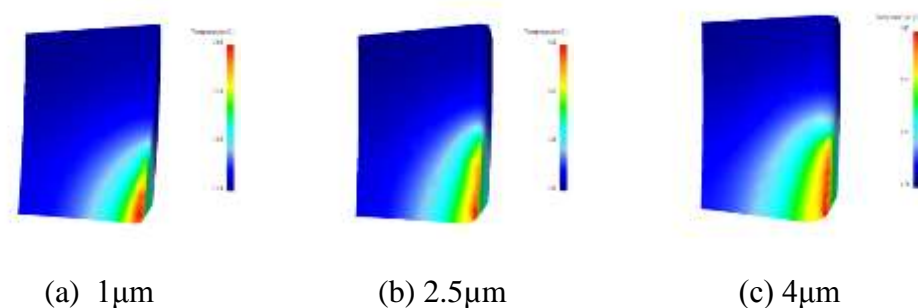
Fig. 4.9 Predicted tool temperature distributions under different cutting edge radius after one cutting pass

4.5.4 Influence of tooling geometry on chip formation and temperatures

Chip formation refers to chip flow directions, shapes and minimum chip thickness. Minimum chip thickness in micro milling is regarded as the smallest radial uncut chip thickness when a chip can be formed. Due to intermittent cutting mechanism and self-breaking capability in micro milling, helical and low temperature chips become more desirable for better surface finish, longer tool life and less energy consumption.

After a half pass (90°) milling, maximum radial depth of cut is approximately equal to feed per tooth. Chips tend to be different in flow directions and shapes using various tools as shown in Fig. 4.10. Resulting from applied boundary constraints on the bottom plane, chip flows both horizontally and vertically with straight cutting edge tool (see Fig. 4.10 (a)), which reflects inaccuracy of chip formation prediction by plane strain models

(Wang et al., 2009). According to comparison of chip flow directions under different helix angles, it is certain that fluent chip ejection can benefit from higher helix angle and also in this circumstance, there is less opportunity for chips interact with tool rake surface, which may reduce the possibility of crater wear. However, for 45° helix angle tools, there are almost no chips produced and only burrs can be formed at the edge of workpiece as a result of plastic deformation, which is obvious demonstrated in Fig. 4.10 (d). Because of worn cutting edge and increasing axial cutting force for 45° cutters, large plastic deformation of work material takes place in axial direction. The existence of burrs may cause significant fluctuations of cutting forces for the subsequent cutting passages, and makes tool wear and life unpredictable. For 30° helix angle tools, burrs appear much less, and also complete spiral chips are formed. As a result, this type of tools not only possesses good chip evacuation capability but also improves machining stability.

(a) 0° (b) 15° (c) 30°

(d) 45° (e) Maximum chip temperatures under different helix angles
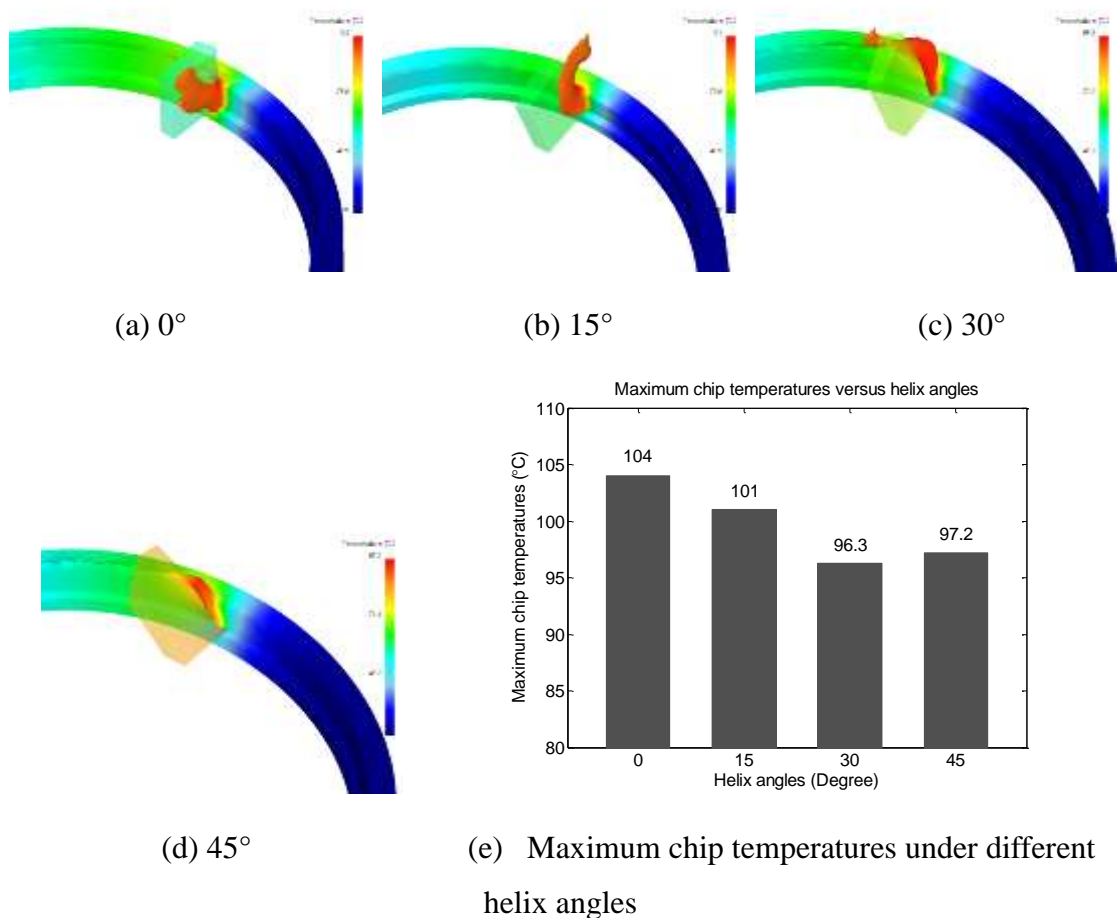
Fig. 4.10 Predicted chip formation and temperatures after a half cutting pass under different helix angles

In addition, predicted maximum chip temperatures using four types of tools, shown in Fig. 4.10 (e), are 104ºC, 101ºC, 96.3 ºC, 97.2 ºC respectively and 30º high helix angle tools generate the lowest chip heat, which may due to reduced contact between tools and work material compared to 0º and 15º tools, and less elastic or plastic deformation compared to 45º tools. From the standpoint of energy saving, 30° helix angle is more suitable for micro tool designs.

According to Fig. 4.11 and Fig. 4.12 (a), it is obvious that positive rake angle facilitates chip formation and evacuation as well as less heat generation. When the tool rake angle becomes more negative, compressing rather than shearing is dominated in material removal and chips can hardly be formed.

(a) -7°   (b) 0°   (c) 7°
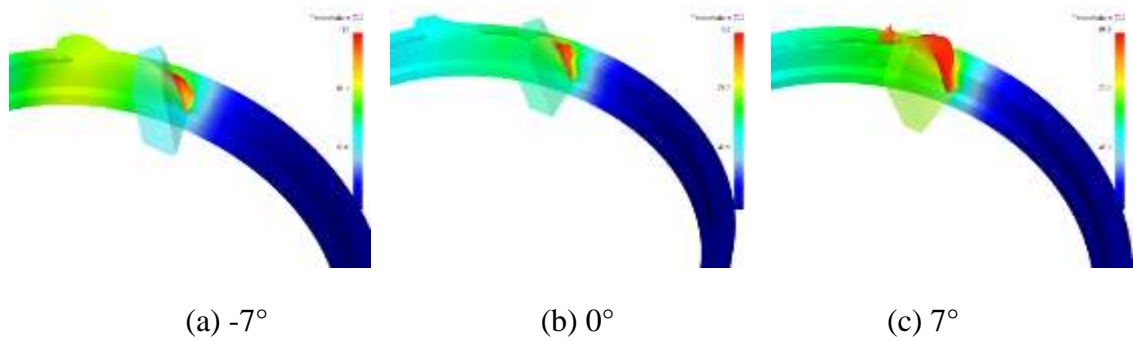
Fig. 4.11 Predicted chip formation after a half cutting pass under different rake angle

(a) Rake angles   (b) Cutting edge radius
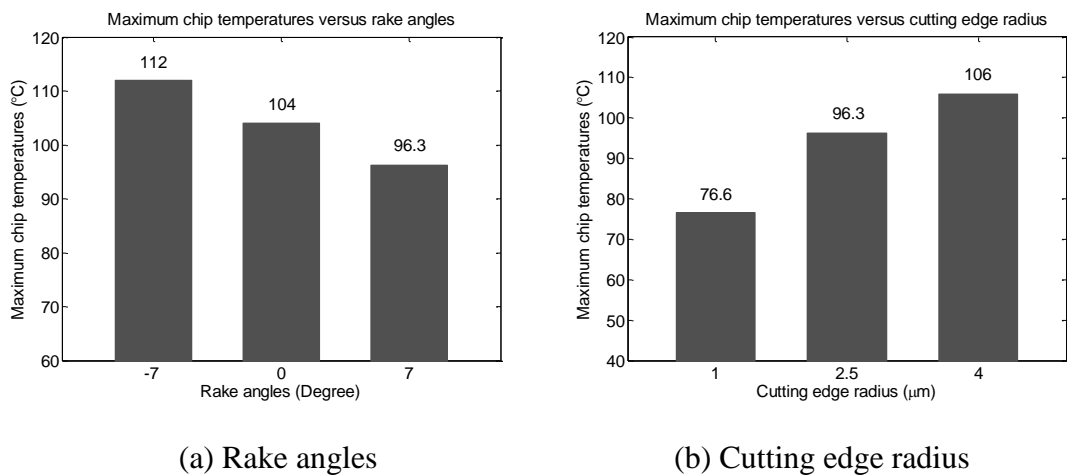
Fig. 4.12 Predicted maximum chip temperatures after a half cutting pass under different tool geometries

(a) 1μm   (b) 2.5μm   (c) 4μm
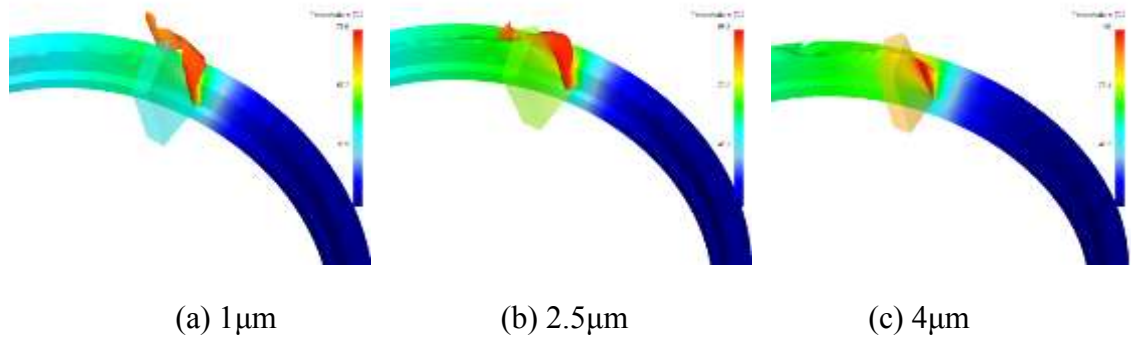
Fig. 4.13 Predicted chip formation after a half cutting pass under different cutting edge radius

Cutting edge radius has significant impact on chip formation and ejection. Continuous spiral shaped and low temperature chips are achieved by small edge corner tools, as illustrated in Fig. 4.13 and Fig. 4.12 (b). From Fig. 4.13 (c), when using a 4μm cutting edge radius tool, only ploughing phenomenon is observed and there are almost no chips formed due to minimum chip thickness effect in micro-scale cutting. Therefore, according to Fig. 4.13 (b) and (c), it is certain that the ratio of minimum chip thickness to the cutting edge radius for AISI 1045 steel under the specific cutting conditions is between 25% and 40%.

Based on above analysis, it is concluded that all helix angle, rake angle and cutting edge radius can affect chip formation and temperatures significantly. Different tool geometries have different response on the chip flow directions, shapes as well as the minimum chip thickness. To achieve better chip evacuation capability and machining stability as well as low heat generation, 30° helix angle, positive rake angle and sharp cutting edge can be more preferable for the specific investigation.

4.6   Conclusions

Comprehensive investigation on tooling geometrical effects in the micro milling process has been conducted by a 3D FE-based method proposed in Chapter 3. Cutting forces, tool stresses, tool temperatures, chip formation and temperatures in cutting AISI 1045 steel with respect to different helix angles, rake angles and cutting edge radius have been predicted, compared and discussed to identify individual geometrical effect. Based on the simulation results, the following conclusions can be drawn:

- Cutting edge radius has the most significant effect on cutting forces, followed by helix angel and rake angle.

- Rising helix angles increases tool stresses steadily. Compared to negative rake angle, the positive rake angle has more impact on the tool stresses. A sharp cutting edge can reduce the level of tool stresses considerably.

- A higher helix angle, positive rake angle and dull cutting edge lead to higher tool temperatures. Compared to helix angle and rake angle, cutting edge radius affects the tool temperature mostly.

- Helix angle, rake angle and cutting edge radius affect the chip directions, shapes and minimum chip thickness as well as chip temperatures significantly. 30° helix angle, positive rake angle and sharp cutting edge are more preferable for the better chip removal capability, machining stability and less power consumption.

According to above conclusions, cutting edge radius is the most influential factor for determining the process performance, followed by helix angle, and rake angle has less impact. By taking comprehensive account of the effects of tooling geometries on cutting forces, tool stresses, tool temperatures, and chip formation and temperatures, it is suggested that in roughing milling for high material removal rate or cutting hard materials, low helix angle and negative rake angle can yield better results as a result of maintaining edge strength and enhancing tool life. Whereas in finish cutting for the best surface finish, 30° helix angle, positive rake angle and sharp edge corner are more practical for the tool configurations.

Chapter 5 Performance Assessment of Diamond-like Carbon and Nano-crystalline Diamond Coatings on Micro Tools

5.1 <u>Introduction</u>

In micro milling, extending the tool life and improving the tooling performance have the great industrial significance and also present great technological challenges. It is universally recognized that, in conventional cutting, appropriate coatings can be used on tools to extend the cost effectiveness and efficiency of the production process in terms of improved surface quality, increased tool life span, reduction in machine downtime and reduction in risk of damage as a result of tool wear or breakages. Coatings enable hardness, toughness and wear resistance of a tool material to be consistently maintained well during machining operations. Moreover, there will be important environmental and economic benefits by enabling the possibility of dry machining due to a lower friction coefficient between coating films and work materials.

Up to now, quite limited work has been conducted on improving the life and enhancing the performance of micro tools by using appropriate coating techniques, diamond coatings in particular. Huge progress has been achieved by applying diamond-like carbon (DLC) and nano-crystalline diamond (NCD) coatings on conventional cutting tools (Almeida et al., 2008; Hu et al., 2008; Meng et al., 2008; Hu et al., 2007; Hanyu et al., 2005; Fukui et al., 2004; Dai et al., 2000). However, application of the two coatings on micro tools is still a big challenge due to complex tool shapes and tiny tooling geometries.

In the work presented in this chapter, DLC and NCD thin films are applied upon micro end mills in an attempt to enhance the tooling performance. Multiple criteria performance of the DLC and NCD coated tools in dry slot milling, including the cutting forces, tool integrity, surface finish and micro-burr formation, are characterized and compared against those of uncoated tungsten carbide tools in both dry and wet cutting

conditions for the evaluation purpose.

5.2   DLC and NCD coating properties and applications

5.2.1   DLC films

DLC is an amorphous carbon (a-C) or hydrogenated amorphous carbon (a-C: H) thin film material and consists of sp^2 bonded (graphite-like) carbon within a sp^3 bonded (diamond-like) matrix. Its properties are strongly dependent on the deposition conditions. DLC films possess many desirable qualities such as mechanical (high hardness), optical (high optical band gap), electrical (high electrical resistivity), chemical (inert) and tribological (anti-adhering, low friction and wear coefficient) properties and can be deposited at substrate temperature lower than 200°C. The typical areas of application for these coatings include machining, moulding, automotive, machinery, optical and biomedical devices, etc.

Bonding strength to the substrates is the largest inherent issue for DLC coatings. The higher the sp^3 percentage in a DLC film, the harder the DLC film but the higher the compressive stress within that film. The internal stress that benefits the hardness of DLC materials makes it difficult to bond such coatings to the substrates to be protected. In extreme cases, such stresses can create unstable interfaces and the film may become prone to delamination.

5.2.2   NCD films

NCD is the main representative of diamond at the nano-scale, and it exhibits most of the notable properties of natural diamonds. It is the hardest known material, has the lowest coefficient of thermal expansion, is chemically inert and wear resistant, offers low friction, has high thermal conductivity, is electrically insulating and optically transparent from the ultra-violet (UV) to the far infrared (IR). NCD finds use in many diverse applications including, its use as a precious gem, but also as a heat sink, as an abrasive, and as inserts and/or wear-resistant coatings for cutting tools (Paul, 1995).

5.3   DLC and NCD films deposition and characterization

Two-flute end mills with Ø500 µm diameter and 30° helix angle (Magaforce 8507-Ø0.5 mm) are selected for DLC and NCD films deposition. The substrate material is K15 carbide, containing 6.5-7% cobalt, with micro grain size between 6µm and 8µm. Before the coating process, qualitative conditions of tungsten carbide tools are examined using a Zeiss Supra 35VP FE-SEM operated at 6kV as micro tool inspection and assessment are of great importance for the ultimate coating quality. The SEM images of an uncoated micro tool are shown in Fig. 5.1, and the cutting edge radius of the tool is measured to be 1.5µm.

(a) Bottom view   (b) Side view

(c) The cutting edge radius measurement
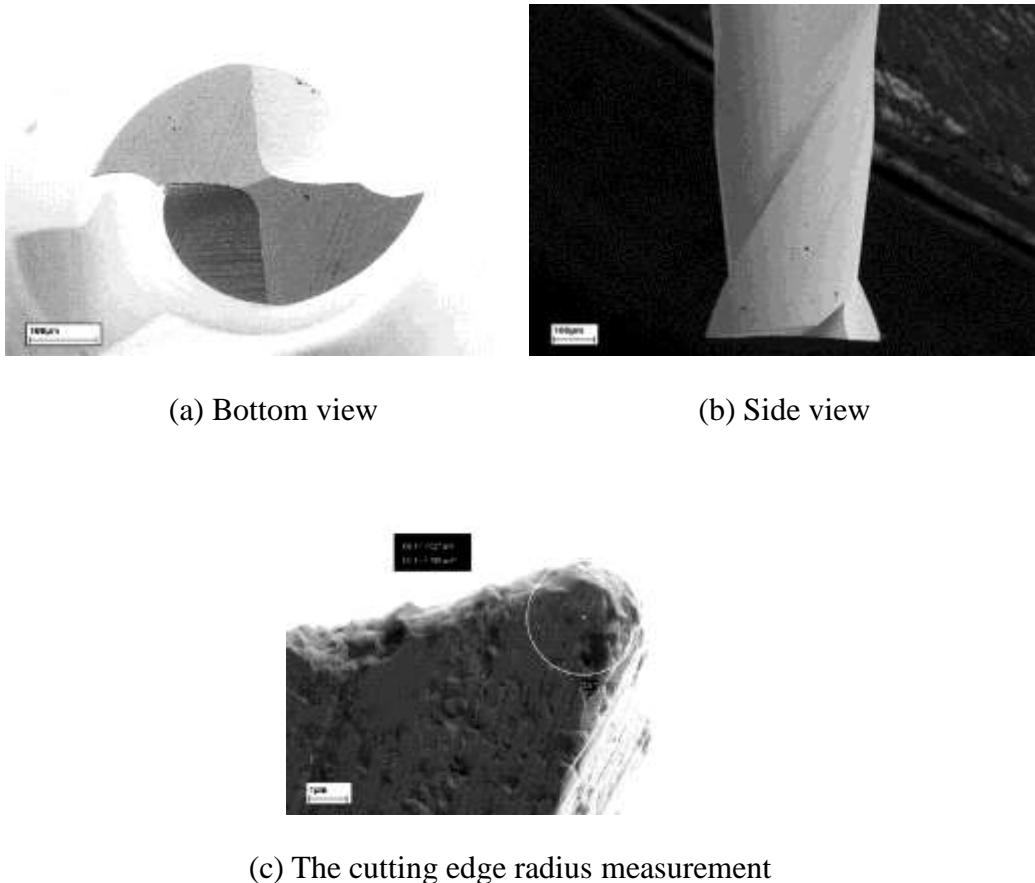
Fig. 5.1 SEM images of an uncoated micro tool

5.3.1   DLC and NCD films deposition

5.3.1.1   DLC films deposition

DLC films are coated by radio frequency plasma enhanced chemical vapour deposition

(PE-CVD) process in Diameter Ltd and the reactor and system are shown in Fig. 5.2. One of the main attributes of this process is that the thermal envelope is at near-room temperature, allowing coatings to be deposited onto thermally sensitive materials.

Fig. 5.2 PE-CVD reactor and system (Diameter Ltd)

The precursor gas is a mixture of acetylene, argon and tetramethylsilane (TMS). The ratio of argon to acetylene is adjusted by controlling the flow rate of these gases individually. Prior to deposition, the sample is ultrasonically cleaned in acetone for 15min, and transferred to vacuum chamber with a background pressure below 8×10^{-5} torr. It is then sputter-cleaned for 30min with argon at flow rate of 30sccm, pressure of 8×10^{-2} torr and a bias voltage of 370V. Subsequently, the bias voltage is adjusted to 450V and an interfacial layer is formed by adjusting argon flow rate to 10sccm, and introducing TMS with flow rate of 25sccm. This layer enhances the adhesion of the film to the carbide substrate. Once the interfacial layer is formed, acetylene gas with flow rate of 60sccm is introduced into the chamber and the rate of TMS gas flowing into the system is reduced by half to form a transition layer. The argon flow rate and bias are maintained constant for the film deposition process. After 15min, the TMS gas flowing into the system is cut off and the DLC films are deposited from argon diluted acetylene gas at a bias voltage of 450V. The coating process continues for another 15min, allowing the DLC films of approximately 2µm in thickness to be produced.

5.3.1.2   <u>NCD films deposition</u>

In the study, NCD films are seeded by hot filament chemical vapour deposition (HF-CVD) at CVD diamond lab based in the school of chemistry at Bristol University. A small hot filament reactor operating at a pressure of 100 torr (13,300 Pa) is used and the source gases are CH_4 and H_2 mixtures. Prior to coating, micro tool is cleaned as the DLC deposition process does. The sample is then dried and dipped into 100nm diamond powder to provide seed crystals. The micro tool is vertically mounted in a holder beneath a filament in the reactor chamber. The distance from the top of the micro tool to the filament is 5mm. The flow rates of CH_4 and H_2 are set to be 5sccm and 200sccm respectively, and maintain constant during the deposition process. The film growth time is 6 hours, which gives a thickness of around 2μm for the NCD coatings. The small HF-CVD reactor and system are shown in Fig.5.3.
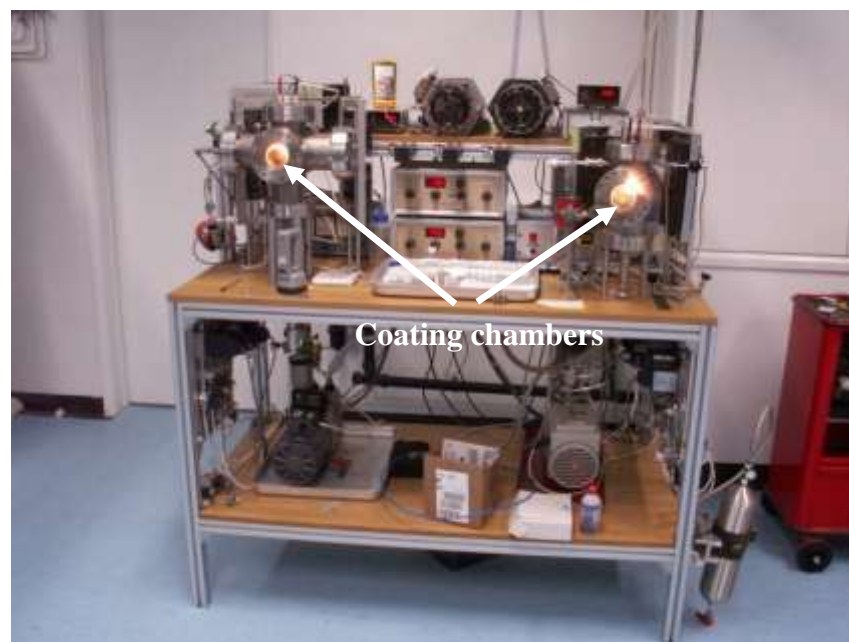
Fig. 5.3 HF-CVD reactor and system (Bristol University)

5.3.2 Characterization of the DLC and NCD films

5.3.2.1   <u>Integrity of the DLC coated micro tool</u>

Integrity of the DLC coated micro end mill is inspected and analyzed after the coating process and the SEM images of the tool together with corresponding coatings are

illustrated in Fig. 5.4.

(a) Bottom view   (b) Bottom coating surface

(c) Delamination on the tip   (d) Coating thickness measurement
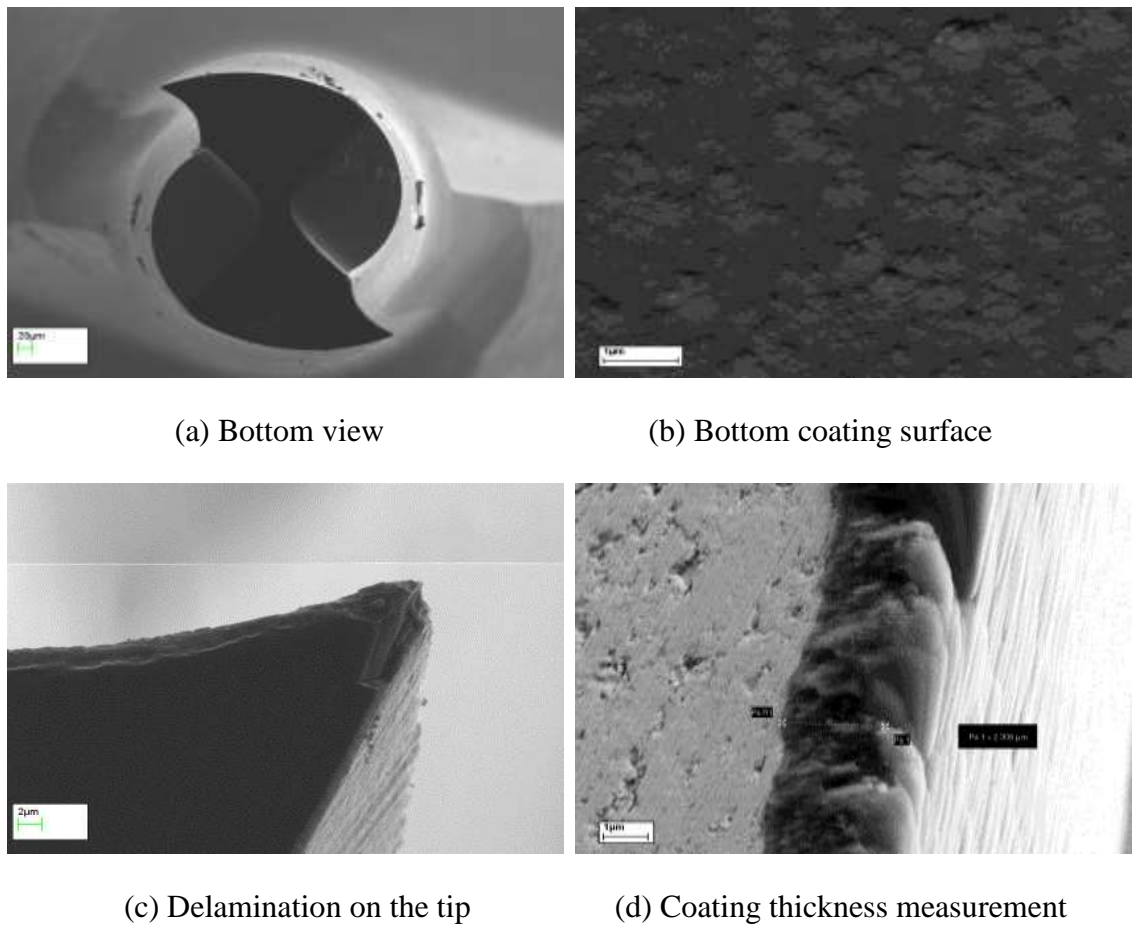
Fig. 5.4 Integrity of the DLC coated micro tool

Fig. 5.5 Zygo NewView 5000
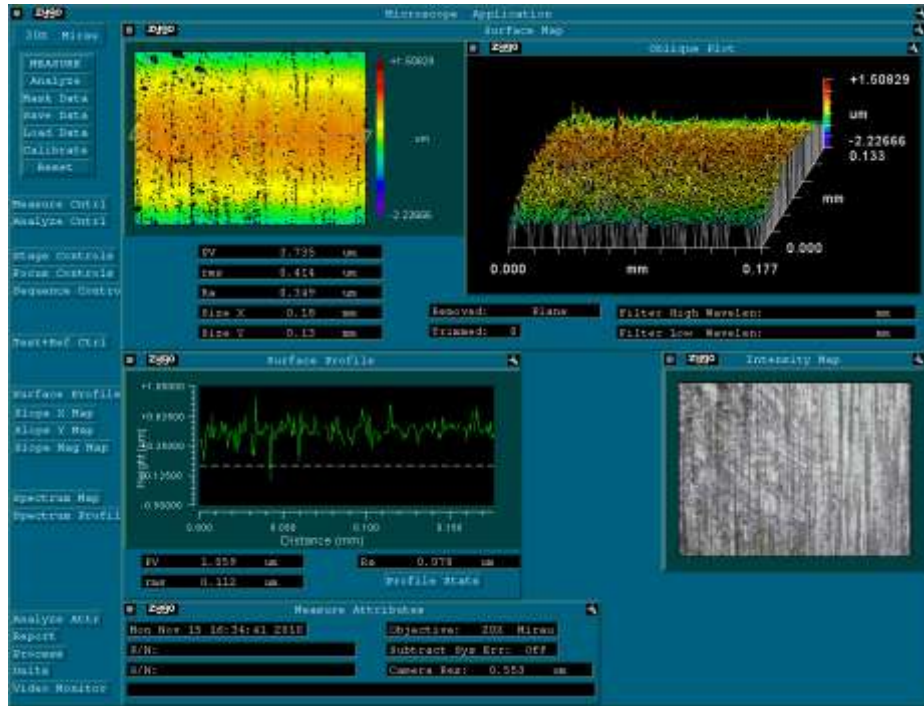
(a) Tungsten carbide micro tool (78 nm)
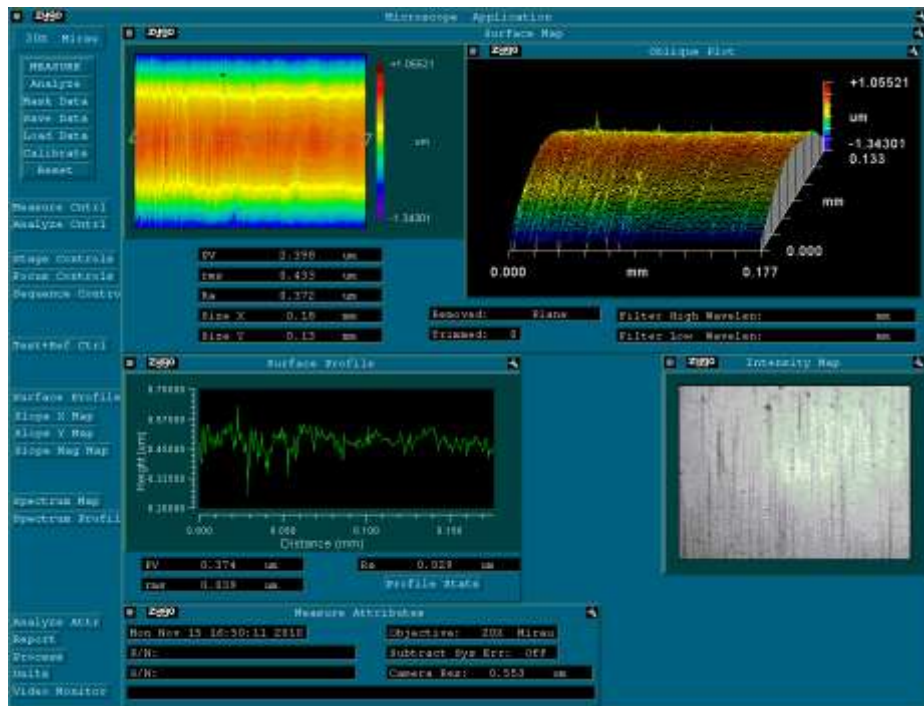
(b) DLC coated micro tool (29 nm)

Fig. 5.6 Measurement of surface roughness on the tool shanks

Due to complex geometrical configuration of micro end mills, it is quite difficult to achieve perfect seeding results. The surface of DLC coatings emerges to be fairly

smooth and the amorphous structure films adhere well to the tungsten carbide substrates, with an exception of slight delamination on the sharp edge corner, as shown in Fig. 5.4 (c). The value of measured coating thickness is around 2μm (see Fig. 5.4 (d)), which matches the estimated one based on the growth time.

The surface roughness, Ra, of DLC coatings on the tool shank is measured using a white light interferometer Zygo NewView 5000 (see Fig. 5.5). The value is 29nm compared with 78nm of an uncoated tungsten carbide micro tool, as given in Fig. 5.6.

5.3.2.2   Integrity of the NCD coated micro tool

The NCD coatings, as shown in Fig. 5.7, are consistently deposited on the tool tips and there is no observable delamination, even at the tool edges. The averaged grain size of the uniform NCD films is 0.6μm. However, larger diamond particles with around 2μm in magnitude are spotted on the tool bottom and flute surface.

(a) Bottom view   (b) Side view

(c) Tool bottom surface   (d) Tool flute surface
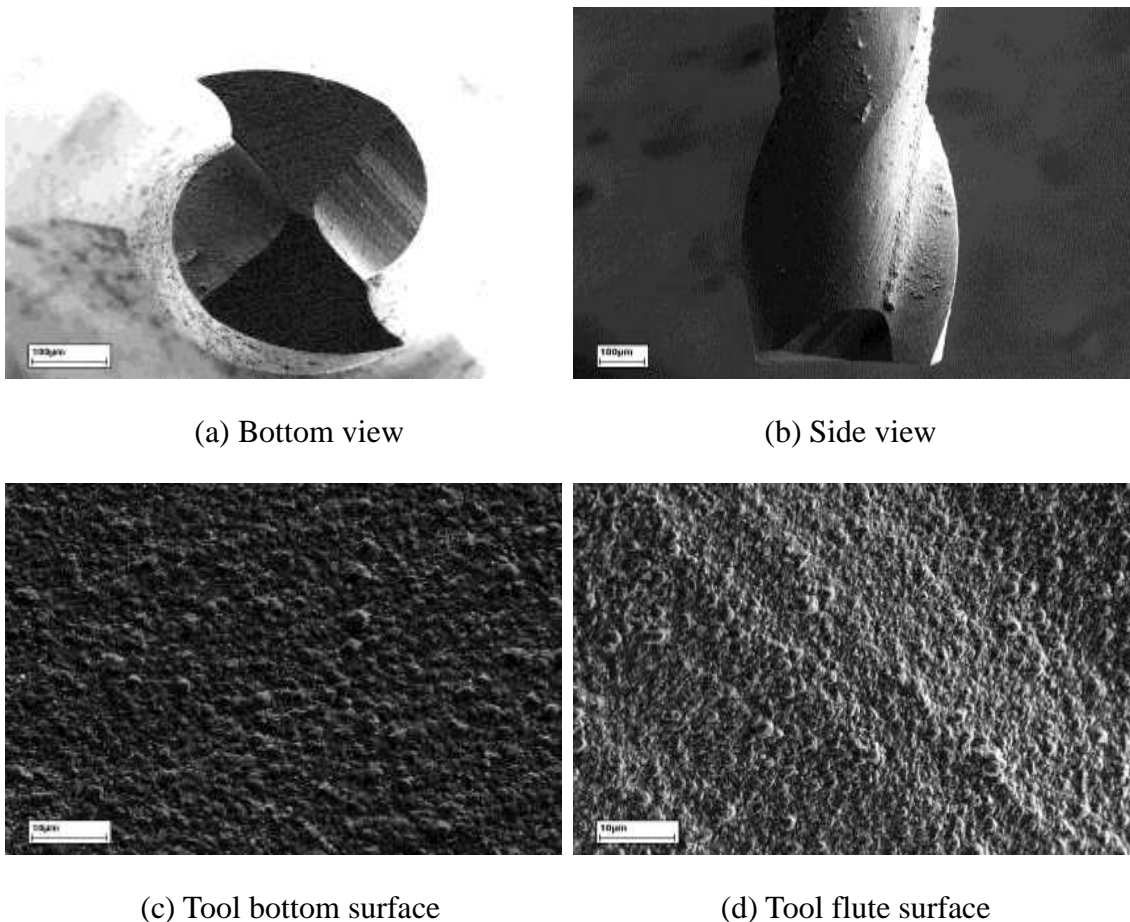
Fig. 5.7 Integrity of the NCD coated micro tool

5.4   **Micro milling trials**

Experiments for the testing are carried out on the ultra-precision machine UltraMill. Fig.5.8 illustrates the detailed experimental setup, which is similar as that in Section 3.6. Cutting forces are recorded by Kistler dynamometer MiniDyn 9256C2 with a charge amplifier 5070A. A/D data acquisition card 2855A4 is used for transferring signals to a desktop computer. A digital camera is employed to assist positioning micro cutter to the workpiece surface in Z axis direction and workpiece is mounted on the top plate of the force dynamometer by four screws.
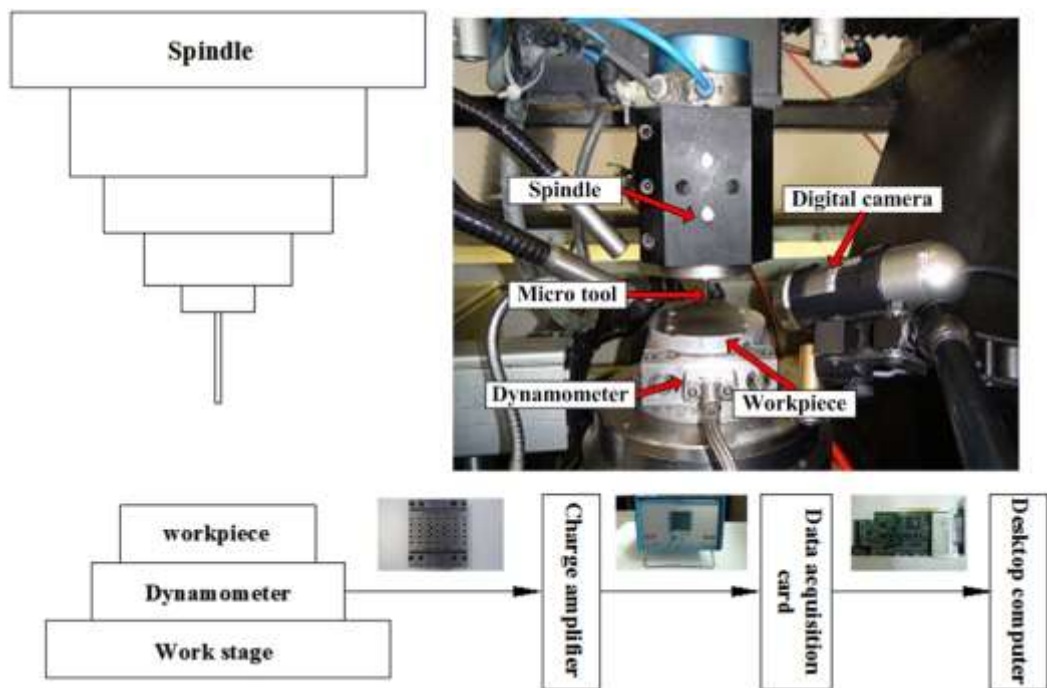
Fig. 5.8 Illustration of the experimental setup

The experiments include full immersion slot milling as illustrated in Fig. 5.9. Before conducting experiments, the top surface of the work sample is well prepared by facing with a Ø2mm diameter end mill. For each testing tool, a total cutting length of 400mm (40mm×10 slots) and 0.5mm in width is milled along –X direction and the gap between adjacent parallel slots is 1.5mm. The work material is chosen as Al 6061-T6 not only because it is suitable for various engineering applications but also no chemical affinity problems occur against the diamond coatings. The most important is that, due to ductility of the aluminium alloy, anti-adhering properties of coatings can be investigated.
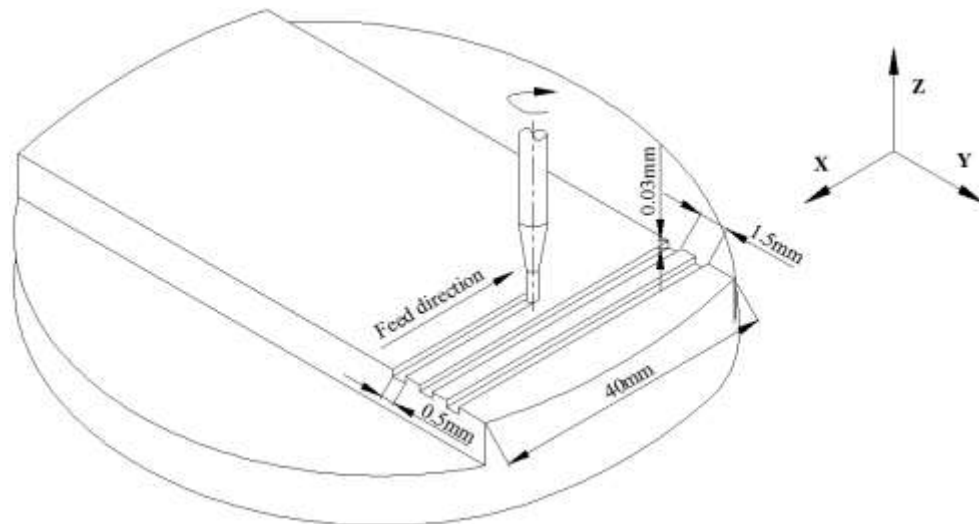
Fig. 5.9 Schematic of the micro milling experiment

The machining conditions used are shown in Table 5.1. The sequence of tests is dry cutting using an uncoated tungsten carbide tool, the DLC coated tool, the NCD coated tool and wet cutting using an uncoated tool. The process parameters, including 94.2m/min cutting speed, 30µm axial depth of cut and 0.5µm feed per tooth, are kept constant for all investigated cutting conditions. In wet cutting at the micro scale, the forces resulting from flowing fluid becomes comparable to the actual cutting forces and it cannot be neglected. To eliminate this influence on the micro force measurement, cutting fluid is sprayed and accumulates on the top surface of workpiece beforehand in wet cutting conditions. The NC codes for the experiment is manually programmed and implemented into the CNC control system of the machine. The details see Appendix V NC codes for the cutting trials in Chapter 5.

Table 5.1 Machining conditions

Work material: Al 6061-T6

Cutting tool properties (Magaforce 8507-Ø0.5):

Diameter (µm): 500

Flute number: 2

Helix angle: 30º

Materials: tungsten carbide, DLC and NCD coatings

Cutting speed (m/min): 94.2

Axial depth of cut (µm) : 30

Feed per tooth (µm): 0.5

Cutting fluid: None or mist

5.5   Results and discussions on the tooling performance

In this section, the experimental results and the associated discussions on the tooling performance are presented. The cutting forces obtained from different conditions are firstly discussed, followed by the tool integrity, surface roughness and micro-burr formation.

5.5.1 Cutting forces

Fig. 5.10 illustrates comparison of the cutting forces under four cutting conditions, including wet cutting using an uncoated tungsten carbide tool (wet WC), dry cutting using an uncoated tungsten carbide (dry WC), the DLC coated (dry DLC) and the NCD coated (dry NCD) tools.
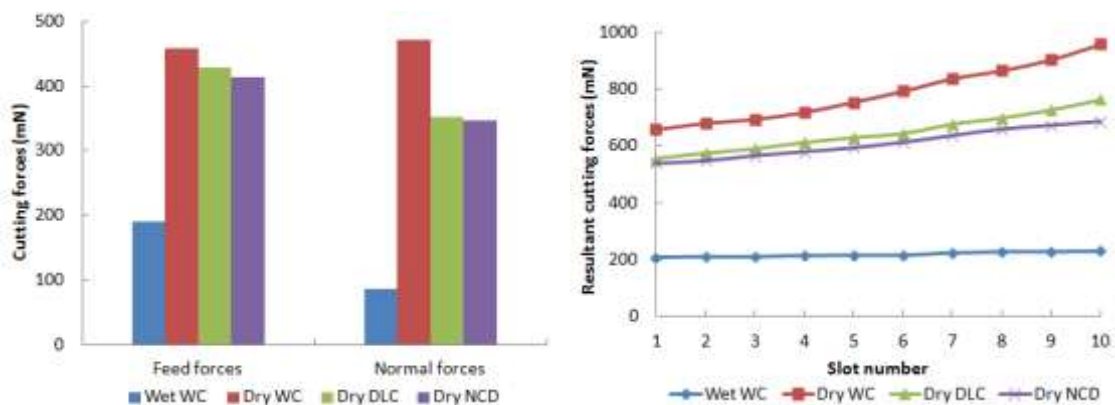
(a) Comparison of the cutting forces at the first slot (b) Comparison of the resultant cutting forces

Fig. 5.10 Cutting force comparison under different conditions

Analysis of the feed forces and normal forces at the first slot shows a slight improvement for the DLC and NCD coated tools compared with the uncoated tool in dry conditions. Dry DLC and NCD produce almost the same amount of cutting forces, which are still dramatically larger than those in wet WC, as clearly seen in Fig. 5.10 (a).

The resultant cutting forces at the beginning of each slot are plotted in Fig. 5.10 (b), and it is obviously seen that dry WC has the largest forces, followed by dry DLC and NCD, and wet WC has the least. The DLC and NCD coated micro tools can almost equally

reduce around 16% forces when compared to the uncoated tool in dry cutting conditions. In addition, the resultant cutting forces increase steadily along with increasing cutting length under dry WC, DLC and NCD cutting conditions whereas those from wet WC nearly remain constant. This phenomenon may be owing to the tool wear, resulting in enlargement of the tool cutting edge radius and leading to larger cutting forces.

5.5.2 Tool integrity

After tests, the micro tools are examined and photographed by a digital microscope Keyence VHX-1000 and the images are shown in Fig. 5.11.

(a) Dry WC   (b) Wet WC

(c) Dry DLC   (d) Dry NCD
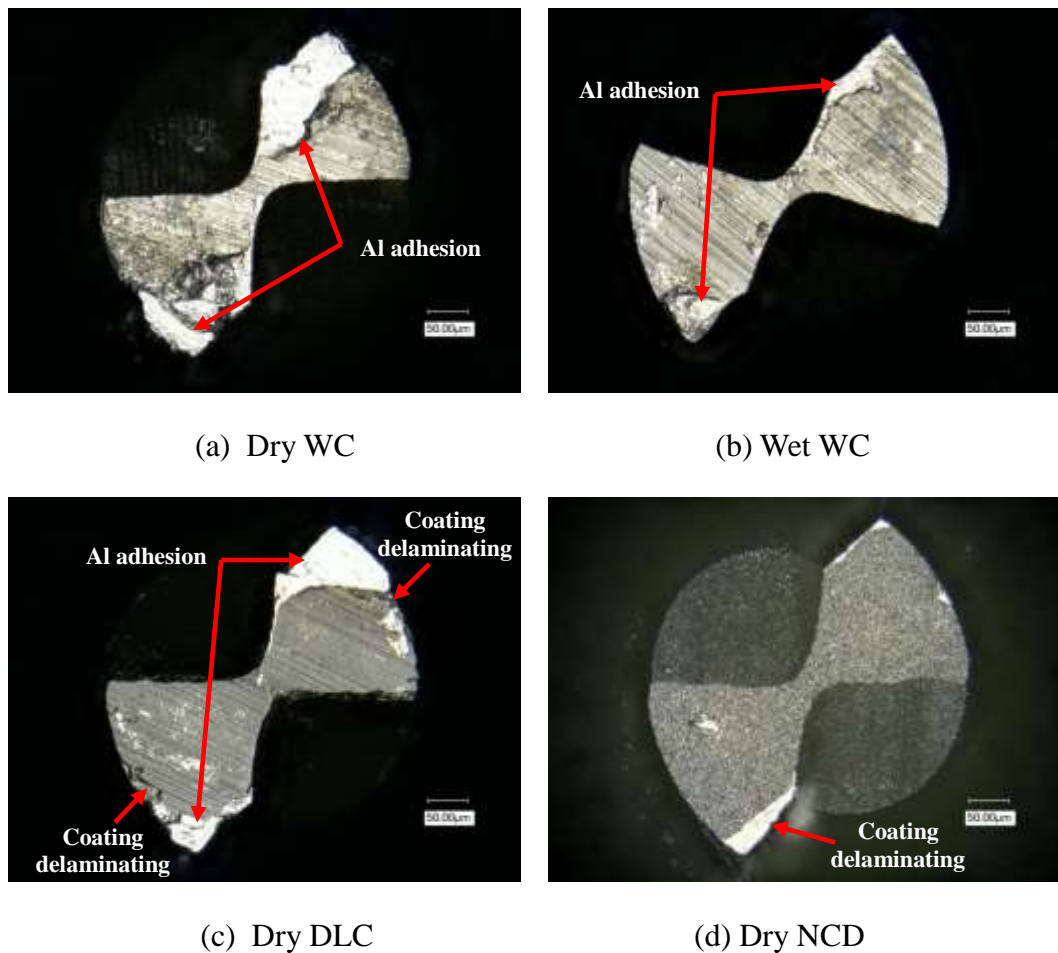
Fig. 5.11 Micro tools after the micro milling tests

There are large portions of adherent chips on the cutting edges of the uncoated micro tool in dry cutting, whereas a significant alleviation in wet cutting, as shown in Fig. 5.11 (a) and Fig. 5.11 (b) respectively. Therefore, the use of cutting fluid makes substantial

improvement with regard to less adhering. From Fig. 5.11 (c), the DLC coated tool experiences large delamination around the two tips and work material aluminium adheres to almost all the delaminating zones. The adhesion is found to be much smaller compared to that of uncoated tool in dry cutting but considerably larger when compared to that in wet cutting. The NCD coated tool does not exhibit much delamination and is almost free from chip adhesion. From this point of view, the NCD coated tool has the best performance, even when compared to that of uncoated tool in wet cutting conditions. Thus, the NCD coatings can act as an efficient interfacial layer in preventing possible chip clogging while cutting.

Tool flank wear is a common wear pattern for micro tools and it is universally used for the criterion of tool life characterization. The flank wear is measured at the bottom face of the micro tool, as shown in Fig. 5.12, and the magnitude can be expressed as:

$$h_f = h_t - h_0 \tag{5.1}$$

Where h_f — Tool flank wear;

h_t — Distance between wear point and reference line of a tool after cutting;

h_0 — Distance between tip point and reference line of a tool before cutting.
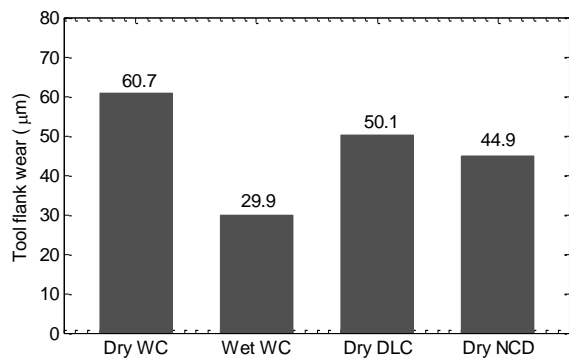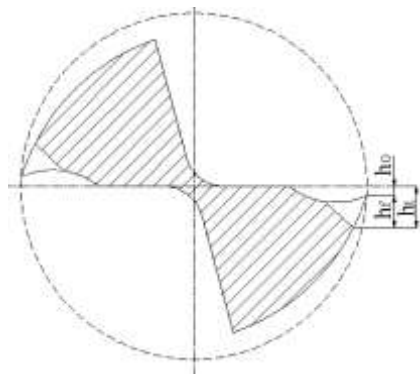
Fig. 5.12 Tool wear characterization   Fig. 5.13 Tool wear under various conditions

Comparative study of frank wear for each tool is shown in Fig.5.13, and the value of flank wear is typically in a few tens of microns under selected cutting conditions. The uncoated tool in dry cutting wears the fastest to around 60μm, and the DLC and NCD coatings respectively slow down the tool wear by approximate 17% and 25% as

compared to that. However, these distinct advantages of the two coatings cannot be comparable to that of cutting fluid as wet WC has the lowest flank wear, which is roughly half of that in dry WC conditions. Therefore, wet WC offers the best performance in reducing tool flank wear followed by dry DLC, NCD and WC respectively.

5.5.3 Surface roughness

Surface roughness is a measurable surface characteristic quantifying high frequency deviations from an ideal surface. The surface roughness at the beginning and in the middle of each micro milled channel on the bottoms is measured along the centreline using the aforementioned white light interferometer and an average value of surface roughness, Ra, is used for the analysis. Table 5.2 shows the details of measured surface roughness.

Table 5.2 Achievable surface roughness under different conditions (unit: nm)

		Dry WC	**Wet WC**	**Dry DLC**	**Dry NCD**
1st slot	Beginning	236	158	153	196
	Middle	222	143	166	190
2nd slot	Beginning	216	159	168	181
	Middle	250	153	165	187
3rd slot	Beginning	243	164	179	208
	Middle	231	162	165	195
4th slot	Beginning	273	154	188	206
	Middle	246	148	166	175
5th slot	Beginning	238	158	168	199
	Middle	259	146	160	203
6th slot	Beginning	270	159	192	191
	Middle	223	147	186	195
7th slot	Beginning	282	169	165	171
	Middle	242	157	186	194
8th slot	Beginning	255	144	192	208
	Middle	275	156	187	213
9th slot	Beginning	220	169	180	200
	Middle	276	172	179	225
10th slot	Beginning	285	169	189	221
	Middle	291	164	184	232

The surface roughness under different cutting conditions is plotted, as a function of cutting length, in Fig. 5.14. The exponential trend lines are also given in the figure. It is obviously revealed that the DLC and NCD coatings on micro tools yield better surface finish than the uncoated tool in dry cutting and poorer than the uncoated tool in wet cutting. Meanwhile, the band widths of surface roughness variations are greatly reduced when applying DLC, NCD coatings and cutting fluid. Additionally, the DLC coated tool produces slightly smoother surface compared to the NCD coated tool although it has considerable delamination and chip adhesion as discussed previously. It is also found that surface finish under the four cutting conditions has similar trend as the resultant cutting forces do, i.e. the longer cutting length, the worse machined surface quality under dry DLC, NCD and WC conditions, and there are no obvious variations for wet cutting using the uncoated tool.
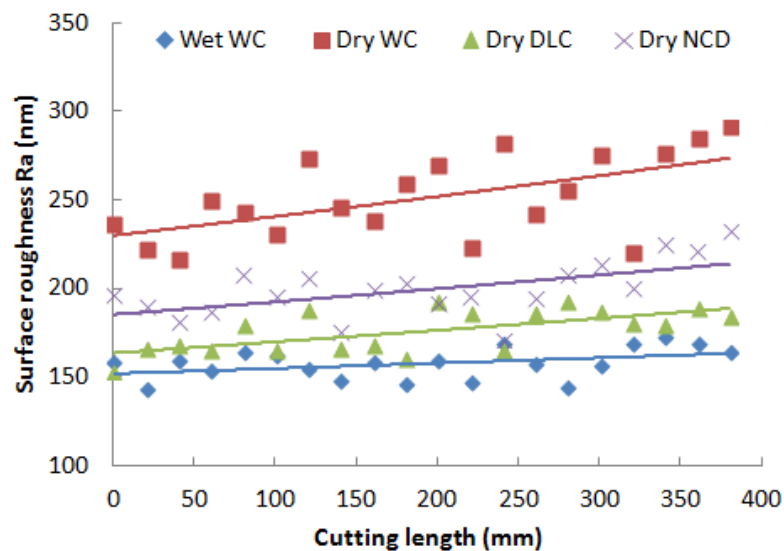
Fig. 5.14 Comparison of achievable surface roughness under different conditions

5.5.4 Micro-burr formation

In micro-scale milling, burr formation is inevitable. Burrs can be classified as entrance, exit, top and bottom burrs according to the position as well as primary, needle-like, feathery and minor burrs according to the shape and amount (Chern et al., 2007). Top burrs on micro milled channels are examined to further evaluate the tools' performance. The burrs from the beginning of each first slot using different cutting conditions are inspected and photographed by the digital microscope Keyence VHX-1000 (see Fig.

5.15), and some examples are shown in Fig. 5.16.
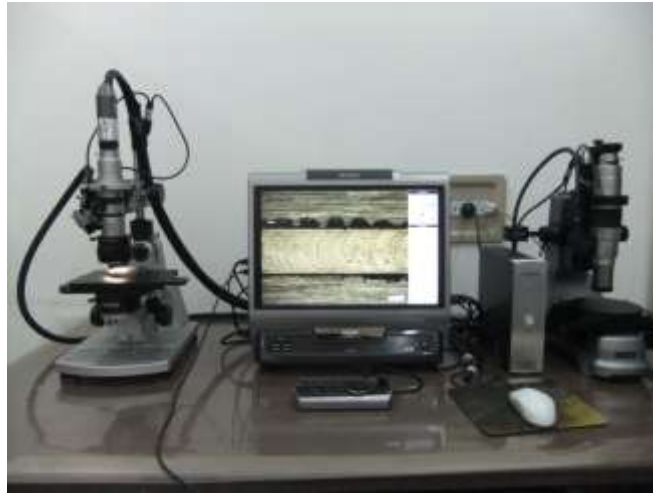
Fig. 5.15 Micro-burr formation inspected by Keyence VHX-1000

(a) Dry WC   (b) Wet WC

(c) Dry DLC   (d) Dry NCD
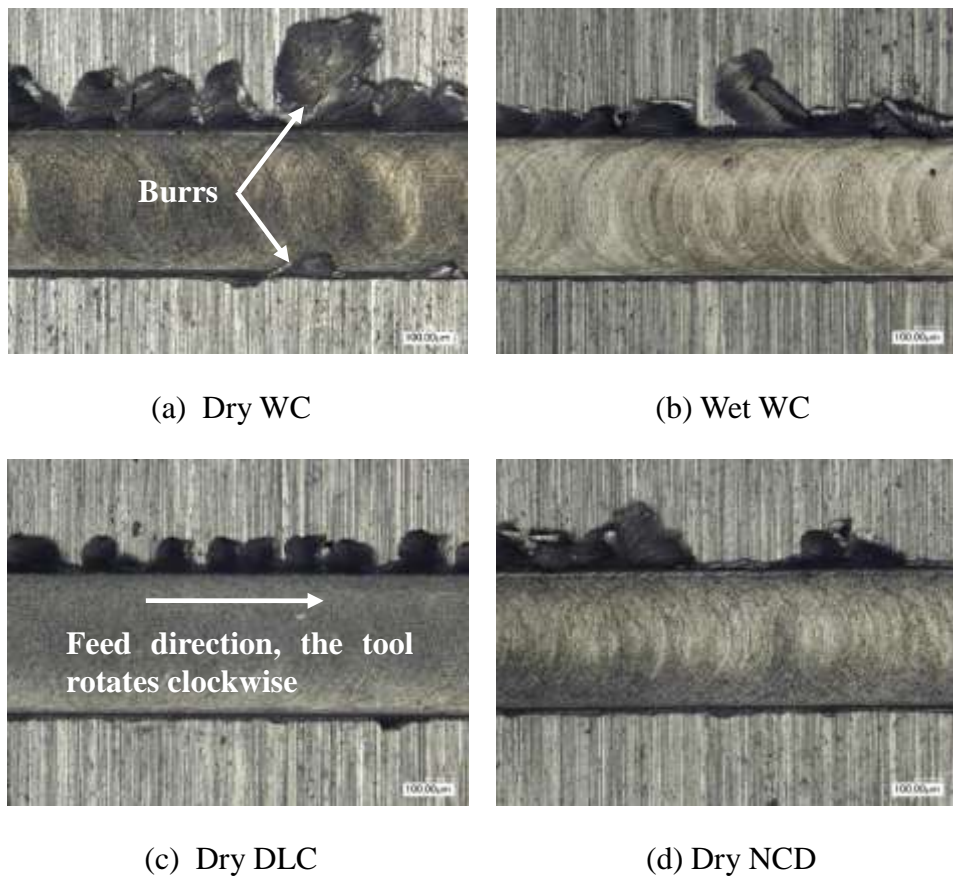
Fig. 5.16 Examples of micro-burr formation under different conditions

Due to ductility of work material, the feather-like burrs are found to be dramatically larger on the top entrance side and negligible on the top exit side under all investigated

conditions. The DLC coated tool in dry cutting and the uncoated tool in wet cutting produce roughly the same and the smallest burrs, and the uncoated tool in dry cutting the biggest. The non-uniform burrs resulting from the NCD coated tool are found slightly larger than the uniform ones produced from the DLC coated tool and the non-uniformity indicates it is possible and promising to further minimize the burrs by optimization of NCD coatings.

5.6 Conclusions

This chapter presents an evaluation of DLC and NCD coatings on ϕ500µm diameter micro end mills in micro machining of Al 6061-T6. The DLC and NCD coated tools in dry cutting together with uncoated tungsten carbide tools in both dry and wet cutting are utilized to create full immersion slots and respective tooling performance including cutting forces, tool integrity, surface finish and micro-burr formation are investigated, compared and discussed. The following conclusions can be drawn from this work:

1. The use of DLC and NCD coatings on micro tools almost equally reduce roughly 16% of cutting forces as compared to the uncoated tool in dry cutting conditions. The performance of these coatings cannot be comparable to influence of cutting fluid which reduces the forces significantly.

2. The DLC coated tool has large portions of aluminium covering on the delaminating area whereas the NCD coated tool has less delamination and is free from chip adhesion.

3. The DLC and NCD coatings help reduce approximately 17% and 25% of the tool flank wear in dry cutting conditions. The performance is still unreachable to the impact from cutting fluid with respect to the reduction of tool wear.

4. Both DLC and NCD coatings facilitate smoother machined surface and the DLC coatings perform better between the two.

5. Applying DLC and NCD coatings on micro tools can minimize burr formation and the DLC coated tool offers the best results among all investigated conditions.

According to above conclusions, major improvements such as reduced cutting forces, lessened chip adhesion, lower tool wear and improved surface roughness as well as smaller burr size can benefit from the DLC and NCD coatings, although the positive impact of these coatings is still weaker than that of cutting fluid. Because of important environmental and economic benefits for dry cutting, it is more desirable and promising to apply DLC and NCD coatings rather than cutting fluid on micro tools in promoting the tooling performance for industrial applications. In addition, the NCD coated tool performs better than the DLC coated tool in terms of coating delaminating, chip adhesion and tool wear, but slightly worse in surface roughness and burr formation. Due to the coating delaminating problems, the DLC coatings in particular, further studies need to be done to optimize the coating conditions so as to enhance bonding strength upon tungsten carbide to meet sustainable manufacturing requirements.

Chapter 6 Influence of Coatings on the Tooling Performance in Micro Cutting

6.1 Introduction

In the former chapter, the performance of DLC and NCD coatings on micro tools has been experimentally studied. It is realized that the use of appropriate coatings can enhance the tooling performance. In this chapter, the coating performance will be further explored and discussed by means of plane-strain FEM.

6.2 Motivation

According to the conclusions from Chapter 5, the DLC and NCD coatings help reduce the chip loads by roughly 16% in dry conditions. However, the advantages achieved are not quite distinctive as expected. Four main possible reasons, as listed in the following, may compromise the cutting performance of micro tools:

1. Partial coating delaminating: Due to the coating delaminating problem, direct contact of chips over the tool substrate appears. And this leads to the increase of friction at the tool-chip and tool-work interfaces, corresponding cutting forces rise accordingly.

2. Chip adhesion: Chip adhesion makes interface contact scheme more complicated. Although sliding mechanism is suitable for low speed cutting, it is inevitable that shearing occurs when chip adhesion is present.

3. Higher coating friction: Although diamond coatings have nominal friction coefficient in the range of 0.1 to 0.2, different deposition conditions or

techniques can result in higher and unstable friction coefficient, which has a direct impact on the cutting forces.

4. The tool cutting edge radius enlargement: Coating thickness would significantly increase the tool cutting edge radius by a few microns, which might change the whole process physics. Based on the simulation results from Chapter 4, the cutting edge radius has the most significant effect on the cutting forces and the larger cutting edge radius, the higher cutting forces. Therefore, coating thickness at the tool edge corners leads to negative effect on the micro machining performance, although the use of coatings has positive influence in terms of good wear resistance and low cutting friction.

From above analysis, all four aspects would more or less affect the cutting performance of coated micro tools. The coating delaminating problem can be well solved by optimized coating conditions or techniques and if no delaminating problem exists, chip adhesion phenomenon can hardly be present, as demonstrated in Fig.5.11 (d). However, in practice, the tool-chip or tool-work interface friction parameters cannot be fairly controlled by proper coating process. The characteristics of friction are mainly dependent on the coating quality, such as coating grain size, grain bonding strength, coating surface smoothness, etc. Besides, the tool cutting edge radius enlargement is unavoidable when the coatings are in good coverage around the tool edge corners.

Comprehensive understandings of the tooling behaviours under various coating circumstances is indispensible for choosing optimum coating conditions so as for improving cutting tool designs. Therefore, it is essential to compare the cutting performance of coated tools with that of uncoated tools, as well as to evaluate the tooling performance under different coating conditions.

6.3   Investigation approach

With the enhancement of computing technology and the development of tailored commercial simulation software, the use of computer to support modelling of cutting becomes more cost-effective and convenient. FEM is adopted in the research as experimental method is quite expensive and time-consuming, whereas mechanistic

modelling method presents great challenge under the complicated coating conditions. The main strength of FEM is to be able to predict cutting forces, chip formation and distribution of tool stresses and temperatures under various cutting conditions.

Metal cutting can be regarded as a process where large deformations are highly concentrated in a small region. In the current research, coatings and corresponding performance rather than the tool geometry are the main focus. Hence, 2D orthogonal plane-strain simulations, which are regarded as the foundations of practical cutting process, are carried out to simplify the analysis. The implicit numerical code DEFORM^{TM}-2D based on an updated Lagrangian formulation, from Scientific Forming Technologies Corporation (SFTC), is used to simulate the cutting process. The process simulation system is designed to analyze 2D flow of various metal forming processes, and it has similar features and capabilities as previously introduced package DEFORM^{TM}-3D.

6.4 **Finite element modelling**

In this section, modelling and simulation of orthogonal cutting using both uncoated WC and coated tools are presented. As NCD films have similar properties and performance as those of DLC coatings, only DLC films without any delaminating and have uniform microstructures are taken into consideration.

6.4.1 Simulation developments

6.4.1.1 Tool modelling, meshing and boundary conditions

An uncoated tungsten carbide tool Magaforce 8507-Ø0.5 mm is used for the benchmarking modelling. The tool geometries including 15.8º rake angle, 23º relief angle and 1.5µm cutting edge radius, are measured by FE-SEM, as shown in Fig. 6.1. If the tool is deposited with DLC films in 2µm thickness and the integrity maintains well, the cutting edge radius becomes 3.5µm.

The cutting tips of both uncoated and DLC coated tools are modelled and meshed using the simulation software, as shown in Fig.6.2. Four-node quadrilateral elements and a fine density window near the cutting points with 0.1 size ratio are used for the meshing.

Approximatly 1500 and 2100 elements are generated for the uncoated and DLC coated tool models respectively. Heat exhange with the environment are defined on the tool rake surface, cutting edges and relief surface for the thermal boundary conditions.

| (a) Rake angle | (b) Relief angle |
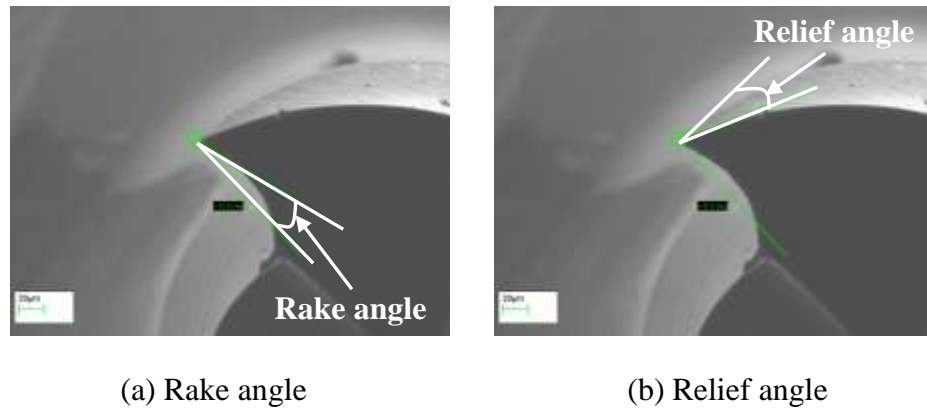
Fig. 6.1 Measurement of the tool geometries

| (a) The uncoated tool | (b) The DLC coated tool |
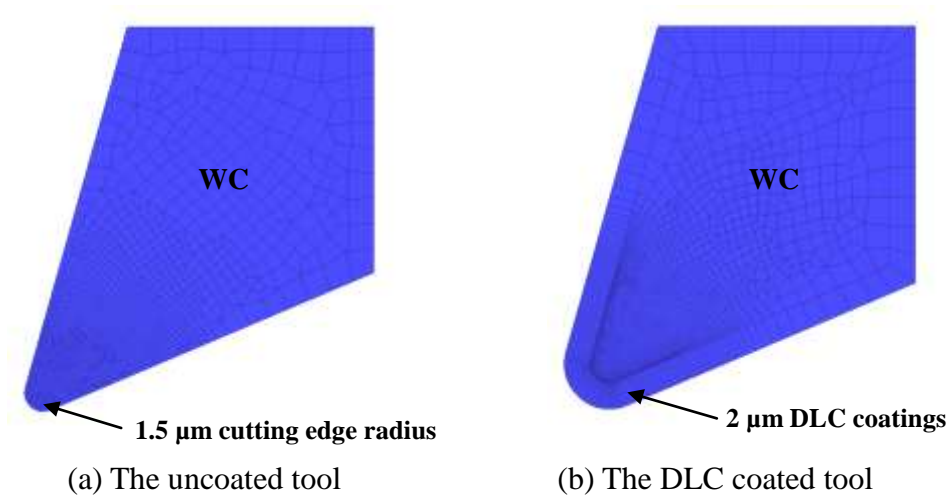
Fig. 6.2 Models and meshing of the uncoated and DLC coated tool tips

6.4.1.2   Workpiece modelling, meshing and boundary conditions

The workpiece is modelled in rectangle shape with 0.08mm in width and 0.02mm in height, as illustrated in Fig. 6.3. It is worth noting that the cutting width of the model is unit '1' mm. With the support of 0.1 size ratio density window, the contact region is highly meshed with the smallest element size reaches around 150nm. During the simulations, the window follows the movement of the cutting tool to ensure finest elements near the tool-chip and tool-work interfaces. The total number of meshing elements inside the initial workpiece model is 4061. The left and bottom surfaces are

fixed with no displacement in the X and Y directions, and heat exchange with environment is predefined on the top and right surfaces.

The initial positions of the tool and workpiece models are also given in Fig. 6.3. The tool has a constant velocity of 94.2m/min along the X direction, which is based on the cutting conditions used in Chapter 5.
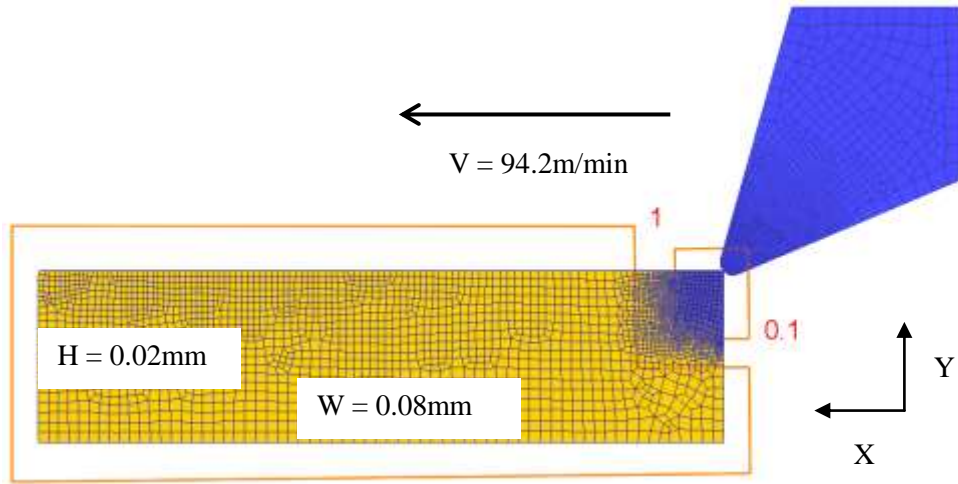
Fig. 6.3 Workpiece modelling, meshing and boundary conditions

6.4.1.3   Workpiece material flow stress model

The workpiece material used is Al 6061-T6. Johnson-Cook model is adopted to represent the flow stress of the material due to its good fit for strain-hardening and thermal softening behavior of metals and its numerical robustness, and it can be easily used in finite element simulation models (Wang et al., 2009). The material constants for the model are listed in Table 6.1,

Table 6.1 Al 6061-T6 constants for Johnson-Cook model (Johnson et al., 1996)

A (MPa)	B (MPa)	C	m	n	T_{melt} (K)	T_{room} (K)
324	114	0.002	1.34	0.42	855	293

6.4.1.4   Summary of simulation inputs

The sliding friction based on Coulomb's law is dominat in micro milling due to

ralatively low cutting speed. The friction factor between tungsten carbide and Al 6061-T6 is chosen as 0.7, obtained from the experiments by Medaska et al.(Medaska et al., 1999). And the friction value between DLC coatings and the work material is 0.1, which is recommended by Diameter Ltd. The mechanical and thermal properties of tungsten cabide, DLC coatings and workpiece material are given in Table 6.2.

Table 6.2 Material properties of tungsten carbide, DLC coatings and workpiece

	Substrate	**Coating**	**Workpiece**
Materials	WC	DLC	Al 6061 T6
Young's modulus (GPa)	690	120	68.9
Poisson's ratio	0.24	0.2	0.33
Thermal expansion (µm)	5.2	1.2	23.6
Thermal conductivity (W/m/K)	84.02	500	167
Heat capacity (J/Kg/K)	203	510	896
Emissivity	0.45	0.9	0.25

6.4.1.5   Simulation setup

In order to reduce computational complexity and save simulation time, the cutting tool is modelled as a rigid body with heat transfer capability, and the deformation of workpiece is treated elastic-plastically with isotropic strain hardening. The time increment for each step is $3 \times e^{-8}$ sec and the simulation is interrupted when the process time reaches $3 \times e^{-5}$ sec. Therefore, roughly 1000 steps are calculated. An adaptive remeshing without manual interruption is triggered when the interface depth is beyond $8 \times e^{-5}$ mm so as to avoid excessive distortion of the elements in the primary and secondary cutting zones. The environment temperature is assigned to be 20ºC, and the heat transfer with workpiece is implemented with a constant convection coefficient of 0.02 N/sec/mm/ ºC.

6.5   Tooling performance for the uncoated and DLC coated tools

In the following, the simulation results at constant and various uncut chip thickness (UCT) for the both uncoated and DLC coated tools, such as chip formation, cutting forces and tool temperatures, are extracted and compared for comprehensive

investigation of respective tooling performance.

6.5.1 Predicted tooling performance at constant UCT

6.5.1.1 Chip formation

Fig. 6.4 shows the predicted chip formation process using the uncoated and DLC coated tools at 0.5µm UCT and velocity of 1570.8 mm/sec.
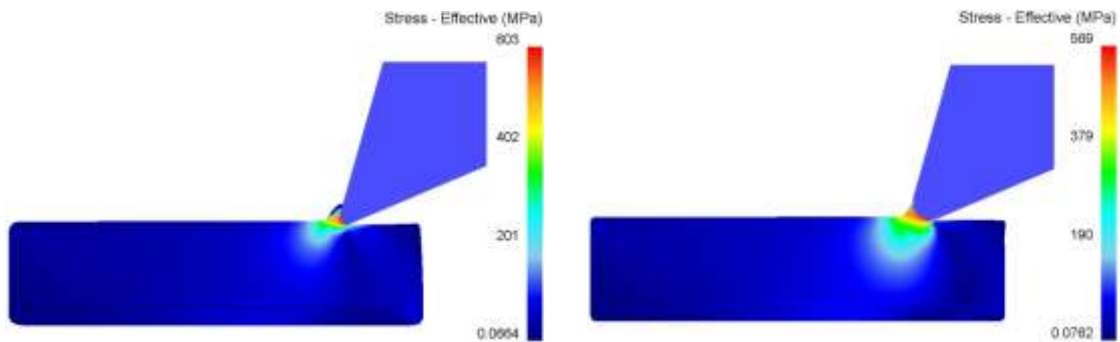
(a) Cutting time: $1\times e^{-5}$ sec (cutting distance: 0.0157mm)
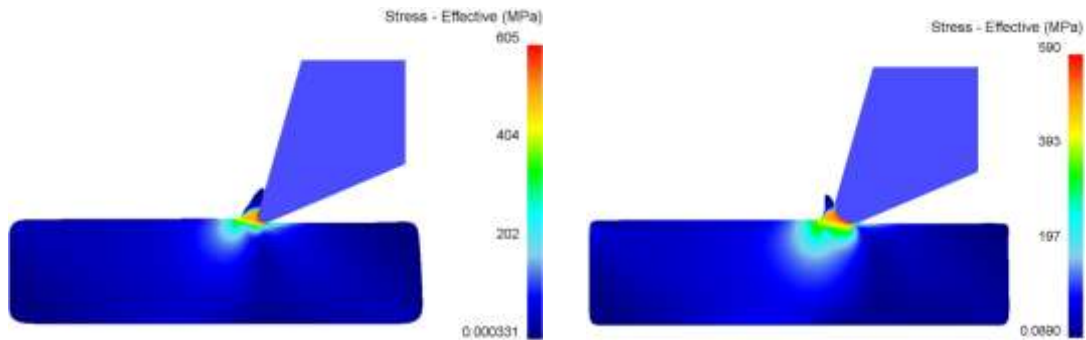
(b) Cutting time: $2\times e^{-5}$ sec (cutting distance: 0.0314mm)
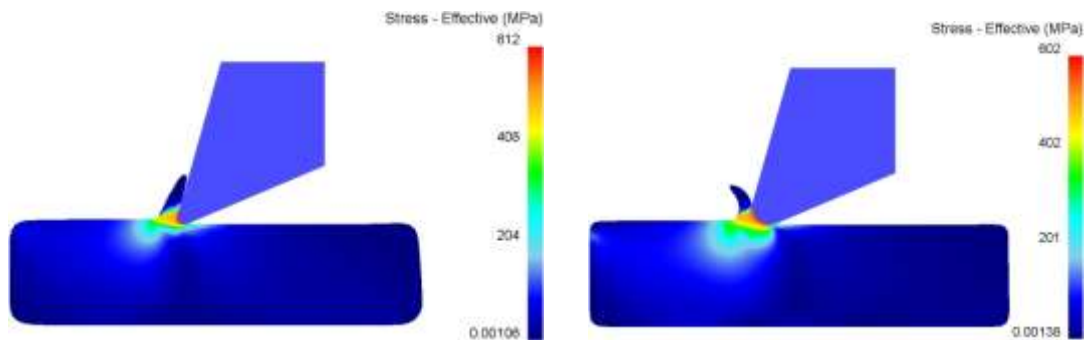
(c) Cutting time: $3\times e^{-5}$ sec (cutting distance: 0.0471mm)

Fig. 6.4 Predicted chip formation under the uncoated and coated tools at different

cutting time

After $1 \times e^{-5}$ sec cutting, as seen from Fig. 6.4 (a), chip begins to be formed for the uncoated tool whereas ploughing phenomenon is found for the DLC coated tool due to the larger cutting edge radius. According to Fig. 6.4 (b-c), the chips produced by the uncoated tool flow along the tool rake surface and have less deformation. For the coated tool, the well-known size effects play a significant role as chips are pushed away from the tool rake surface as a result of the tool negative rake angle effect.

6.5.1.2   Cutting forces

The variations of simulated feed and normal force components with respect to cutting distance using different tools are shown in Fig.6.5. The feed and normal forces refer to the cutting forces in the horizontal and vertical directions respectively.
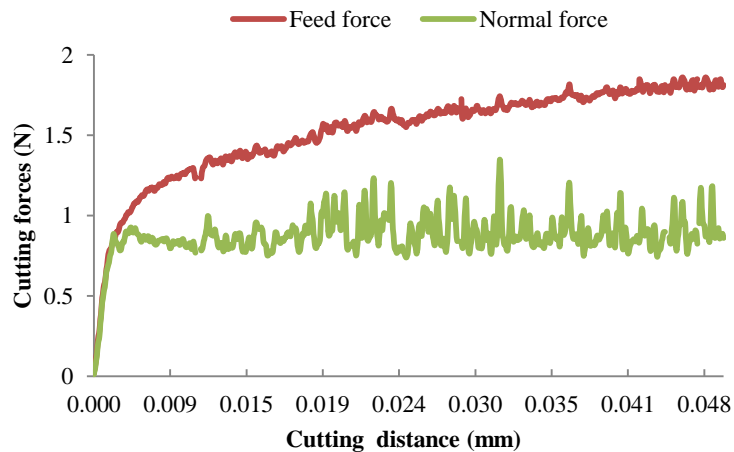
(a) The uncoated tool
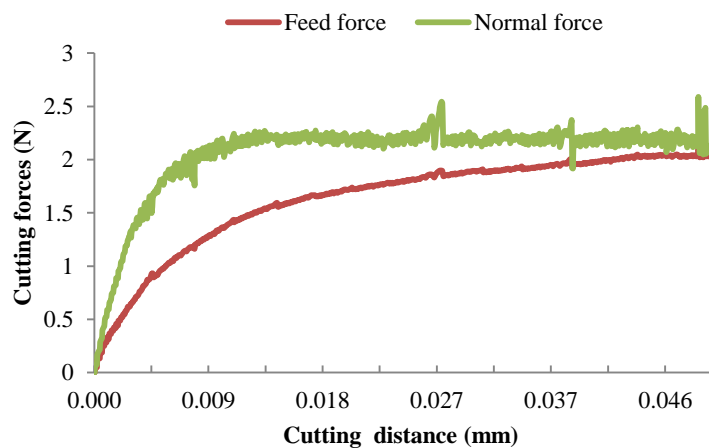
(b) The DLC coated tool

Fig. 6.5 The variations of predicted forces using the uncoated and coated tools

For the both uncoated and coated tools before around 0.04mm travel stroke, the longer cutting distance, the larger feed loads, whereas the normal forces almost remain constant after an initial cutting distance. After 0.04mm, the slopes of feed forces become almost level, thus it is assumed that the cutting has reached the steady state at $3 \times e^{-5}$ sec cutting (0.471mm). The averaged feed and normal force components for the uncoated tool are predicted to be 1.86N and 0.925N, respectively, as compared with 2.03N and 2.19N for the DLC coated tool. Hence, the DLC coated tool has the lager resultant cutting forces, which means the benefit of reduced cutting friction cannot complete offset the negative effect of the cutting edge radius enlargement. From Fig.6.5 (b), the magnitude of normal force surpasses that of feed force, indicating that compression rather than shearing becomes dominant with the increase of cutting edge radius under the specified UCT.

6.5.1.3   Tool stresses and temperatures

Predicted tool stresses and temperatures at $3 \times e^{-5}$ sec cutting under different tools are given in Fig. 6.6 and Fig. 6.7 respectively.
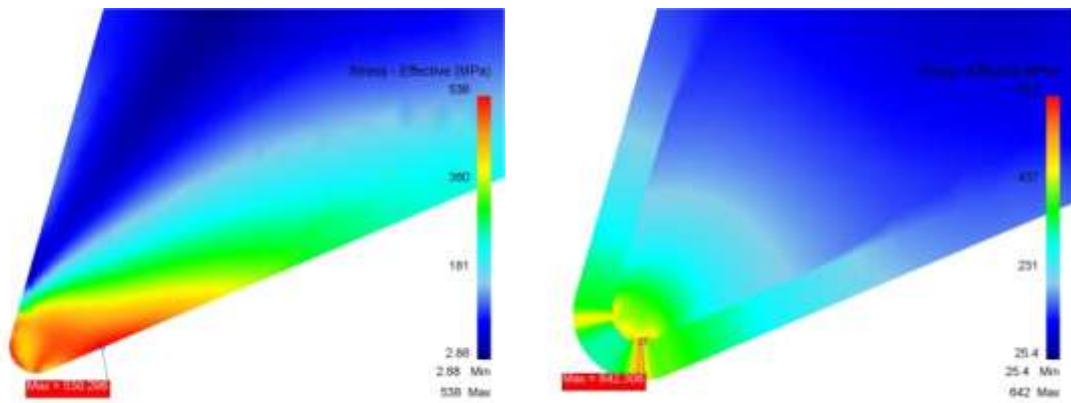
(a) The uncoated tool   (b) The DLC coated tool

Fig. 6.6 Predicted tool stresses at $3 \times e^{-5}$ sec cutting under different tools

The tools are defined as elastic bodies for the stress prediction. As described in the force prediction section, the feed force is two times larger than the normal force for the uncoated tool, but the values become comparable for the DLC coated tool. Therefore, the highest tool stress is located on the relief surface for the uncoated tool, whereas

around edge radius area for the coated tool, as demonstrated in Fig. 6.6. The highest stress (642Mpa) for the DLC coated tool lies at the DLC-WC interface and it is larger than that (538MPa) of the uncoated tool due to the larger cutting load. Hence, coatings are prone to be delaminating and high bonding strength to the substrate is essential for maintaining the integrity of coated tools so as for promoting sustainable cutting operations.

(a) The uncoated tool   (b) The DLC coated tool
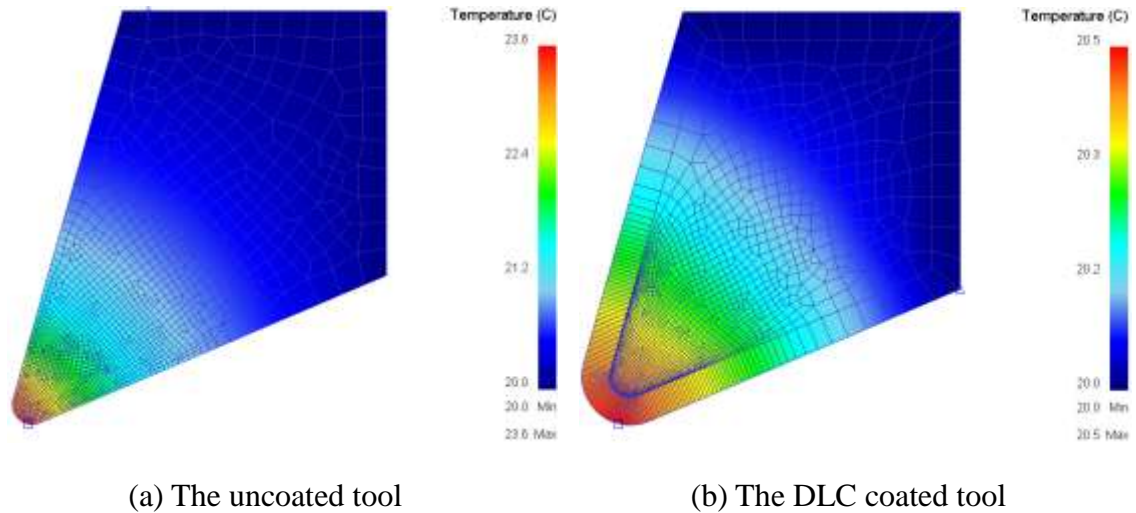
Fig. 6.7 Predicted tool temperatures at $3 \times e^{-5}$ sec cutting under different tools

Temperatures in the primary and secondary cutting zones in the workpiece are predicted to be around 29-35°C using the uncoated and DLC coated tools. From Fig. 6.7, it is observed that the highest tool temperatures are located near the tool-work rather than the tool-chip interface, and the value on the coated tool (20.5°C) is much lower than that on the uncoated tool (23.6°C). Two possible reasons, including high thermal conductivity for the coatings and low cutting friction, might directly associated with the advantage. In order to identify this, two additional simulations are performed, one is using an uncoated tool with 3.5µm cutting edge radius and another is using a virtual DLC coated tool with 0.7 coating friction coefficient to the workpiece.

Fig. 6.8 shows predicted tool temperature distribution at $3 \times e^{-5}$ sec cutting using the virtual uncoated and coated tools. For the virtual uncoated tool, as compared with Fig. 6.7(a), it is clearly seen that, with the increase in the tool cutting edge radius from 1.5µm to 3.5µm, the highest tool temperature rise slightly from 23.6°C to 24.5°C, although thermal conductivity region also increases for the more blunt tool.

(a) The virtual uncoated tool   (b) The virtual coated tool
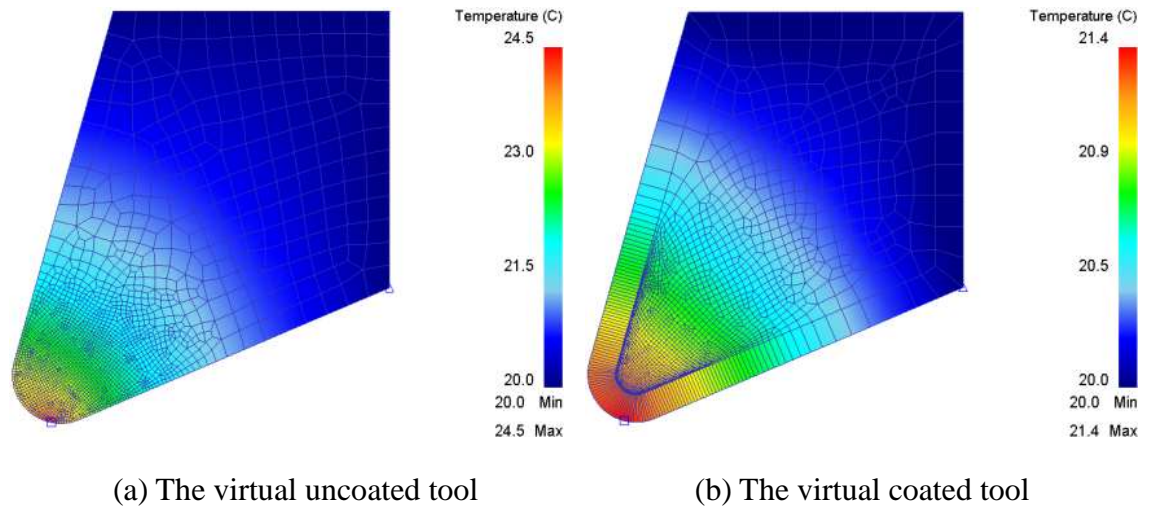
Fig. 6.8 Predicted tool temperatures at $3 \times e^{-5}$ sec cutting under the virtual tools

The tools used in Fig. 6.8 and Fig. 6.7(b) have the same geometries. Predicted maximum tool temperature reduces from 24.5°C to 21.4°C due to the high thermal conductivity of coatings, and further reduction to 20.5°C can be achieved when the friction parameter decreases from 0.7 to 0.1. Therefore, both cutting friction and coating thermal conductivity play an important role on the reduction of heat generation. As tool failure can be due to temperature-dependent accelerated wear rate, appropriate coatings can be employed as effective layers for preventing the tool abrasive wear.

6.5.2 Predicted tooling performance at various UCT

In this section, the UCT is varied at 0.1µm, 0.25µm, 0.5µm, 0.75µm, 1.0µm, 1.5µm, 2.5µm, 3.5µm and 5.0µm respectively at a constant velocity of 1570.8mm/sec. The wide range of UCT is chosen based on the values of feed per tooth used for practical micro milling operations. The simulated data are obtained after $3 \times e^{-5}$ sec cutting for further investigation of the tooling performance.

6.5.2.1   Chip formation

Comparison of the chip formation under different UCT is given in Fig. 6.9.

For the 0.1µm UCT, ploughing dominates the cutting mechanism for both tools and no chips are formed. Complete chips are generated since 0.25µm UCT for the uncoated tool, and 0.5µm UCT for the DLC coated tool. Hence, it is revealed that the lager

cutting edge radius of tools, the higher minimum chip thickness.

(a) 0.1μm UCT
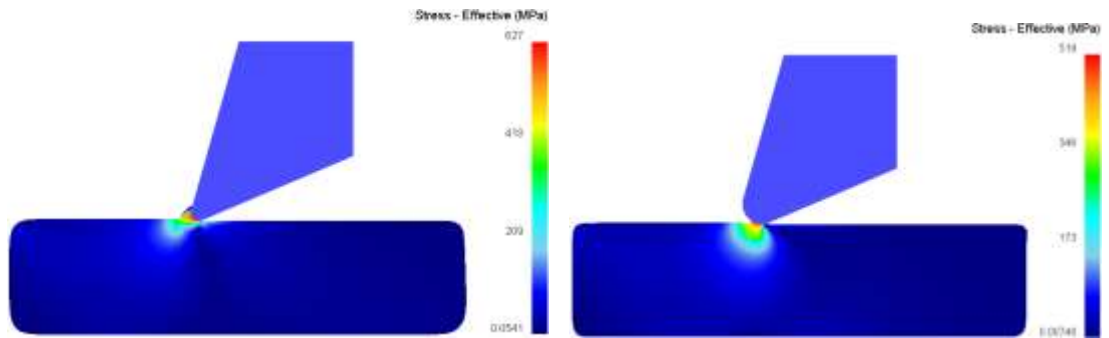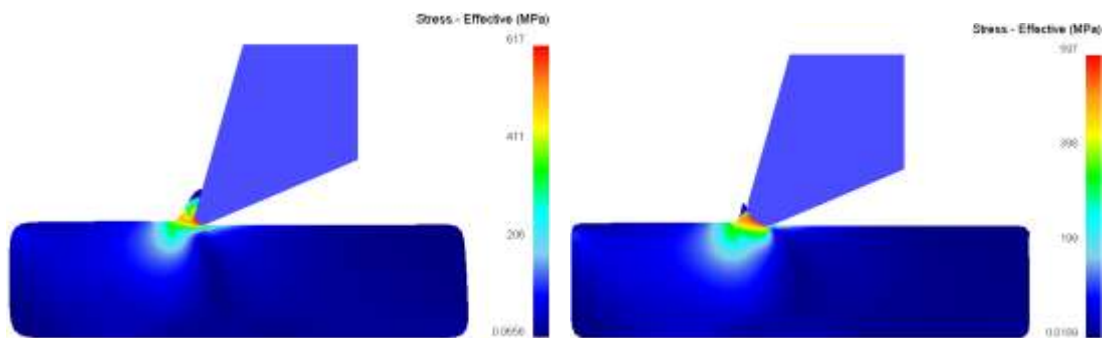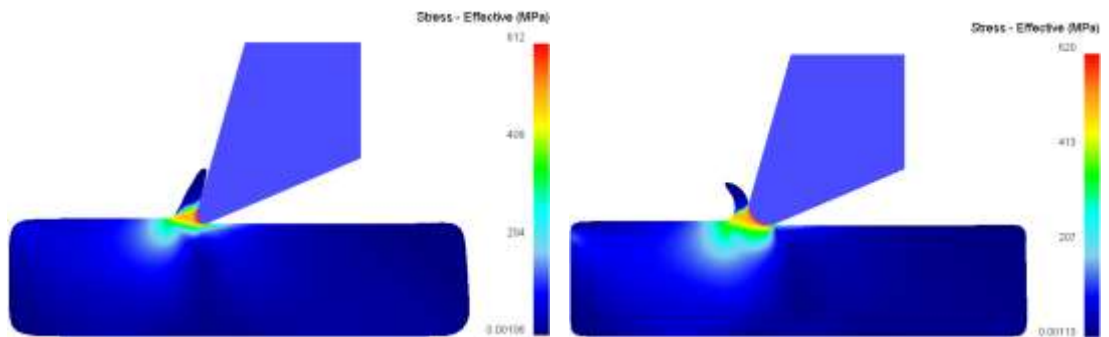
(b) 0.25μm UCT
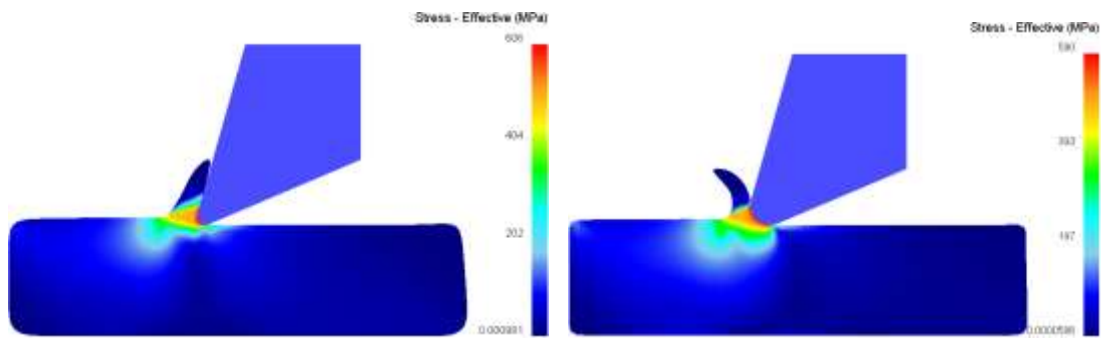
(c) 0.5μm UCT

(d) 0.75μm UCT
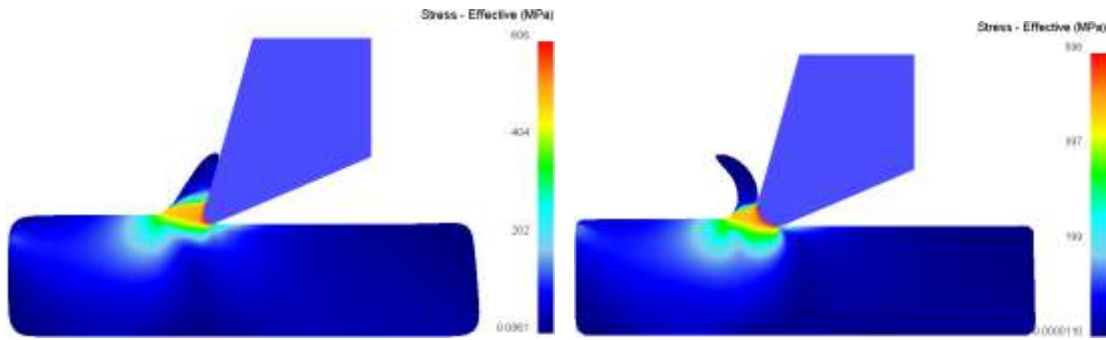
(e) 1.0μm UCT
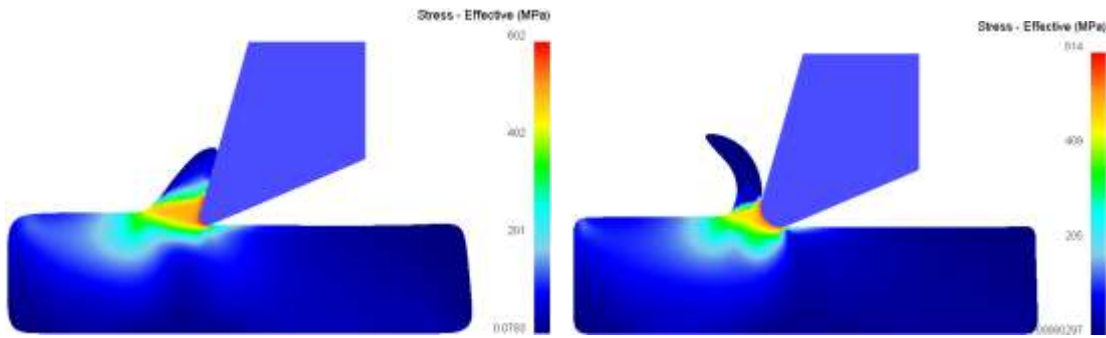
(f) 1.5μm UCT
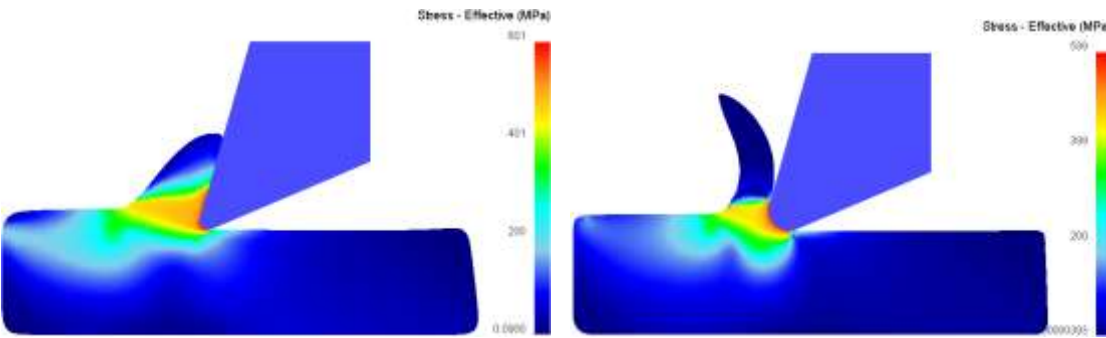
(g) 2.5μm UCT
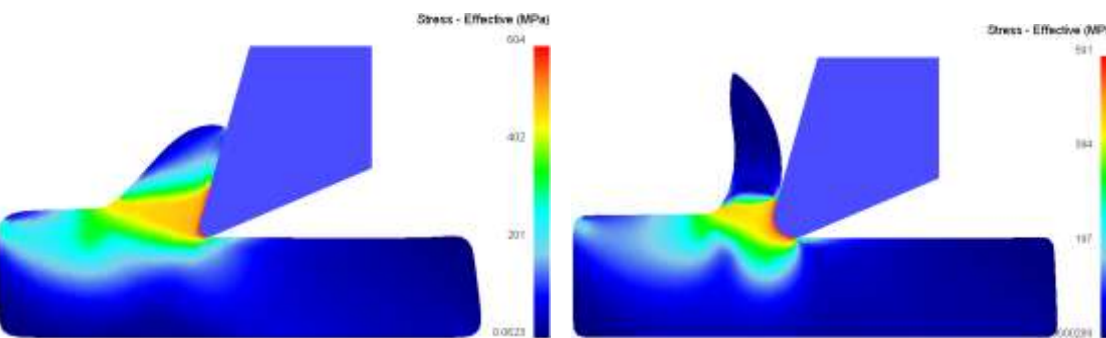
(h) 3.5μm UCT

(i) 5.0µm UCT
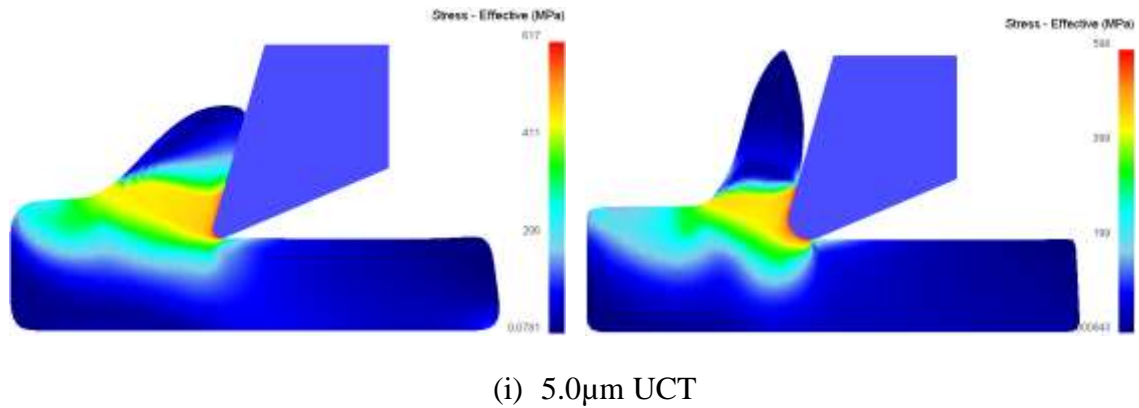
Fig. 6.9 Predicted chip formation at $3 \times e^{-5}$ sec cutting under various UCT

As mentioned previously, the chips produced by the uncoated tool are prone to slide along the tool rake surface. In this case, the nominal rake angle has great effects. Although the 5µm UCT has the largest chip size, the ratio of tool-chip contact length to the chip thickness is the smallest. This phenomenon may be due to the increasing frictional stress on the tool rake surface, leading to the chip movement more difficult along the rake surface direction.

For the DLC coated tool, the larger tool edge radius affects the cutting mechanism significantly, resulting in relatively larger deformation of generated chips as compared to those of the uncoated tool. From 0.5µm to 5µm UCT, the effective rake angle varies from negative to positive and the curvature of deformed chips becomes smaller, which indicates the nominal tool rake angle takes gradual effect with the increasing UCT.

6.5.2.2   Cutting forces and specific cutting energy

Table 6.3 gives the detailed information about the predicted feed and normal forces at various UCT, and the resultant cutting forces are plotted in Fig. 6.10, as a function of UCT for the two types of cutting tools.

It can be observed that, the resultant cutting forces have a tendency to increase with simultaneous increase in UCT for both tools. The force values of the DLC coated tool are slightly larger when UCT is smaller than 1.5µm. However, when the UCT is greater than 1.5µm, those become smaller and have a relatively slower increase as compared to those of the uncoated tool. This trend gives evidence that in micro-scale cutting, the cutting forces at small and large UCT are mainly affected by the tool edge radius and

the friction properties respectively, and there is a complete trade-off between the tool edge radius effect and cutting friction effect at 1.5µm UCT.

Table 6.3 Predicted forces for the uncoated and coated tools under various UCT

No.	Uncut chip thickness (µm)	The uncoated tool		The DLC coated tool	
		Feed force (N)	Normal force (N)	Feed force (N)	Normal force (N)
1	0.1	1.12	0.727	0.559	1.37
2	0.25	1.64	0.886	1.65	2.08
3	0.5	1.86	0.925	2.03	2.21
4	0.75	2.26	1.03	2.26	2.26
5	1.0	2.72	1.18	2.52	2.32
6	1.5	3.51	1.44	2.82	2.18
7	2.5	4.51	1.69	3.41	2.20
8	3.5	5.55	2.11	3.96	2.06
9	5	6.91	2.46	5.07	1.90
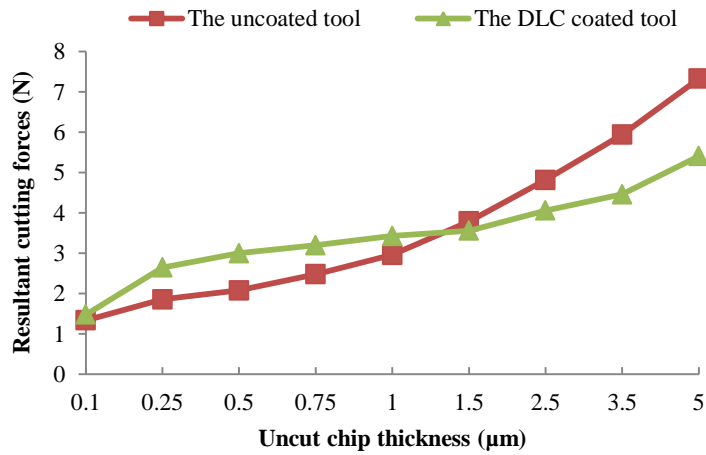
Fig. 6.10 Predicted resultant cutting forces under various UCT

From above, if the uncut chip thickness is less than 1.5µm, the larger cutting edge radius of micro tools, the larger resultant cutting forces. The results are not in accordance with the conclusion drawn from Fig. 5.10 (b) as the use of DLC coatings could help reduce the magnitude of cutting forces. It could be explained by coating delaminating on the tool edges at the first cut, which makes the tool edge corner smaller. Besides, coating films could consistently take effects when there is no or partial delaminating on the tool rake and relief surfaces.

The specific cutting energy is defined as the resultant cutting forces per unit area of cutting section, and it can be represented as:

$$E = F_r/(h_c \cdot w) \tag{6.1}$$

where F_r – The resultant cutting forces;

h_c – The value of UCT;

w – The width of cutting section (unit '1' mm).
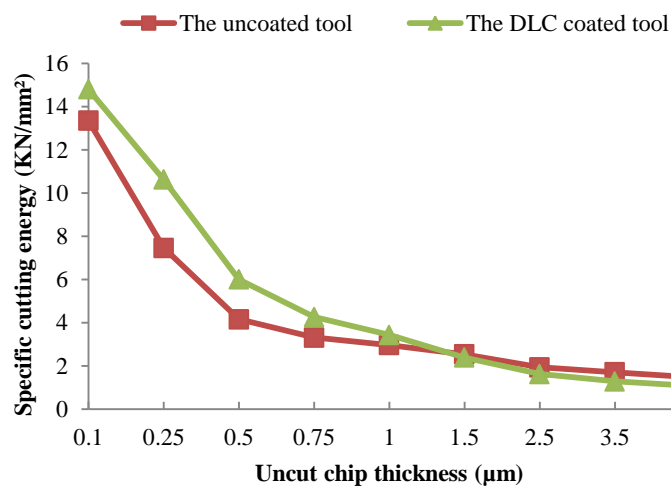
Fig. 6.11 The specific cutting energy under various UCT

The specific energy has a significant increase at small UCT, as obviously shown in Fig. 6.11. In this case, the effective rake angle of tools becomes more negative and results in ploughing which contributes substantially to the energy. In addition, the DLC coated tool has a lager specific energy, and it indicates that the specific cutting energy is closely related to the cutting edge radius of tools. When the UCT is larger than 1.5µm, the energy consumption of both uncoated and coated tools becomes much lower. Therefore, if power consumption is the greatest concern, UCT should be chosen above 1.5µm under the specific cutting conditions.

6.5.2.3   Tool temperatures

The influence of UCT on the maximum tool temperatures is shown in Fig. 6.12 and the examples of temperature distributions at 0.1µm and 5µm UCT are given in Fig. 6.13.
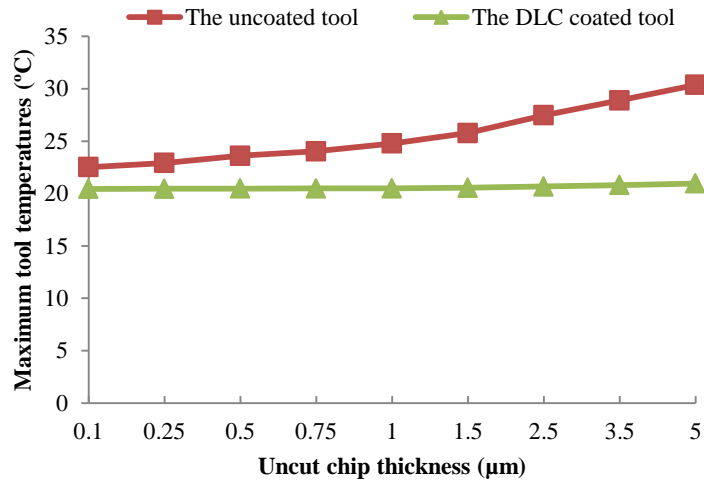
Fig. 6.12 Predicted maximum tool temperatures under various UCT
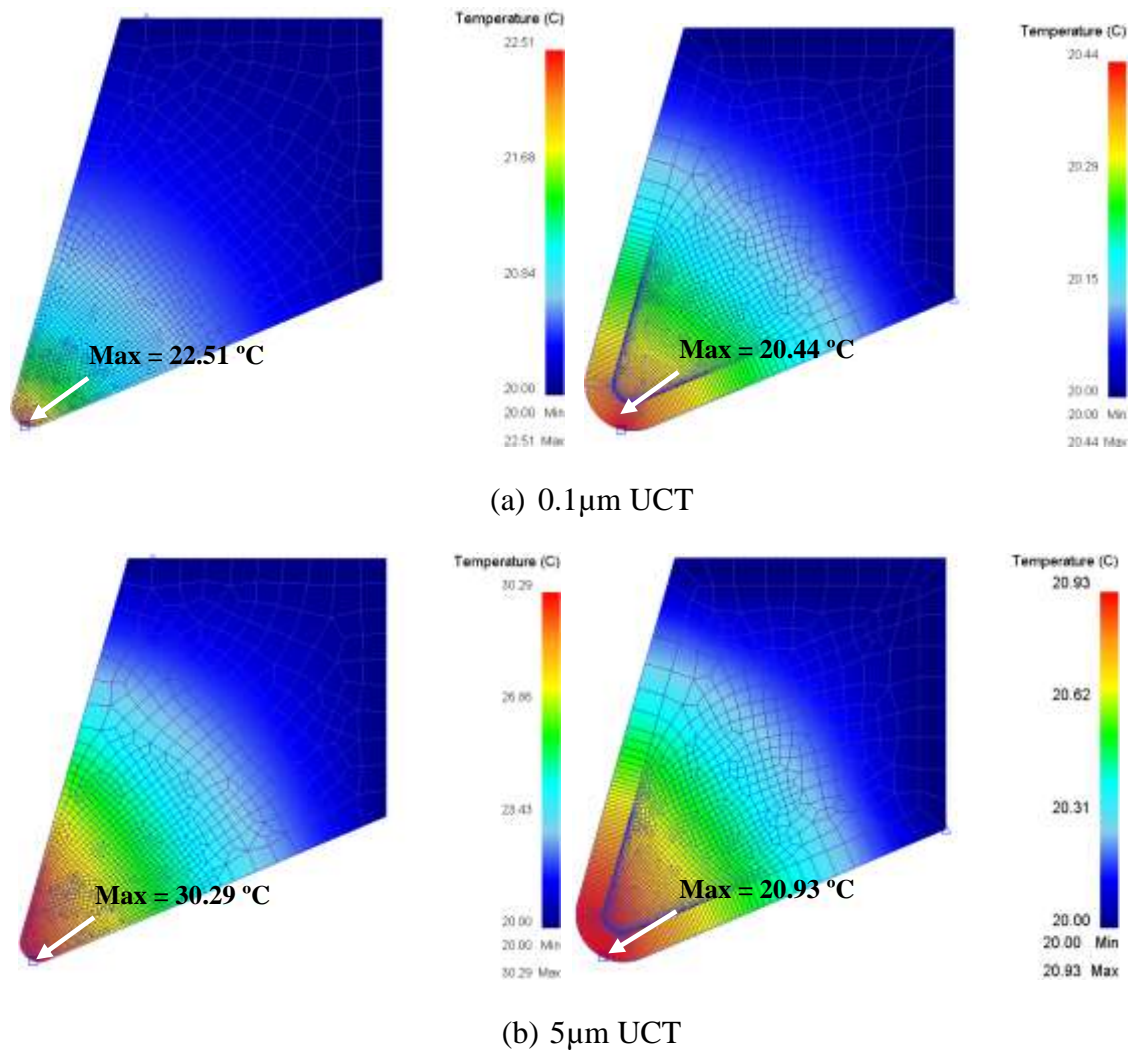
(a) 0.1μm UCT

(b) 5μm UCT

Fig. 6.13 Predicted tool temperature distributions at 0.1μm and 5μm UCT

It is seen that the maximum tool temperatures increase with increase in UCT for the uncoated tool, whereas those are almost UCT independent for the DLC coated tool. The uncoated tool has comparatively higher temperatures under the investigated cutting conditions. From Fig. 6.13, the highest temperature points on the uncoated and DLC coated tools under 0.1µm and 5µm UCT are located at the cutting edges close to the relief surfaces. It indicates compressing rather than shearing dominates the heat generation. However, the higher temperature zones (in red areas) move from around the relief surface to the rake surface with rising UCT, which gives evidence that the ploughing behaviour is shifting to shearing cutting mechanism as the tool effective rake angle becomes more positive.

6.6 <u>Verification of the orthogonal cutting model</u>

Based on the simulation results achieved in section 4.5.1, the planar cutting forces in micro milling have fairly minor variations when the helix angle of a tool is reduced to zero. If the planar force components rather than the axial forces are of great concern, a plane-strain model can be used to represent the micro milling with acceptable deviations for the force prediction. Therefore, the proposed orthogonal cutting model can be verified by comparison of predicted cutting forces with measured planar force data.

It is noted that the feed and normal forces in the orthogonal cutting model have different definitions as those in micro milling, and the two components respectively refer to the tangential force (F_{ta}) and radial force (F_{ra}) in micro milling, as illustrated in Fig. 6.14.
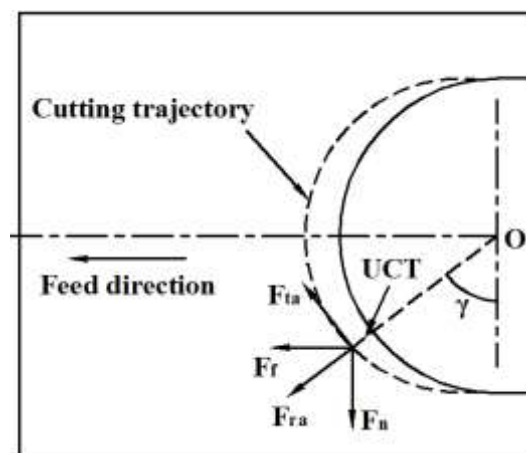
Fig. 6.14 Schematic of the planar force components in micro slot milling

For one cutting pass, the cutting rotation angle is in the range of 0º to 180º. The value of UCT varies from zero to feed per tooth and then reduced to zero along the cutting trajectory, and it can be calculated by:

$$h_c = f_z \cdot sin\gamma \tag{6.1}$$

Where f_z and γ represent feed per tooth and cutting rotation angle respectively.

The cutting forces in the tangential and radial directions can be expressed as:

$$F_{ta} = F_f cos\gamma - F_n sin\gamma \tag{6.2}$$

$$F_{ra} = F_f sin\gamma + F_n cos\gamma \tag{6.3}$$

Where F_{ta} — Cutting force component tangential to cutting direction;

F_{ra} — Cutting force component in the radial direction;

F_f — Cutting force component in the feed direction;

F_n — Cutting force component in the normal direction;

And the resultant force can be given as:

$$F_r = \sqrt{F_{ta}^2 + F_{ra}^2} = \sqrt{F_f^2 + F_n^2} \tag{6.4}$$

It must be mentioned that due to large fluctuations of cutting forces caused by possible coating delaminating, as explained in section 6.5.2.2, only the uncoated tool in dry cutting is used for the validation. According to the process conditions used in chapter 5, the feed per tooth is 0.5µm and axial depth of cut is 0.03mm. The forces at 15º angular intervals in the feed and normal directions are extracted in five consecutive cycles and the averaged values are utilised for calculation of the resultant cutting forces along one cutting locus. These planar forces are divided by the axial UCT so as to obtain corresponding counterparts with unit '1' mm axial DOC. The predicted resultant cutting forces derived from the orthogonal cutting model at $3 \times e^{-5}$ sec cutting are compared with the measured ones for the verification, and the data are given in Table 6.4.

Table 6.4 Comparison of the measured and predicted resultant cutting forces

No.	Cutting rotation angle	Uncut chip thickness (µm)	Measured resultant cutting forces (N)	Predicted resultant cutting forces (N)	Deviations
1	15°	0.1294	1.58	1.47	-7.0%
2	30°	0.25	2.02	1.88	-7.0%
3	45°	0.3536	2.36	1.94	-17.8%
4	60°	0.433	2.35	2.11	-10.2%
5	75°	0.483	2.34	2.12	-9.4%
6	90°	0.5	2.33	2.08	-10.7%
7	105°	0.483	2.34	2.12	-9.4%
8	120°	0.433	2.12	2.11	-0.5%
9	135°	0.3536	1.92	1.94	+1.0%
10	150°	0.25	1.92	1.88	-1.6%
11	165°	0.1294	1.69	1.47	-13.0%

Deviation analysis of the simulated and experimental resultant forces is carried out and the maximum percentage errors are within 18%, which shows favourably in terms of the magnitude. Hence, it is believed that the developed orthogonal cutting model is correct and could be capable of effectively investigating the cutting mechanics of micro tools.

6.7 Influence of coating properties and UCT on the tooling performance

Various combinations of coating properties and UCT may produce different tooling performance. The primary goal of this study is to find out how the friction coefficient (µ), coating thickness (t_c) and UCT (h_c) will influence the cutting forces and tool temperatures, and determine which variable has a significant effect.

6.7.1 Design of simulation

Design of experiment (DOE) is an efficient and scientific strategy for planning experiments in a structured, mathematical way. It can be applied when investigating a phenomenon in order to gain understanding or improve performance. By collecting and analysing multivariate data, valid and objective conclusions can be realized. The general

procedures of conducting DOE are: defining the objective and clarifying the problem; selection of the response variables; choice of factors, levels and range; choice of experimental design; performing the experiment; collection and statistical analysis of the data; and conclusion of the experiment (Montgomery, 2001). DOE has found broad applications, particularly in engineering design activities. Some applications include evaluation of alternatives, sort out important variables, achieve a response criterion, maximize or minimize a target, find the optimum conditions, etc.

Based on the fundamental principles of DOE, the response data achieved from 2D orthogonal simulations rather than from experiments are used for the investigation. This approach, termed as design of simulation, has the similar strength and design procedures as those of DOE.

In the present study, a full factorial design consists of three input factors is introduced. The friction coefficient and coating thickness have three discrete levels. The range of UCT is divided into low and high domains with three levels respectively but has five levels in total, so there are 45 factorial points for taking on all possible combinations of these levels across all factors. Such a simulation design allows studying the effect of each factor on the response variable, as well as the effects of interactions between factors on the response variable.

The selection of levels for friction factor is based on the nominal friction coefficient between DLC coatings and Al 6061-T6, taking into account slightly higher variations. In practice, the thickness of thin-film coatings always lies between 1μm and 3μm so as to reduce the cutting edge radius effect. The tool models and meshing with 1μm, 2μm and 3μm thickness of DLC coatings are shown in Fig. 6.15.

Besides, the values of UCT are varied from 0.1μm to 5μm. From the simulation results presented in the section 6.5.2.2, 1.5μm UCT is the transition point for the predicted cutting forces and specific cutting energy. Thus, the value is assumed as a critical and dividing level between the low and high UCT regions.

(a) 1μm   (b) 2μm   (c) 3μm
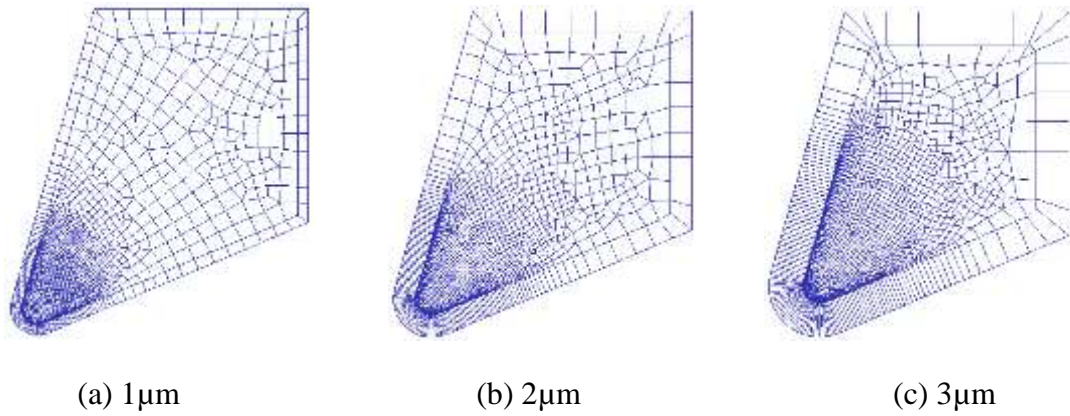
Fig. 6.15 Tool models and meshing with different coating thickness

The levels of the input variables are given in Table 6.5, and the design matrix of simulations together with corresponding response are summarized in Table 6.6. With the support of a commercial and statistical software Minitab, the predicted cutting forces and tool temperatures data in the table are used for analysing the full factorial design.

Table 6.5 Levels of the input variables

Factors	Levels		
	Low	Medium	High
Friction coefficient, μ	0.1	0.2	0.3
Coating thickness, t_c (μm)	1	2	3
Low UCT, h_{cl} (μm)	0.1	0.8	1.5
High UCT, h_{ch} (μm)	1.5	3.25	5

Table 6.6 Design matrix of simulations and corresponding responses

Run No.	Friction coefficient	Coating thickness (µm)	UCT (µm)	Cutting forces (N)		Maximum tool temperature (ºC)
				Feed forces	Normal forces	
1	0.1	1	0.1	0.817	1.37	20.573
2	0.2	1	0.1	1.06	1.35	20.877
3	0.3	1	0.1	1.21	1.32	21.066
4	0.1	2	0.1	0.559	1.37	20.439
5	0.2	2	0.1	0.992	1.48	20.664
6	0.3	2	0.1	1.15	1.45	20.879
7	0.1	3	0.1	0.432	1.29	20.329
8	0.2	3	0.1	0.936	1.72	20.595
9	0.3	3	0.1	1.12	1.55	20.719
10	0.1	1	0.8	1.85	1.58	20.704
11	0.2	1	0.8	2.07	1.52	21.085
12	0.3	1	0.8	2.28	1.45	21.357
13	0.1	2	0.8	2.30	2.25	20.507
14	0.2	2	0.8	2.61	2.13	20.794
15	0.3	2	0.8	2.85	1.97	20.964
16	0.1	3	0.8	2.70	2.73	20.417
17	0.2	3	0.8	3.08	2.71	20.674
18	0.3	3	0.8	3.32	2.43	20.814
19	0.1	1	1.5	2.31	1.65	20.811
20	0.2	1	1.5	2.63	1.57	21.309
21	0.3	1	1.5	2.82	1.49	21.775
22	0.1	2	1.5	2.82	2.18	20.547
23	0.2	2	1.5	3.16	2.26	20.826
24	0.3	2	1.5	3.38	2.06	21.099
25	0.1	3	1.5	3.26	2.89	20.449
26	0.2	3	1.5	3.62	2.76	20.734
27	0.3	3	1.5	3.89	2.67	20.889
28	0.1	1	3.25	3.34	1.34	21.217
29	0.2	1	3.25	3.87	1.27	22.150
30	0.3	1	3.25	4.34	1.43	22.744
31	0.1	2	3.25	3.81	2.12	20.761
32	0.2	2	3.25	4.43	2.02	21.216
33	0.3	2	3.25	5.05	2.32	21.559
34	0.1	3	3.25	4.40	2.8	20.566
35	0.2	3	3.25	4.93	2.51	20.850
36	0.3	3	3.25	5.37	2.63	21.227
37	0.1	1	5.0	4.56	1.14	21.582
38	0.2	1	5.0	5.17	1.32	22.573
39	0.3	1	5.0	5.76	1.43	23.482
40	0.1	2	5.0	4.86	1.86	20.970
41	0.2	2	5.0	5.69	2.04	21.526
42	0.3	2	5.0	6.63	2.41	21.963
43	0.1	3	5.0	5.71	2.88	20.621
44	0.2	3	5.0	6.39	2.49	20.975
45	0.3	3	5.0	7.01	3.06	21.440

6.7.2 Results and discussions

6.7.2.1   Cutting forces

The main effects and two-way interaction plots for the resultant cutting forces are given in Fig, 6.16 and Fig. 6.17 respectively.
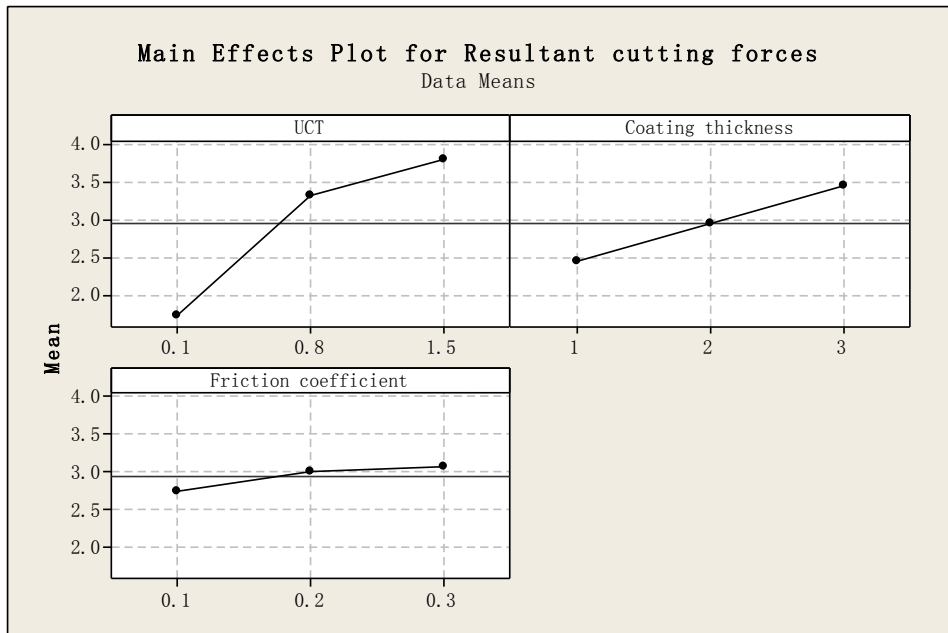
(a) Low UCT
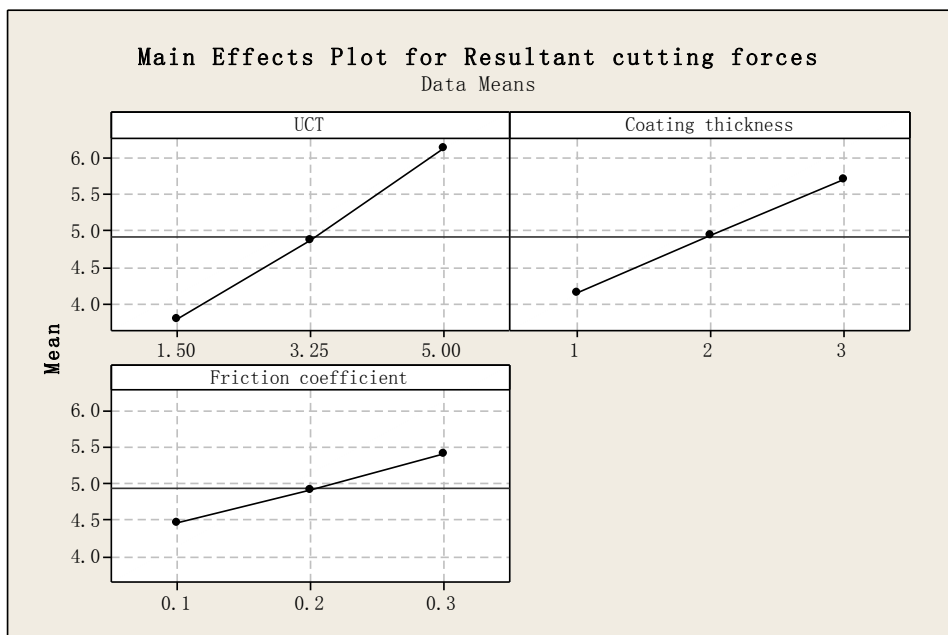
(b) High UCT

Fig. 6.16 Main effects plots for the resultant cutting forces at low and high UCT
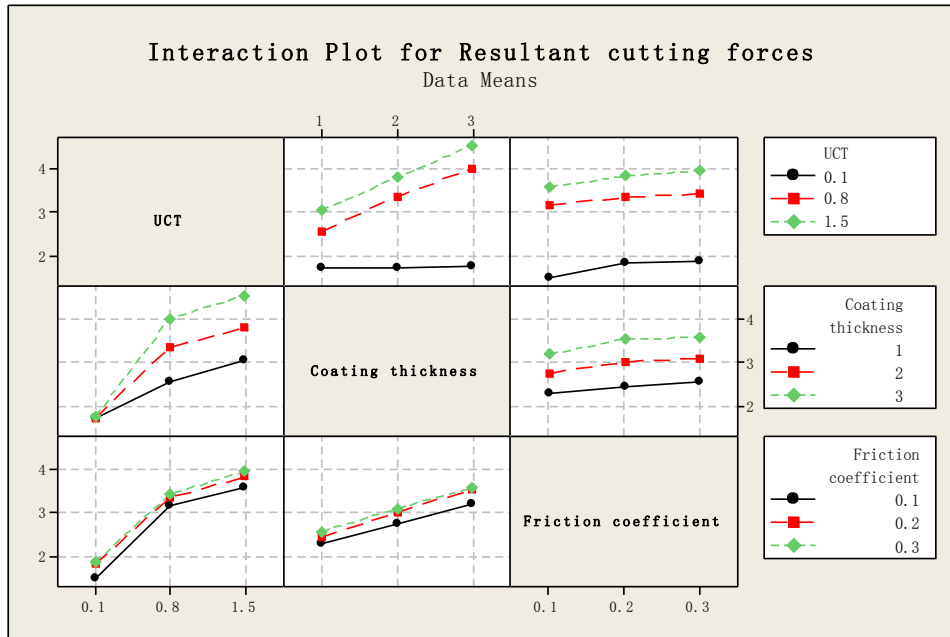
(a) Low UCT
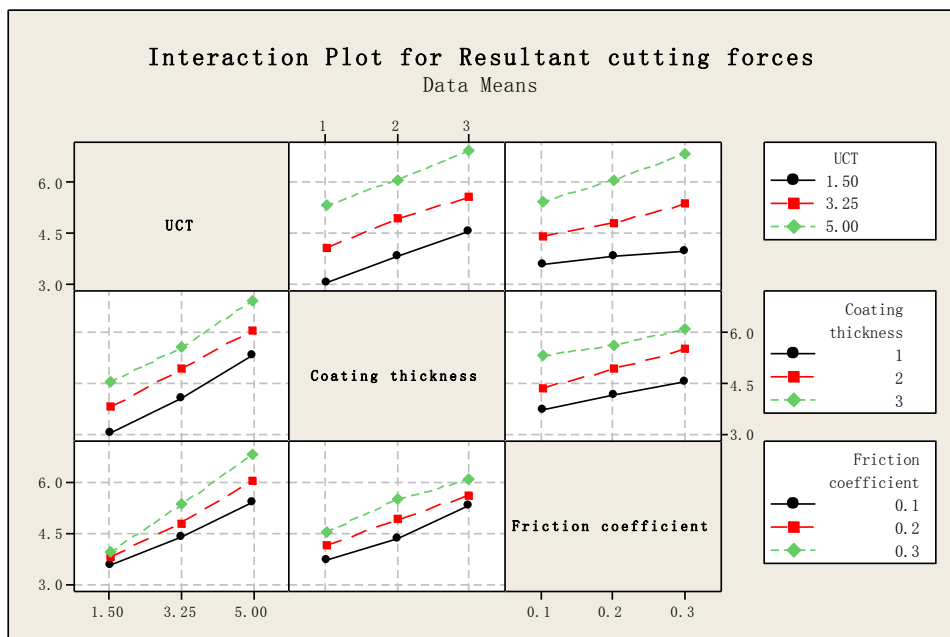
(b) High UCT

Fig. 6.17 Interaction plots for the resultant forces at low and high UCT

For the main effects plots, if the line is horizontal, there is no main effect present. The response does not change depending on the factor level. If the line is not horizontal, there may be a main effect present, and the greater the slope of the line, the stronger the effect.

As illustrated from Fig. 6.16, UCT has the most important effect on the resultant cutting forces, followed by coating thickness and friction coefficient. As expected, increasing the three independent variables from low level to high level would give rise to the cutting forces in both low and high UCT conditions. At low UCT, if the UCT is chosen to be less than 0.8μm, corresponding influence is considerably stronger. In addition, when the friction coefficient increases from 0.1 to 0.3, the magnitude of cutting forces has fairly slight variations.

In the interaction plots, if the lines are parallel to each other, there is no interaction present. The change in the response from the low to the high level of a factor does not depend on the level of a second factor. If the lines are not parallel to each other, there may be an interaction present. The change in the response from the low to the high level of a factor depends on the level of a second factor. The greater the degree of departure from being parallel, the stronger the effect.

According to Fig. 6.17, the interaction between UCT and coating thickness is significant at low UCT, but not significant at high UCT domain. Besides, the interaction behaviour between UCT and friction coefficient displays different and opposite results, and there is no obvious correlation between coating thickness and friction coefficient.

Analysis of variance for the resultant cutting forces, as illustrated in Table 6.7, is conducted to further determine which of the effects are statistically significant. The analysis of variance table consists of the variability due to the differences among the three main factors and their two-way interactions. It contains six columns: the first one (Source) is the cause of variability; the second one is the degrees of freedom; the third one is adjusted sums of squares; the fourth one is adjusted mean squares, which is calculated by Adj SS/ DF; the fifth one refers to the F statistic, which is used to determine P-value. The last column (P-value) determines the appropriateness of rejecting the null hypothesis in a hypothesis test. In general, if the P-value is less than the critical value 0.05, the effect is significant. Otherwise, the effect has less significance.

According to the values of F statistics and P-values, it is clearly seen that UCT, coating thickness, UCT*Coating thickness and friction coefficient have sequentially significant

contribution to the cutting forces at low UCT, whereas at high UCT, the sequence changes to UCT, coating thickness, friction coefficient and UCT*Friction coefficient.

Accordingly, the relationship between UCT and coating thickness has great impact in the low UCT range. As coating thickness is closely related to the tool cutting edge radius, it can be concluded that the effect of cutting edge radius depends more on the level of UCT than friction coefficient in such case. When the UCT is increased to the high domain, friction coefficient has a gradually significant effect and the interaction between UCT and friction coefficient cannot be neglected any more. Simultaneously, the dependence of coating thickness to UCT on cutting forces reduces dramatically.

Hence, in micro cutting, the tool cutting edge radius effect and cutting friction effect on cutting forces are dominant at low and high UCT respectively, which are consistent with the results drawn in section 6.5.2.2.

Table 6.7 Analysis of variance for the resultant forces at low and high UCT

UCT range	Source	DF	Adj SS	Adj MS	F	P
Low UCT domain	UCT	2	21.2573	10.6286	1889.33	0.000
	Coating thickness	2	4.5198	2.2599	401.72	0.000
	Friction coefficient	2	0.5530	0.2765	49.15	0.000
	UCT*Coating thickness	4	2.0781	0.5195	92.35	0.000
	UCT*Friction coefficient	4	0.0242	0.0060	1.07	<u>0.429</u>
	Coating thickness*Friction coefficient	4	0.0284	0.0071	1.26	<u>0.360</u>
	Error	8	0.0450	0.0056		
	Total	26	28.5057			
	S = 0.0750040 R-Sq = 99.84% R-Sq(adj) = 99.49%					
High UCT domain	UCT	2	24.6766	12.3383	1383.87	0.000
	Coating thickness	2	10.8182	5.4091	606.69	0.000
	Friction coefficient	2	3.9019	1.9509	218.82	0.000
	UCT*Coating thickness	4	0.0411	0.0103	1.15	<u>0.399</u>
	UCT*Friction coefficient	4	0.8982	0.2245	25.18	0.000
	Coating thickness*Friction coefficient	4	0.1163	0.0291	3.26	<u>0.073</u>
	Error	8	0.0713	0.0089		
	Total	26	40.5237			
	S = 0.0944236 R-Sq = 99.82% R-Sq(adj) = 99.43%					

6.7.2.2   Tool temperatures

The similar analysis is performed to study coating properties and UCT effects on the maximum tool temperatures.
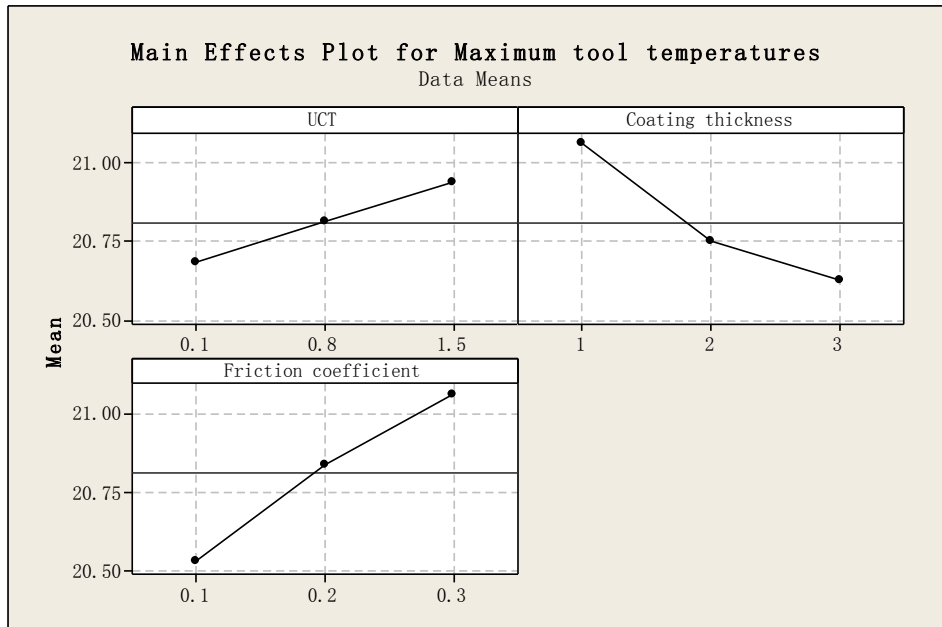
(a) Low UCT
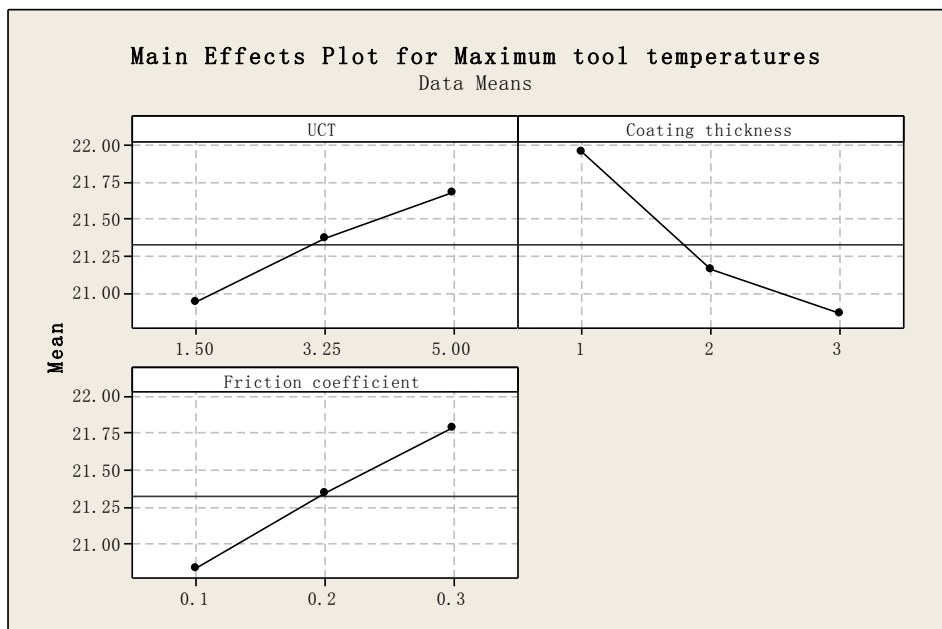
(b) High UCT

Fig. 6.18 Main effects plots for the maximum tool temperatues at low and high UCT
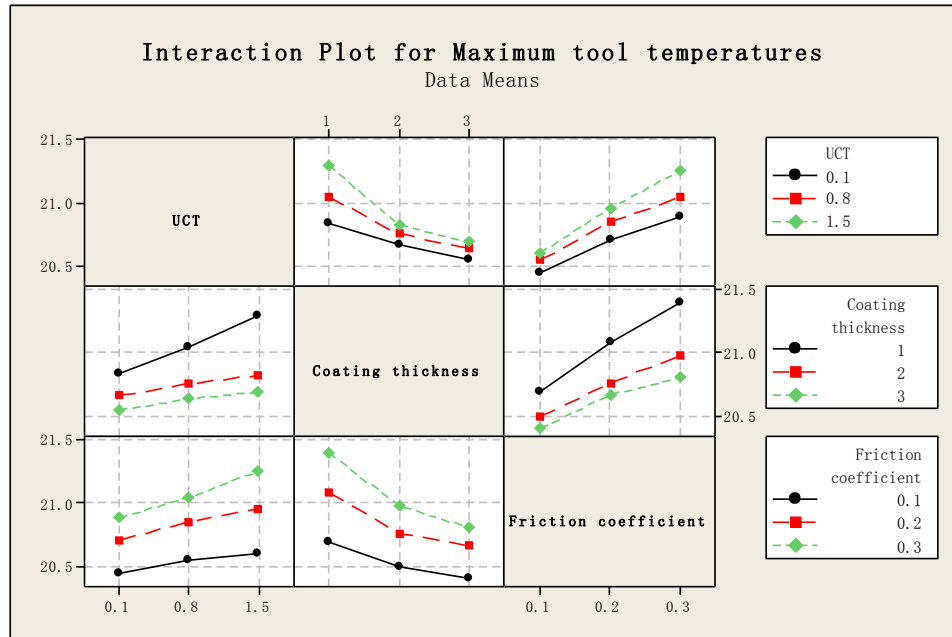
(a) Low UCT
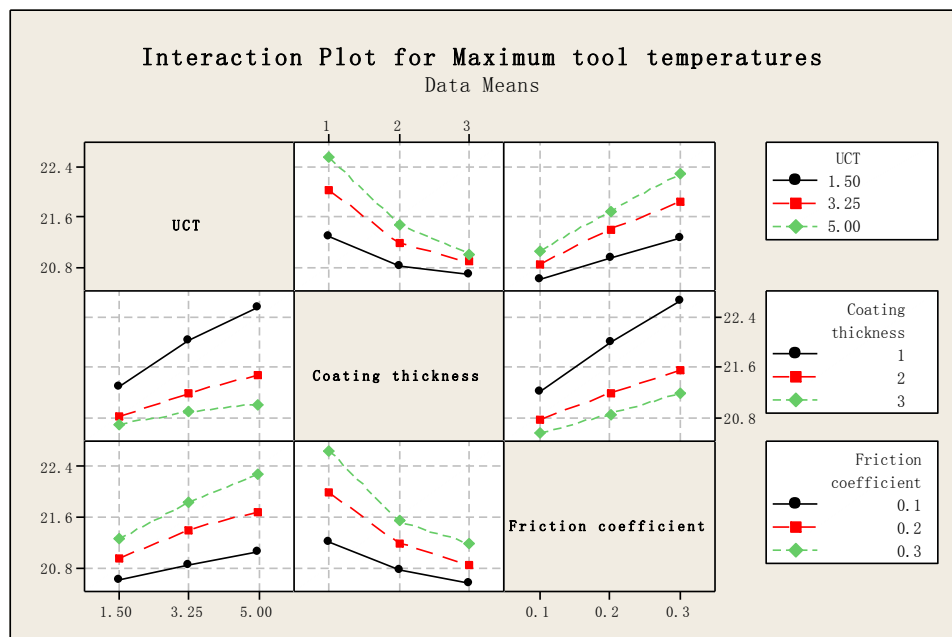
(b) High UCT

Fig. 6.19 Interaction plots for the maximum tool temperatures at low and high UCT

Fig. 6.18 shows the main effects for the response, and the trend of temperature variations between the low and high UCT plots has no noticeable difference. Increase UCT and friction coefficient from low level to high level will lead to greater tool temperatures, but if the coating layer is getting thicker, the response becomes more

positive and there is less heat on the tool tips. The possible reason for the observation could be larger thermal conductivity area of DLC coatings on the tool tips.

From the tool temperature interaction plots as given in Fig. 6.19, it seems that all lines are unparalleled, which generally indicates that all input factors may interact with each other to some extent. In order to present accurate and detailed comparisons, it is essential to evaluate the significance by looking at the effects in the analysis of variable table, as shown in Table 6.8.

Table 6.8 Analysis of variance for the tool temperatures at low and high UCT

UCT range	Source	DF	Adj SS	Adj MS	F	P
Low UCT domain	UCT	2	0.29343	0.14671	42.48	0.000
	Coating thickness	2	0.91711	0.45856	132.79	0.000
	Friction coefficient	2	1.28375	0.64188	185.87	0.000
	UCT*Coating thickness	4	0.09581	0.02395	6.94	0.010
	UCT*Friction coefficient	4	0.03620	0.00905	2.62	<u>0.115</u>
	Coating thickness*Friction coefficient	4	0.07215	0.01804	5.22	0.023
	Error	8	0.02763	0.00345		
	Total	26	2.72608			
	S = 0.0587654 R-Sq = 98.99% R-Sq(adj) = 96.71%					
High UCT domain	UCT	2	2.50743	1.25377	162.15	0.000
	Coating thickness	2	5.80457	2.90228	375.34	0.000
	Friction coefficient	2	4.16768	2.08384	269.50	0.000
	UCT*Coating thickness	4	0.66845	0.16711	21.61	0.000
	UCT*Friction coefficient	4	0.26164	0.06541	8.46	0.006
	Coating thickness*Friction coefficient	4	0.58997	0.14749	19.07	0.000
	Error	8	0.06186	0.00773		
	Total	26	14.06170			
	S = 0.0879337 R-Sq = 99.56% R-Sq(adj) = 98.57%					

Almost all investigated main and two-way sources under both UCT domains have great impact on the response except for the UCT*Friction coefficient. The P-value of UCT*Friction coefficient (0.115) at low UCT is larger than 0.05 and that at high UCT (0.006) is less than 0.05, which means less significant and significant respectively. This trend of relationship indicates that the effect of the coating friction effect to the

maximum tool temperatures, similar as its influence to the resultant cutting forces, plays a gradually important role when UCT is getting larger. Apart from that, evidence exists of significant effects of the other three main factors and two interaction factors as the corresponding P-values are less than 0.05.

The extent of significance of sources on the yield can be determined by comparing of the F statistics. Among the three main sources, friction coefficient is the most significant at low UCT but coating thickness has the greatest importance at high UCT. Therefore, The heat generated on the tool tips is mainly affected by the friction work at cutting interfaces at small UCT, but thermal conductivity area of coatings at large UCT.

6.8   Conclusions

In order to better understand the coating performance on micro tools, the cutting performance of DLC coated tool has been extensively studied and compared with that of the uncoated tool using 2D thermo-mechanical simulations. The proposed simulation models have been validated at different UCT. Besides, the influence of coating friction coefficient, coating thickness as well as UCT on cutting forces and tool temperatures has been statistically analysed through design of simulation method. The conclusions are made as follows:

- At 0.5µm UCT, the use of DLC coatings on micro tool gives rise to the cutting forces but reduces heat generation as compared to the performance of the uncoated tool. The highest stress for the coated tool lies at the coating-substrate interface, which may attribute to possible coating delaminating.

- At 1.5µm UCT, there is a complete trade-off between the tool edge radius enlargement effect and coating friction effect on the cutting forces and specific cutting energy for the coated tool.

- If UCT is chosen to be above minimum chip thickness, the larger tool cutting edge radius, the severer chip deformations.

- As compared to the performance of the uncoated tool, the DLC coated tool has less heat on the tips and the coatings help reduce more heat with increasing UCT.

- UCT has the most important effect on the cutting forces, followed by coating thickness and friction coefficient. The larger the three variables, the higher cutting forces. In micro cutting using coated tools, the negative effect of tool cutting edge radius enlargement and the positive effect of reduced coating friction on the cutting forces are dominant at low and high UCT respectively.

- Increase UCT and friction coefficient lead to higher tool temperatures, whereas increase coating thickness results in lower heat on the tool tips. Cutting friction at low UCT and coating thickness at high UCT have comparatively greater influence on the tool temperatures.

From above conclusions, appropriate UCT in micro machining is of the greatest importance for achieving desirable coating performance of micro tools. Thus, it is definitely necessary to determine proper process variables before conducting cutting trials. In Chapter 8, the influence of process variables on the tooling performance will be studied comprehensively dedicated for process planning and optimization purpose.

Chapter 7 Tooling Performance in Micro Milling of Common Metals

7.1 <u>Introduction</u>

Mechanical, chemical and physical properties of work materials have a direct influence on the cutting performance of micro tools. Practically, a thorough understanding of their influence will help production engineers in effective planning the process so as to achieve optimum tooling performance.

The tooling performance for a work material at the micro-scale is closely related to its micro-machinability, which is commonly assessed by means of a combination of characterization factors, including cutting forces, surface roughness, tool wear, micro-burr formation and power consumption. Usually good machinability translates to cutting with small chip loads, good surface finish, minimum tool wear, free burrs and low energy. Due to the well-known size effects, existing knowledge with respect to machinability available in conventional cutting cannot be directly applied at the micro-scale. Accordingly, it is much need to determine the micromachining characteristics of frequently used engineering materials so as for cost-effective industrial applications.

The objective of this chapter is to experimentally investigate the micro milling behaviours of some general purpose engineering materials, including Al 6061-T6, copper C101, carbon steel AISI 1045, stainless steel 304 and tool steel P20. These materials are selected as tested targets primarily due to their engineering importance for a variety of industries. The comparisons of related performance as well as their changes with the tool wear progression are undertaken in an attempt to identify their respective micro-machinability. Moreover, the effects of process variables on the cutting performance of C101, AISI 1045, and 304 are also analyzed.

7.2   Properties of the investigated work materials

The material conditions or characteristics, such as microstructure, grain size, heat treatment, chemical composition, hardness, thermal conductivity, work hardening, individually and in combinations, directly influence the tooling performance. Chemical composition is a major factor in determining a material's micro-machinability and those for the five investigated metals are summarized in Table 7.1.

Table 7.1 Chemical compositions of the investigated work materials (Weight. %)

	Work materials				
	Al 6061-T6	**C101**	**AISI 1045**	**304**	**P20**
Cr	0.04-0.35	—	≤ 0.2	18-20	1.4-2.0
Cu	0.15-0.40	≥ 99.99	≤ 0.3	—	0.25
Fe	≤ 0.7	—	97.6-98.8	66.345-74	97
Mg	0.8-1.2	—	0.6-0.9	—	—
Si	0.4-0.8	—	0.15-0.35	≤ 1.0	0.2-0.8
Mn	≤ 0.15	—	0.6-0.9	≤ 2.0	0.60-1.00
S	—	—	≤ 0.035	≤ 0.03	≤ 0.03
P	—	—	≤ 0.03	≤ 0.045	≤ 0.03
C	—	—	0.42-0.48	≤ 0.08	0.28-0.40
Mo	—	—	—	—	0.30-0.55
Ni	—	—	0.2	8.0-10.5	—
Al	95.8-98.6	—	—	—	—

Al 6061-T6 is a soft, lightweight metal with good corrosive resistance and weldability, and it possesses great strength for its weight. To increase the strength and hardness, the material is often alloyed with silicon, iron, manganese and chromium. C101 is an oxygen-free high conductivity (OFHC) pure cooper which is widely used for its superior electrical conductivity, corrosion resistance and ease in formability.

Among the three ferrous metals, AISI 1045 is a medium tensile low hardenability carbon steel, which has fairly good strength and impact properties, plus reasonable weldability. 304 is the most versatile and widely used grade stainless steel with extremely low carbon content, and it features excellent forming and welding

characteristics. P20 is a general high tensile mould steel which is readily machinable in the hardened and tempered conditions. For steels basically, the carbon content greatly affects their machinability. High carbon steels are difficult to cut because of their strength and containing carbides that abrade the micro tool. On the other hand, low carbon steels are soft and ductile, resulting in a possible built up edge that shortens the tool life (George Schneider, 2002).

An overview of typical mechanical and thermal properties for the investigated work materials is presented in Table 7.2. A material with high yield and tensile strengths is more difficult to machine as it requires a high level of force to initiate chip formation. In conventional cutting, hardness is considered as a common reference for evaluating a material's machinability and the definition of it is the tendency to resist deformation. It is distinct that P20 is the hardest metal, followed by AISI 1045, 304, Al 6061-T6 and C101. Hence, among the five materials, cutting P20 presents the greatest difficulty.

Table 7.2 Mechanical and thermal properties for the investigated work materials

	Work materials				
	Al 6061-T6	**C101**	**AISI 1045**	**304**	**P20**
Density ($\times 10^3$ kg/m^3)	2.7	8.92	7.85	8.0	7.85
Poisson's Ratio	0.33	0.31	0.29	0.29	0.29
Elastic Modulus (GPa)	68.9	115	205	200	205
Tensile Strength (MPa)	310	455	569	505	1030
Yield Strength (MPa)	276	365	343	215	862
Hardness (Vickers)	107	90	188	129	300
Thermal Expansion (10^{-6}/ºC)	23.6	16.9	15.1	17.8	12.8
Thermal Conductivity (W/m-K)	167	391.1	49.8	16.2	32

A low thermal conductivity material will not dissipate heat freely and therefore, heat might be accumulated in or near the cutting zone when micromachining this material, which will accelerate the tool wear and reduce the tool life. Large thermal expansion of a material will make holding close finish tolerances extremely difficult, as a small rise in temperature will cause the deterioration of dimensional accuracy (George Schneider, 2002).

7.3   <u>Experimental procedures</u>

Micro milling operations are applied on the five materials in coolant mist with full tool diameter being engaged. The experiment has the same setup as Fig.5.8. The ultra-precision machine UltraMill and cutting tool Magaforce 8500-Ø0.5mm are again used for the cutting trials. A dynamometer MiniDyn 9256C2 together with a digital camera is employed, respectively, for recording the forces and aligning the tool positions.

Micro-grain WC tools from the same batch are selected so as to ensure the tool material and geometry used are the same. Prior to the cutting, defects inspection on these tools are undertaken from the side to the bottom by an optical microscope TESA VISIO 200, and examples of the tool checking interfaces are shown in Fig. 7.1.
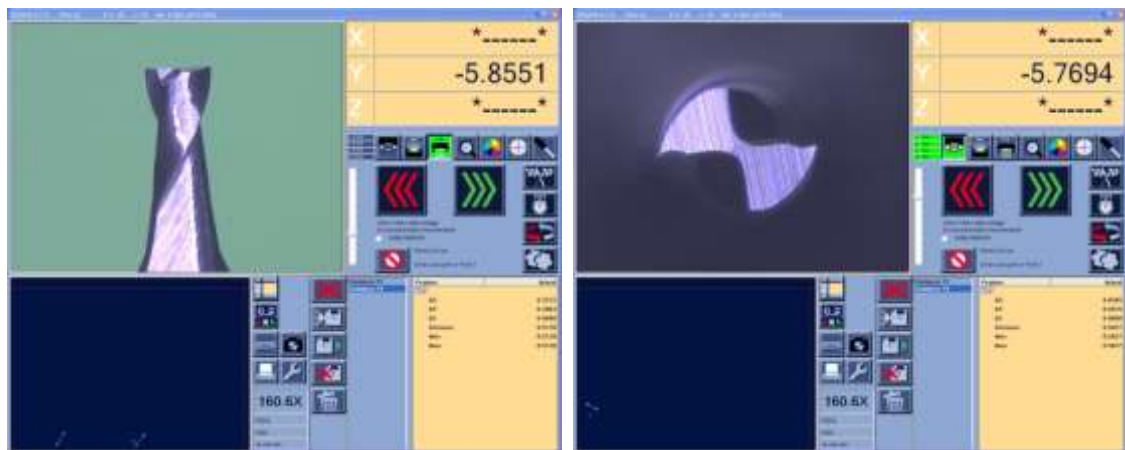
(a) Side view   (b) Bottom view

Fig. 7.1 Examples of the tool checking interfaces using TESA VISIO 200

The work materials are supplied in the form of a cylindrical bar with three inches in diameter. The samples are well prepared by a conventional CNC milling machine in the workshop in Brunel University. Among them, the work surfaces on the three steels are grinded to be smoother and leveller. These five workpieces have the similar shape and geometries, but different type of materials. Two sets of full-immersion milling are conducted on C101, AISI 1045, 304 samples, and the arrangement of these cutting trials is illustrated in Fig.7.2. For the Al 6061-T6 and tool steel P20 samples, only the first set of cutting trials is performed.
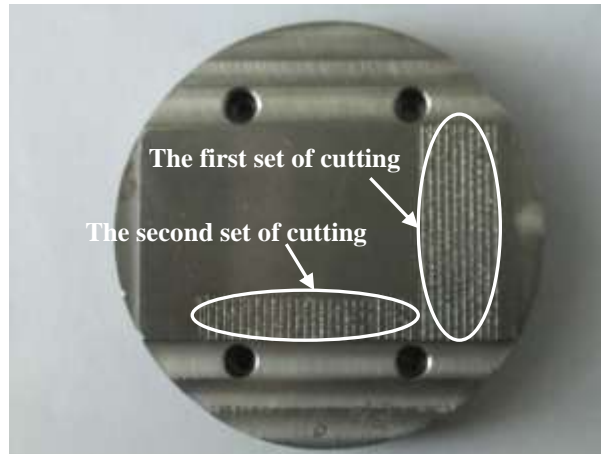
Fig. 7.2 Two sets of cutting trials on the AISI 1045 sample

The first set of cutting is primarily designed to investigate the tooling performance, particularly along with the progression of tool wear, under constant cutting conditions. The process variables are fixed at 0.25µm/tooth feed rate, 94.2m/min and 20µm axial depth of cut. Thus at the initial stage of cutting, the ratio of feed per tooth to the tool cutting edge radius is 16.7%. The cutting conditions used are quite low due to lacking of corresponding experience as well as concerning tool premature breakages in machining the hard tool steel P20. The total cutting distance for each sample is 400mm, with ten channels in 40mm length each. A brand new tool is used for each set of cutting trials and the gap between two adjacent slots is 2mm. The corresponding NC codes are programmed in Appendix V.

The performance of work materials may have different sensitivity to the cutting conditions. In the second set of cutting, three levels of feed rate, cutting speed and axial depth of cut are employed, in order to determine the material characteristics of AISI 1045, C101 and 304 under various process variables. The feed is varied at 0.2µm, 0.4µm and 0.6µm per tooth, which enables the ratio of the feed per tooth to the tool edge radius to be between 13.3% and 40%. The cutting speed is varied at 62.8m/min, 94.2m/min and 125.6m/min, and the axial depth of cut is varied at 10µm, 20µm and 30µm respectively. Thus the overall quantity of the micro-milled slots is 27. The cutting distance for each process variable combinations is 10mm. The experimental runs are randomized by a statistical software Minitab and the order is given in Table 7.3.

Table 7.3 Sequence of process variable combinations for the second set of cutting

Run order	Depth of cut (mm)	Spindle speed (rpm)	Cutting speed (m/min)	Feed per tooth (µm)	Feed rate (mm/min)
1	0.02	40,000	62.8	0.2	16
2	0.01	80,000	125.6	0.2	32
3	0.03	40,000	62.8	0.6	48
4	0.01	60,000	94.2	0.4	48
5	0.03	60,000	94.2	0.6	72
6	0.01	40,000	62.8	0.2	16
7	0.01	60,000	94.2	0.6	72
8	0.03	60,000	94.2	0.2	24
9	0.02	80,000	125.6	0.4	64
10	0.03	40,000	62.8	0.2	16
11	0.01	60,000	94.2	0.2	24
12	0.03	80,000	125.6	0.6	96
13	0.02	40,000	62.8	0.6	48
14	0.02	60,000	94.2	0.4	48
15	0.02	60,000	94.2	0.2	24
16	0.01	40,000	62.8	0.6	48
17	0.02	80,000	125.6	0.2	32
18	0.01	80,000	125.6	0.4	64
19	0.03	80,000	125.6	0.2	32
20	0.03	60,000	94.2	0.4	48
21	0.02	60,000	94.2	0.6	72
22	0.03	80,000	125.6	0.4	64
23	0.03	40,000	62.8	0.4	32
24	0.01	40,000	62.8	0.4	32
25	0.02	40,000	62.8	0.4	32
26	0.02	80,000	125.6	0.6	96
27	0.01	80,000	125.6	0.6	96

7.4   Results and discussions

7.4.1 Tooling performance in the first set of cutting trials

In this section, the tooling performance derived from the first set of cutting trials are examined, and discussed based on different evaluation indicators, including cutting forces, tool integrity, surface finish, and micro-burr formation.

7.4.1.1 Cutting forces and variations with the tool wear progression

Elementary characteristics for the description of the cutting process are the tool-work interactions. Cutting forces contain important information on the mechanics and dynamics of machining processes and the forces encountered for a tool to cut through a material is directly related to the power consumed. To understand an overall perspective of the force variations with the tool wear progression, the magnitude of cutting forces are measured in micro cutting the final parts of the first and last channels of each tested materials. The considerably low forces in the axial direction are ignored, and the force components in both feed and normal directions together with their resultant values and ratios are given in Table 7.4.

Table 7.4 The measured cutting forces in micro milling various materials

No.	Materials	The first channel				The last channel			
		Cutting forces (mN)			The ratio of feed to normal force	Cutting forces (mN)			The ratio of feed to normal force
		Feed forces	Normal forces	Resultant forces		Feed forces	Normal forces	Resultant forces	
1	Al 6061-T6	108.8	96.4	145.5	1.13	120.0	117.6	168.0	1.02
2	C101	192.2	77.8	207.3	2.47	221.3	88.3	238.3	2.51
3	AISI 1045	218.9	90.5	236.9	2.42	275.4	107.2	295.5	2.57
4	304	326.6	222.6	395.2	1.47	362.0	238.6	433.6	1.52
5	P20	350.6	124.9	372.2	2.81	438.1	156.3	465.1	2.80

At the machining of the first channel, Al 6060-T6 has the lowest chip load at 145.5mN whereas stainless steel 304 has the highest at 395.2mN. The forces for the copper, carbon steel and tool steel are measured respectively at 207.3mN, 236.9mN and 372.2mN. In conventional case, the force required for cutting P20 is always the highest but it is strange that the stainless steel gives the largest load. This observation may be due to the enlarged tool nose radius caused by possible built up edges on the tool tips, making the relatively ductile material the most difficult to machine.

The extent of MCT effect on a material can be determined by the ratio of feed to normal force. Al 6061-T6 has the lowest value and the normal force becomes comparable to the feed force, which indicates that there is a dominant MCT effect when using the 0.25μm feed per tooth. The ratio of feed to normal force for 304 is calculated to be 1.47, which

also means the MCT effect is strong. The other metals show less MCT effect as the feed forces are over two times larger than the normal forces. It might reach a general conclusion that the more ductile a material, the greater the MCT effect under the specific cutting conditions.

At the machining of the last channel for all the materials, the forces increase due to the tool wear effect. From Al 6060-T6, C101, AISI 1045, 304 to P20, the values respectively rise by 22.5mN, 31.0mN, 58.6mN, 38.4mN and 92.9mN. The resultant load for P20 exceeds those of 304, and becomes the most prominent. Therefore, it might be realized that the tool wear effect plays the most important role on P20 in terms of the cutting forces, but it has the least significance on Al 6061-T6.

7.4.1.2 Tool integrity

After 400mm length cutting, the five micro tools are ultrasonic cleaned and further examined. The state of these tools is given in Fig. 7.3, and from the bottom view it is clearly seen that the cutting tips of tools become blunt but no premature failures or breakages of the tool shafts are present.

(a) Al 6061-T6	(b) C101	(c) AISI 1045

(d) 304	(e) P20
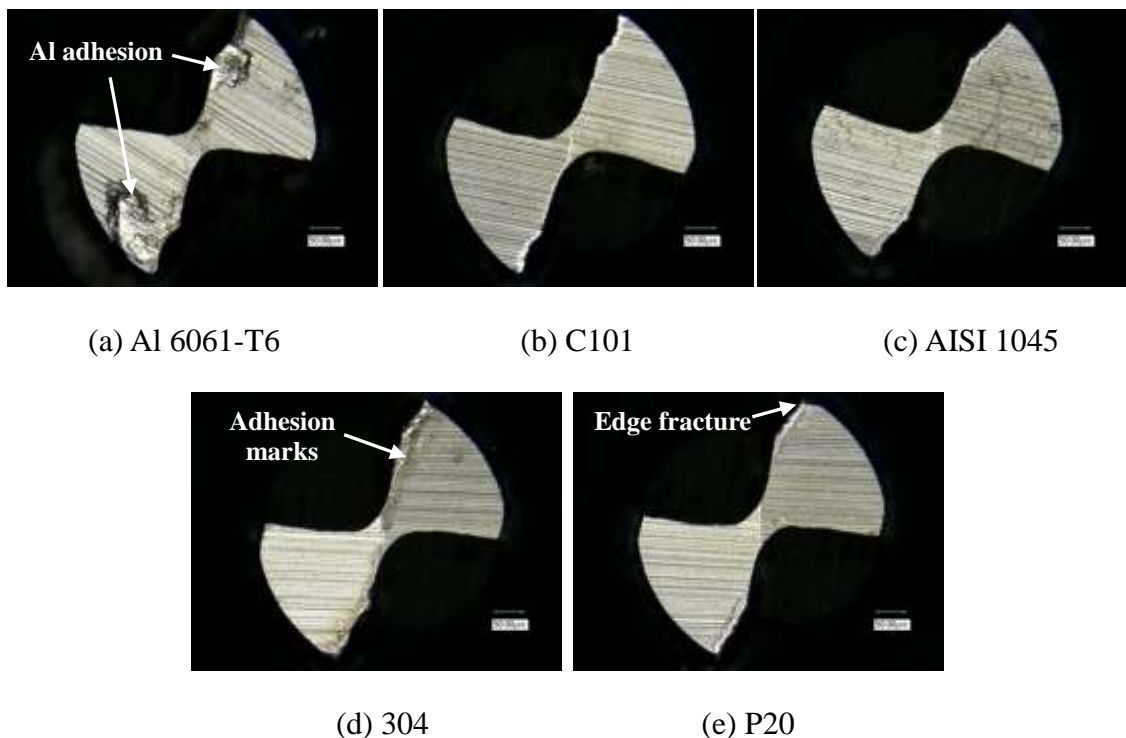
Fig. 7.3 Integrity of micro tools after micromachining various materials

For the tool after machining Al 6061-T6, large-sized built up edges seize close to the two cutting tips, owing to low elastic modulus and ductility of the work material. Although C101 is harder than Al 6061-T6, the tool condition is observed to be as new. After micromachining the ferrous materials, the tools experience substantial material loss and the geometries cannot be well maintained as C101 does. Concerning the tool for cutting 304, chip adhesion marks and slightly minor chip adhesion on the tool edges are spotted, indicating that there are possible build up edges during the cutting process. The build up edges may be removed by the subsequent slot cutting, careless handling or the ultrasonic cleaning process before the examination. In addition, edge fracture occurs on one cutting tip of the tool when micromachining the hardest material P20, as obviously seen from Fig.7.3 (e).

The wear characterization defined in Chapter 5 is employed as a means of assessing the flank wear on the two tips, and the values are averaged and compared in Fig. 7.4. C101 has the lowest averaged tool wear at 3.78µm, followed by Al 6061-T6 at 13.48µm, and the three steels have the highest at around 25µm. The wear behaviour from micromachining C101 indicates a fair improvement as compared to that of Al 6061-T6, which reveals a better machinability in terms of the tool life. As Al 6061-T6 presents the lower forces than C101, it is considered that chip adhesion or MCT effect may be responsible for the more tool wear.
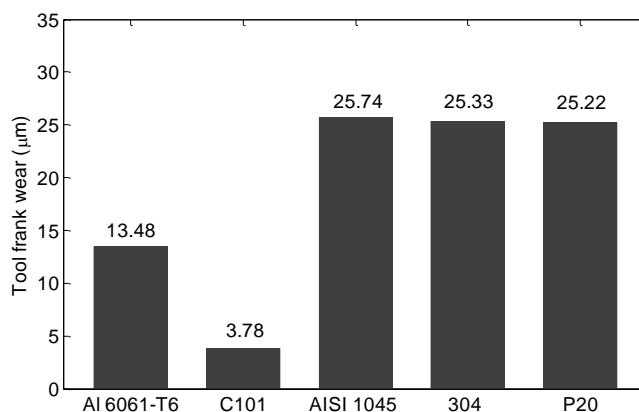
Fig. 7.4 Comparison of the tool flank wear after cutting the work materials

It is worth to note that the ferrous materials have almost the same levels of tool flank wear. These observations are out of accord with those of conventional machining, in

which the hardest tool steel P20 usually results in the most rapid wear. For AISI 1045, the cutting tool wears more and it is probably due to the negative effect of the high carbon content in the micro-scale cutting. For 304, MCT effect or possible chip adhesion may lead to the tool life deterioration significantly. Except for the hardness, MCT effect and chip adhesion, other factors such as the material thermal properties may also contribute to their equal wear behaviours. However, among the three materials, P20 still gives the worst result due to the obvious edge breakages.

Based on the above observations and discussions, it is demonstrated that the tool wear and life in micro-scale cutting is not only determined by the work material properties but also by the cutting mechanism and mechanics.

7.4.1.3 Surface finish and variations with the tool wear progression

Fig.7.5 shows images of the machined surface profiles at the bottom of the first slots for the five work materials. There is some dirt attached to these surfaces that can hardly be removed by an ultrasonic cleaning process. The appearances of the surfaces differ from each other. Al 6061-T6 and P20 present the much rougher surfaces, and the quality for C101, AISI 1045 and 304 seems fairly better.

(a) Al 6061-T6   (b) C101   (c) AISI 1045

(d) 304   (e) P20
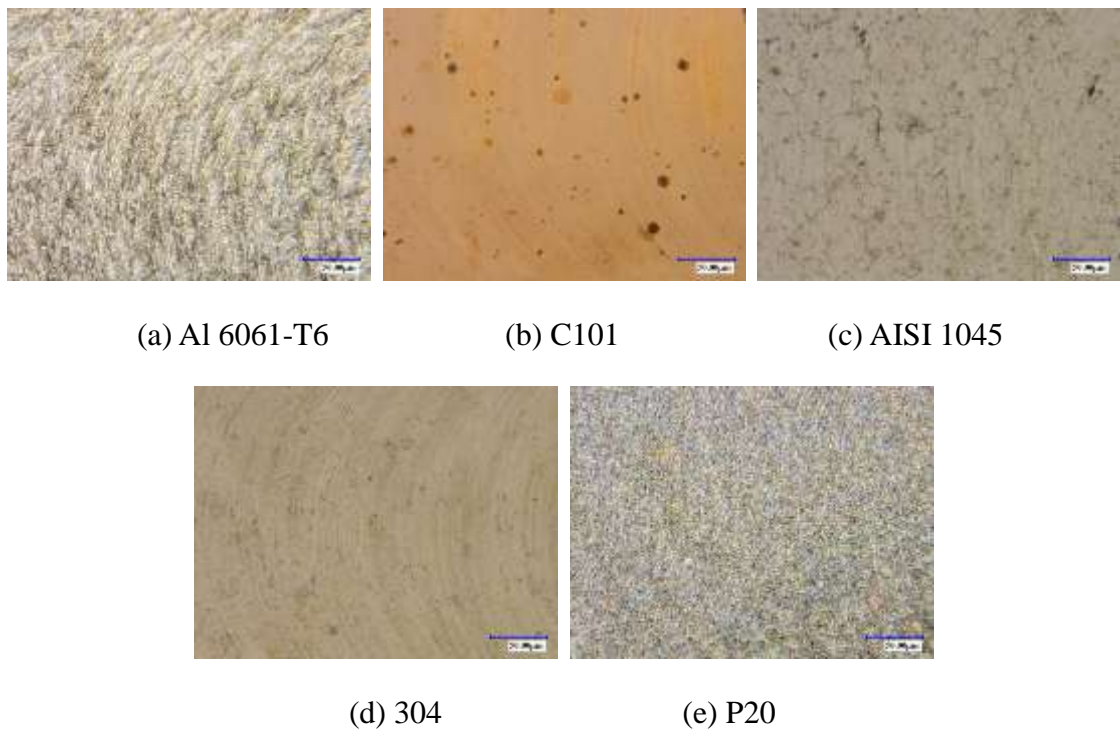
Fig. 7.5 Surface profiles at the bottom of the first slots for the work materials

Measurements of the surface roughness, Ra, with the assistance of Zygo NewView 5000 are carried out for quantitatively determining the surface finish variations with the tool wear progression. The values are recorded near the exit points of each slot, and they are compiled and plotted as a function of cutting distance, as depicted in Fig.7.6, in which the corresponding exponential trend lines are also given.
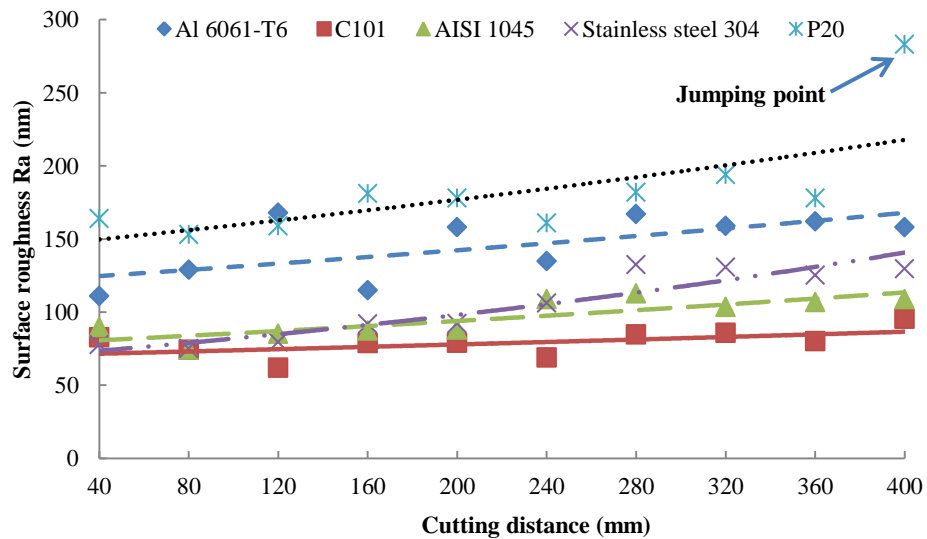
Fig. 7.6 Surface roughness variations for the work materials

At the beginning, C101, AISI 1045 as well as 304 result in almost the same and the best level of smoothness, and P20 gives the worst performance mainly because of the low stiffness of the micro tool and possible vibrations during cutting the hardest material. In addition, Al 6061-T6 has the comparatively poor surface generation primarily due to the severe MCT effect and the chip adhesion on the tool. From the five trend lines, it is obvious that the wear progression of the cutting edges negatively influences the surface roughness. Along with the increasing cutting distance, the surface roughness for Al 6061-T6, AISI 1045, 304 and P20 rises slightly, whereas that for C101 roughly keeps constant at around 75nm. After the 10th slot milling, the best to the poorest surface quality is obvious, and the sequence is from C101, AISI 1045, 304 to Al 6061-T6 and P20. Stainless steel 304 gives a poorer roughness as compared to AISI 1045 because it is gummier and tends to work hardening very rapidly.

The tool edge fracture greatly affects the surface roughness, as evidence shows that a sudden jumping point at 283nm appears at machining the last channel of P20. As a

result of the edge breakage, machining instability is likely to occur, leading to the considerable performance deterioration. This phenomenon demonstrates that the tooling edge strength act as an important role for achieving a favourable machining quality and acceptable tool life, particularly in case of micromachining a hard material. Except for P20, Al 6061-T6 has relatively large roughness variations as the built up edges, which change the instantaneous cutting tool profile, may have the great influence on the cutting mechanism and mechanics.

7.4.1.4 Micro-burr formation

The micro burrs on the top of slots are the research targets. The examples upon the first slots of each work materials are shown in Fig. 7.7. Generally these visible burrs are in the feathery and wavy type.

| (a) Al 6061-T6 | (b) C101 | (c) AISI 1045 |

| (d) 304 | (e) P20 |
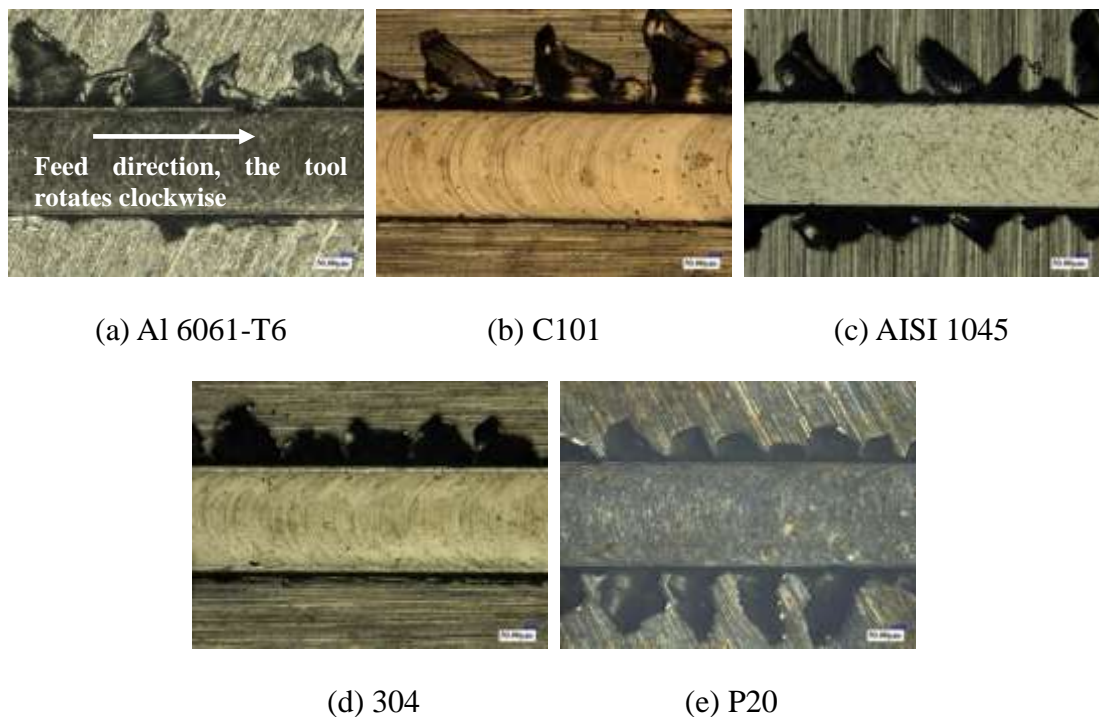
Fig. 7.7 Examples of micro-burr formation upon the first slots for the work materials

The entrance and exit burrs are formed respectively by up and down milling, and they have different characteristics on the five investigated materials. Burr height and thickness are the most frequently and easily measured burr quantities, but they cannot reflect the burr size precisely in the study. Therefore, a comparative study on the micro-burr formation is undertaken so as to determine which material gives the best or the

worst performance.

Al6061-T6, C101 and 304 can be categorized as a group due to almost free of exit burrs. At the entrance side, C101 exhibits the slightly larger burr size than Al 6061-T6, and stainless steel 304 has the smallest. In the other group, the burrs on AISI 1045 and P20 samples are distributed at the both entrance and exit sides. At the entrance side, the burrs for AISI 1045 are approximately two times larger than those of P20, but they are much smaller at the other side. In contrast, P20 at the exit side is prone to achieve the largest size of burrs, even when compared to those of AISI 1045 at the entrance side. According to the observations from the two groups, hardness may be considered to be an influential factor for the micro-burr formation in terms of size and location. The softer the work materials, the bigger the entrance burrs. Meanwhile, the harder the work materials, the larger the exit burrs.

In some practical cases, a deburring process is of prime importance for maintaining the accuracy and functionality of a micro-milled part. For a hard work material, the micro burrs are easily fractured and thus removed. On the other hand, if a work material is more ductile, the burrs elimination presents a big challenge as further plastic deformation may take place, leading to excessive dimensional errors and high tensile residual stresses. From this point and regardless of burr size, the second group including P20 and AISI 1045 may give the better performance than the first group that contains Al6061-T6, C101 and 304.

7.4.2 Tooling performance in the second set of cutting trials

In this section, emphasis is placed on the cutting performance of C101, AISI 1045 and 304 under three groups of cutting conditions. The first group is cutting with 94.2m/min speed and 20µm axial depth of cut, but variable feed per tooth from 0.2µm, 0.4µm to 0.6µm, in order to investigate the feed effect on different material samples. In the second group, cutting speed varies at 62.8m/min, 94.2m/min and 125.6m/min with 0.4µm feed per tooth and 30µm axial depth of cut. Three levels of axial depth of cut including 10µm, 20µm and 30µm are studied in the third group using the highest level of feed rate at 0.6µm/tooth and cutting speed at 125.6m/min. Consequently, the tooling performance obtained from the nine typical slots is selected for the investigation.

7.4.2.1 Cutting forces

The resultant forces for C101, AISI 1045 and 304 are investigated in the planar directions and these values are plotted in Fig. 7.8, in an attempt to find out the trend of their changes under the above specified conditions.

(a) Feed per tooth

(b) Cutting speed

(c) Axial depth of cut
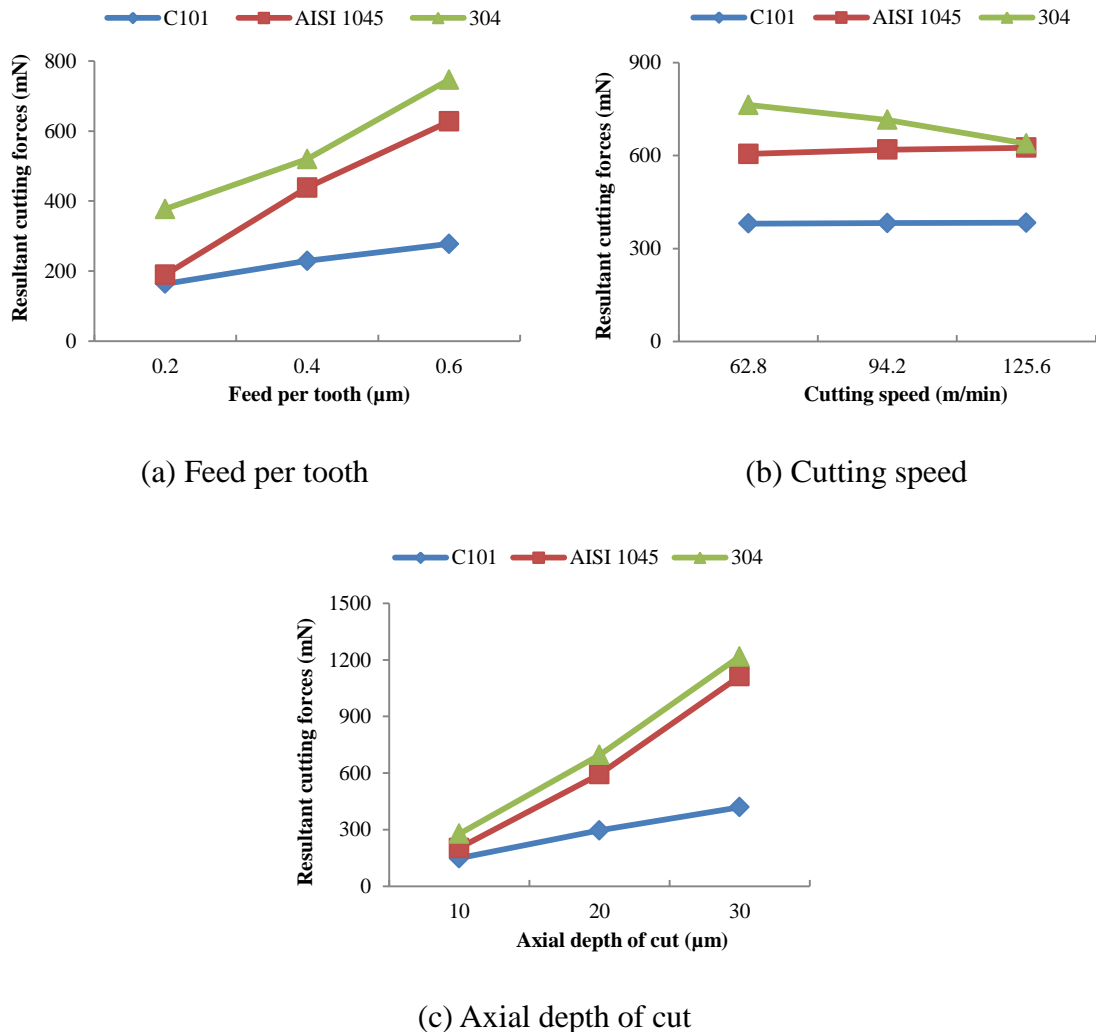
Fig. 7.8 Resultant force variations for the three materials under various conditions

For the three work materials, the resultant forces have a general increase with the feed rate, and the feed effect is shown to be more prominent for the two steels than that for C101. If the feed per tooth varies from 0.2µm to 0.6µm, the force for 304 rises from 377mN to 746.7mN, and for AISI 1045 from 190mN to 627mN, whereas that for C101 only has a minor increase by 114.1mN.

Cutting speed has the less influence except for 304. From 62.8m/min to 125m/min, the chip loads for AISI 1045 and C101 remain level to be around 615mN and 382mN respectively. But that for the stainless steel are slightly reduced when the spindle rotates at a faster speed. It decreases from 763mN to the same level as that of AISI 1045 at the cutting speed of 125.6m/min (see Fig. 7.8(b)). As 304 has the lowest thermal conductivity, more heat tends to be accumulated in the cutting zone at the higher speed, and thus the force reduction is probably caused by the thermal softening effect.

Among the three process variables, axial depth of cut has the strongest influence. At the lowest level, the forces for C101, AISI 1045 and 304 are measured to be 148.2mN, 202.2mN and 278mN respectively. While at the highest level, the loads surge to over 1,100mN for the two steels, but only 420mN for C101. The variation of axial depth of cut presents roughly the more and same effect for AISI 1045 and 304, but much less for C101, as illustrated in Fig.7.8(c).

From above analysis, in general, stainless steel 304 induces the largest resultant forces under the three levels of cutting conditions, followed by AISI 1045, and C101 has the considerably lowest loads. Hence, the power consumed for micromachining C101 is the least, AISI 1045 is in the intermediate rank and that of 304 is the most.

7.4.2.2   Surface roughness

Fig. 7.9 (a-c) respectively shows the effect of feed per tooth, cutting speed and axial depth of cut on the surface roughness Ra for the C101, AISI 1045 and 304 samples.

It is found that the feed effect on C101 is less obvious, but more on AISI 1045 and 304 as the roughness values decreases slightly when the feed varies from 0.2μm to 0.6μm per tooth. For AISI 1045, the value changes from 109nm to 86nm, whereas that for 304 from 120.3nm to 97.7nm. This implies that the size effects might be dominant on the surface generation of AISI 1045 and 304 under the used feed domain. In addition, the machining quality for C101 is the best and that for 304 is the poorest.

Cutting speed has almost no obvious effects under the investigated conditions, except for micromachining 304 at a higher speed. In such case, the machining quality can be fairly improved, even better than that of AISI 1045. However, C101 still gives the best

surface roughness at around 70nm, which is 30% less than that of AISI 1045.

(a) Feed per tooth

(b) Cutting speed
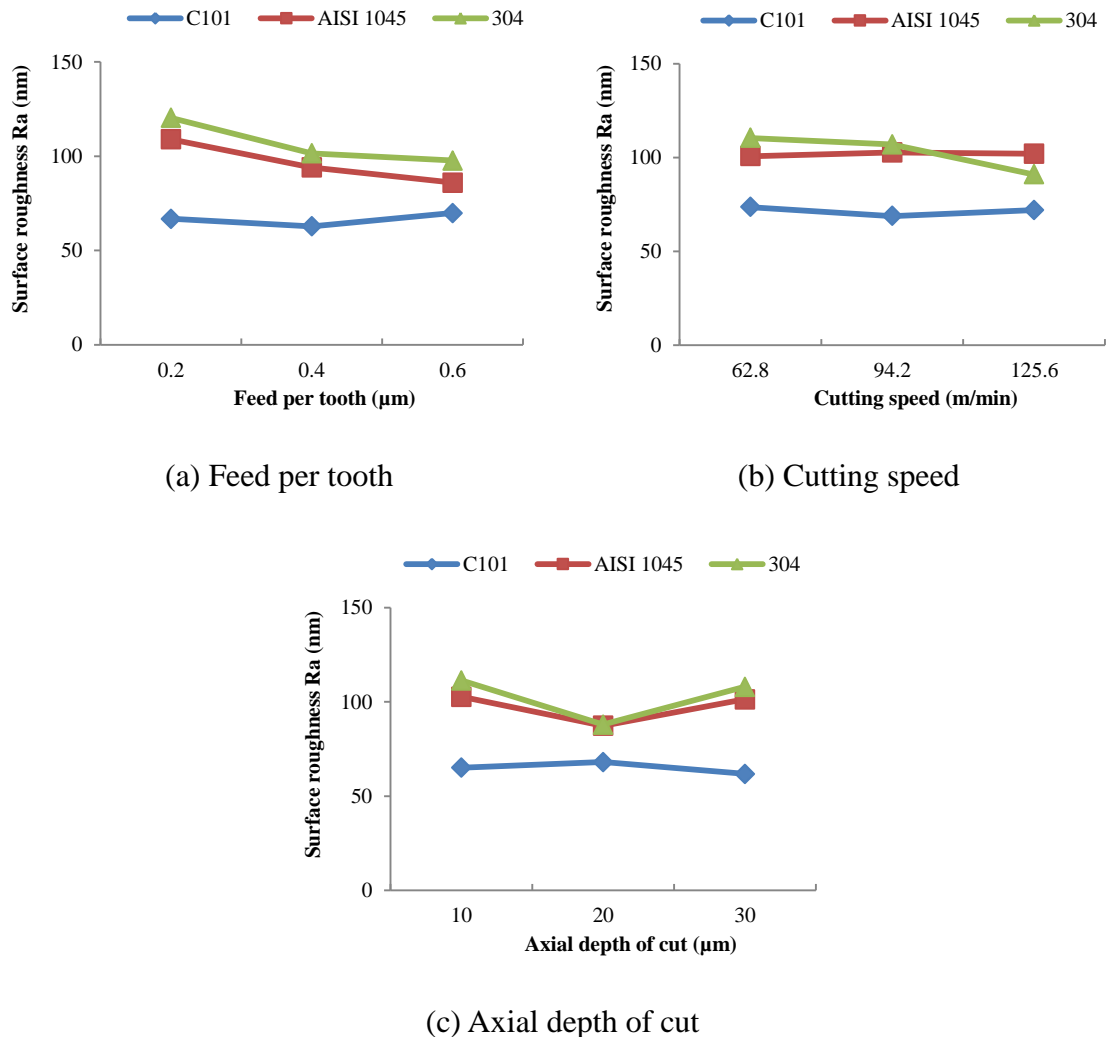
(c) Axial depth of cut

Fig. 7.9 Surface roughness variations for the three materials under various conditions

It is interesting to note that the roughness for C101 remains constant regardless of the axial depth of cut. For the other two materials, the values have a decrease then increase trend when the axial depth of cut changes from 10μm, 20μm to 30μm. This phenomenon demonstrates that there exist size effects in the axial cutting direction for the surface generation. For AISI 1045 and 304, an optimum micromachining can be achieved if the axial depth of cut is appropriately selected. Apart from that, this trend also implies that the MCT value for C101 is much smaller than those for AISI 1045 and 304. From Fig.7.9 (a-c), in general, the sequence of the best to the worst achievable surface is C101, AISI 1045 and 304.

7.4.2.3   Micro-burr formation

Table 7.5 collectively shows images of micro-burr formation under the three typical groups of cutting conditions, and there exist substantial differences concerning burr size and location for the three investigated materials.

In contrast to the conventional tendency that the higher feed the bigger burrs, the adverse feed effect appears for C101 and 304 in the first group. The influences on micro-burr formation are clearly observed, in which generally the lower feed, the much larger burrs. Simultaneously at the exit side, minor burrs tend to be formed at the low feed, but there are no observable burrs at the high level. For AISI 1045, burrs are generated at the both up and down milling sides of the slots, and the size or volume at the three feeds are seen without any noticeable differences. At the 0.2µm feed per tooth, C101 produces the largest burrs, followed by 304 and AISI 1045. If the value increases to 0.6µm, the size of micro-burrs for C101 and 304 is greatly reduced, even smaller than that for AISI 1045. Therefore, it is concluded that the feed plays a more important role in terms of burr size and location for a ductile material.

In the second group under 0.4µm feed per tooth and 30µm depth of cut, cutting speed shows independence on the micro-burr formation for the ductile materials, such as C101 and 304. But for AISI 1045, the entrance burrs increase and the exit burrs decrease along with the rising cutting speed. At the same level of cutting speed, it is observed that C101 produces the biggest and 304 the smallest burrs.

Axial depth of cut influences the micro-burr formation more than the other controllable process parameters, as is evident in the third group. For all the three materials, the entrance burrs rise dramatically and the exit burrs just emerge or become slightly larger if the axial depth of cut increases from 10µm to 30µm. At the 10µm axial depth of cut, there are almost no burrs on C101, and little burrs on 304 but relatively larger burrs at both entrance and exit sides for AISI 1045. At the 30µm axial depth of cut, C101 gives the worst performance with respect to the burr size, and stainless steel 304 is considered to be the best. Therefore, the axial depth of cut presents the most sensitive variable with respect to the micro-burr formation for C101 than the other two materials.

Table 7.5 Micro-burr formation under the three groups of cutting conditions

		Work materials		
		C101	**AISI 1045**	**304**
The first group (94.2m/min cutting speed and 20μm depth of cut and various feed per tooth)	**0.2μm**			
	0.4μm			
	0.6μm			
The second group (0.4μm feed per tooth and 30μm depth of cut and various cutting speed)	**62.8 m/min**			
	94.2 m/min			
	125.6 m/min			
The third group (0.6μm feed per tooth and 125.6m/min cutting speed and various axial depth of cut)	**10μm**			
	20μm			
	30μm			

7.5   <u>Summary of the cutting performance for the five materials</u>

Based on the observations obtained from the two sets of micro milling trials, the cutting performance for the five investigated work materials is summarized in Table 7.6.

Table 7.6 Summary of the cutting performance for the work materials

| | | | | Work materials | | | |
			Al 6061-T6	C101	AISI 1045	304	P20
The first set of cutting	**Averaged cutting forces (mN)**		156.8	222.8	266.2	414.4	418.7
	Force variations (mN)		22.5	31.0	58.6	38.4	92.9
	Tool state		Large BUE	As new	Excessive wear	Potential BUE	Edge fracture
	Tool flank wear (μm)		13.48	3.78	25.74	25.33	25.22
	Averaged surface roughness (nm)		146.2	79.2	96.5	104.1	183.3
	Roughness variations (nm)		57	33.3	38.6	57.3	130
	Micro-burr formation		Ultra large, on up-milling side	Ultra large, on up milling side	Large, on both side	Small, on up-milling side	Large, on both side
The second set of cutting	**Resultant Cutting forces (mN)**	**Feed per tooth (μm)** 0.2	—	163.6	190	377	—
		0.4		229	438.5	519.8	
		0.6		277.7	627	746.7	
		Cutting speed (m/min) 62.8	—	380.4	604.9	763	—
		94.2		382.2	618.9	715	
		125.6		383	625.3	638.5	
		Axial DOC (μm) 10	—	148.2	202.2	278	—
		20		295.9	593.7	695.4	
		30		418.7	1113	1218	
	Surface roughness (nm)	**Feed per tooth (μm)** 0.2	—	66.8	62.8	69.8	—
		0.4		109	94	86	
		0.6		120.3	101.5	97.7	
		Cutting speed (m/min) 62.8	—	73.6	100.7	110.5	—
		94.2		68.8	102.7	107	
		125.6		72	102	91	
		Axial DOC (μm) 10	—	65.1	102.7	111.4	—
		20		68.1	87.4	88	
		30		61.8	101.4	108	
	Micro-burr formation in general		—	Large	Medium	Small	—

Comparison of the averaged cutting forces in the first set of cutting trails indicates that Al 6061-T6 is the easiest metal to machine, and P20 together with 304 are the most difficult under the specified cutting conditions. In addition, Al 6061-T6 has the smallest force variations and P20 the largest along with the tool wear or fracture progression. In terms of the micro tool integrity, surface roughness and variations, C101 presents the best and P20 appears to be the worst. However, C101 and Al 6061-T6 form the largest burrs, but 304 much smaller.

The second set of cutting trials is undertaken to further examine the cutting performance of C101, AISI 1045 and 304 under various cutting conditions. From the general information given in the table, C101 experiences the best performance except for the micro-burr formation and 304 the weakest among the three materials. The results are in well consistency with those obtained from the first set of cutting trials.

By comprehensively considering the cutting performance of the five work materials, the micro-machinability of C101 is considered to be very good and by some definitions, excellent. That of Al 6061-T6 ranks as the second place due to the lowest forces and less tool wear but large BUE and micro-burr formation as well as poor surface roughness. AISI 1045 is in the medium place, and P20 presents the poorest even when compared to stainless steel 304 with regard to all the evaluation indicators, including the cutting forces, tool integrity, surface roughness and micro-burr formation.

7.6 Conclusions

This chapter presents an experimental study on the cutting performance of the five most common metals that consist of Al 6061-T6, copper C101, carbon steel AISI 1045, stainless steel 304 and tool steel P20. The properties and characteristics of the work materials are briefly introduced. Two sets of micro milling trials on C101, AISI 1045 and 304 samples and one set on Al 6061-T6 and P20 samples are conducted with coolant, in order to analyze the cutting forces, tool wear, surface roughness, and micro-burr formation under the specified process conditions.

The cutting behaviours of the five materials are observed, discussed and summarized. The easiest to the most difficult machined materials are from Al 6061-T6, C101, and

AISI 1045,304 to P20. However, if the comprehensive cutting performance is of concern, the general sequence from the best to the poorest becomes C101, Al 6061-T6, AISI 1045, 304 and P20.

The study also demonstrates that a material's performance is not only affected by its conditions or properties but also by the cutting mechanism and mechanics. Cutting conditions play an important role on the micromachining characteristics of a work material and the MCT effect may have a negative influence. Therefore, in case the micro milling machine, cutting tool and work material are predefined for a specific application, proper selection of cutting conditions is of prime importance for achieving an optimum performance.

Chapter 8 Influence of Process Variables on the Tooling Performance

8.1 Introduction

In micro milling, feed rate, cutting speed and axial depth of cut constitute the complete set of process variables. Due to fragility of the micro tools and size effects in micro-scale cutting, pure geometrical downscaling based on the knowledge available for conventional milling appears inappropriate for the selection of process conditions, as it may lead to excessive tool deflections, premature tool failures and edge fractures. Simultaneously, negative effects on the cutting performance, such as machining inaccuracy and low productivity, become prominent.

At present, the emerging manufacturing technology is not fully understood and the existing knowledge and experiences are limited. There are no good methods for selecting suitable cutting conditions and the recommendations from tool suppliers or the trial-and-error method cannot always guarantee a successful micro milling. Due to the high cost of micro tools, the process variables adopted in practice are quite conservative. Therefore, systematic knowledge on the effects of process variables on the tooling performance is indispensable for engineers as it has potential benefits for the extension of tool life and selecting optimum cutting conditions.

This chapter aims to comprehensively investigate the effects of process variables based on both FEM and experimental approaches. Firstly, preliminary determination of feed rate based on the MCT value is discussed. Simulation based approach is then used to predict the cutting forces, tool stresses, tool temperatures as well as chip formation and temperatures, and finally experiments based approach is adopted to study the surface roughness under various process variables. The comparisons of the tooling performance are presented so as to provide scientific knowledge for the process planning and optimization.

8.2   Preliminary determination of feed rate based on the MCT value

In orthogonal cutting, the reduction of UCT does not linearly decrease the cutting forces, as indicated in Fig. 6.10. Accordingly, in micro milling, the cutting loads have nonlinear trend along with decreasing feed per tooth. If feed per tooth is selected to be smaller than the value of MCT, complete ploughing phenomenon occurs and no chip forms, which significantly affects the machining performance in terms of cutting force vibrations (Vogler et al., 2004b), large burr formation (Lee et al., 2002), high specific cutting energy (Liu et al., 2007; Ng et al., 2006; Lucca et al., 1991), poor surface quality (Vogler et al., 2004a), etc. Hence, it is important to identify the value of MCT and choose appropriate feed rate in an effort to enhance the tooling performance.

Son et al. (Son et al., 2005) proposed a simple analytical model to estimate the MCT in micro-scale cutting. Two factors including friction coefficient between the tool and workpiece, and the tool cutting edge radius, determine the value of MCT in the model, and it can be formulated as:

$$t_m = r \left(1 - cos \left(\frac{\pi}{4} - \frac{\varphi}{2} \right) \right) \qquad (8\text{-}1)$$

where t_m − The value of MCT;

$\quad$ r − The tool cutting edge radius;

$\quad$ φ − The friction angle between tool and chip;

$$\varphi = \arccos \left(\frac{1}{\sqrt{1 + \mu^2}} \right) \qquad (8\text{-}2)$$

$\quad$ μ − Coefficient of friction.

Literature review in Chapter 2 demonstrates that, the ratio of MCT to the tool cutting edge radius (normalized MCT) is not only affected by the friction coefficient and the tool cutting edge radius, but also the thermo-mechanical properties of work materials and cutting conditions. According to Liu et al. (Liu et al., 2006), an increase in the cutting speed and the tool cutting edge radius leads to increased normalized MCT. This is due to the predominance of thermal softening over strain hardening effects. When the cutting temperature rises, thermal softening enables work material more ductile and less

easy to form chips. An increase in the composition content of a work material also leads to a rise in the normalized MCT. Based on above discussions, due to the simplification, the analytical model given in equation (8-1) is only partially suitable for describing the complex process and thus it underestimates the value of MCT.

Experimental method is a direct way for the estimation of MCT, but in some cases it appears to be costly, tedious, time-consuming and less practical. Furthermore, the accuracy will be strongly affected by experimental uncertainties.

FEM based methodology, as proposed in Chapter 3 and Chapter 6, can comprehensively and simultaneously take into account the tool geometries, thermo-mechanical properties of work materials, cutting conditions as well as the tool-work contact scheme, and it emerges as a more feasible and promising approach. In principle, a 2D orthogonal model as given in Chapter 6 is more convenient to determine the specific value of MCT as a 3D model with a helix angle is relatively complex and requires specific knowledge for developing the tool and workpiece models.

According to the discussions from investigating tooling geometrical effects in Chapter 4, the normalized MCT is estimated to be between 25% and 40% for AISI 1045 steel. For the micro tool Magaforce 8500-Ø0.3mm with 2.5µm edge radius, the value of MCT for AISI 1045 steel is in the range of 0.625µm to 1µm. Similarly, the value of MCT under Magaforce 8507-Ø0.5mm with 1.5µm edge radius falls into 0.375µm and 0.6µm domain. Therefore, in order to avoid possible complete ploughing phenomenon and improve the tooling performance, the feed per tooth used should be set to or above 1µm and 0.6 µm respectively for the two types of tools.

8.3   Simulation based study on the tooling performance

In the following section, the FEM simulation based approach proposed in Chapter 3 is used to study the influence of process variables on the cutting forces, tool stresses, tool temperatures as well as chip formation and temperatures in micro milling of AISI 1045 in dry conditions.

8.3.1 Simulation inputs

Investigation on the effects of process variables on micro milling performance is similar to study the tooling geometrical effects as described in Chapter 4. Simulations are carried out using uniform tool geometries, i.e. Ø0.3mm diameter, 7° rake angle, 15° relief angle, 30° helix angle and 2.5µm cutting edge radius.

Various process variables, as shown in Table 8.1, are applied. There are three input groups, which consist of group 1 for three levels of feed per tooth, group 2 for three levels of cutting speed and group 3 for three levels of axial depth of cut. The three levels of cutting speed correspond to the spindle speed with 15,000rpm, 30,000rpm and 45,000rpm. In the same group, when a specified variable changes, other process parameters remain constant. Seven simulations in total, including the benchmarking simulation in Chapter 3, are performed in dry cutting and the associated tooling performance are presented and analyzed in the following sub-sections.

Table 8.1 Process variables for the simulation inputs

	Feed per tooth (µm)	Cutting speed (m/min)	Axial depth of cut (µm)
Group 1	1, 1.5, 2	28.26	20
Group 2	1	14.13, 28.26, 42.39	20
Group 3	1	28.26	15, 20, 25

8.3.2 Process variable effects on the micro milling performance

8.3.2.1 Cutting forces

Fig. 8.1 illustrates the predicted maximum cutting force components under three levels of feed per tooth, cutting speed and axial depth of cut. It is obviously seen that the maximum normal, feed and axial forces increase gradually with increasing feed per tooth and axial depth of cut whereas there are almost no variations under different cutting speed. Therefore, both feed per tooth and axial depth of cut play a vital role on determining the magnitude of cutting forces, and cutting speed has less importance.

(a) Feed per tooth   (b) Cutting speed

(c) Axial depth of cut
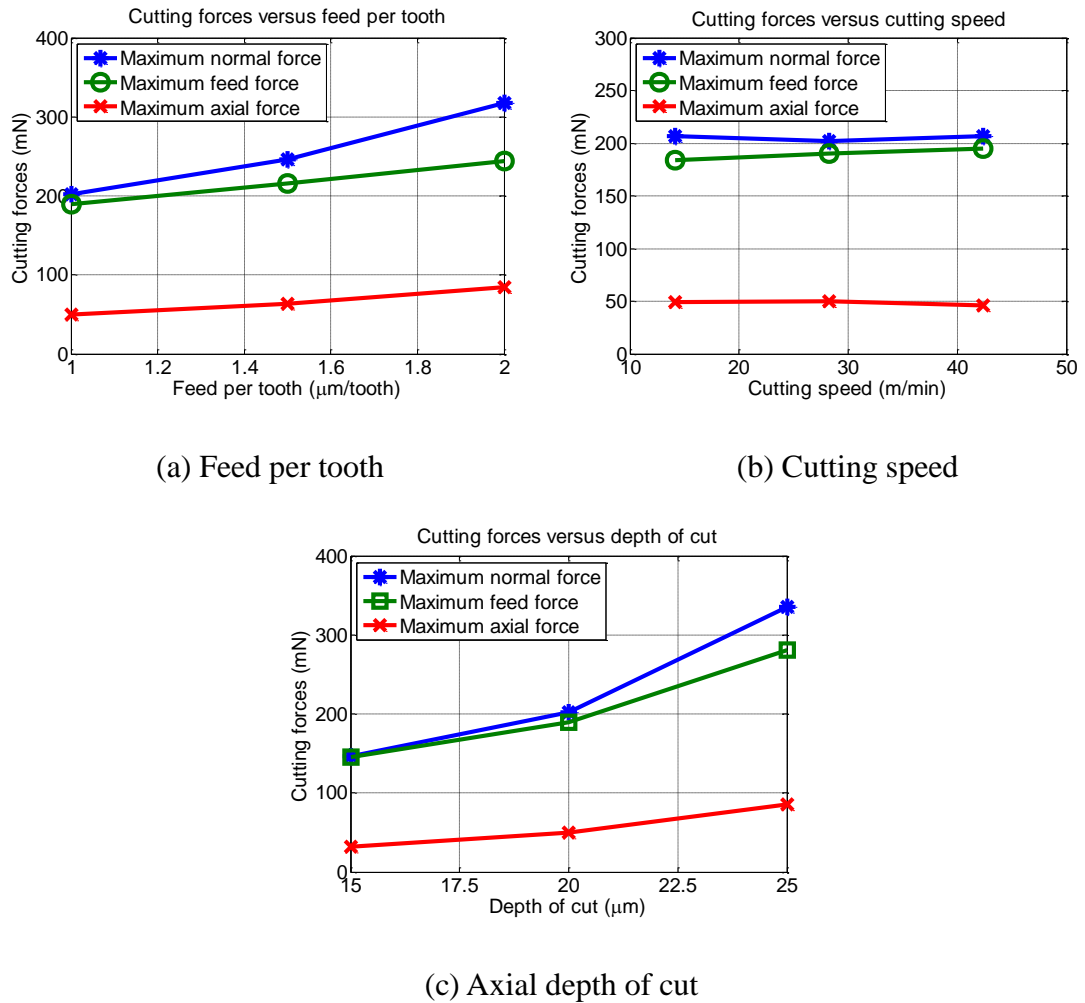
Fig. 8.1 Predicted cutting forces under different process variables

In micro milling, when the cutting forces approach the strength of a tool within a few rotations, premature tool failures or edge fractures take place. In general, small feed per tooth and axial depth of cut are more desirable for the cutting force reduction but result in low productivity. Once feed per tooth is reduced to or smaller than the minimum chip thickness of the machined material, elastic recovery resulting from ploughing dominates the cutting, which contributes to significant deterioration of the tooling performance, as pointed out in section 8.2. Thus, there exists an optimum feed per tooth for the best performance. It is well established that high cutting speed leads to better cutting performance, and from Fig. 8.1(b), cutting speed can hardly affect the cutting forces, thus it could be employed as high as possible. Due to the small diameter of micro tools, micro milling machines are commonly equipped with high speed spindles so as to achieve good tooling performance and acceptable productivity. In practice, from cutting forces perspective, axial depth of cut is always determined based on the

recommendations of tool suppliers or experiences of machine operators so as to avoid excessive tool deflection or premature failures.

8.3.2.2   Tool stresses

The predicted maximum effective stresses at the primary cutting edges of micro tools under the highest resultant forces during one cutting pass are shown in Fig. 8.2.

(a) Feed per tooth   (b) Cutting speed

(c) Axial depth of cut
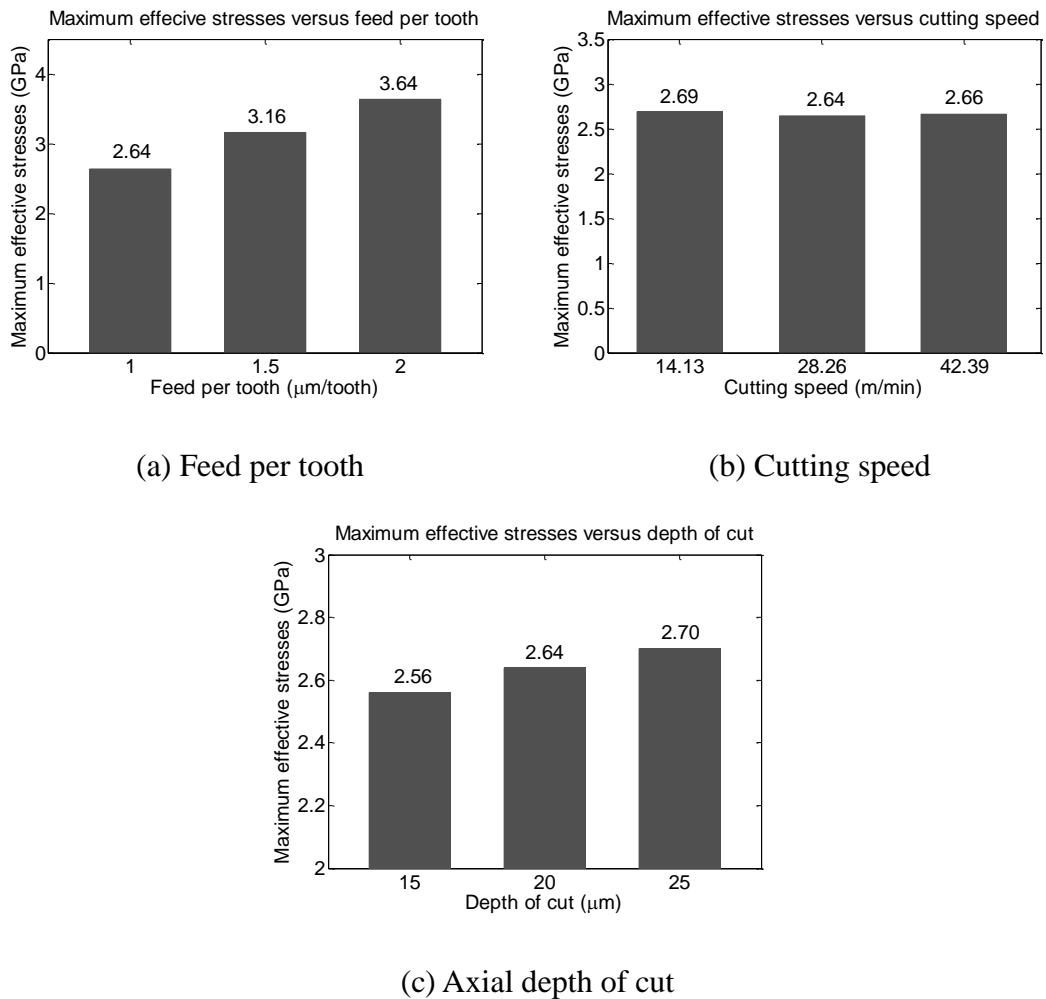
Fig. 8.2 Predicted maximum tool stresses under different process variables

Rising feed per tooth from 1µm to 2µm leads to steadily increasing the tool stresses (see Fig. 8.2 (a)), and the maximum tool stresses under different cutting speed levels have minor variations (see Fig. 8.2 (b)), which matches corresponding trend of cutting forces prediction. With respect to axial depth of cut, although the predicted cutting forces increase considerably (See Fig. 8.1 (c)), the maximum tool stresses only rise slightly as

shown in Fig. 8.2 (c), mainly attributing to the extension of tool-work interface contact length. Among all the three process variables, feed per tooth is the most important factor on affecting the effective tool stresses, followed by axial depth of cut and cutting speed has less importance.

8.3.2.3 Tool temperatures

Temperature distributions on micro tools after 180º rotation angles cutting employing different feed per tooth, cutting speed and axial depth of cut are predicted in Fig. 8.3, Fig. 8.4, and Fig. 8.5 respectively. It is clearly seen that more heat tends to be accumulated at the cutting edges of micro tools and at the cutting tip points in particular.

| (a) 1µm | (b) 1.5µm | (c) 2µm |
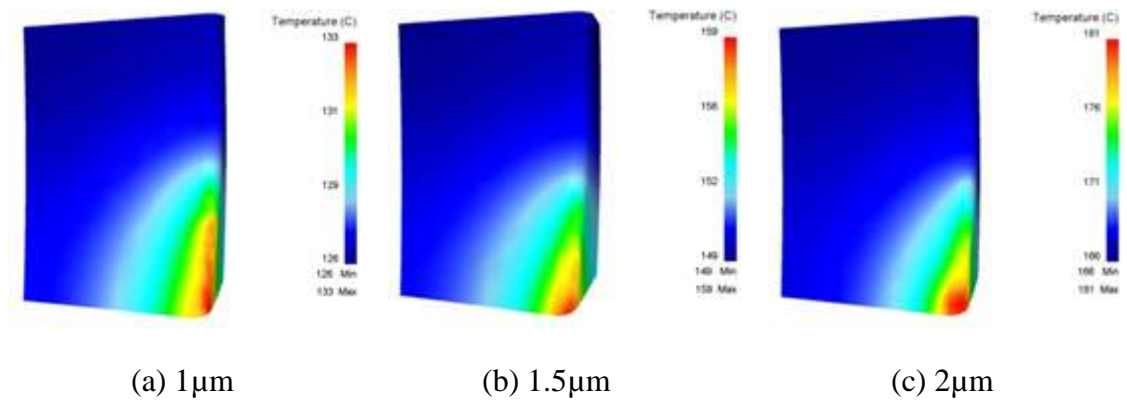
Fig. 8.3 Predicted tool temperature distributions under different feed per tooth after one cutting pass

| (a) 14.13m/min | (b) 28.26m/min | (c) 42.39m/min |
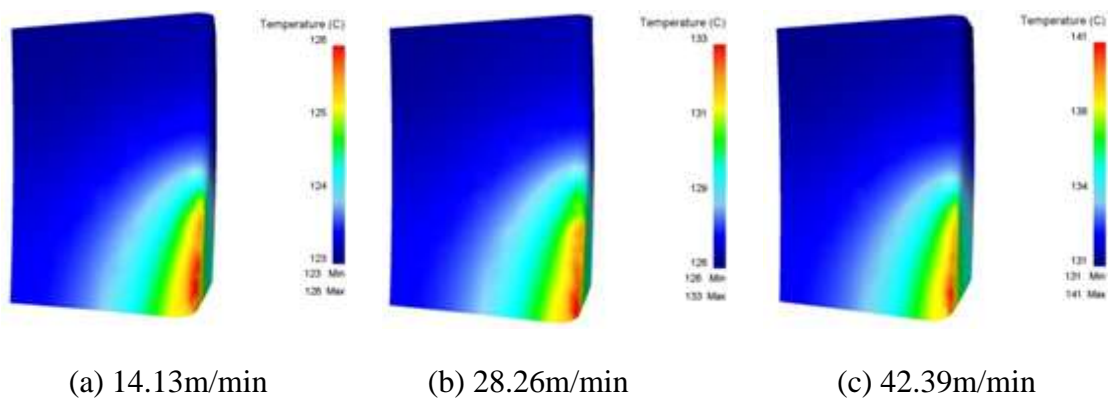
Fig. 8.4 Predicted tool temperature distributions under different cutting speed after one cutting pass

(a) 15μm　　　　　　　　(b) 20μm　　　　　　　　(c) 25μm
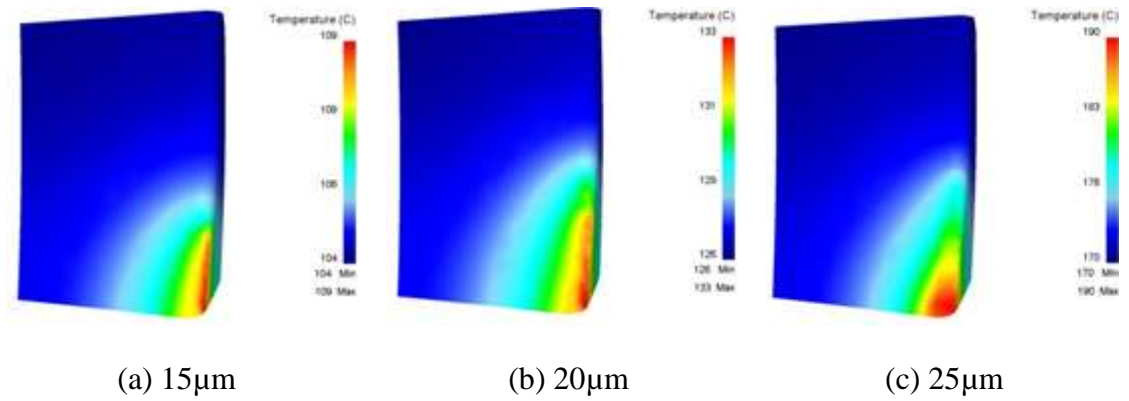
Fig. 8.5 Predicted tool temperature distributions under different axial depth of cut after one cutting pass

(a) Feed per tooth　　　　　　　　　　　　(b) Cutting speed

(c) Axial depth of cut
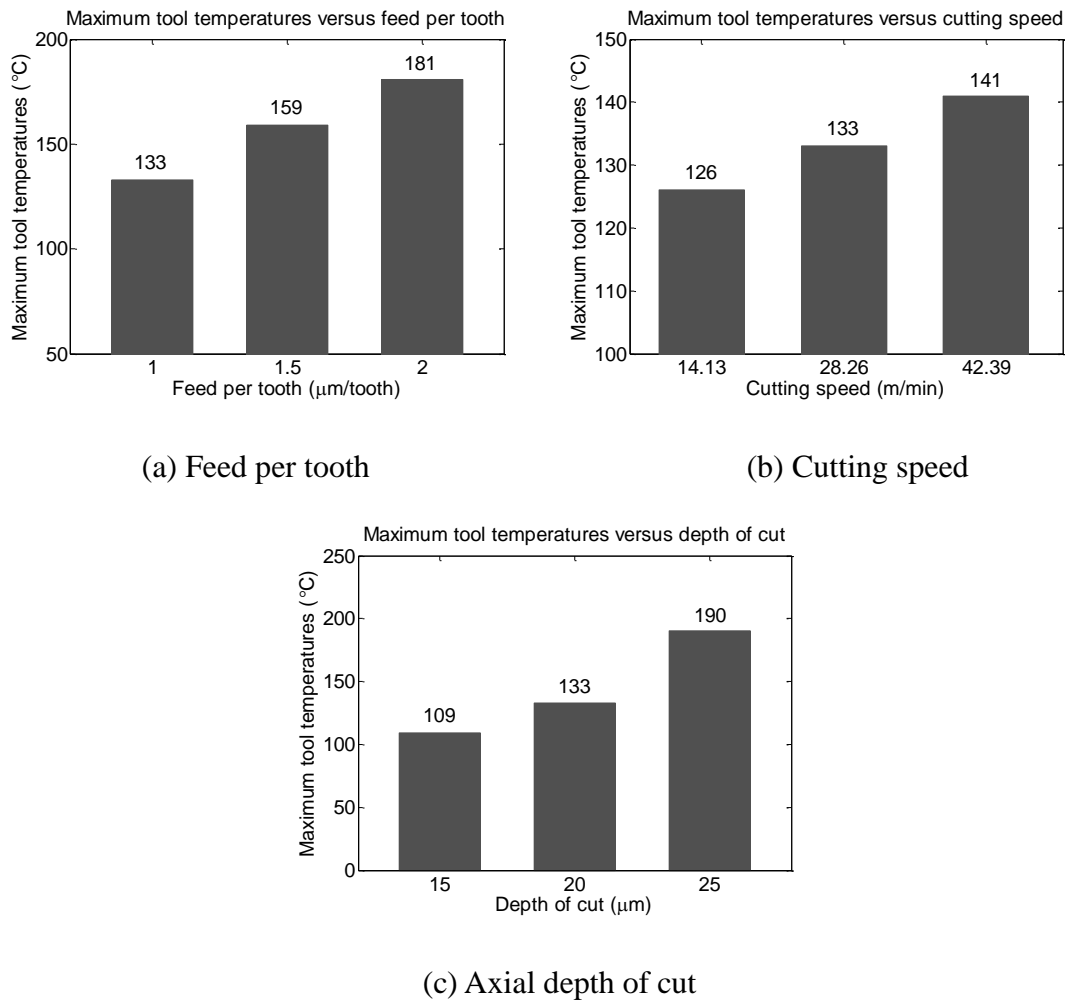
Fig. 8.6 Predicted maximum tool temperatures under different process variables after one cutting pass

According to comparison of the maximum tool temperatures, as illustrated in Fig. 8.6,

all the three process factors have considerable impact on the heat generation. Rising feed per tooth, cutting speed as well as axial depth of cut gives rise to the tool temperatures, which means higher tool wear rate and shorter tool life. Hence, micro milling may not suitable for high duty operations due to more heat generation and excessive tool wear problems.

8.3.2.4   Chip formation and temperatures

Good chip evacuation capabilities as well as low temperature chips contribute to better tooling performance, such as longer tool life and less energy consumption. Predicted chip morphologies at 60° rotation angle cutting under different process conditions are given in Fig. 8.7, Fig. 8.8 and Fig. 8.9 respectively.

From Fig. 8.7, all three levels of feed per tooth generate both spiral and continuous chips. For 1μm feed per tooth, chip shape emerges to be slightly straight, owing to prominent negative rake angle effect. The phenomenon is mainly caused by the small ratio of radial depth of cut to the cutting edge radius of micro tools. Additionally, 1μm feed per tooth has the least maximum chip temperature at 95.2ºC whereas 2μm feed has the most at 111ºC. If the feed per tooth becomes higher, thicker chips can be formed, leading to possible chip crowding inside tool flutes. Chip crowding often results in chip hammering, excessive energy consumption, crater wear, or even catastrophic edge failures. Hence, high feed per tooth is not suitable for micro-scale machining, and among all investigated feed per tooth, 1μm feed delivers the best results in terms of good chip ejection and low chip temperatures.

(a) 1μm   (b) 1.5μm   (c) 2μm
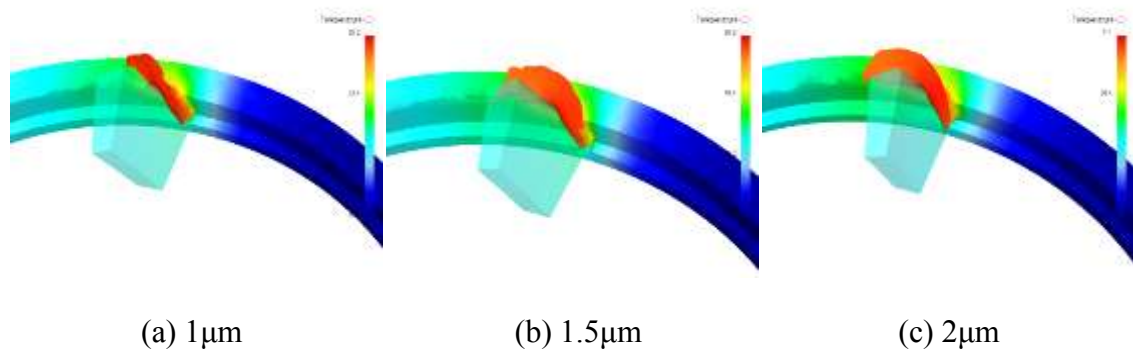
Fig. 8.7 Chip formation at 60° rotation angle under different feed per tooth

(a) 14.13m/min   (b) 28.26m/min   (c) 42.39m/min
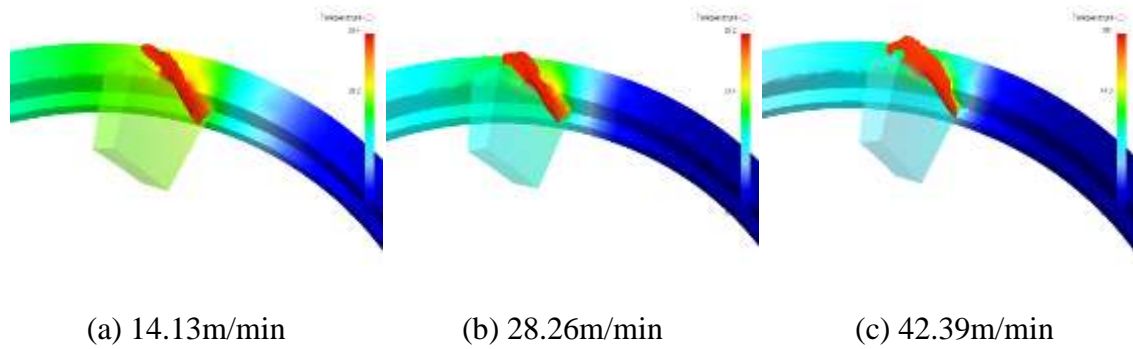
Fig. 8.8 Chip formation at 60° rotation angle under different cutting speed

(a) 15μm   (b) 20μm   (c) 25μm
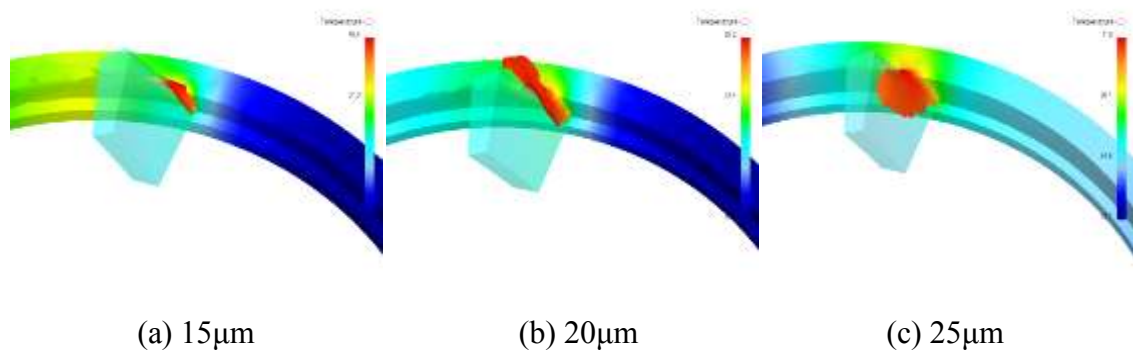
Fig. 8.9 Chip formation at 60° rotation angle under different axial depth of cut

Increasing cutting speed gives rise to more heat generation. The maximum chip temperatures are predicted to be 65.4ºC, 85.2ºC and 101ºC when using 14.13m/min, 28.26m/min and 42.39m/min cutting speeds. However, almost identical chip shapes and flow directions are found, as depicted in Fig. 8.8.

Different axial depth of cut has different response on the chip formation. According to Fig. 8.9, small depth of cut is beneficial for the chip evacuation, and the smaller depth of cut, the lower chip temperatures. In some cases, because of small depth of cut and dull cutting edge of micro tools, large plastic deformation takes place in the axial cutting direction. Material removal is mainly achieved by protrusion rather than shearing and no chips but burrs are formed, as an example is shown in Fig.8.9 (a). On the other hand, from Fig. 8.9 (c), high axial depth of cut is prone to form a straight and large volume chip, which is difficult to flow out of the tool flutes as more energy is required for the deformation.

8.3.3 Summary of the simulation based study

The influence of process variables on the cutting forces, tool stresses, tool temperatures, chip formation and temperatures have been investigated using 3D FEM-based approach. Three levels of feed per tooth, cutting speed and axial depth of cut are used for the simulation inputs, and corresponding tooling performance are predicted and compared so as to determine respective influence. The following conclusions can be drawn:

1. Rising feed per tooth and axial depth of cut lead to gradually increasing the magnitude of cutting forces whereas cutting speed causes minor variations.

2. Feed per tooth is the most important factor on determining the maximum effective tool stresses, followed by axial depth of cut, and cutting speed has less importance.

3. Rising feed per tooth, cutting speed as well as axial depth of cut gives rise to more heat generation at the cutting edges of micro tools.

4. Both feed per tooth and axial depth of cut affect chip formation significantly. Cutting speed has less influence on the chip shapes and flow directions but more impact on chip temperatures.

8.4 <u>Experimental study on the surface roughness</u>

Due to the 3D FEM-based approach lacking the capability of predicting the surface generation, in this section, the influence of process variables on the quality of machined surface is further studied by means of experiments. Besides, the MCT effect acting on the surface finish is also discussed.

8.4.1 Experimental details

Micro slot milling on a AISI 1045 steel sample is carried out using the same machine and micro tool as in Chapter 7, and oil based coolant mist is sprayed onto the cutting zone throughout the experiments.

When investigating the influence of feed rate on surface roughness, the feed per tooth is

varied at 0.1µm, 0.2µm, 0.4µm, 0.6µm, 1µm, 1.5µm, 2µm, 2.5µm, 3µm, and 4µm, respectively at a constant spindle speed of 60,000rpm and axial depth of cut of 20µm. The wide range of feed ensures that the MCT of work material can fall into this range so that the MCT effect can be investigated. In case investigating cutting speed and axial depth of cut effects, the spindle speed is varied at 20,000rpm, 40,000rpm, 60,000rpm and 80,000rpm, and the axial depth of cut changes from 10µm, 20µm, 30µm to 40µm with 0.6µm feed per tooth.

The cutting distance under each process condition combinations is 10mm and the tool wear effect is thus regarded as negligible. After the experiments, the topography on the floor of the slots is analyzed for assess the machining quality, using Taylor Hobson non-contact surface profiler CCI2000, as shown in Fig. 8.10. Surface roughness is measured in three different positions across the length of each slot and an averaged value is calculated so as to reduce the measurement uncertainty and assess repeatability.

Fig. 8.10 Non-contact surface profiler Taylor Hobson CCI2000

8.4.2 Results and discussions

8.4.2.1 Influence of feed rate

The averaged surface roughness under different feed rate is shown in Fig. 8.11. It is found that the achievable surface roughness could be between 75-180nm, and the smallest value, 79.3nm, is observed at 1µm feed per tooth. Besides, from the underlying

micro cutting mechanics and characteristics point of view, the wide range of investigated feed can be classified into three zones, namely, ploughing dominant zone, transition zone and shearing dominant zone.
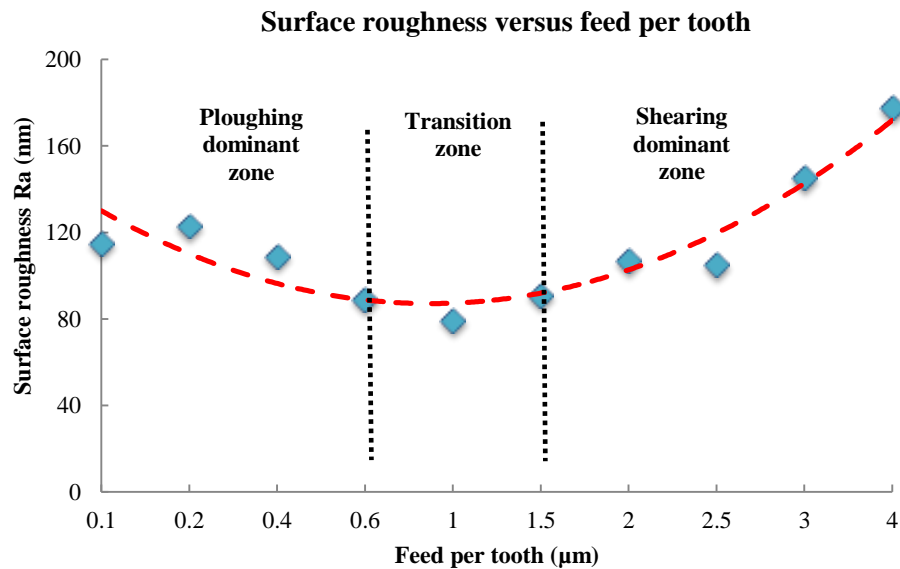
Fig. 8.11 Averaged surface roughness under different feed rate

If the feed per tooth is chosen to be less than 0.6μm, surface roughness has a rough tendency to decrease steadily with an increase of feed rate. Representative images of the machined surface topographies at the 0.2μm and 0.6μm feed per tooth are given in Fig. 8.12. This phenomenon can be explained by alleviating severe ploughing effect for higher feed rate, resulting in less elastic recovery of the work material. In this zone, the ploughing mechanism dominates the cutting. The specific value, 0.6μm per tooth, is largely dependent on MCT of the work material.

The middle range is when the feed per tooth is greater than 0.6μm, and less than 1.5μm, there are fewer variations for the machined surface quality. Both ploughing and shearing mechanisms interact and play an important role in the transition zone. When the feed per tooth increases, the ploughing mechanism reduces surface roughness whereas shearing based on conventional feed effects lead to poor surface quality. Therefore, there is a trade-off between the two cutting mechanisms, and an optimal feed rate exists in the zone that the best surface finish can be produced.

(a) 0.2μm/tooth   (b) 0.6μm/tooth
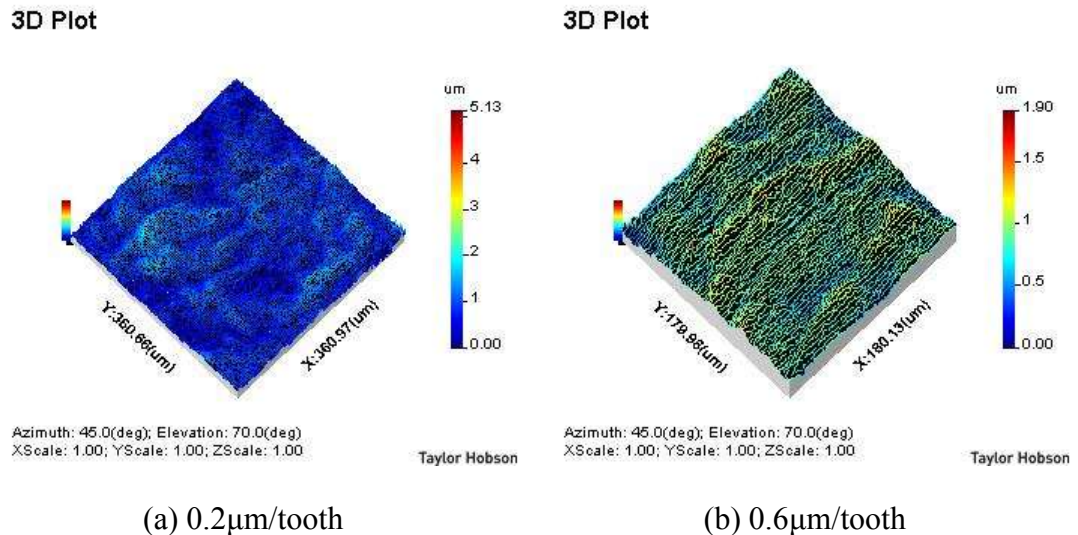
Fig. 8.12 Representative images of surface topographies under different feed rate at the ploughing dominant zone

As in the shearing dominant zone where the feed per tooth exceeds the tool cutting edge radius, the influence of feed per tooth has the same trend as occurring in conventional milling. Although the ploughing effect still exists, it has less significance on the feed marks. The larger feed per tooth, the worse surface finish, which agrees with the conclusions Klocke et al. (Klocke et al., 2009) have drawn.

According to above discussions, optimum surface roughness appears when the feed per tooth is larger than the value of MCT and less than the tool cutting edge radius. Therefore, it is important to determine the two parameters so as to choose appropriate cutting conditions if the surface quality is of great concern.

8.4.2.2   Influence of cutting speed and axial depth of cut

Fig. 8.13 shows the averaged surface roughness, as a function of four levels of cutting speed and depth of cut under 0.6μm feed per tooth.

The cutting speed at 31.4mm/min, 62.8mm/min, 94.2mm/min and 125.6mm/min in the plot corresponds to the spindle speed at 20,000rpm, 40,000rpm, 60,000rpm and 80,000rpm respectively. The surface profiles at the 125.6mm/min cutting speed and 0.6μm/tooth feed rate under different axial depth of cut are illustrated in Fig. 8.14.
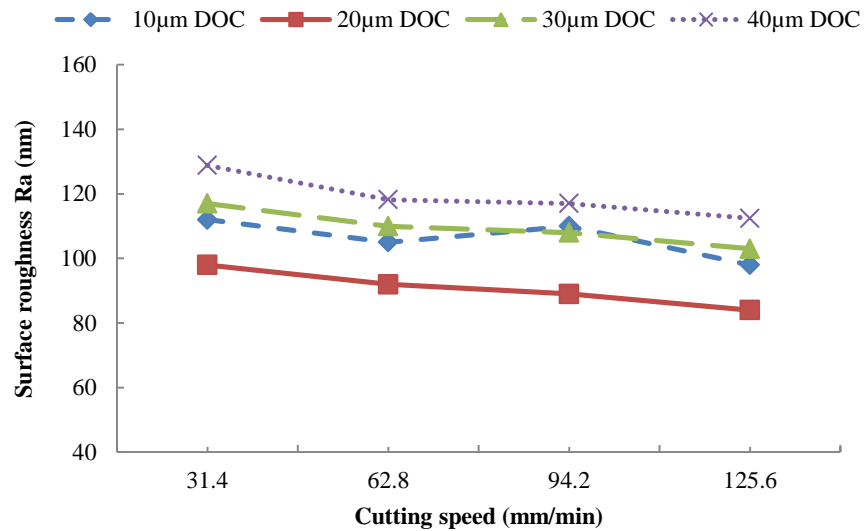
Fig. 8.13 Surface roughness variations at 0.6µm feed per tooth under different cutting speed and axial depth of cut

It can be observed that, in general, higher cutting speed results in slightly smoother surfaces. The cutting speed has positive impact on the surface generation under all levels of depth of cut, which indicates that the spindle speed used for practical operations should be selected as fast as possible so as to achieve good machining quality.

In conventional milling, reducing axial depth of cut sometimes leads to a better surface finish due to less chatter or tool deflection. Nevertheless, in micro milling, this is not always an effective method for improving the machining quality. At constant 0.6µm/tooth, according to Fig. 8.13, the reduction of axial depth of cut from 40µm to 20µm has favourably positive effect on the surface roughness. For example, at 125.6mm/min feed rate, the roughness reduces from 112.4nm to 84nm. If the axial depth of cut decrease continues to 10µm, the surface finish will be slightly deteriorated to be 98nm, probably owing to the prominent size effects as well as the thermal softening of the work materials. In this case, the axial depth of cut becomes the same order of the tool bottom edge radius, and compressing or rubbing phenomenon as well as large elastic recovery will occur in the axial cutting direction, which dominates the material removal mechanism and chip generation physics, and eventually influences the machining process including surface generation. Thus, similar as the characteristics of feed rate influence, there also exists an optimum axial depth of cut at which micro

milling produces the best surface finish. The results achieved are not in consistent with the literature (Vogler et al., 2004a), in which the authors stated that the axial depth of cut has less influence on the surface generation.

(a) 10μm

(b) 20μm

(c) 30μm

(d) 40μm
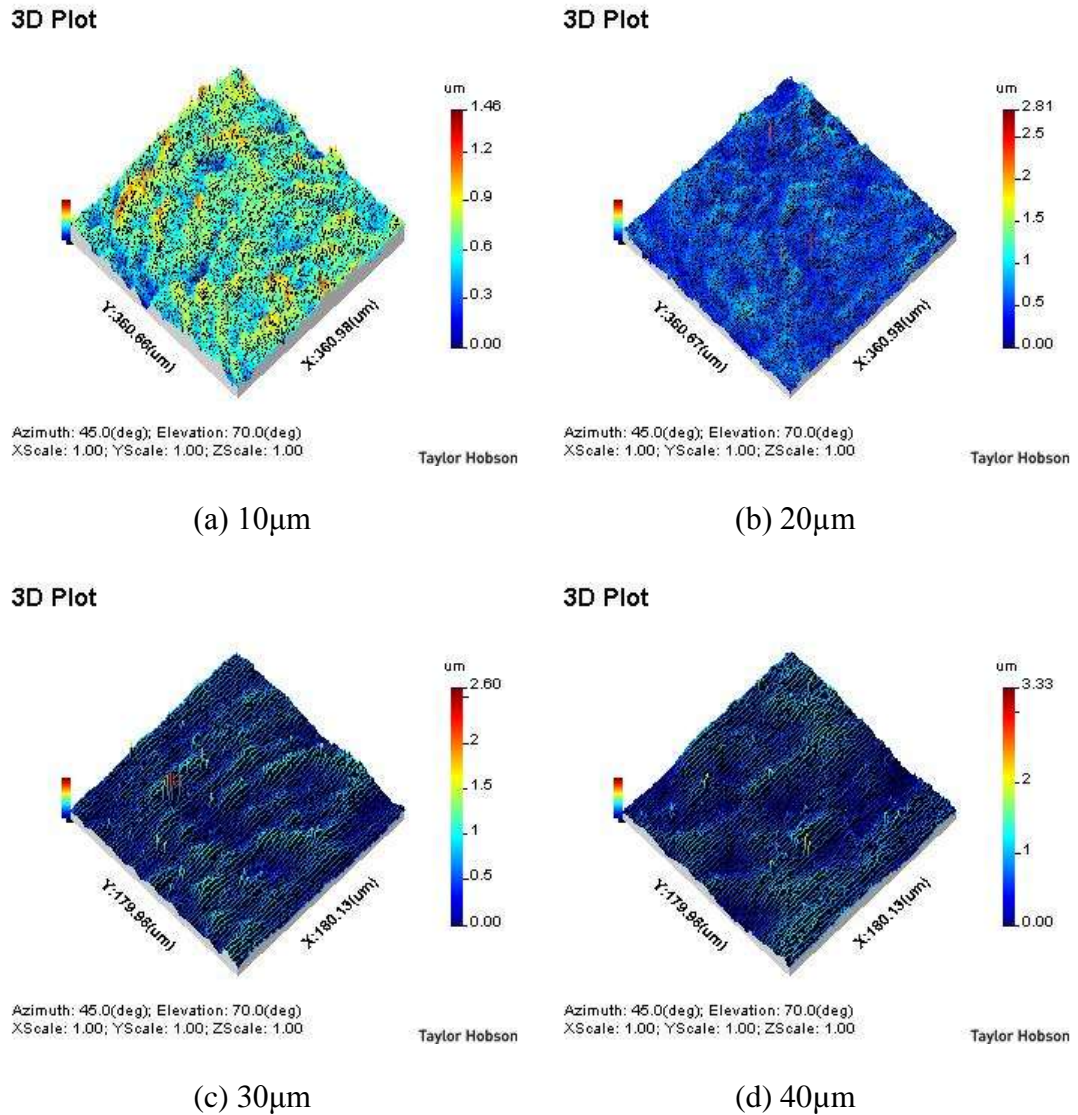
Fig. 8.14 Surface profiles under different axial depth of cut at 125.6mm/min cutting speed and 0.6μm feed per tooth

From improving machining efficiency point of view, the axial depth of cut should be selected as large as possible, assuming there are no critical issues on tool premature failures or excessive tool wear. Practically, recommended data from tool suppliers or experiences of machine operators are more appropriate to apply as they are usually based on the tool configuration and comprehensive performance considerations, such as the tool life, machining quality and material removal rate, etc.

8.5   <u>Conclusions</u>

This chapter presents comprehensively investigating the effects of process variables on the cutting performance of micro tools in micro milling of AISI 1045 steel. 3D finite element and experiments based approaches are utilized to analyse the cutting forces, tool stresses, tool temperatures, chip formation and temperatures as well as surface roughness. Among the three process factors, generally, feed rate has the most influence, followed by axial depth of cut, and cutting speed has less impact.

Based on the research results obtained, it suggests that for practical applications, the determination of appropriate feed per tooth is mainly dependent on the minimum chip thickness of work materials and the cutting edge radius of micro tools. Cutting speed relies more on the applicable maximum spindle speed of micro milling machines and in order to achieve an optimum tooling performance, axial depth of cut is preferably selected according to the available experiences or recommended parameters from tool suppliers.

Chapter 9 Conclusions and Recommendations for Future Work

9.1 <u>Conclusions</u>

According to the results and discussions from previous chapters, the conclusions can be summarized as follows:

1) Based on continuum cutting mechanics, a three-dimensional finite element method has been proposed for modelling and simulation of the micro milling process, and validation through well-designed micro milling trials demonstrates that the approach is capable of characterizing the milling process effectively.

2) Cutting edge radius is the most influential geometrical feature on the tooling performance, followed by helix angle and rake angle. Lower helix angle and more negative rake angle perform better in heavy-duty operations. On the other hand, 30° helix angle, more positive rake angle and sharper edge corner are more beneficial for light or finish cutting.

3) From experimental study on the micro milling performance using the coated and WC micro tools, reduced cutting forces, less chip adhesion, lower tool wear, improved surface roughness as well as smaller burrs can benefit from the DLC and NCD coatings in dry cutting conditions. However, the coating performance is unreachable to the positive influence resulting from the coolant.

4) There is a trade-off between the tool edge radius enlargement and coating friction effects on the tooling performance, and appropriate UCT plays a greatest important role for achieving desirable coating performance. At low UCT, the coating thickness effect on cutting forces and coating friction effect on tool temperatures are comparatively prominent. Whereas at high UCT, coating

friction and coating thickness play an important role in the reduction of chip loads and tool temperatures respectively.

5) By comparing micro milling characteristics of the five work materials, sequence of the easiest to the most difficult materials is from Al 6061-T6, C101, and AISI 1045, 304 to P20. C101 shows the best cutting performance, then Al 6061-T6, AISI 1045 and 304, and P20 presents the poorest. A material's micro-machinability is not only affected by its conditions or properties but also by the cutting mechanism and mechanics.

6) Feed rate exhibits the most effect on the tooling performance, followed by axial DOC, and cutting speed has less impact. The size effects on the surface generation exist in both feed and axial cutting directions. Appropriate feed rate is determined by both the MCT of work materials and the tool edge radius. Cutting speed depends more on the maximum spindle speed and axial DOC is preferably selected based on the available experiences or recommended data from the tool suppliers.

9.2 <u>Contribution to knowledge</u>

The innovations and contributions to knowledge from this research are summarised in the following:

1) A 3D FEM-based model has been proposed for modelling and simulation of the micro milling process, particularly for tooling geometrical effects on micro milling performance.

2) DLC and NCD coatings have been successfully applied on micro end mills and corresponding tooling performance have been improved. The performance of the coated and uncoated tools has been compared by plane-strain simulations. The effects of coating properties and UCT on the cutting forces and tool temperatures have been determined.

3) Micro milling process characterization of five common materials has been carried out with well-designed evaluation trials. The process variable influences on the tooling performance have been identified and the optimization of process parameters explored.

9.3 <u>Recommendations for future work</u>

As regarding the future work for the research, the following areas are recommended:

1) Taking into account the dynamic performance of micro milling machine, such as the spindle run-out and chatter for further study.

2) Fabrication of bespoke micro tools with different geometries by appropriate manufacturing technology so as to experimentally investigate and optimize the cutting performance of micro tools.

3) Effective optimization of the coating process so as to increase the bonding strength of DLC and NCD coatings to the substrates at the cutting edges.

4) Increasing the knowledge related to the micro cutting characteristics for a wide range of work materials, including non-metals and some other metals, such as PMMA, silicon, ceramics, cast iron and titanium alloys.

References

Adams, D.P., Vasile, M.J., Benavides, G. and Campbell, A.N., 2001. 'Micromilling of metal alloys with focused ion beam–fabricated tools'. Precision Engineering, 25(2), pp. 107-113.

Afazov, S.M., Ratchev, S.M. and Segal, J., 2010. 'Modelling and simulation of micro-milling cutting forces'. Journal of Materials Processing Technology, 210(15), pp. 2154-2162.

Ali, M.Y. and Ong, A.S., 2006. 'Fabricating micromilling tool using wire electrodischarge grinding and focused ion beam sputtering'. International Journal of Advanced Manufacturing Technology, 31(5-6), pp. 501-508.

Almeida, F.A., Sacramento, J., Oliveira, F.J. and Silva, R.F., 2008. 'Micro- and nano-crystalline CVD diamond coated tools in the turning of EDM graphite'. Surface and Coatings Technology, 203(3-4), pp. 271-276.

Alting, L., Kimura, F., Hansen, H. and Bissacco, G., 2003. 'Micro engineering'. CIRP Annals - Manufacturing Technology, 52(2), pp. 635-657.

Aramcharoen, A., Mativenga, P.T. and Yang, S., 2007. 'The effect of AlCrTiN coatings on product quality in micro-milling of 45 HRC hardened H13 die steel'. Proceedings of the 35th International MATADOR Conference, pp. 203-206.

Aramcharoen, A. and Mativenga, P.T., 2009. 'Evaluation of critical parameters in micro machining of hardened tool steel'. International Journal of Nanomanufacturing, 3(1-2), pp. 100-111.

Aramcharoen, A., Mativenga, P.T., Yang, S., Cooke, K.E. and Teer, D.G., 2008. 'Evaluation and selection of hard coatings for micro milling of hardened tool steel'. International Journal of Machine Tools and Manufacture, 48(14), pp. 1578-1584.

Aurich, J.C., Dornfeld, D., Arrazola, P.J., Franke, V., Leitz, L. and Min, S., 2009. 'Burrs—Analysis, control and removal'. CIRP Annals - Manufacturing Technology, 58(2), pp. 519-542.

Baker, M., 2006. 'Finite element simulation of high-speed cutting forces'. Journal of Materials Processing Technology, 176(1-3), pp. 117-126.

Bang, Y.B., Lee, K.M. and Oh, S., 2005. '5-axis micro milling machine for machining micro parts'. International Journal of Advanced Manufacturing Technology, 25(9-10), pp. 888-894.

Bao, W.Y. and Tansel, I.N., 2000c. 'Modeling micro-end-milling operations. Part III: influence of tool wear'. International Journal of Machine Tools and Manufacture, 40(15), pp. 2193-2211.

Bao, W.Y. and Tansel, I.N., 2000b. 'Modeling micro-end-milling operations. Part II: tool run-out'. International Journal of Machine Tools and Manufacture, 40(15), pp. 2175-2192.

Bao, W.Y. and Tansel, I.N., 2000a. 'Modeling micro-end-milling operations. Part I: analytical cutting force model'. International Journal of Machine Tools and Manufacture, 40(15), pp. 2155-2173.

Biermann, D. and Kahnis, P., 2010. 'Analysis and simulation of size effects in micromilling'. Production Engineering, 4(1), pp. 25-34.

Bissacco, G., Hansen, H.N. and De Chiffre, L., 2005. 'Micromilling of hardened tool steel for mould making applications'. Journal of Materials Processing Technology, 167(2-3), pp. 201-207.

Brecher, C., Wenzel, C. and Klar, R., 2008. 'Characterization and optimization of the dynamic tool path of a highly dynamic micromilling machine'. CIRP Journal of Manufacturing Science and Technology, 1(2), pp. 86-91.

Bruno, F., Friedrich, C. and Warrington, R.O., 1995. 'The miniaturization technologies: past, present and future'. IEEE Transactions on Industrial Electronics, 42(5), pp. 423-430.

Chae, J., Park, S.S. and Freiheit, T., 2006. 'Investigation of micro-cutting operations'. International Journal of Machine Tools and Manufacture, 46(3-4), pp. 313-332.

Cheng, X., Wang, Z.G., Nakamoto, K. and Yamazaki, K., 2009. 'Design and development of a micro polycrystalline diamond ball end mill for micro/nano freeform machining of hard and brittle materials'. Journal of Micromechanics and Microengineering, 19(11), No.115022.

Chern, G.L., Wu, Y.J.E., Cheng, J.C. and Yao, J.C., 2007. 'Study on burr formation in micro-machining using micro-tools fabricated by micro-EDM'. Precision Engineering, 31(2), pp. 122-129.

Cheung, C., To, S. and Lee, W., 2002. 'Anisotropy of surface roughness in diamond turning of brittle single crystals'. Materials and Manufacturing Processes, 17(2), pp. 251-267.

Childs, T.H.C., Maekawa, K., Obikawa, T. and Yamane, Y., 2000. 'Metal machining: theory and applications'. Arnold, London.

Chuzhoy, L., Devor, R.E., Kapoor, S.G. and Bammann, D.J., 2002. 'Microstructure-Level modeling of ductile iron machining'. Journal of Manufacturing Science and Engineering, 124(2), pp. 162-169.

Dai, M., Zhou, K., Yuan, Z., Ding, Q. and Fu, Z., 2000. 'The cutting performance of diamond and DLC-coated cutting tools'. Diamond and Related Materials, 9(9-10), pp. 1753-1757.

Davim, J.P., Reis, P., Maranhao, C., Jackson, M.J., Cabral, G. and Gracio, J., 2010. 'Finite element simulation and experimental analysis of orthogonal cutting of an aluminium alloy using polycrystalline diamond tools'. International Journal of Materials and Product Technology, 37(1-2), pp. 46-59.

Deng, W.J., Xia, W. and Tang, Y., 2009. 'Finite element simulation for burr formation near the exit of orthogonal cutting'. The International Journal of Advanced Manufacturing Technology, 43(9-10), pp. 1035-1045.

Dhanorker, A. and Ozel, T., 2008. 'Meso/micro scale milling for micro-manufacturing'. International Journal of Mechatronics and Manufacturing Systems, 1(1), pp. 23-42.

Dhanorker, A. and Özel, T., 2006. 'An experimental and modeling study on meso/micro end milling process'. Proceedings of 2006 ASME Conference on Manufacturing Science and Engineering, No. 21127.

Dimov, S., Pham, D.T., Ivanov, A., Popov, K. and Fansen, K., 2004. 'Micromilling strategies: Optimization issues'. Proceedings of the Institution of Mechanical Engineers, Part B: Journal of Engineering Manufacture, 218(7), pp. 731-736.

Dornfeld, D., Min, S. and Takeuchi, Y., 2006. 'Recent advances in mechanical micromachining'. CIRP Annals - Manufacturing Technology, 55(2), pp. 745-768.

Egashira, K. and Mizutani, K., 2003. 'Milling using ultra-small diameter ball end mills fabricated by electrical discharge machining'. Seimitsu Kogaku Kaishi/Journal of the Japan Society for Precision Engineering, 69(10), pp. 1449-1453.

Fang, F.Z., Wu, H., Liu, X.D., Liu, Y.C. and Ng, S.T., 2003. 'Tool geometry study in micromachining'. Journal of Micromechanics and Microengineering, 13(5), pp. 726-731.

Filiz, S., Conley, C.M., Wasserman, M.B. and Ozdoganlar, O.B., 2007. 'An experimental investigation of micro-machinability of copper 101 using tungsten carbide micro-endmills'. International Journal of Machine Tools and Manufacture, 47(7-8), pp. 1088-1100.

Filiz, S., Xie, L., Weiss, L.E. and Ozdoganlar, O.B., 2008. 'Micromilling of microbarbs for medical implants'. International Journal of Machine Tools and Manufacture, 48(3-4), pp. 459-472.

Fleischer, J., Deuchert, M., Ruhs, C., Kühlewein, C., Halvadjiysky, G. and Schmidt, C., 2008. 'Design and manufacturing of micro milling tools'. Microsystem Technologies, 14(9-11), pp. 1771-1775.

Friedrich, C.R. and Vasile, M.J., 1996. 'Development of the micromilling process for high-aspect-ratio microstructures'. Journal of Microelectromechanical Systems, 5(1), pp. 33-38.

Fukui, H., Okida, J., Omori, N., Moriguchi, H. and Tsuda, K., 2004. 'Cutting performance of DLC coated tools in dry machining aluminum alloys'. Surface and Coatings Technology, 187(1), pp. 70-76.

Gandarias, E., Dimov, S., Pham, D., Ivanov, A., Popov, K., Lizarralde, R. and Arrazola, P., 2006. 'New methods for tool failure detection in micromilling'. Proceedings of the Institution of Mechanical Engineers, Part B: Journal of Engineering Manufacture, 220(2), pp. 137-144.

George Schneider, J., 2002. 'Machinability of metals'. in: 'Cutting tool applications'. GMRS Associates.

Gietzelt, T., Eichhorn, L. and Schubert, K., 2008. 'Manufacturing of microstructures with high aspect ratio by micromachining'. Microsystem Technologies, 14(9-11), pp. 1525-1529.

Grum, J. and Kisin, M., 2003. 'Influence of microstructure on surface integrity in turning - Part II: The influence of a microstructure of the workpiece material on cutting forces'. International Journal of Machine Tools and Manufacture, 43(15), pp. 1545-1551.

Grzesik, W., Zalisz, Z. and Nieslony, P., 2002. 'Friction and wear testing of multilayer coatings on carbide substrates for dry machining applications'. Surface and Coatings Technology, 155(1), pp. 37-45.

Hanyu, H., Kamiya, S., Murakami, Y. and Kondoh, Y., 2005. 'The improvement of cutting performance in semi-dry condition by the combination of DLC coating and CVD smooth surface diamond coating'. Surface and Coatings Technology, 200(1-4), pp. 1137-1141.

Heaney, P.J., Sumant, A.V., Torres, C.D., Carpick, R.W. and Pfefferkorn, F.E., 2008. 'Diamond coatings for micro end mills: Enabling the dry machining of aluminium at the micro-scale'. Diamond and Related Materials, 17(3), pp. 223-233.

Hu, J., Chou, Y.K. and Thompson, R.G., 2008. 'Nanocrystalline diamond coating tools for machining high-strength Al alloys'. International Journal of Refractory Metals and Hard Materials, 26(3), pp. 135-144.

Hu, J., Chou, Y.K., Thompson, R.G., Burgess, J. and Street, S., 2007. 'Characterizations of nano-crystalline diamond coating cutting tools'. Surface and Coatings Technology, 202(4-7), pp. 1113-1117.

Huang, B.W., Cai, J.Z. and Hsiao, W.L., 2010. 'Cutting force estimation in a micro milling process'. Proceedings of the Institution of Mechanical Engineers, Part B: Journal of Engineering Manufacture, 224(10), pp. 1615-1619.

Huo, D. and Cheng, K., 2010. 'Experimental investigation on micromilling of oxygen-free, high-conductivity copper using tungsten carbide, chemistry vapour deposition, and single-crystal diamond micro tools'. Proceedings of the Institution of Mechanical Engineers, Part B: Journal of Engineering Manufacture, 224(6), pp. 995-1003.

Huo, D., Cheng, K. and Wardle, F., 2009a. 'Design of a five-axis ultra-precision micro-milling machine-UltraMill. Part 1: holistic design approach, design considerations and specifications'. International Journal of Advanced Manufacturing Technology, 47(9-12), pp. 867-877.

Huo, D., Cheng, K. and Wardle, F., 2009b. 'Design of a five-axis ultra-precision micro-milling machine-UltraMill. Part 2: integrated dynamic modelling, design optimisation and analysis'. International Journal of Advanced Manufacturing Technology, 47(9-12), pp. 879-890.

Jackson, M.J., Gill, M.D.H., Sein, H. and Ahmed, W., 2003. 'Manufacture of diamond-coated cutting tools for micromachining applications'. Proceedings of the Institution of Mechanical Engineers, Part L: Journal of Materials: Design and Applications, 217(1), pp. 77-83.

Jackson, M.J., Robinson, G.,M. and Ahmed, W., 2006. 'Micromachining selected metals using diamond coated cutting tools'. International Journal of Nanomanufacturing, 1(2), pp. 304-317.

Jaspers, S., 2002. 'Material behaviour in conditions similar to metal cutting: flow stress in the primary shear zone'. Journal of Materials Processing Technology, 122(2-3), pp. 322-330.

Johnson, G.R. and Cook, W.H., 1983. 'A constitutive model and data for metals subjected to large strains, high strain rates, and high temperatures'. Proceedings of the 7th International Symposium on Ballistics, pp. 541-547.

Johnson, G.R., Stryk, R.A., Holmquist, T.J. and Beissel, S.R., 1996. 'User instruction for the 1996 version of the EPIC code'. Alliant Techsystems Inc.

Jun, M.B.G., DeVor, R.E. and Kapoor, S.G., 2006b. 'Investigation of the dynamics of Micro end milling-Part II: model validation and interpretation'. Journal of Manufacturing Science and Engineering, 128(4), pp. 901-912.

Jun, M.B.G., Joshi, S.S., DeVor, R.E. and Kapoor, S.G., 2008. 'An experimental evaluation of an atomization-based cutting fluid application system for micromachining'. Journal of Manufacturing Science and Engineering, Transactions of the ASME, 130(3), pp. 0311181-0311188.

Jun, M.B.G., Liu, X., DeVor, R.E. and Kapoor, S.G., 2006. 'Investigation of the dynamics of micro end milling-Part I: model development'. Journal of Manufacturing Science and Engineering, 128(4), pp. 893-900.

Kang, I.S., Kim, J.S., Kim, J.H., Kang, M.C. and Seo, Y.W., 2007. 'A mechanistic model of cutting force in the micro end milling process'. Journal of Materials Processing Technology, 187-188(0), pp. 250-255.

Kang, I.S., Kim, J.S. and Seo, Y.W., 2008. 'Cutting force model considering tool edge geometry for micro end milling process'. Journal of Mechanical Science and Technology, 22(2), pp. 293-299.

Khalili, K. and Safaei, M., 2009. 'FEM analysis of edge preparation for chamfered tools'. International Journal of Material Forming, 2(4), pp. 217-224.

Kim, C.J., Mayor, J.R. and Ni, J., 2004. 'A static model of chip formation in microscale milling'. ASME Journal of Manufacturing Science and Engineering, 126(4), pp. 710-718.

Klocke, F., Quito, F., Arntz, K. and Souza, A., 2009. 'A Study of the influence of cutting parameters on micro milling of steel with cubic boron nitride (CBN) Tools'. Proceedings of SPIE - The International Society for Optical Engineering, No.7204.

Klocke, F., Raedt, H.W. and Hoppe, S., 2001. '2D-FEM simulation of the orthogonal high speed cutting process'. Machining Science and Technology, 5(3), pp. 323-340.

Lai, X., Li, H., Li., C., Lin, Z. and Ni, J., 2008. 'Modelling and analysis of micro scale milling considering size effect, micro cutter edge radius and minimum chip thickness'. International Journal of Machine Tools and Manufacture, 48(1), pp. 1-14.

Lee, D.E., Hwang, I., Valente, C.M.O., Oliveira, J.F.G. and Dornfeld, D.A., 2006. 'Precision manufacturing process monitoring with acoustic emission'. International Journal of Machine Tools and Manufacture, 46(2), pp. 176-188.

Lee, K. and Dornfeld, D.A., 2002. 'An experimental study on burr formation in micro milling aluminum and copper'. Trans. North American Manufacturing Research Institute, 30, pp. 255-262.

Lee, K. and Dornfeld, D., 2005. 'Micro-burr formation and minimization through process control'. Precision Engineering, 29(2), pp. 246-252.

Lee, S.W., Mayor, R. and Ni, J., 2006. 'Dynamic analysis of a mesoscale machine tool'. Journal of Manufacturing Science and Engineering, Transactions of the ASME, 128(1), pp. 194-203.

Li, C., Lai, X., Peng, L., Li, H. and Ni, J., 2007. 'Modeling of three-dimensional cutting forces in micro-end-milling'. Journal of Micromechanics and Microengineering, 17(4), pp. 671.

Li, H., Lai, X., Li, C., Lin, Z., Miao, J. and Ni, J., 2008. 'Development of meso-scale milling machine tool and its performance analysis'. Frontiers of Mechanical Engineering in China, 3(1), pp. 59-65.

Li, P., 2009. 'Micromilling of hardened tool steels'. PhD thesis, Delft University of Technology.

Litwinski, K.M., Min, S., Lee, D.E., Dornfeld, D.A. and Lee, N., 2006. 'Scalability of tool path planning to micro machining'. Proceedings of the 1st International Conference on Micromanufacturing - ICOMM, pp. 174-179.

Liu, K. and Melkote, S.N., 2007. 'Finite element analysis of the influence of tool edge radius on size effect in orthogonal micro-cutting process'. International Journal of Mechanical Sciences, 49(5), pp. 650-660.

Liu, X., DeVor, R.E. and Kapoor, S.G., 2007b. 'Model-based analysis of the surface generation in microendmilling---Part II: experimental validation and analysis'. Journal of Manufacturing Science and Engineering, 129(3), pp. 461-469.

Liu, X., DeVor, R.E. and Kapoor, S.G., 2007a. 'Model-based analysis of the surface generation in microendmilling---Part I: model development'. Journal of Manufacturing Science and Engineering, 129(3), pp. 453-460.

Liu, X., DeVor, R.E. and Kapoor, S.G., 2006. 'An analytical model for the prediction of minimum chip thickness in micromachining'. Journal of Manufacturing Science and Engineering, 128(2), pp. 474-481.

Liu, X., DeVor, R.E., Kapoor, S.G. and Ehmann, K.F., 2004a. 'The mechanics of machining at the microscale: assessment of the current state of the science'. Journal of Manufacturing Science & Engineering, 126(4), pp. 666-678.

Liu, X., Jun, M.B.G., DeVor, R.E. and Kappor, S.G., 2004b. 'Cutting mechanisms and their influence on dynamic forces, vibrations and stability in micro-endmilling'. ASME Conference Proceedings, 62416(47136), pp. 583-592.

Lucca, D.A., Rhorer, R.L. and Komanduri, R., 1991. 'Energy dissipation in the ultraprecision machining of copper'. CIRP Annals - Manufacturing Technology, 40(1), pp. 69-72.

Malekian, M., Park, S.S., Jun, M.B.G. and Jun, M.B.G., 2009. 'Tool wear monitoring of micro-milling operations'. Journal of Materials Processing Technology, 209(10), pp. 4903-4914.

Mamalis, A., 2001. 'Finite element simulation of chip formation in orthogonal metal cutting'. Journal of Materials Processing Technology, 110(1), pp. 19-27.

Medaska, M.K., Nowag, L. and Liang, S.Y., 1999. 'Simultaneous measurement of the thermal and mechanical effectiveness of cutting fluid'. Journal of Machining Science and Technology, 3(2), pp. 221-237.

Meng, X.M., Tang, W.Z., Hei, L.F., Li, C.M., Askari, S.J., Chen, G.C. and Lu, F.X., 2008. 'Application of CVD nanocrystalline diamond films to cemented carbide drills'. International Journal of Refractory Metals and Hard Materials, 26(5), pp. 485-490.

Min, S., Dornfeld, D., Inasaki, I., Ohmori, H., Lee, D., Deichmueller, M., Yasuda, T. and Niwa, K., 2006. 'Variation in machinability of single crystal materials in micromachining'. CIRP Annals - Manufacturing Technology, 55(1), pp. 103-106.

Montgomery, D.C., 2001. 'Design and analysis of experiments'. John Wiley & Sons, Inc.

Ng, C.K., Melkote, S.N., Rahman, M. and Senthil, K.A., 2006. 'Experimental study of micro- and nano-scale cutting of aluminum 7075-T6'. International Journal of Machine Tools and Manufacture, 46(9), pp. 929-936.

Okazaki, Y., Mishima, N. and Ashida, K., 2004. 'Microfactory - Concept, history, and developments'. Journal of Manufacturing Science and Engineering, Transactions of the ASME, 126(4), pp. 837-844.

Okazaki, Y., Mori, T. and Morita, N., 2001. 'Desk-top NC milling machine with 200 krpm spindle'. ASPE Annual MeetingProceedings of 2001 ASPE Annual Meeting, pp. 192-195.

Oxley, P.L.B.,1989. 'Mechanics of machining: an analytical approach to assessing machinability'. Ellis Horwood, Chichester,West Sussex, London.

Özel, T., 2006. 'The influence of friction models on finite element simulations of machining'. International Journal of Machine Tools and Manufacture, 46(5), pp. 518-530.

Özel, T., Liu, X. and Dhanorker, A., 2007. 'Modelling and simulation of micro-milling process'. CIRP 4th International Conference and Exhibition on Design and Production of Machines and Dies/Molds4th International Conference and Exhibition on Design and Production of Machines and Dies/Molds, pp. 21-23.

Park, J.B., Wie, K.H., Park, J.S. and Ahn, S.H., 2009. 'Evaluation of machinability in the micro end milling of printed circuit boards'. Proceedings of the Institution of Mechanical Engineers, Part B: Journal of Engineering Manufacture, 223(11), pp. 1465-1474.

Paul, W.M., 1995. 'CVD diamond - a new technology for the future?'. Endeavour Magazine, 19(3), pp. 101-106.

Pham, D., Elkaseer, A., Popov, K., Dimov, S., Olejnik, L. and Rosochowski, A., 2009. 'Micromilling of coarse-grained and ultrafine-grained Cu99.9E: Effects of material microstructure on machining conditions and surface quality'. 4M/ICOMM 2009 - The Global Conference on Micro Manufacture, pp. 241-244.

Popov, K., Dimov, S., Pham, D.T., Minev, R., Rosochowski, A., Olejnik, L. and Richert, M., 2006a. 'The effects of material microstructure in micro-milling'. in: '4M 2006 - Second International Conference on Multi-Material Micro Manufacture'., eds. Wolfgang Menz, Stefan Dimov and Bertrand Fillon, Elsevier.Oxford, pp. 127-130.

Popov, K.B., Dimov, S.S., Pham, D.T., Minev, R.M., Rosochowski, A. and Olejnik, L., 2006b. 'Micromilling: material microstructure effects'. Proceedings of the Institution of Mechanical Engineers, Part B: Journal of Engineering Manufacture, 220(11), pp. 1807-1813.

Rahman, M., Senthil Kumar, A. and Prakash, J.R.S., 2001. 'Micro milling of pure copper'. Journal of Materials Processing Technology, 116(1), pp. 39-43.

Rusnaldy, Ko, T.J. and Kim, H.S., 2008. 'An experimental study on microcutting of silicon using a micromilling machine'. International Journal of Advanced Manufacturing Technology, 39(1-2), pp. 85-91.

Rusnaldy, Ko, T.J. and Kim, H.S., 2007. 'Micro-end-milling of single-crystal silicon'. International Journal of Machine Tools and Manufacture, 47(14), pp. 2111-2119.

Sartkulvanich, P., 2007. 'Determination of material properties for use in FEM simulations of machining and roller burnishing'. The Ohio State University.

Schaller, T., Bohn, L., Mayer, J. and Schubert, K., 1999. 'Microstructure grooves with a width of less than 50 μm cut with ground hard metal micro end mills'. Precision Engineering, 23(4), pp. 229-235.

Schmidt, J., Spath, D., Elsner, J., Hüntrup, V. and Tritschler, H., 2002. 'Requirements of an industrially applicable microcutting process for steel micro structures'. Microsystem Technologies, 8(6), pp. 402-408.

Schmidt, J. and Tritschler, H., 2004. 'Micro milling of steels'. Microsystem Technologies, 10(3), pp. 167-174.

Schueler, G.M., Engmann, J., Marx, T., Haberland, R. and Aurich, J.C., 2010. 'Burr formation and surface characteristics in micro-end milling of titanium alloys'. in: 'Burrs - Analysis, Control and Removal'. pp. 129-138.

Sheikh, M.A., Mativenga, P.T. and Iqbal, S.A., 2007. 'Characterization of machining of AISI 1045 steel over a wide range of cutting speeds. Part 2: evaluation of flow stress models and interface friction distribution schemes'. Proceedings of the Institution of Mechanical Engineers, Part B: Journal of Engineering Manufacture, 221(5), pp. 917-926.

Shelton, J.A. and Shin, Y.C., 2010a. 'Comparative evaluation of laser-assisted micro-milling for AISI 316, AISI 422, TI-6AL-4V and Inconel 718 in a side-cutting configuration'. Journal of Micromechanics and Microengineering, 20(7), No.075012.

Shelton, J.A. and Shin, Y.C., 2010b. 'Experimental evaluation of laser-assisted micromilling in a slotting configuration'. Journal of Manufacturing Science and Engineering, Transactions of the ASME, 132(2), No.021008.

Shimada, S., Ikawa, N., Tanaka, H., Ohmori, G., Uchikoshi, J. and Yoshinaga, H., 1993. 'Feasibility study on ultimate accuracy in microcutting using molecular dynamics simulation'. CIRP Annals - Manufacturing Technology, 42(1), pp. 91-94.

Shirakashi, T. and Usui, E., 1970. 'Effect of temperature and strain rate upon flow stress of metal in compression'. Bulletin of the Japan Society of Precision Engineering, 1-4(1), pp. 91-98.

Simoneau, A., Ng, E. and Elbestawi, M.A., 2007. 'Grain size and orientation effects when microcutting AISI 1045 steel'. CIRP Annals - Manufacturing Technology, 56(1), pp. 57-60.

Simoneau, A., Ng, E. and Elbestawi, M.A., 2006a. 'Chip formation during microscale cutting of a medium carbon steel'. International Journal of Machine Tools and Manufacture, 46(5), pp. 467-481.

Simoneau, A., Ng, E. and Elbestawi, M.A., 2006b. 'The effect of microstructure on chip formation and surface defects in microscale, mesoscale, and macroscale cutting of steel'. CIRP Annals - Manufacturing Technology, 55(1), pp. 97-102.

Son, S.M., Lim, H.S. and Ahn, J.H., 2005. 'Effects of the friction coefficient on the minimum cutting thickness in micro cutting'. International Journal of Machine Tools and Manufacture, 45(4-5), pp. 529-535.

Sreeram, S., Kumar, A.S., Rahman, M. and Zaman, M.T., 2006. 'Optimization of cutting parameters in micro end milling operations in dry cutting condition using genetic algorithms'. International Journal of Advanced Manufacturing Technology, 30(11-12), pp. 1030-1039.

Takeuchi, Y., Suzukawa, H., Kawai, T. and Sakaida, Y., 2006. 'Creation of ultra-precision microstructures with high aspect ratios'. CIRP Annals - Manufacturing Technology, 55(1), pp. 107-110.

Tanaka, M., 2001. 'Development of desktop machining microfactory'. Riken Review, 34, pp. 46-49.

Tansel, I., Rodriguez, O., Trujillo, M., Paz, E. and Li, W., 1998a. 'Micro-end-milling—I. Wear and breakage'. International Journal of Machine Tools and Manufacture, 38(12), pp. 1419-1436.

Tlusty, J. and Macneil, P., 1975. 'Dynamics of cutting forces in end milling'. Annals of CIRP, 24(1), pp. 21-25.

Torres, C.D., Heaney, P.J., Sumant, A.V., Hamilton, M.A., Carpick, R.W. and Pfefferkorn, F.E., 2009. 'Analyzing the performance of diamond-coated micro end mills'. International Journal of Machine Tools and Manufacture, 49(7-8), pp. 599-612.

Uhlmann, E., Piltz, S. and Schauer, K., 2005. 'Micro milling of sintered tungsten–copper composite materials'. Journal of Materials Processing Technology, 167(2-3), pp. 402-407.

Vasile, M.J., Friedrich, C.R., Kikkeri, B. and McElhannon, R., 1996. 'Micrometer-scale machining: Tool fabrication and initial results'. Precision Engineering, 19(2-3), pp. 180-186.

Vogler, M.P., DeVor, R.E. and Kapoor, S.G., 2004a. 'On the modeling and analysis of machining performance in micro-end milling, Part I: Surface generation'. Journal of Manufacturing Science and Engineering, 126(4), pp. 685-694.

Vogler, M.P., DeVor, R.E. and Kapoor, S.G., 2003. 'Microstructure-level force prediction model for micro-milling of multi-phase materials'. Journal of Manufacturing Science and Engineering, Transactions of the ASME, 125(2), pp. 202-209.

Vogler, M.P., Kapoor, S.G. and DeVor, R.E., 2004b. 'On the modeling and analysis of machining performance in micro-endmilling, part II: Cutting force prediction'. Journal of Manufacturing Science and Engineering, Transactions of the ASME, 126(4), pp. 695-705.

Wang, J.S., Gong, Y.D., Abba, G., Antoine, J.F. and Shi, J.S., 2009. 'Chip formation analysis in micromilling operation'. The International Journal of Advanced Manufacturing Technology, 45(5-6), pp. 430-447.

Weck, M., Hennig, J. and Hilbing, R., 2001. 'Precision cutting processes for manufacturing of optical components'. Proceedings of SPIE - The International Society for Optical Engineering, 4440, pp. 145-151.

Weinert, K., Kahnis, P., Petzoldt, V. and Peters, C., 2005. 'Micro-milling of steel and NiTi SMA'. 55th CIRP General Assembly, STC-C section meeting presentation file, Antalya, Turkey.

Weinert, K. and Petzoldt, V., 2008. 'Machining NiTi micro-parts by micro-milling'. Materials Science and Engineering: A, 481-482, pp. 672-675.

Weule, H., Hüntrup, V. and Tritschle, H., 2001. 'Micro-cutting of steel to meet new requirements in miniaturization'. CIRP Annals - Manufacturing Technology, 50(1), pp. 61-64.

Yan, J., Uchida, K., Yoshihara, N. and Kuriyagawa, T., 2009. 'Fabrication of micro end mills by wire EDM and some micro cutting tests'. Journal of Micromechanics and Microengineering, 19(2), No.025004.

Yen, Y., 2004. 'Estimation of tool wear in orthogonal cutting using the finite element analysis'. Journal of Materials Processing Technology, 146(1), pp. 82-91.

Yuan, Z.J., Lee, W.B., Yao, Y.X. and Zhou, M., 1994. 'Effect of crystallographic orientation on cutting forces and surface quality in diamond cutting of single crystal'. CIRP Annals - Manufacturing Technology, 43(1), pp. 39-42.

Yuan, Z.J., Zhou, M. and Dong, S., 1996. 'Effect of diamond tool sharpness on minimum cutting thickness and cutting surface integrity in ultraprecision machining'. Journal of Materials Processing Technology, 62(4), pp. 327-330.

Zaman, M.T., Kumar, A.S., Rahman, M. and Sreeram, S., 2006. 'A three-dimensional analytical cutting force model for micro end milling operation'. International Journal of Machine Tools and Manufacture, 46(3-4), pp. 353-366.

Zerilli, F.J. and Armstrong, R.W., 1995. 'Constitutive equation for HCP metals and high strength alloy steels'. High Strain Rate Effects on Polymer, Metal and Ceramic Matrix Composites and other Advanced Materials, 48, pp. 121-126.

Abaqus, 2011. Available at: http://www.3ds.com/ (Accessed: 6/8/2011).

AdvantEdge, 2011. Available at: http://www.thirdwavesys.com/ (Accessed: 6/8/2011).

ANSYS LS-DYNA, 2011. Available at: http://www.ansys.com/ (Accessed: 6/8/2011).

Cimatron Group, 2010. Available at: http://www.cimatron.com/ (Accessed: 10/15/2010).

Datron Dynamics, 2010. Available at: http://www.datron.com/ (Accessed: 10/15/2010).

DEFORM, 2011. Available at: http://www.deform.com/ (Accessed: 6/8/2011).

Design News, 2010. Available at: http://www.designnews.com/ (Accessed: 10/15/2010).

Fanuc, 2010. Available at: http://www.fanuc.co.jp/ (Accessed: 7/13/2010).

Inventables, 2010. Available at: http://www.inventables.com/ (Accessed: 10/15/2010).

Kaleido Technology, 2010. Available at: http://www.kaleido-technology.com/ (Accessed: 10/15/2010).

Kern, 2010. Available at: http://www.kern-microtechnic.com/ (Accessed: 7/13/2010).

Kistler, 2010. Available at: http://www.kistler.com/ (Accessed: 8/23/2010).

Kugler, 2010. Available at: http://www.kuglerofamerica.com/ (Accessed: 7/13/2010).

Makino, 2010. Available at: http://www.makino.com/ (Accessed: 7/13/2010).

Matweb, 2009. Available at: http://www.matweb.com/ (Accessed: 11/12/2009).

Moore, 2010. Available at: http://www.nanotechsys.com/ (Accessed: 7/13/2010).

Performance Micro Tool, 2010. Available at: http://www.pmtnow.com/ (Accessed: 7/13/2010).

PMPA: Precision Machined Products Association, 2010. Available at: http://www.pmpa.org/ (Accessed: 10/15/2010).

Sodick, 2010. Available at: http://www.sodick.com/ (Accessed: 7/13/2010).

Taylor Hobson, 2010. Available at: http://www.taylor-hobson.com (Accessed: 8/27/2010).

Union Tool, 2010. Available at: http://www.uniontool.co.jp/ (Accessed: 7/13/2010).

Veeco, 2010. Available at: http://www.veeco.com/ (Accessed: 8/27/2010).

Willemin Macodel, 2010. Available at: http://www.willemin-macodel.com/ (Accessed: 10/15/2010).

Yole Developpement, 2010. Available at: http://www.yole.fr/ (Accessed: 10/15/2010).

Zeiss, 2010. Available at: http://www.zeiss.com/ (Accessed: 8/27/2010).

Zygo, 2010. Available at: http://www.zygo.com/ (Accessed: 8/27/2010).

Appendices

Appendix I

List of Publications Resulting from the Research

List of Publications Resulting from the Research

1. T. Wu, K. Cheng. 3D FE-based modelling and simulation of the micro milling process. Proceedings of Precision Engineering and Nanotechnology, Key Engineering Materials, 2012, Vol.516, pp.634-639

2. T. Wu, K. Cheng. An investigation on the cutting performance of nano-crystalline diamond coatings on a micro-end mill. Proceedings of the Institution of Mechanical Engineers, Part B: Journal of Engineering Manufacture, 2012, Vol.226, No.8, pp.1421-1424

3. T. Wu, K. Cheng, R. Rakowski. Investigation on tooling geometrical effects of micro tools and the associated micro milling performance. Proceedings of the Institution of Mechanical Engineers, Part B: Journal of Engineering Manufacture, 2012, Vol.226, No.9, pp.1442-1453

4. T. Wu, K. Cheng. Investigation on the effects of process variables and the associated micro milling performance. Proceedings of the 10th International Conference on Frontiers of Design and Manufacturing, June 10~12, 2012, Chongqing, China

5. T. Wu, K. Cheng. Book chapter: Micro milling: the state-of-the-art approach towards applications, in: Micro Cutting: Fundamentals and Applications, John Wiley & Sons, 2012 (In press)

6. T. Wu, K. Cheng. Micro milling performance assessment of diamond-like carbon coatings on a micro end mill. Proceedings of the Institution of Mechanical Engineers, Part J: Journal of Engineering Tribology, 2012 (Accepted)

Appendix II

Summary of Facilities in the Research

Summary of Facilities in the Research

Micro milling machine	Five-axis ultra-precision micro milling machine UltraMill
Cutting tools	1. Magaforce 8500-Ø0.3mm 2. Magaforce 8507-Ø0.5mm 3. Magaforce 8507-Ø0.5mm with DLC coatings 4. Magaforce 8507-Ø0.5mm with NCD coatings
Work materials	1. Al 6061-T6 2. Copper C101 3. Carbon steel AISI 1045 4. Stainless steel 304 5. Tool steel P20
Instrument and metrology	1. White light interferometer Zygo NewView 5000 2. Surface profiler Taylor Hobson CCI2000 3. Field emission scanning electron microscope Zeiss Supra 35VP 4. Digital microscope Keyence VHX-1000 5. Optical microscope TESA VISIO-200 6. Dynamometer Kistler MiniDyn 9256C2 with a charge amplifier 5070A 7. Digital camera Dino-Lite AD413TL

Appendix III

Specifications of Micro Milling Machine UltraMill

Specifications of Micro Milling Machine UltraMill

General	Description
System Configuration	Ultra-precision 5-axis bench-top micro milling machine with gantry frame
Base Material	Natural granite
Machining Envelope	150 mm x 150 mm x 80 mm (vertical)
Workpiece Material	Ferrous or nonferrous metal, plastics and crystals
Control System	Delta Tau PC-based multi-axis CNC motion controller (UMAC), in a Windows environment; Compact control enclosure - drawer cabinet mounted underneath the machine base to minimise overall machine footprint.
CNC Front-End	Delta Tau Advantage 900 system; 15'' flat panel monitor; Customized CNC software with 5-axis machining capability; wireless or cable pendant.
Space Requirement	1.1 m wide x 0.8 m deep x 2.1 m high

Machining Spindle	Performance
Type	Water cooled aerostatic bearing
Stiffness	Radial: 4N/μm; Axial: 3N/μm
Maximum Speed	200,000 rpm
Load Capacity	Radial: 55N at spindle nose; Axial: 45N
Drive System	DC brushless motor
Power	400 Watts at 200,000 rpm
Motion Accuracy	<1.0 μm axial TIR and <2.0 μm radial TIR
Tool Clamping	3 mm collet, manual or automatic (optional)

Linear Axes	X	Y	Z
Type	Air bearing slides fitted with squeeze film dampers		
Stroke	230 mm	225 mm	160 mm
Feedrate	0-3000 mm/min	0-3000 mm/min	0-3000 mm/min
Drive System	DC brushless linear motor	DC brushless linear motor	DC brushless linear motor
Feedback	Optical linear encoder	Optical linear encoder	Optical linear encoder
Resolution	5 nm	5 nm	5 nm
Motion Accuracy	<1.0 μm over total travel	<1.0 μm over total travel	<1.0 μm over total travel

Rotational Axes	B (Spindle Swivelling)	C (Workpiece Rotary Table)
Type	Precision ball bearing	Air bearing fitted with squeeze film dampers
Stroke	± 90°	360°
Rotational Speed	0-30 rpm	0-100 rpm
Drive System	DC brushless torque motor	DC brushless torque motor
Feedback	Optical rotary encoder	Optical rotary encoder
Resolution	0.026 arcsec	0.02 arcsec
Motion Accuracy	<1.0 μm over 180° in axial and radial direction	<0.1 μm in axial and radial direction

Supply	Air	Electrical
	220 l/min at 6 Bar dry compressed air	440VAC, 3 phase mains supply

Appendix IV

Specifications of Kistler Dynamometer MiniDyn 9256C2

Specifications of Kistler Dynamometer MiniDyn 9256C2

Force

KISTLER
measure. analyze. innovate.

MiniDyn

Multicomponent Dynamometer up to 250 N

Type 9256C...

Multicomponent dynamometer for measuring the three orthogonal components of a force. Its very low threshold allows measuring extremely small forces.

- For cutting force measurements in ultra precise machining
- Small design
- High sensitivity and natural frequency
- Small temperature error
- Top plate made of titanium

Type 9256C2

Description

The dynamometer consists of four 3-component force sensors mounted under high preload between the cover plate and the two lateral base plates.

A low temperature error is obtained by this special mounting of the sensors. Each force sensor contains three crystal rings, of which one is sensitive to pressure in the y-direction and the two others to shear in the x- and z-directions. The forces are measured practically without displacement.

The outputs of the four mounted force sensors are fed to the 7-pole flanged socket. There are also multicomponent force-moment measurements possible.

The four sensors are fitted so that they are ground-isolated. This largely eliminates ground loop problems.

The dynamometer is corrosion-resistant and protected against penetration by splashing water or cutting fluid. The dynamometer including connecting cable Type 1696A5 or Type 1697A5 meets the degree of protection IP67.

Examples of Application

- Cutting force measurement in precision machining such as:
  - cutting wafers
  - grinding hard-disk read heads
  - diamond turning
  - high speed machining
  - micromachining
- Ultra-high precision machining of brittle hard materials
- Multicomponent force measurement of small forces
- Force measurement in confined spaces

Technical Data

Measuring range	F_x, F_y, F_z	N	$-250 \ldots 250$
Type 9256C1	M_x, M_z	N·m	$-8 \ldots 8$
Type 9256C2	M_x, M_z	N·m	$-11 \ldots 11$
Calibrated measuring range			
100 %	F_x, F_y, F_z	N	$0 \ldots 250$
10 %	F_x, F_y, F_z	N	$0 \ldots 25$
Overload	F_x, F_y, F_z	N	$-300/300$
Threshold		N	$<0{,}002$
Sensitivity	F_x, F_z	pC/N	≈ -26
	F_y	pC/N	≈ -13
Linearity, all ranges		%FSO	$\leq \pm 0{,}4$
Hysteresis, all ranges		%FSO	$\leq 0{,}5$
Crosstalk		%	$\leq \pm 2$
Rigidity	c_x, c_z	N/µm	>250
	c_y	N/µm	>300
Natural frequency (mounted on rigid base)			
Type 9256C1	$f_n (x)$	kHz	$\approx 5{,}1$
	$f_n (y)$	kHz	$\approx 5{,}5$
	$f_n (z)$	kHz	$\approx 5{,}6$
Type 9256C2	$f_n (x)$	kHz	$\approx 4{,}0$
	$f_n (y)$	kHz	$\approx 4{,}8$
	$f_n (z)$	kHz	$\approx 4{,}6$
Operating temperature range		°C	$0 \ldots 70$
Insulation resistance		Ω	$>10^{13}$
Ground isolation		Ω	$>10^8$
Degree of protection EN60529 (with connecting cable Type 1696A5/1697A5)			IP67
Weight			
Dynamometer	Type 9256C1/C2	kg	$0{,}75/0{,}87$
Top plate	Type 9256C1/C2	kg	$0{,}24/0{,}36$
Clamping area			
Type 9256C1		mm	39x80
Type 9256C2		mm	55x80

Appendix V

NC Codes for the Micro Milling Experiments

NC codes for the cutting trials in Chapter 5

```
G21 G54 G90 G94
G52 X8 Y-43 Z28.6195 B-25.2862 C28.405                    /*Reference point*/
S60000 M04                                          /*Spindle speed 60,000 rpm*/
G04 P30
G00 X0
Y0 Z5 C0 B0
G00 Z0.5
G01 Z-0.03 F5                                          /*Depth of cut 0.03mm*/
X45 F60                            /*1st slot machining, feed rate 60mm/min */

G00 Z5
G04 P40
Y1.5
X0 Z0.5
G01 Z-0.03 F5
X45 F60                                              /*2nd slot machining*/

G00 Z5
G04 P40
Y3
X0 Z0.5
G01 Z-0.03 F5
X45 F60                                              /*3rd slot machining*/

G00 Z5
G04 P40
Y4.5
X0 Z0.5
G01 Z-0.03 F5
X45 F60                                              /*4th slot machining*/

G00 Z5
G04 P40
Y6
X0 Z0.5
G01 Z-0.03 F5
X45 F60                                              /*5th slot machining*/

G00 Z5
G04 P40
Y7.5
X0 Z0.5
G01 Z-0.03 F5
X45 F60                                              /*6th slot machining*/

G00 Z5
G04 P40
Y9
X0 Z0.5
G01 Z-0.03 F5
X45 F60                                              /*7th slot machining*/
```

```
G00 Z5
G04 P40
Y10.5
X0 Z0.5
G01 Z-0.03 F5
X45 F60                                                    /*8th slot machining*/

G00 Z5
G04 P40
Y12
X0 Z0.5
G01 Z-0.03 F5
X45 F60                                                    /*9th slot machining*/

G00 Z5
G04 P40
Y13.5
X0 Z0.5
G01 Z-0.03 F5
X45 F60                                                    /*10th slot machining*/

G00 Z5
G00 Y100
G04 P10
G00 Y0
G52 X0 Y0 Z0 B0 C0
M5
M30
```

NC codes for the first set of cutting in Chapter 7

```
G21 G54 G90 G94
G52 X8 Y-57 Z30.536 B-25.2862 C28.405                    /*Reference point*/
S60000 M04                                               /*Spindle speed 60,000 rpm*/
G04 P30
G00 X0
Y0 Z5 C0 B0
G00 Z0.5
G01 Z-0.02 F5                                            /*Depth of cut 0.02mm*/
X45 F30                                  /*1st slot machining, feed rate 30mm/min */

G00 Z5
G04 P40
Y2
X0 Z0.5
G01 Z-0.02 F5
X45 F30                                                 /*2nd slot machining*/

G00 Z5
G04 P40
Y4
X0 Z0.5
G01 Z-0.02 F5
X45 F30                                                 /*3rd slot machining*/

G00 Z5
G04 P40
Y6
X0 Z0.5
G01 Z-0.02 F5
X45 F30                                                 /*4th slot machining*/

G00 Z5
G04 P40
Y8
X0 Z0.5
G01 Z-0.02 F5
X45 F30                                                 /*5th slot machining*/

G00 Z5
G04 P40
Y10
X0 Z0.5
G01 Z-0.02 F5
X45 F30                                                 /*6th slot machining*/

G00 Z5
G04 P40
Y12
X0 Z0.5
G01 Z-0.02 F5
X45 F30                                                 /*7th slot machining*/
```

```
G00 Z5
G04 P40
Y14
X0 Z0.5
G01 Z-0.02 F5
X45 F30                                                    /*8th slot machining*/

G00 Z5
G04 P40
Y16
X0 Z0.5
G01 Z-0.02 F5
X45 F30                                                    /*9th slot machining*/

G00 Z5
G04 P40
Y18
X0 Z0.5
G01 Z-0.02 F5
X45 F30                                                    /*10th slot machining*/

G00 Z5
G00 Y100
G04 P10
G00 Y0
G52 X0 Y0 Z0 B0 C0
M5
M30
```

NC codes for the second set of cutting in Chapter 7

```
G21 G54 G90 G94
G52 X8 Y-38 Z30.217 B-25.2862 C28.405                    /*Reference point*/
S40000 M04                                      /*Spindle speed 40,000 rpm*/
G04 P30
G00 X0
Y0 Z5 C0 B0
G00 Z0.5
G01 Z-0.02 F5                                      /*Depth of cut 0.02mm*/
X10 F16                          /*1st slot machining, feed rate 16mm/min */
G01 Z0.5 F5

G00 Z5
M05
G04 P20
S80000 M04                                      /*Spindle speed 80,000 rpm*/
G04 P30
Y2
X0 Z0.5
G01 Z-0.01 F5                                      /*Depth of cut 0.01mm*/
X10 F32                          /*2nd slot machining, feed rate 32mm/min */
G01 Z0.5 F5

G00 Z5
M05
G04 P20
S40000 M04                                      /*Spindle speed 40,000 rpm*/
G04 P20
Y4
X0 Z0.5
G01 Z-0.03 F5                                      /*Depth of cut 0.03mm*/
X10 F48                          /*3rd slot machining, feed rate 48mm/min */
G01 Z0.5 F5

G00 Z5
M05
G04 P20
S60000 M04                                      /*Spindle speed 60,000 rpm*/
G04 P20
Y6
X0 Z0.5
G01 Z-0.01 F5                                      /*Depth of cut 0.01mm*/
X10 F48                          /*4th slot machining, feed rate 48mm/min */
G01 Z0.5 F5

G00 Z5
M05
G04 P20
S60000 M04                                      /*Spindle speed 60,000 rpm*/
G04 P20
Y8
X0 Z0.5
```

```
G01 Z-0.03 F5                              /*Depth of cut 0.03mm*/
X10 F72                          /*5th slot machining, feed rate 72mm/min */
G01 Z0.5 F5


G00 Z5
M05
G04 P20
S40000 M04                                 /*Spindle speed 40,000 rpm*/
G04 P20
Y10
X0 Z0.5
G01 Z-0.01 F5                              /*Depth of cut 0.01mm*/
X10 F16                          /*6th slot machining, feed rate 16mm/min */
G01 Z0.5 F5


G00 Z5
M05
G04 P20
S60000 M04                                 /*Spindle speed 60,000 rpm*/
G04 P20
Y12
X0 Z0.5
G01 Z-0.01 F5                              /*Depth of cut 0.01mm*/
X10 F72                          /*7th slot machining, feed rate 72mm/min */
G01 Z0.5 F5


G00 Z5
M05
G04 P20
S60000 M04                                 /*Spindle speed 60,000 rpm*/
G04 P20
Y14
X0 Z0.5
G01 Z-0.03 F5                              /*Depth of cut 0.03mm*/
X10 F24                          /*8th slot machining, feed rate 24mm/min */
G01 Z0.5 F5


G00 Z5
M05
G04 P20
S80000 M04                                 /*Spindle speed 80,000 rpm*/
G04 P20
Y16
X0 Z0.5
G01 Z-0.02 F5                              /*Depth of cut 0.02mm*/
X10 F64                          /*9th slot machining, feed rate 64mm/min */
G01 Z0.5 F5


G00 Z5
M05
G04 P20
S40000 M04                                 /*Spindle speed 40,000 rpm*/
G04 P20
Y18
X0 Z0.5
```

```
G01 Z-0.03 F5                                          /*Depth of cut 0.03mm*/
X10 F16                                   /*10th slot machining, feed rate 16mm/min */
G01 Z0.5 F5


G00 Z5
M05
G04 P20
S60000 M04                                          /*Spindle speed 60,000 rpm*/
G04 P20
Y20
X0 Z0.5
G01 Z-0.01 F5                                          /*Depth of cut 0.01mm*/
X10 F24                                   /*11th slot machining, feed rate 24mm/min */
G01 Z0.5 F5


G00 Z5
M05
G04 P20
S80000 M04                                          /*Spindle speed 80,000 rpm*/
G04 P20
Y22
X0 Z0.5
G01 Z-0.03 F5                                          /*Depth of cut 0.03mm*/
X10 F96                                   /*12th slot machining, feed rate 96mm/min */
G01 Z0.5 F5


G00 Z5
M05
G04 P20
S40000 M04                                          /*Spindle speed 40,000 rpm*/
G04 P20
Y24
X0 Z0.5
G01 Z-0.02 F5                                          /*Depth of cut 0.02mm*/
X10 F48                                   /*13th slot machining, feed rate 48mm/min */
G01 Z0.5 F5


G00 Z5
M05
G04 P20
S60000 M04                                          /*Spindle speed 60,000 rpm*/
G04 P20
Y26
X0 Z0.5
G01 Z-0.02 F5                                          /*Depth of cut 0.02mm*/
X10 F48                                   /*14th slot machining, feed rate 48mm/min */
G01 Z0.5 F5


G00 Z5
M05
G04 P20
S60000 M04                                          /*Spindle speed 60,000 rpm*/
G04 P20
Y28
X0 Z0.5
```

```
G01 Z-0.02 F5                                    /*Depth of cut 0.02mm*/
X10 F24                             /*15th slot machining, feed rate 24mm/min */
G01 Z0.5 F5


G00 Z5
M05
G04 P20
S40000 M04                                    /*Spindle speed 40,000 rpm*/
G04 P20
Y30
X0 Z0.5
G01 Z-0.01 F5                                    /*Depth of cut 0.01mm*/
X10 F48                             /*16th slot machining, feed rate 48mm/min */
G01 Z0.5 F5


G00 Z5
M05
G04 P20
S80000 M04                                    /*Spindle speed 80,000 rpm*/
G04 P20
Y32
X0 Z0.5
G01 Z-0.02 F5                                    /*Depth of cut 0.02mm*/
X10 F32                             /*17th slot machining, feed rate 32mm/min */
G01 Z0.5 F5


G00 Z5
M05
G04 P20
S80000 M04                                    /*Spindle speed 80,000 rpm*/
G04 P20
Y34
X0 Z0.5
G01 Z-0.01 F5                                    /*Depth of cut 0.01mm*/
X10 F64                             /*18th slot machining, feed rate 64mm/min */
G01 Z0.5 F5


G00 Z5
M05
G04 P20
S80000 M04                                    /*Spindle speed 80,000 rpm*/
G04 P20
Y36
X0 Z0.5
G01 Z-0.03 F5                                    /*Depth of cut 0.03mm*/
X10 F32                             /*19th slot machining, feed rate 32mm/min */
G01 Z0.5 F5


G00 Z5
M05
G04 P20
S60000 M04                                    /*Spindle speed 60,000 rpm*/
G04 P20
Y38
X0 Z0.5
```

```
G01 Z-0.03 F5                                    /*Depth of cut 0.03mm*/
X10 F48                              /*20th slot machining, feed rate 48mm/min */
G01 Z0.5 F5


G00 Z5
M05
G04 P20
S60000 M04                                  /*Spindle speed 60,000 rpm*/
G04 P20
Y40
X0 Z0.5
G01 Z-0.02 F5                                    /*Depth of cut 0.02mm*/
X10 F72                              /*21st slot machining, feed rate 72mm/min */
G01 Z0.5 F5


G00 Z5
M05
G04 P20
S80000 M04                                  /*Spindle speed 80,000 rpm*/
G04 P20
Y42
X0 Z0.5
G01 Z-0.03 F5                                    /*Depth of cut 0.03mm*/
X10 F64                              /*22nd slot machining, feed rate 64mm/min */
G01 Z0.5 F5


G00 Z5
M05
G04 P20
S40000 M04                                  /*Spindle speed 40,000 rpm*/
G04 P20
Y44
X0 Z0.5
G01 Z-0.03 F5                                    /*Depth of cut 0.03mm*/
X10 F32                              /*23rd slot machining, feed rate 32mm/min */
G01 Z0.5 F5


G00 Z5
M05
G04 P20
S40000 M04                                  /*Spindle speed 40,000 rpm*/
G04 P20
Y46
X0 Z0.5
G01 Z-0.01 F5                                    /*Depth of cut 0.01mm*/
X10 F32                              /*24th slot machining, feed rate 32mm/min */
G01 Z0.5 F5


G00 Z5
M05
G04 P20
S40000 M04                                  /*Spindle speed 40,000 rpm*/
G04 P20
Y48
```

```
X0 Z0.5
G01 Z-0.02 F5                                          /*Depth of cut 0.02mm*/
X10 F32                               /*25th slot machining, feed rate 32mm/min */
G01 Z0.5 F5


G00 Z5
M05
G04 P20
S80000 M04                                    /*Spindle speed 80,000 rpm*/
G04 P20
Y50
X0 Z0.5
G01 Z-0.02 F5                                          /*Depth of cut 0.02mm*/
X10 F96                               /*26th slot machining, feed rate 96mm/min */
G01 Z0.5 F5


G00 Z5
M05
G04 P20
S80000 M04                                    /*Spindle speed 80,000 rpm*/
G04 P20
Y52
X0 Z0.5
G01 Z-0.01 F5                                          /*Depth of cut 0.01mm*/
X10 F96                               /*27th slot machining, feed rate 96mm/min */
G01 Z0.5 F5


G00 Z5
G00 Y100
G04 P10
G00 Y0
G52 X0 Y0 Z0 B0 C0
M5
M30
```

NC codes for the cutting trials in Chapter 8

```
G21 G54 G90 G94
G52 X8 Y-58.8 Z28.3685 B-25.2862 C28.405                    /*Reference point*/
S60000 M04                                        /*Spindle speed 60,000 rpm*/
G04 P30
G00 X0
Y0 Z5 C0 B0
G00 Z0.5
G01 Z-0.02 F5                                        /*Depth of cut 0.02mm*/
X10 F12                                /*1st slot machining, feed rate 12mm/min*/

G01 Z0.5 F5
G00 Z5
G04 P20
Y2
X0 Z0.5
G01 Z-0.02 F5
X10 F24                                /*2nd slot machining, feed rate 24mm/min*/

G01 Z0.5 F5
G00 Z5
G04 P20
Y4
X0 Z0.5
G01 Z-0.02 F5
X10 F48                                /*3rd slot machining, feed rate 48mm/min*/

G01 Z0.5 F5
G00 Z5
G04 P20
Y6
X0 Z0.5
G01 Z-0.02 F5
X10 F72                                /*4th slot machining, feed rate 72mm/min*/

G01 Z0.5 F5
G00 Z5
G04 P20
Y8
X0 Z0.5
G01 Z-0.02 F5
X10 F120                              /*5th slot machining, feed rate 120mm/min*/

G01 Z0.5 F5
G00 Z5
G04 P20
Y10
X0 Z0.5
G01 Z-0.02 F5
X10 F180                              /*6th slot machining, feed rate 180mm/min*/
```

```
G01 Z0.5 F5
G00 Z5
G04 P20
Y12
X0 Z0.5
G01 Z-0.02 F5
X10 F240                            /*7th slot machining, feed rate 240mm/min*/

G01 Z0.5 F5
G00 Z5
G04 P20
Y14
X0 Z0.5
G01 Z-0.02 F5
X10 F300                            /*8th slot machining, feed rate 300mm/min*/

G01 Z0.5 F5
G00 Z5
G04 P20
Y16
X0 Z0.5
G01 Z-0.02 F5
X10 F360                            /*9th slot machining, feed rate 360mm/min*/

G01 Z0.5 F5
G00 Z5
G04 P20
Y18
X0 Z0.5
G01 Z-0.02 F5
X10 F480                            /*10th slot machining, feed rate 480mm/min*/

G00 Z5
M05
G04 P20
S20000 M04                          /*Spindle speed 20,000 rpm*/
G04 P30
Y20
X0 Z0.5
G01 Z-0.01 F5                       /*Depth of cut 0.01mm*/
X10 F24                             /*11th slot machining, feed rate 24mm/min */

G01 Z0.5 F5
G00 Z5
G04 P20
Y22
X0 Z0.5
G01 Z-0.02 F5                       /*Depth of cut 0.02mm*/
X10 F24                             /*12th slot machining, feed rate 24mm/min*/

G01 Z0.5 F5
G00 Z5
G04 P20
Y24
X0 Z0.5
```

```
G01 Z-0.03 F5                                    /*Depth of cut 0.03mm*/
X10 F24                                          /*13th slot machining, feed rate 24mm/min*/


G01 Z0.5 F5
G00 Z5
G04 P20
Y26
X0 Z0.5
G01 Z-0.04 F5                                    /*Depth of cut 0.04mm*/
X10 F24                                          /*14th slot machining, feed rate 24mm/min*/


G00 Z5
M05
G04 P20
S40000 M04                                       /*Spindle speed 40,000 rpm*/
G04 P30
Y28
X0 Z0.5
G01 Z-0.01 F5                                    /*Depth of cut 0.01mm*/
X10 F48                                          /*15th slot machining, feed rate 48mm/min */


G01 Z0.5 F5
G00 Z5
G04 P20
Y30
X0 Z0.5
G01 Z-0.02 F5                                    /*Depth of cut 0.02mm*/
X10 F48                                          /*16th slot machining, feed rate 48mm/min*/


G01 Z0.5 F5
G00 Z5
G04 P20
Y32
X0 Z0.5
G01 Z-0.03 F5                                    /*Depth of cut 0.03mm*/
X10 F48                                          /*17th slot machining, feed rate 48mm/min*/


G01 Z0.5 F5
G00 Z5
G04 P20
Y34
X0 Z0.5
G01 Z-0.04 F5                                    /*Depth of cut 0.04mm*/
X10 F48                                          /*18th slot machining, feed rate 48mm/min*/


G00 Z5
M05
G04 P20
S60000 M04                                       /*Spindle speed 60,000 rpm*/
G04 P30
Y36
X0 Z0.5
G01 Z-0.01 F5                                    /*Depth of cut 0.01mm*/
X10 F72                                          /*19th slot machining, feed rate 72mm/min */
```

```
G01 Z0.5 F5
G00 Z5
G04 P20
Y38
X0 Z0.5
G01 Z-0.02 F5                                        /*Depth of cut 0.02mm*/
X10 F72                              /*20th slot machining, feed rate 72mm/min*/

G01 Z0.5 F5
G00 Z5
G04 P20
Y40
X0 Z0.5
G01 Z-0.03 F5                                        /*Depth of cut 0.03mm*/
X10 F72                              /*21st slot machining, feed rate 72mm/min*/

G01 Z0.5 F5
G00 Z5
G04 P20
Y42
X0 Z0.5
G01 Z-0.04 F5                                        /*Depth of cut 0.04mm*/
X10 F72                              /*22nd slot machining, feed rate 72mm/min*/


G00 Z5
M05
G04 P20
S80000 M04                                           /*Spindle speed 80,000 rpm*/
G04 P30
Y44
X0 Z0.5
G01 Z-0.01 F5                                        /*Depth of cut 0.01mm*/
X10 F96                              /*23rd slot machining, feed rate 96mm/min */

G01 Z0.5 F5
G00 Z5
G04 P20
Y46
X0 Z0.5
G01 Z-0.02 F5                                        /*Depth of cut 0.02mm*/
X10 F96                              /*24th slot machining, feed rate 96mm/min*/

G01 Z0.5 F5
G00 Z5
G04 P20
Y48
X0 Z0.5
G01 Z-0.03 F5                                        /*Depth of cut 0.03mm*/
X10 F96                              /*25th slot machining, feed rate 96mm/min*/

G01 Z0.5 F5
G00 Z5
G04 P20
Y50
```

```
X0 Z0.5
G01 Z-0.04 F5                                    /*Depth of cut 0.04mm*/
X10 F96                                    /*26th slot machining, feed rate 96mm/min*/

G00 Z5
G00 Y100
G04 P10
G00 Y0
G52 X0 Y0 Z0 B0 C0
M5
M30
```